Dissertation

submitted to the combined faculties for the Natural Sciences and for Mathematics of the Ruperto-Carola University of Heidelberg, Germany

for the degree of

Doctor of Natural Sciences

presented by

M. Sc. **Karin Mössenböck**

born in Linz, Austria

date of oral presentation: June 19th 2015, Heidelberg

A Story in Brown and White

Regulation of Metabolic Homeostasis by Brown Adipose Tissue

Referees

Prof. Dr. Peter Angel

Prof. Dr. Stephan Herzig

ABSTRACT

Adipose tissue exists in three shades: White adipose tissue (WAT), the site of energy storage, brown adipose tissue (BAT), which burns nutrients to generate heat and maintain body temperature, and brown in white adipose tissue (brite AT), which represents WAT adapting BAT features in cold exposure. Thermogenically active BAT has been discovered in adult humans and inversely correlates with obesity and insulin resistance. The link between impaired insulin sensitivity and the browning of adipose tissue has not been clear however. While the necessity for insulin for normal development of adipose tissues is well recognised, the dependence of the recruitment of brite adipocytes in functional insulin signalling has not been investigated before. We show that β3-adrenergic stimulation can overcome insulin deficiency and fully activate the brown program in WAT. Vice versa, while it is known that the presence of brite AT allows enhanced glucose clearance, it has not previously been investigated whether this tissue is more insulin sensitive than white. Surprisingly we found that brite cells and tissues demonstrated markedly elevated glucose uptake even in the absence of insulin, and while insulin augmented glucose uptake to both white and brite AT, the degree of this response did not differ between the two types of adipose tissue. In line with these findings, we observed a marked induction of the insulin independent glucose transporter solute carrier family 2 (GLUT-1) upon browning of WAT. Thus we demonstrate for the first time that insulin signalling is dispensable for brite recruitment and not improved in browned cells or tissues.

The nuclear receptor co-regulator Transducin (beta)-like 1 X-linked receptor 1 (TBLR) is a known transcriptional master-regulator that carries out distinct metabolic roles in liver and WAT. We show that, being part of the machinery of a general regulatory mechanism, the actions of TBLR depend largely on its environment, since TBLR deficiency in BAT lead to a distinct phenotype compared to other tissues and its role in mature cells differs from its role during adipogenic differentiation. During differentiation, TBLR balanced growth versus differentiation cues and its depletion reduced glucose import and metabolic activity of mature adipocytes. In thermogenically active mature brown adipocytes or BAT, *Tblr* expression was found to be cold-inducible downstream of the MAPK pathway. BAT-specific knock out of TBLR could be largely compensated for, since gene expression, adiposity, lipid or glucose handling and respiration in these mice (BATKO mice) were normal. However, BATKO mice had impaired maximal thermogenic capacity upon acute β3-adrenergic stimulation. Surprisingly, BAT-specific TBLR KO had systemic effects on gene expression and lead to reduced serum very low density lipoprotein (VLDL) both in the cold and at thermoneutrality. After excluding altered hepatic production or loss to feces, we observed elevated lipid deposition to WAT. Based on our findings, we hypothesise that BATKO mice differentially secrete factors that affect peripheral metabolism.

Understanding the recruitment and regulation of different shades of adipose tissue is a crucial step towards pharmaceutically targeting a disadvantageous metabolic state. This thesis offers new insights on the dependence of whole body metabolism on the function of thermogenically active adipose tissue.

ZUAMMENFASSUNG

Fettgewebe kommt in drei Formen vor: Klassisches weißes Fettgewebe (white adipose tissue, WAT), ein Energiespeicherorgan, braunes Fettgewebe (brown adipose tissue, BAT), das im Gegensatz zu WAT Nährstoffe verbrennt um Wärme zu erzeugen und die Körpertemperatur aufrecht zu erhalten, und sogenanntes „brite“ (brown in white) Fett, welches sich wie BAT verhält und in der Kälte in WAT rekrutiert wird („browning“). Wärme-erzeugendes BAT wurde kürlich entgegen früherer Annahmen in Erwachsenen nachgewiesen und korreliert negativ mit Adipositas und Typ 2 Diabetes, jedoch war unbekannt, welche Verbindung zwischen verringerter Insulin-Sensitivität und WAT „browning“ besteht. Wir zeigen hier, dass es durch β3-adrenerge Stimulation möglich ist, die Auswirkungen von Insulindefizienz auf „brite“ Fett zu kompensieren und das braune Programm in WAT zur Gänze zu aktivieren. Weiters wurde nie spezifiziert ob „brite“ Fett per se insulin-sensitiver ist als weißes. Überraschenderweise konnten wir nachweisen, dass „browned“ Fett bereits ohne Insulin mehr Glukose aufnimmt. Insulinstimulation führte zur Steigerung der Aufnahmerate, jedoch war das Ausmaß dieser Antwort jeweils gleich stark. Im Einklang dazu beobachteten wir einen substanziellen Anstieg des insulin-unabhängigen Glukosetransporters „solute carrier family 2“ (GLUT-1) beim „browning“ von WAT. Wir zeigen also erstmals, dass WAT „browning“ nicht von Insulin-Signalen abhängt, und dass Insulinsensitivität von „browned“ gegenüber weißen Zellen und Gewebe nicht verbessert ist.

Der Kernrezeptor Koregulator Transducin (beta)-like 1 X-linked receptor 1 (TBLR) ist als Master-Regulator bekannt, der in Leber und WAT metabolische Aufgaben übernimmt. Wir zeigen, dass TBLR in seiner Funktion stark von seiner Umgebung abhängt, da sich TBLR Defizienz in BAT anders auswirkte als in anderen Geweben, und in differenziertem BAT anders als während der Adipogenese. Während der Differenzierung balancierte TBLR Wachstums- gegen Differenzierungssignale aus und das Ausschalten („knock out“, KO) von TBLR hatte zur Folge, dass diese Zellen zu metabolisch weniger aktiven Fettzellen reiften und weniger Glukose importierten. In differenziertem BAT war *Tblr* Expression kälteinduzierbar. Mäuse ohne TBLR im BAT (BATKO) konnten den Verlust großteils kompensieren und zeigten normale Genexpression, Adiposität, und Fett- und Glukosestoffwechsel. Die akute β3-adrenerge Stimulation der maximalen BAT Kapazität von BATKO Mäusen war jedoch beeinträchtigt. Überraschenderweise hatten diese Tiere reduzierte Spiegel von very low density lipoprotein (VLDL) im Serum, sowohl in der Kälte als auch unter thermoneutralen Bedingungen. Dieser Unterschied rührte weder von unterschiedlicher hepatischer VLDL Produktion noch von Energieverlust an Fäces her, allerdings kommt es zu vermehrter Lipidablagerung in WAT. Basierend darauf vermuten wir, dass BATKO Mäuse sich von Kontrolltieren bezüglich der BAT-mediierten Sekretion von Faktoren unterscheiden, die periphäre Gewebe beeinflussen.

Um einen nachteilhaften metabolischen Status verbessern zu können, ist eine vielversprechende Strategie, die Regulierung verschiedener Formen von Fettgewebe zu verstehen und zu beeinflussen. Diese Arbeit eröffnet neue Erkenntnisse zur Abhängigkeit des Stoffwechsels eines ganzen Organismus von der Funktion von braunem Fettgewebe.

ACKNOWLEDGEMENTS

Looking back on the last 4 years, I can only say that it was a fantastic experience. None of this would have been possible without the help of all those people constantly supporting me.

I want to thank you, Stephan, for accepting me into your lab, and despite it consisting of so many and so different members that sometimes we greeted new faces every week, never losing touch to the individual members and their project. Not only did I never feel doubt that you were interested in the people and projects, but also your optimism is incredibly containgious, leading me to walk out from every meeting filled with new enthusiasm. Alex, thank you for having been incredibly patient with me when introducing me to the lab, topic and methods, I think there could not have been a single person from whom I could have learned more, not only because of your patience, but also your dedication to detail. Of course the whole group was amazing. This bunch of brilliant people not only helped me more than I deserve, but also created this positive atmosphere in which it was a pleasure to work. Oksana, I was always looking forward to our preps just because it gave us the time to talk. Kati, you fought like a lion with all the hassles we encountered with breeding of our mice, thank you. Thank you Mauricio, for never being as annoyed as you would have every right to be with my never ending stupid questions. I want to thank all the technicians, you are the foundation pillars of all of our success and without you not a single project would have been possible. Thanks Ashley and Adriano for reading my thesis and putting up with my English. Thanks Maria, you made my transition to TBLR so smooth, even just by email from the island. And thank you all A170ies! I also want to thank my TAC committee members, Marcel Scheideler, who crossed the alps every time just to be here and support me, and Aurelio Teleman, who gave me so much useful input. Thanks also to our collaborators, Carsten Sticht who analysed microarray data galore for me and always took time to explain its meaning, and Anne Loft for the patient support with ChIPseq and a million of questions. Thank you, Prof. Rüdiger Hell, Prof. Peter Angel and Prof. Karin Müller-Decker for taking the time and effort to constitute my defense commission. Thank you Lindsay and the Graduate School for being so supportive during my time in the Student Council.

Whom I probably owe most to is my family, who never stopped believing in me and gave me all I need and so much more. Papa, you are the one that lighted the spark of fascination for wisdom and science in me, since as early as I can think back. Mama, you know me better than I know myself, and the knowledge that you will always be there if I fall gives me the courage to try flying high. Stefan, Omas, Opas, thank you for believing in me! Thanks to the crazy bunch I left in Austria, but who never stopped travelling here just to see me. Who would have thought that I'd be Doctor Miss Commander one day? At the same time, I found incredible people here that are at the same time friends and family and more. I do not want to imagine Heidelberg without our 10-girls-in-a-room cooking sessions. Thank you Chiara, my sister in caffeine and Nutella! Ece, health to your hands! Anna, thanks for the szarlotka! Thanks for being fed your mums in Italy, Turkey and Poland! And finally, thank you so much, Angelo, for even in your pixelated form being able to make every bit of stress go away and make me laugh like a moron with just a word and a smile.

“Whether you succeed or not is irrelevant - there is no such thing. Making your unknown known is the important thing - and keeping the unknown always beyond you.”

Georgia O’Keeffe

INDEX

INTRODUCTION

Obesity is a pandemic

For the first time in the history of mankind, over-nutrition accounts for a higher death toll than under-nutrition. An imbalance in energy intake over energy expenditure causes excessive accumulation of fat, which is classified as overweight if the body mass index (BMI,the body weight in kilograms (kg) divided by the square of body height in meters, kg/m^2), exceeds 25, and as obesie if the BMI exceeds 30. Roughly 40 % of the world's population is overweight and more than 1 out of 10 individuals is obese, numbers that have doubled in the last 30 years. This correlates with an increased risk for the globally leading source of death, cardiovascular disease, as well as for diabetes and certain cancers (WHO (2015) Fact sheet No. 311, Obesity and overweight).

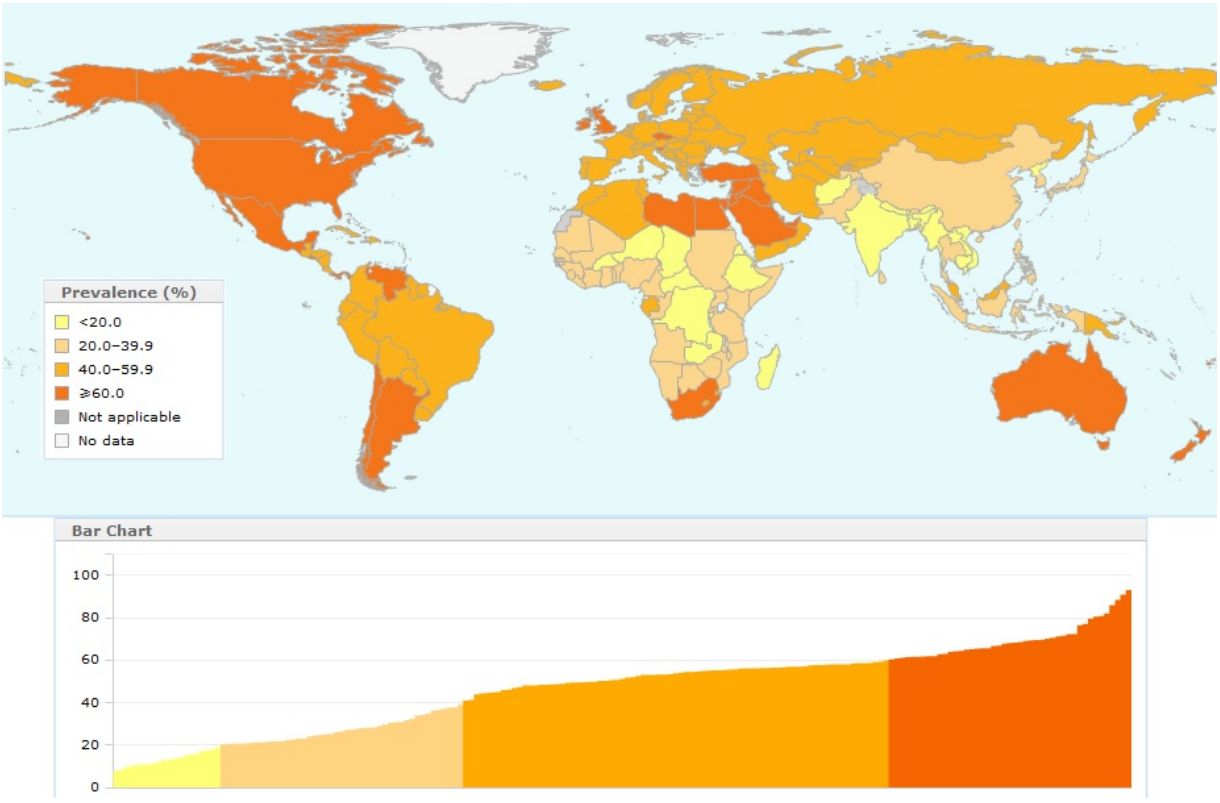

Figure 1. Worldwide prevalence of overweight*. The percentage of overweight (BMI > 25 kg/m^2) inhabitants age 20+ (male and female) in 2008 is shown. © Copyright World Health Organization (WHO), 2015.*

In order to identify strategies to counteract the deleterious consequences of obesity, the underlying causes need to be understood as well as the mechanisms by which, upon onset of obesity, systemic adverse effects are mediated. It is widely accepted that lifestyle, namely

diet or nutritional status and physical activity, translate to body composition and as such there is a strong correlation between socioeconomic status and obesity [10, 11]. Additionally, genetic predispositions contribute to the development of obesity [12, 13], making it clear that adipose tissue biology needs to be correctly regulated to maintain a healthy status.

Obesity leads to the metabolic syndrome and to diabetes

As a consequence of being overweight or obese, a plethora of deleterious health conditions are described. These co-morbidities comprise the so-called metabolic syndrome, which is defined by glucose intolerance or insulin resistance, accompanied by further factors such as obesity, hypertension or an altered serum lipid profile (dyslipidemia) [14]. One of the underlying causes of insulin resistance are toxic by-products of metabolic overload [15]. Mainly this equates to elevated levels of circulating fatty acids (FAs), either produced by lipolysis in lipid stores in adipose tissue, or by lipoprotein lipolysis in other tissues through the action of lipoprotein lipase (LPL) [16]. This in turn leads to FA-mediated dampening of insulin signalling [17-19] and to adipocyte death followed by chronic inflammation and macrophage infiltration [20, 21]. Furthermore, the abundance and composition of triglyceride and cholesterol-rich lipoproteins, which transport lipids through the bloodstream, is disturbed [14], due to both fatty acid induced elevated production of very low density lipoprotein (VLDL) in the liver [22], and due to diminished clearance of peripheral cholesterol following a reduction in levels of high density lipoprotein (HDL) [23, 24].

The metabolic syndrome is a strong determinant for the subsequent development of type 2 diabetes [25, 26].

Fat does not equal fat: Multiple shades of adipose tissue

When examining obesity and overabundance of fat, it is crucial to clearly define the location and nature of lipid depots.

The major site of fat storage in mammals is white adipose tissue (WAT) [27], most of which is located either intra-abdominally (also referred to as visceral), embedding inner organs, or subcutaneously in the form of inguinal (around the hips) or intrerscapular (between the shoulder blades) fat [28]. Over-abundance of subcutaneous fat bears less risk for the development of diabetes than excessive accumulation of intra-abdominal fat [29].

This can to some extent be attributed to the fact that adipose tissue acts as an endocrine organ in a depot-specific manner [30]. Adipose tissue secretes factors that act either in a paracrine manner, on neighbouring cells, or in an endocrine manner, being secreted into the

circulation. Among those factors are cytokines such as leptin and tumor necrosis factor alpha (TNFα), complement factors such as adipsin and adiponectin or proteins involved in lipid homepstasis such as lipoprotein lipase (LPL) or apolipoproteins [31].

In addition to the location, the composition of adipose tissue can vary between individuals. Adipose tissue is comprised not only of adipocytes (mature fat cells), but also connective tissue and the stromal vascular fraction of cells, which containins stem cells that can differentiate into mature adipocytes [32]. Excess of nutrients leads to expansion of adipose tissue, and while in adult-onset of obesity this mainly means filling of already present adipocytes with lipids (hypertrophy), in early onset obesity this is accompanied by increased cell number, termed hyperplasia [33].

Finally, in contrast to energy storing white adipose tissue, brown adipose tissue comprises a functionally diverse fat depot, dissipating nutrients to generate heat via the mitochondrial pore protein uncoupling protein 1 (UCP-1) [34]. The recent discovery that brown adipocytes can be detected in adult humans [35-37] has drawn interest to elucidate its therapeutic potential in the setting of obesity. While most of the conventional approaches to pharmaceutically target obesity have shown only limited success, such as inhibition of intestinal nutrient uptake [38] or of white adipose tissue (WAT) formation [39, 40], the activation of brown adipose tissue (BAT) is a promising approach, having been proven to help maintain normal glucose homeostasis [41-43].

Brown and white adipocytes differ morphologically

Brown adipocytes differ morphologically from classical white adipocytes, having small multilocular lipid droplets rather than one large droplet, and by possessing and increased number and size of mitochondria [44], which can be seen in Figure 2. Brown adipocyte mitochondria are numerous, ovoid in shape and densely packed with laminar cristae [2]. Also, BAT is highly vascularised [45, 46], conferring its darker colour compared to white adipose tissue, which is visible even upon gross inspection [2]. Finally, brown adipocytes, in contrast to white, are characterised by the expression of uncoupling protein 1 (UCP-1, also thermogenin) [47, 48], which is the basis of their differential function as will be explained below.

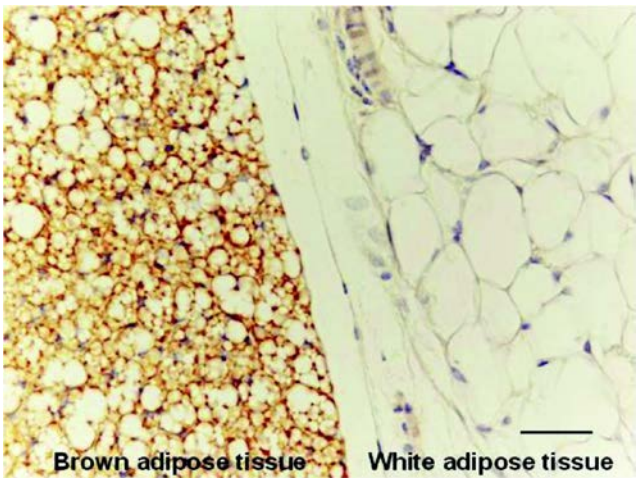

Figure 2. Differential morphology of brown and white adipose tissue*. Adjacent brown and white adipose tissu depots stained with an antibody against the brown fat-specific protein uncoupling protein 1 (UCP-1) [1, 2]*

Brown and white adipocytes have different origins

Brown adipose tissue, although being rich in lipids just like white, is not a fat depot in the classical sense. Instead, it shares more common features with muscle, as it is designed for lipid catabolism rather than storage, it is innervated by the sympathetic nervous system and is rich in mitochondria [49].

In general, brown as well as white adipocytes differentiate from mesodermal stem cells (MSCs) into adipocytes in two steps, first committing either to the white or the brown preadipocyte lineage, followed by terminal differentiation [27]. Each of these steps is controlled by individual subsets of regulatory proteins. The commitment step is mainly regulated by bone morphogenic proteins (BMPs) [50, 51], the hedgehog pathway [52] and the Wnt pathway [53, 54], while terminal differentiation is regulated by insulin [55], cAMP responsive element binding (CREB) [56], and in response to insulin and CREB subsequently by CCAAT/enhancer-binding protein beta and delta (C/EBPβ, C/EBPδ) [57, 58] and after that by C/EBPα and peroxisome proliferator-activated receptor gamma (PPARγ) [59-62].

It was recently confirmed that brown fat cells and muscle cells, in contrast to white fat cells, derive from a common myogenic factor 5 (Myf5) expressing precursor and they can be inter-converted during differentiation under the control of PRD1-BF1-RIZ1 homologous domain containing 16 (PRDM16) [63, 64].

In addition to classical brown adipose tissue, white adipose tissue can respond to the demand for thermogenesis upon cold exposure by so called “browning”, that is, the emergence of adipocytes with brown properties within classical WAT depots [65-68]. While the morphology and function, including UCP-1 expression, of these “brite” (brown in white, sometimes also referred to as beige) adipocytes resembles that of brown, they differ from brown adipocytes found in classical BAT depots as they do not descend of Myf5 expressing

precursors [69-71]. It is currently not resolved whether brite cells exclusively arise exclusively from brite precursor cells residing in white fat depots [72, 73], or if, as numerous studies suggest [2, 74-77], even fully differentiated white adipocytes can trans-differentiate into brite cells [8].

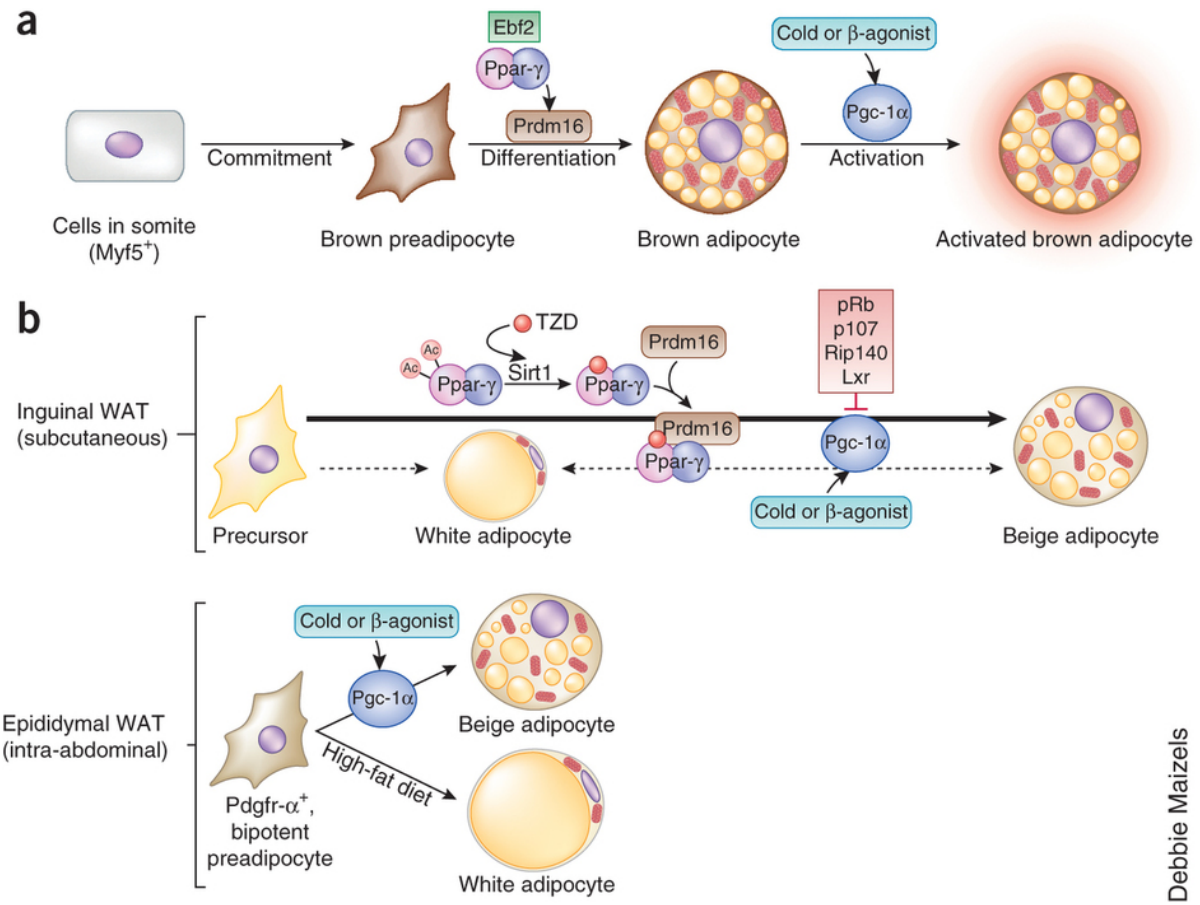

Figure 3. White, brite and brown adipocytes arise from different precursors*. While brown adipocytes arise, like muscle cells, from Myf5 expressing precursors and can be acutely activated by cold exposure (a), white and brite adipocytes derive from adipocyte precursors (b). Different mechanisms were suggested to influence the fate determination between white and brite adipocytes, such as cold and dietary stimuli during differentiation (b). [8]*

Brown and white adipocytes differ functionally

Higher vascularisation of BAT compared to WAT is necessary, since the function of BAT is to use the energy from food intake for the production of heat if challenged by cold-exposure [78], as opposed to white adipose tissue that stores excess energy as triglyceride depots [79]. This allows animals to adapt to cold challenges and switch from shivering to more

energy-conserving non-shivering thermogenesis, a process dependant on the mitochondrial pore protein UCP-1 [47, 48].

In general, to gain energy from food, nutrients are oxidised and electrons resulting from this breakdown are gradually transferred to oxygen (O_2). This process allows for the generation of adenosine triphosphate (ATP) from adenosine diphosphate (ADP) and inorganic phosphate (P_i), a process referred to as oxidative phosphorylation. The breakdown of nutrients leads to the production of reduction equivalents by transferring electrons (e^-) to NAD^+, reducing it to NADH. In the mitochondria of each cell, those electrons are then step-wise handed through a chain of protein-complexes in the inner mitochondrial membrane. Those complexes consist of

- Complex I (NADH:ubiquinone oxidoreductase, transfers e^- from NADH to ubiquinone, reducing it to ubiquinol)
- Complex II (succinate:ubiquinone oxidoreductase, alternative entry point for succinate-derived e^- directly from the citric acid cycle)
- Complex III (ubiquinone:cytochrome c oxidoreductase, transfers e^- from ubiquinol to cytochrome c)
- Complex IV (cytochrome c oxidase, transfers e^- from cytochrome c to O_2)
- Complex V (ATP synthase, creates ATP from ADP and P_i powered by the proton (H^+) gradient over the inner mitochondrial membrane)

Complex I, III and IV pump protons from the mitochondrial matrix into the intermembrane space between the permeable outer and the impermeable inner mitochondrial membrane, which creates a gradient and thus force, both in concentration and charge. The last step of this process limits the reaction as an equilibrium is reached until ATP is again hydrolysed to ADP + P_i. [80].

Brown adipocyte mitochondria however possess a unique feature, as they express a protein, uncoupling protein 1 (UCP-1) that permeabilises the inner mitochondrial membrane, thereby dissipating the electrochemical gradient and uncoupling respiration from the need of ATP synthesis and use. By disrupting the equilibrium and releasing heat rather than ATP, the reaction allows the continual breakdown of nutrients, which, in the absence of uncoupling, would require ATP to be hydrolysed (for example by powering muscle contraction) [81, 82]. Phrased simply, in the cold BAT burns energy stores without requiring physical activity.

The events occurring during oxidative phosphorylation and uncoupled respiration are illustrated in Figure 4.

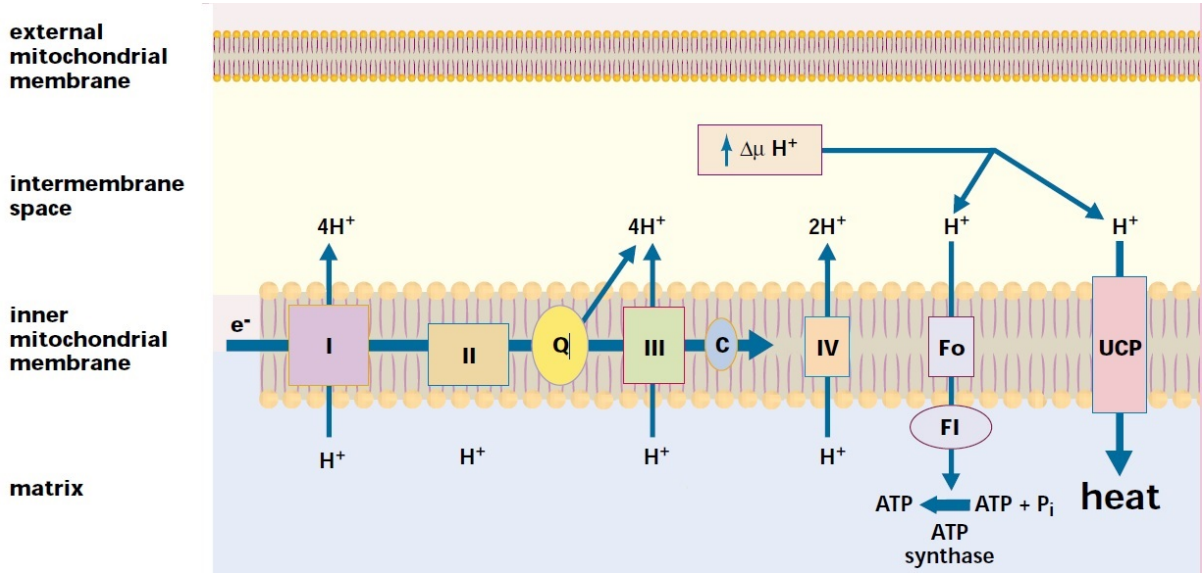

Figure 4. Ucp1 uncouples respiration by dissipating the proton gradient. *Gradual electron transport through the complexes of the electron transport chain in the inner mitochondrial membrane lead to the buildup of an electrochemical gradient, which is the driving force of ATP production. Dissipation of this gradient through the pore protein UCP-1 uncouples respiration from ATP generation and leads to the production of heat (Figure adapted from [7]*

UCP-1 is regulated both transcriptionally and functionally

Without control, the existence of brown adipose tissue would, in a futile cycle, lead to depletion of energy and consequently death. Thus brown adipose tissue function, in particular UCP-1 meadiated events, are tightly controlled to assure uncoupling only takes place when required. This control is exerted on the one hand transcriptionally, allowing adipocytes to gradually express increasing amounts of UCP-1 during the course of cold adaptation, and on the other hand on protein activation levels, allowing for acute UCP-1 activation upon β-adrenergic stimulation [78].

In both cases, the initial steps are the same. Cold exposure leads to norepinephrine (NE, equal to noradrenalin) release [83] and activation of the adipose β3-adrenergic receptor (β3-AR) [84, 85]. The β3-AR is a G-protein coupled receptor (GPCR) and upon activation of the membrane bound G-protein GS [86], adenylyl cyclase is activated which triggers an increase in the second messenger molecule cyclic adenosine monophosphate (cAMP) [87] and subsequent activation of protein kinase A (PKA) [88].

PKA can then mediate both the transcriptional response required for cold adaption, and acute UCP-1 activation. The former is achieved by phosphorylating and activating cAMP response element binding (CREB) and subsequent gene expression programs [89, 90].

Those include direct *Ucp1* binding by CREB [91] and also phosphorylation and activation of the p38 mitogen-activated protein kinase (MAP kinase) pathway [92] and subsequently the PPARγ co-regulator PGC-1α [93], which can again bind the *Ucp1* promoter [94].

Even in the presence of high UCP-1 expression, mitochondria in BAT stay coupled and UCP-1 inactivated until stimulated, which can occur in a matter of minutes [78]. In the physiological state, UCP-1 is maintained inactive through inhibition by purin nucleotides such as GDP and ADP [46, 95]. However in the cold, upon activation of PKA as described above, lipolysis is induced and free fatty acids are produced [96-98]. Those fatty acids do not only serve as fuel to power the electron transport chain as described above, but also activate UCP-1 [82, 99]. In fact, despite the fact that fatty acids possess, to some degree, even UCP-1-independent capability to drive respiration, by acting as fuel or even as detergents with inherent uncoupling capability [100], the activation of thermogenesis is still fully dependent on UCP-1. This is proven by the findings that FAs fail to induce thermogenesis in UCP-1 knockout cells [101] and that on the other hand unmetabolisable FA analogues are still capable of UCP-1 induction [102].

Brown and brite fat are glucose sinks burning away nutrients

The function of thermogenically active adipose tissue, as explained above, together with the discovery of its presence in adult humans, make it an interesting candidate for counteracting nutrient overload, obesity and diabetes. There are speculations that one of the physiological functions of BAT is to prevent obesity [103, 104]. High fat diets have been shown to activate thermogenesis [105], however it is not fully understood whether defects in BAT function have the potential to facilitate obesity. While some previous reports suggest that BAT-deficient animals are obese [106], other studies found that UCP-1 knockout animals were not overweight or obese [107]. In humans, BAT activity negatively correlates with adiposity [108], and despite the small amount of BAT present in humans, it is estimated that brown fat could contribute up to 20% of daily energy expenditure [109].

Upon cold-induced activation of BAT, glucose uptake is increased [110], and this has the potential to systemically clear glucose and thereby improve insulin sensitivity in humans [42, 43], which makes targeting of BAT a promising strategy in the prevention and treatment of obesity-induced diabetes [41].

Additionally, recent studies demonstrated that BAT has the potential to correct another hallmark of the metabolic syndrome, hypertriglyceridemia, by clearing triglyceride rich proteins from the circulation via on LPL activity [111].

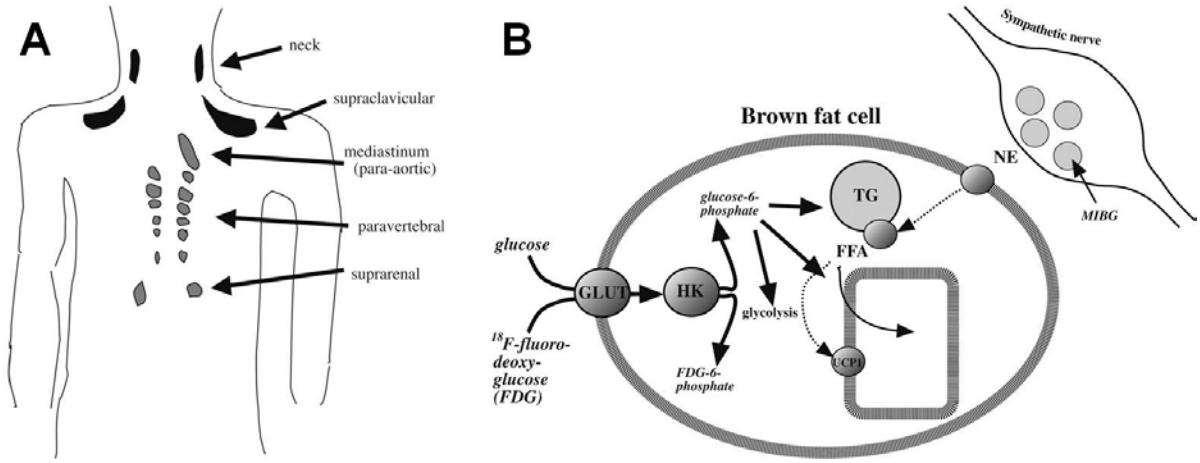

***Figure 5. Brown fat is existent in humans and clears glucose and fat**. (A) ^{18}F-fluorodeoxiglucose (^{18}F-FDG) uptake studies revealed sites of high glucose uptake in adult human subjects, confirmed to being adipose tissue by computed-tomography coupled positron emission tomoscintigraphy (PET-CT) scans in follow up studies. (B) Brown fat cells import glucose which is broken down by glycolysis or converted to lipids. Upon adrenergic activation, intracellular lipolysis creates free fatty acids, serving both as activators and as fuel for thermogenesis. (Figure adapted from [9])*

Transcriptional co-regulation of gene expression depends on multiprotein complexes

Gene expression is coordinated depending on cell type, developmental stage or specific requirement in response to environmental changes. The latter is largely possible by regulating gene expression programs through nuclear receptors (NRs), proteins that can be activated by ligand binding, translocate to the nucleus and regulate target gene expression [112]. These ligands are often lipophilic hormones, such as steroids and thyroids, that instead of binding to surface receptors enter the cell and bind to NRs. In addition to hormone activated nuclear receptors, there are so-called orphan receptors for which their ligands have not yet been identified [113, 114]. NRs, once in the nucleus, bind as homo- or heterodimers to palindromic response elements (REs) [115]. The structure of NRs is modular and outlined in Figure 6.

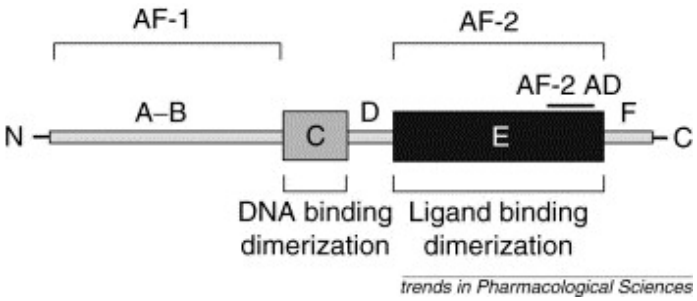

Figure 6. Nuclear receptors are modular proteins*. Apart from a N-terminal receptor specific activating domain (AF-1), NRs consist of a C-terminal ligand dependent activating domain (AF-2), those two being separated by a DNA binding domain [6].*

In addition to being controlled by the presence and absence of ligands, NRs interact with co-regulators, proteins that mediate activation (co-activators) or repression (co-repressors) of NR target genes [116]. The latter is achieved by recruiting proteins that interact with un-bound NRs and form a co-repressor complex at target gene promoters. The two best characterised co-repressors are the nuclear receptor co-repressor NCoR [117], and SMRT (Silencing Mediator of Retinoid and Thyroid Receptors [118]. Those proteins interact with NRs [119] and exert repressive function [120]. Diverse interactions have been described, in which NCoR or SMRT form complexes with histone deacetylase 3 (HDAC3), transducin-β-like 1X-linked (TBL1X, or also TBL) and its related protein transducin-β -like 1 X-linked receptor 1 (TBL1XR1, or also TBLR). In these complexes, HDAC3 is responsible for the repressing function by deacetylating chromatin, which causes heterochromatin formation and shut down of gene expression [121-123]. This complex is illustrated in Figure 7.

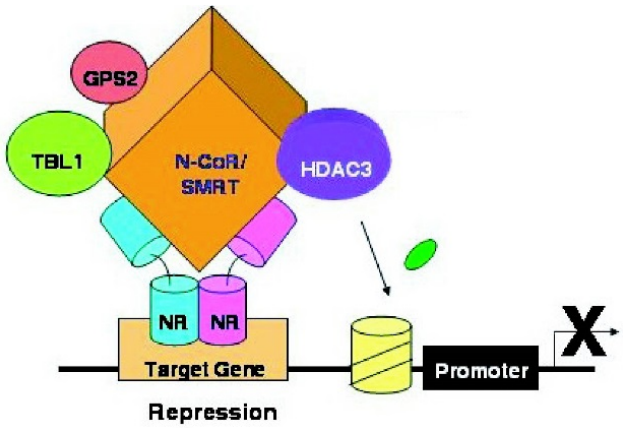

Figure 7. Co-repressor complexes consist of multiple proteins*. NRs not bound by ligands recruit co-repressor complexes to mediate silencing of target gene repressors. Co-repressors such as NCoR and SMRT interact with further proteins such as HDAC3, TBL or TBLR to mediate heterochromatin formation and gene repression (figure adapted from[5]).*

Finally, co-regulators themselves are target of regulation, and a variety of post-transcriptional modifications has been reported to being able to transmit signals by activating or inactivating NR co-regulators. For example mitogen triggered activation of the MAPK pathway can lead to co-repressor phosphorylation and export from the nucleus, thereby activating gene expression [124]. Also acetylation [125] or ubiquitinylation [126] have been described. Intriguingly, this allows a common co-repression machinery to being activated or de-activated for specific targets in a tissue-specific way. One example is the co-activator PGC-1α that in brown fat is described as to interact with PPARγ and TR to activate *Ucp1* transcription [127]. The same factor however in liver is known to, upon cAMP signalling-mediated CREB phosphorylation, facilitate glucocorticoid signalling-dependent expression of gluconeogenic genes [93]. Thus, not only differential expression but also distinct regulation of NR co-regulators can determine tissue-specific responses. It is even speculated that co-regulators, being amplifiers of gene expression responses, are the missing link to explain how small sets of genetic mutations can give rise to a wide-spread spectrum of phenotypes [112].

TBLR and TBL are co-regulators with known metabolic roles

As outlined above, NRs work in cooperation with multiprotein-complexes mediating repressive or activating function and those co-regulators can be targeted and modified in order to change their function.

Two proteins sharing roughly 90 % sequence homology, TBLR and TBL, together with HDAC3, are part of the NCoR or SMRT co-repressor complex. They are, like HDAC3, essential for NCoR repressive function [128]. However, NCoR repressive function depends on HDAC3 but not on TBLR/TBL, suggesting that they regulate the co-repressor complex in a different way than the actual de-acetylating function [129]. One way they do so seems to be targeting of the NCoR complex to histones, in order to, upon initial weak de-acetylation capability, recruit the complex to its site of action and thereby enhance its potency [130]. Further, both proteins harbour an F-box/WD40 repeat motif, which is known to allow for target protein poly-ubiquitinylation and degradation [131], suggesting that they can function by altering the stability of the NCoR complex. In fact, TBLR and TBL do not only mediate gene repression, but have also been shown to activate gene expression. TBLR and TBL can serve as nuclear exchange factors, recruiting the ubiquitin conjugating/19S proteasome complex, which leads to the exchange of co-repressors (NCoR or SMRT) for co-activators [132].

While both factors have been described as functionally redundant [128], subsequent research showed they differ in 5 phosphorylation sites, which allows for differential

regulation. TBL possesses unique sites phosphorylated by glycogen synthase kinase 3 (GSK3), while TBLR harbours a unique site targeted by protein kinase C-δ (PKCdelta) [3].

Figure 8 illustrates the action of TBLR and TBL in the NCoR or SMRT co-repressor complex.

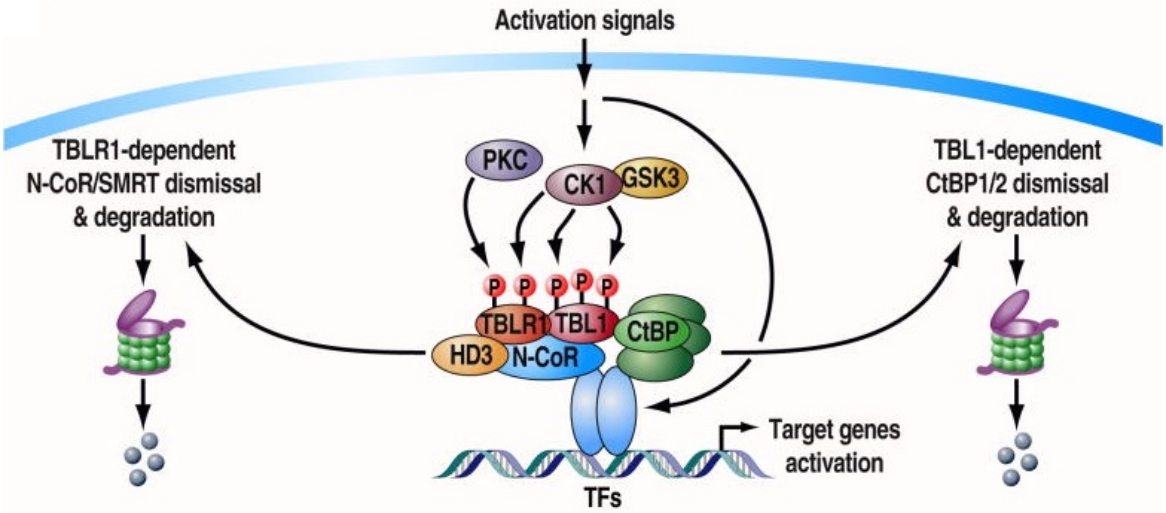

Figure 8. TBLR and TBL can be phosphorylated to mediate nuclear co-regulator exchange. *Activating signals lead to kinase mediated phosphorylation of TBLR and / or TBL on distinct sites. In turn they recruit the ubiquitin conjugating/19S proteasome complex, thereby eliminating co-repressors and exchanging them for co-activators (figure adapted from [3]).*

Conceivably, being part of the machinery that exerts one very common mechanism of gene regulation, both TBLR and TBL have been associated with disease development if aberrantly expressed. TBLR mutations are associated with autism and mental disabilities [133-135].

Further, they regulate the balance between pro- and anti-proliferative effects, depending on their interaction partners. For example, TBLR was recently demonstrated to interact with the androgen receptor (AR) in order to switch from pro- to anti-proliferative programs, suppressing prostate cancer growth [136]. In the setting of cervical cancer however, TBLR was found to promote metastasis [137]. TBL was demonstrated to interact with nuclear factor κB (NF-κB), thereby activating pro-proliferative programs and enhancing breast cancer invasiveness [138].

Finally, metabolic roles were reported for both TBLR and TBL, and notably, depending on the tissue, they can mediate specific roles without being completely functionally redundant, leading to strong phenotypes upon deletion of TBLR-only in adipose tissue or of TBL-only in the liver. Our group demonstrated that in white adipose tissue, TBLR interacts with PPARγ and retinoid X receptor alpha (RXRα) to allow cAMP-mediated activation of lipid mobilization,

thus potentially being protective against the development of obesity [139]. In the liver, TBL, together with TBLR and PPARα, is responsible for fatty acid oxidation, its absence inducing hypertriglyceridemia and hepatic steatosis ("fatty liver") [140]. In embryonic stem cells, TBL deletion blocks adipogenic differentiation [132].

Aim of the projects

This thesis is comprised of two related projects, the first focusing on insulin signalling and the browning of white adipose tissue, the second elucidating the role of nuclear receptor co-regulator TBLR in brown adipose tissue.

Due to the potential of brown and brite fat to counteract obesity, it is crucial to understand how brown adipocytes can be recruited and how they are regulated. The first part of this thesis will describe the interplay between insulin signalling and the recruitment of brite adipocytes. It is known that insulin and insulin-like growth factor (IGF)-1 are indispensable for adipogenic differentiation [141, 142], their absence leading to reduced adipose depots and basal brown fat thermogenesis in vivo [143]. Interestingly, the capability of β3-adrenergic stimulation was maintained regardless of insulin [143]. These studies did however not cast light on the influence of insulin signalling on brite recruitment within white adipose tissue. We hypothesised that in states of impaired insulin signalling, white adipose tissue browning may be impaired, which may partially explain lower BAT abundance in obese and thus insulin resistant patients. Further we speculated that, from the opposing point of view, recruitment of brite adipocytes might improve insulin sensitivity. While it is known that browning increases glucose clearance, it is not described whether brite cells and tissues are more insulin sensitive, that is, reacting stronger to insulin stimulation than white adipose tissue.

The second part of this thesis will focus on nuclear receptor co-regulator-mediated regulation of brown adipose tissue function. Based on the known metabolic roles of TBL [140] and TBLR [139] we hypothesised that also other metabolically active tissues may be hotspots for TBLR- or TBL-mediated regulation. Since previous studies failed to distinguish between different fat depots, it was not previously clear if and which effects of ablation of TBLR in total adipose tissue [139] are attributable to brown fat function. In order to understand the role of TBLR in this functionally distinct adipose depot, in vitro and in vivo studies were employed to examine the role of TBLR and TBL in brown adipocytes and subsequent implications on systemic metabolic homeostasis.

With these two approaches this study aims to enhance the understanding of the regulation of the function of thermogenic active brown adipocyte cells and tissues by hormones such as insulin and by transcriptional regulators such as TBLR.

RESULTS

The goal of this project was to broadly contribute to the understanding of the functional regulation of thermogenic active brown, as well as brite (brown in white) adipose cells and tissues. The first part of this thesis will provide insights on the complex interplay between glucose uptake, insulin signalling and white adipose tissue browning, while the second part will investigate how the metabolic master-regulator Transducin (beta)-like 1 X-linked Receptor 1 (TBL1XR1, or also TBLR) integrates brown adipose tissue-specific mechanisms and systemic metabolic regulation.

BROWNING OF WHITE ADIPOSE TISSUE UNCOUPLES GLUCOSE UPTAKE FROM INSULIN SIGNALLING

C57Bl6 is a robust strain to investigate white adipose tissue browning

In the beginning of this project the role of mouse strain and gender was tested in regard of their effect on browning potential. Primary inguinal white adipose tissue (iWAT) stromal vascular fraction (SVF)-derived $Lin^{-}Sca1^{+}$ [144] adipocyte progenitors from C57Bl6 (BL6) and 129S6/SvEvTac (SV129) male and female mice were differentiated in vitro in the presence or absence of carbaprostacyclin ($cPGI_2$), which had previously been reported to induce browning of white adipocytes by acting downstream of β-adrenergic signalling. This resulted in “white” (ethanol (EtOH) vehicle-treated) or “brite” ($cPGI_2$-treated) adipocytes. The brite state of white adipocytes was defined based on the elevated mRNA expression of uncoupling protein 1 (*Ucp1*). SV129-derived adipocytes expressed higher levels of *Ucp1* even in the absence of $cPGI_2$, indicating an already brite state in basal conditions. In both, BL6- and Sv129-derived adipocytes, basal Ucp1 expression was lower in cells from females, and in all samples *Ucp1* expression was inducible by chronic $cPGI_2$ treatment. Based on the largest relative change by browning cues, female BL6 mice were chosen for further studies (Figure 9).

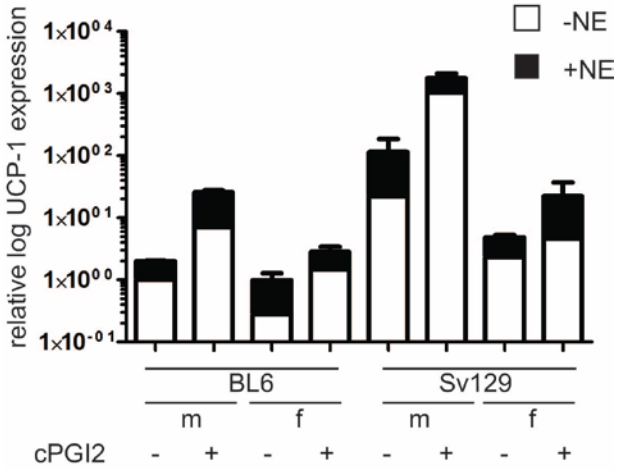

Figure 9. iWAT adipocytes of BL6 mice are white and can turn brite. *Ucp1 mRNA expression of primary iWAT SVF-derived adipocyte progenitors from BL6 and SV120 male and female mice differentiated in vitro into white (EtOH treatment) or brite (cPGI2 treatment) adipocytes. All values are expressed as means ± SEM, n = 3 mice for cell isolation. Three way ANOVA proved, both in basal and in NE stimulated state, p<0.001 for white (EtOH-treated) vs. brite (cPGI2 treated) cells, for BL6 vs. SV129, and for male vs. female.*

Lack of insulin does not impair browning capacity of primary adipocyte progenitors

To address the question of whether insulin signalling during adipocyte differentiation is required for brite recruitment, iWAT SVF-derived primary adipocyte progenitors were isolated from BL6 female mice. Differentiation was induced in the absence or presence of $cPGI_2$ and/or insulin, and the cells were harvested 24 hours later. The capability of adipocyte progenitors to respond to insulin at this timepoint of differentiation was confirmed by Western Blot analysis, detecting phospho-AKT (Figure10.A,B). RNA of harvested cells was subjected to microarray analysis with Affymetrix chips. As expected, bioinformatic analysis of gene expression data revealed that $cPGI_2$ induced distinct gene expression patterns, resulting in the samples from brite-induced cells to group clearly in a hierarchical clustering analysis on correlations. However the presence or absence of insulin during the first 24 hours of differentiation hardly affected gene expression in white as well as in brite-induced cells (Figure 10.C). Next, primary adipocyte progenitors were differentiated for 8 days into mature white or brite adipocytes with insulin present or absent in the medium. The role of insulin in the differentiation to the respective adipocyte type was assessed based on the expression patterns of marker genes. In general, the activation of the adipogenic program, as judged by the expression of the early adipogenic genes peroxisome proliferator activated receptor

gamma (Pparg) [145] and its co-factor peroxisome proliferator activated receptor gamma (Ppargc1a), was not largely compromised by the lack of insulin (Figure 10.D). However, insulin appeared to be essential for full differentiation into mature adipocytes, since cells differentiated without insulin exhibited lower levels of the white adipogenesis marker resistin (Retn) and of the late adipogenesis marker fatty acid binding protein 4 (Fabp4) (Figure 10.E). Fabp4 levels could only be partially rescued by the stimulating effect of $cPGI_2$ on adipogenesis in the absence of insulin (Figure 10.E). The brite adipogenesis markers *Ucp1* and Cell death-inducing DNA fragmentation factor, alpha subunit-like effector A (*Cidea*) were only marginally affected by the lack of insulin in the white state (Figure 10.F). $cPGI_2$ was still capable of inducing their expression, albeit to a compromised extent, in line with impaired general adipogenesis (Figure 10.F). Altogether, this data show that insulin is crucial for regular adipocyte differentiation while it does not arrest the browning process.

Osmotic pumps are a valuable tool for constant-flow administration of browning agents to mice

For in vivo studies of recruitment of brite adipocytes, the standard method used previously in our lab was daily intraperitoneal (i.p.) injection of 1 mg/kg bodyweight of the β3-adrenergic sympathomimetic agonist CL316243 (CL) for 10 consecutive days. However we chose to apply CL by a constant flow administered by implanted osmotic pumps (equal daily dose and duration) after comparing both methods. We found that mice reacted to both administration methods with browning of WAT as indicated by increased food intake (Figure11.A) without changes in body weight (Figure11.B), while magnetic resonance imaging (MRI) analysis even showed a trend to decreased body fat content (Figure11.C). Likewise, with both methods WAT weight was decreased to a similar extent while BAT weight was unaffected (Figure11.D). Finally, mRNA expression levels of marker genes for WAT browning (*Ucp1*, *Cidea* and the mitochondrial factors cytochrome c oxidase subunit VIIa 1 (*Cox7a1*) and VIIIb (*Cox8b*)) were found to be induced equally by either application method, while the expression of the WAT marker gene Retn was unaffected (Figure11.E, inguinal white adipose tissue (iWAT), the same was found in abdominal WAT (aWAT), data not shown). Further, pump-implanted animals did not suffer from any adverse side effects as compared to injected animals. On the contrary, i.p.-injected animals exhibited signs of higher stress levels, such as slight browning even in the basal state (indicative of a generally elevated adrenergic tone) (Figure11.E), as well as a larger relative liver weight (Figure11.F) compared to pump-implanted animals. Based on these results we chose to continue using osmotic pump implantation as a method of inducing browning of WAT in vivo.

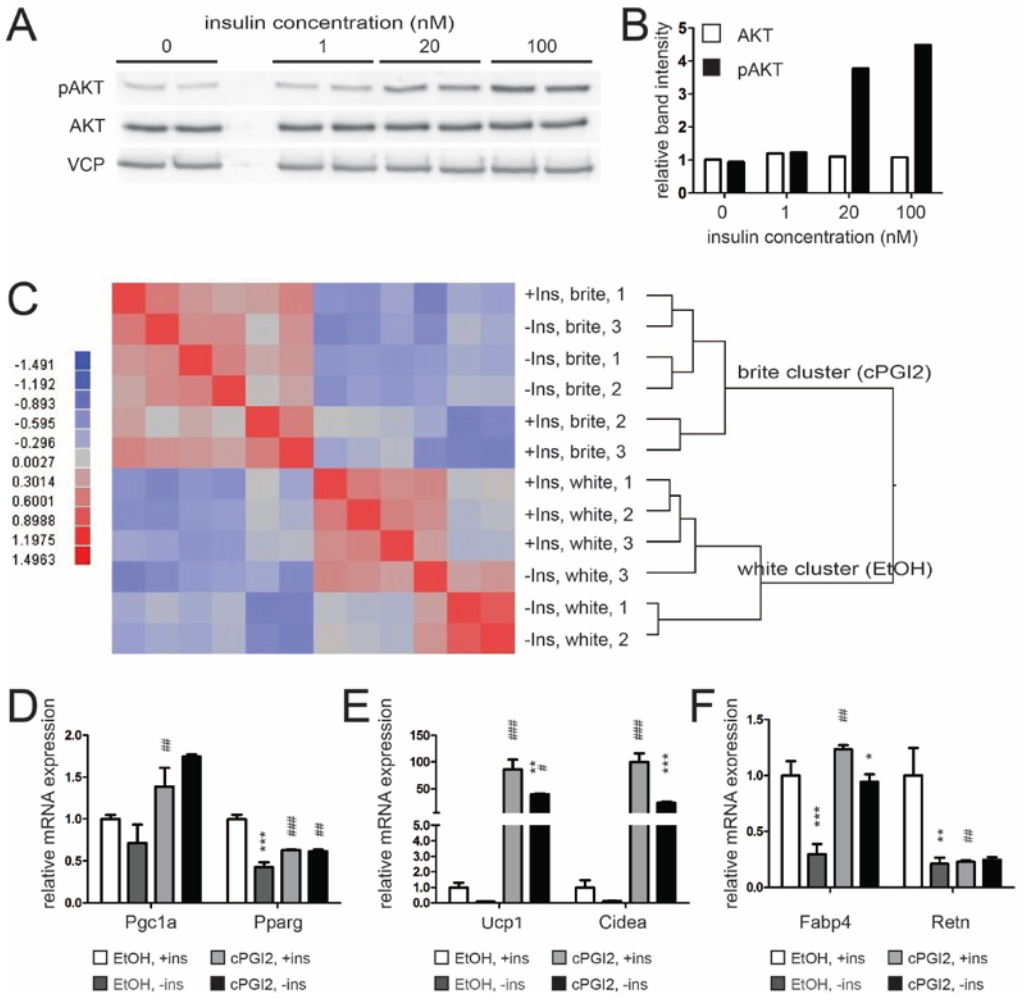

Figure 10. Lack of insulin does not impair browning capacity of primary adipocyte progenitors. *(A) Western Blot and (B) corresponding quantification with ImageJ of iWAT SVF-derived primary adipocyte progenitors at 80% confluency, stimulated with the indicated doses of insulin for 15 minutes. (C) Heatmap showing differential mRNA expression between confluent iWAT SVF-derived primary adipocyte progenitors differentiated for 24 h with white (EtOH-treated) or brite ($cPGI_2$ treated) differentiation cocktail and between absence or presence of insulin (Ins) in the medium. Higher and lower expression is displayed in red and blue, respectively. (D) mRNA expression of Pgc1a and Pparg or (E) Fabp4 and Retn or (F) Ucp1 and Cidea in iWAT SVF-derived primary adipocyte progenitors differentiated into white or brite adipocytes for 8 days with insulin present or absent in the differentiation medium. All values in bar graphs are expressed as means ± SEM, n = 3 animals for cell isolation, #p<0.05, ##p<0.01, ###p<0.001 white (EtOH-treated) vs. brite ($cPGI_2$ treated) cells, *p<0.05, **p<0.01, ***p<0.001 normal conditions vs. insulin deprived conditions.*

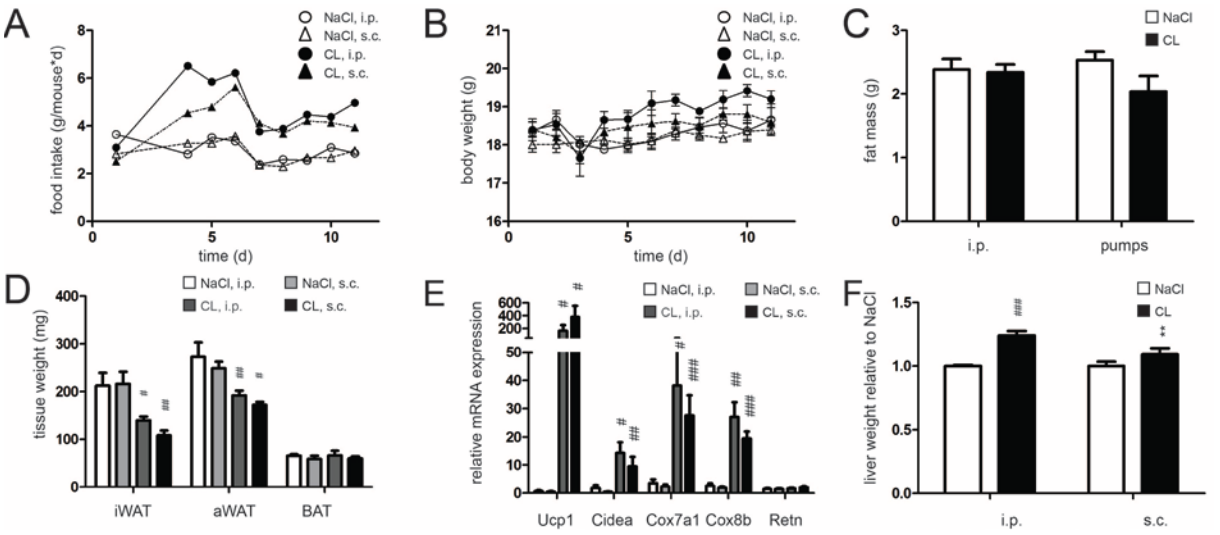

Figure 11. Drug delivery by osmotic pumps induces WAT browning equally efficient as by i.p. injections*. Female BL6 mice were subjected to recruitment of brite adipose tissue by administering 1 mg/kg body weight CL for 10 days either by i.p. injections (i.p.) or by implanted osmotic pumps (s.c.). (A) Food intake, (B) body weight, (C) body fat mass as assessed by MRI, (D) iWAT weight, (E) mRNA expression of brite and white marker genes and (F) liver weight in response to CL-treatment. medium. All values in bar graphs are expressed as means ± SEM, n = 5, #p<0.05, ##p<0.01, ###p<0.001 white (NaCl-treatment) vs. brite (CL-treatment), *p<0.05, **p<0.01, ***p<0.001 i.p. injections vs. osmotic pumps.*

Browning of white adipose tissue is functional in diabetes mouse models

Analogously to the in vitro data shown above, the importance of insulin signalling on the recruitment of brite adipocytes in vivo was studied in established experimental models of insulin insufficiency. We used streptozotocin (STZ)-induced β-cell ablation to create mice lacking insulin, mimicking Type I diabetes [146], and high fat diet (HFD) versus low fat diet (LFD) feeding to generate obese, insulin resistant mice, mimicking Type II diabetes [147]. The pathological settings were confirmed by measuring blood glucose and insulin levels, revealing high blood glucose levels accompanied by a lack of insulin in STZ-treated mice as well as high blood glucose levels despite elevated insulin levels typical for HFD-fed mice (Figure12.A, B). Metabolic abnormality in these animals was further confirmed by demonstration of weight and adipose tissue loss in the STZ and gain of weight and adiposity in the HFD model (Figure12.C, D).

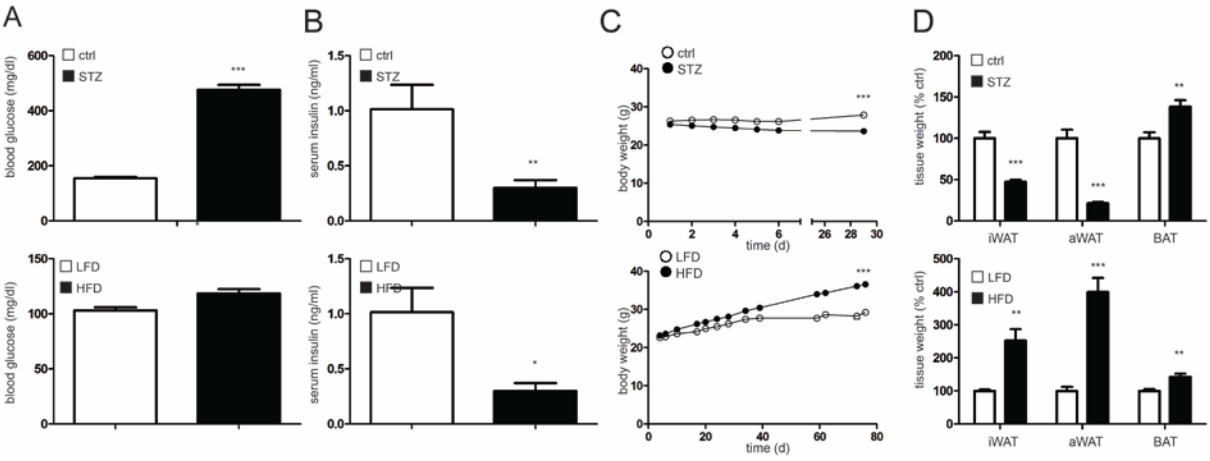

Figure 12. STZ treated mice show a Type I diabetic phenotype while HFD-fed mice show a Type II diabetic phenotype. *(A) Random fed blood glucose levels and (B) serum insulin levels of streptozotocin (STZ, 60 µg/day/g bw) injected and control (upper panels) or 12 weeks low fat diet (LFD) or high fat diet (HFD) fed (lower panels) mice. (C) Body weight over time and (D) inguinal and abdominal white or brown adipose tissue (iWAT, aWAT and BAT, respectively) weights at time of sacrifice of STZ-injected and control (upper panels) or LFD and HFD-fed (lower panels) mice. All values in bar graphs are expressed as means ± SEM, n = 7-10, *p<0.05, **p<0.01, ***p<0.001 control vs. STZ and LFD vs. HFD-fed animals.*

Upon implantation of osmotic pumps to recruit iWAT browning by CL administration, all groups responded to the cue by a loss of fat mass (Figure13.A) and reduced WAT weight, while the masses of BAT and other tissues were not affected (Figure13.B), with the exception of STZ-injected animals that hardly had any body fat mass even before the induction of browning (Figure13.D). Also serum insulin levels were reduced in response to CL-treatment (Figure13.C). Gene expression analysis of iWAT and aWAT depots of STZ-treated animals showed that in the white (no CL) state, brite marker genes (*Ucp1*, *Cidea*, carnitine palmitoyltransferase 1b (*Cpt1b*), *Cox7a1*, *Cox8b*) were expressed at lower levels in insulin-deficient animals (Figure13.D, E). However, CL-treatment could fully overcome the defect, leading to brite marker genes expressed at high levels regardless of the presence of insulin in the serum of the mice (Figure13.D, E). Given the markedly lowered basal expression, the fold change of brite marker mRNAs in response to CL was even higher in STZ-treated mice. Analogously in HFD-fed animals iWAT and aWAT gene expression analysis showed lowered basal levels of brite markers in insulin resistant animals which could be strongly induced by CL-treatment, albeit still not fully reaching the same levels as in LFD-fed controls (Figure13.F, G). Still, also in the Type II diabetes model, the fold induction

of brite markers was even stronger in animals with impaired insulin signalling. To confirm these results, immunohistological analysis of UCP-1 expression in iWAT and aWAT of LFD and HFD-fed animals was performed, the results reflecting the gene expression data, namely that while HFD-fed animals expressed lowered basal UCP-1 levels, CL-treatment was able to increase the amount of UCP-1 protein also in the insulin resistant animals (Figure13.H, I).

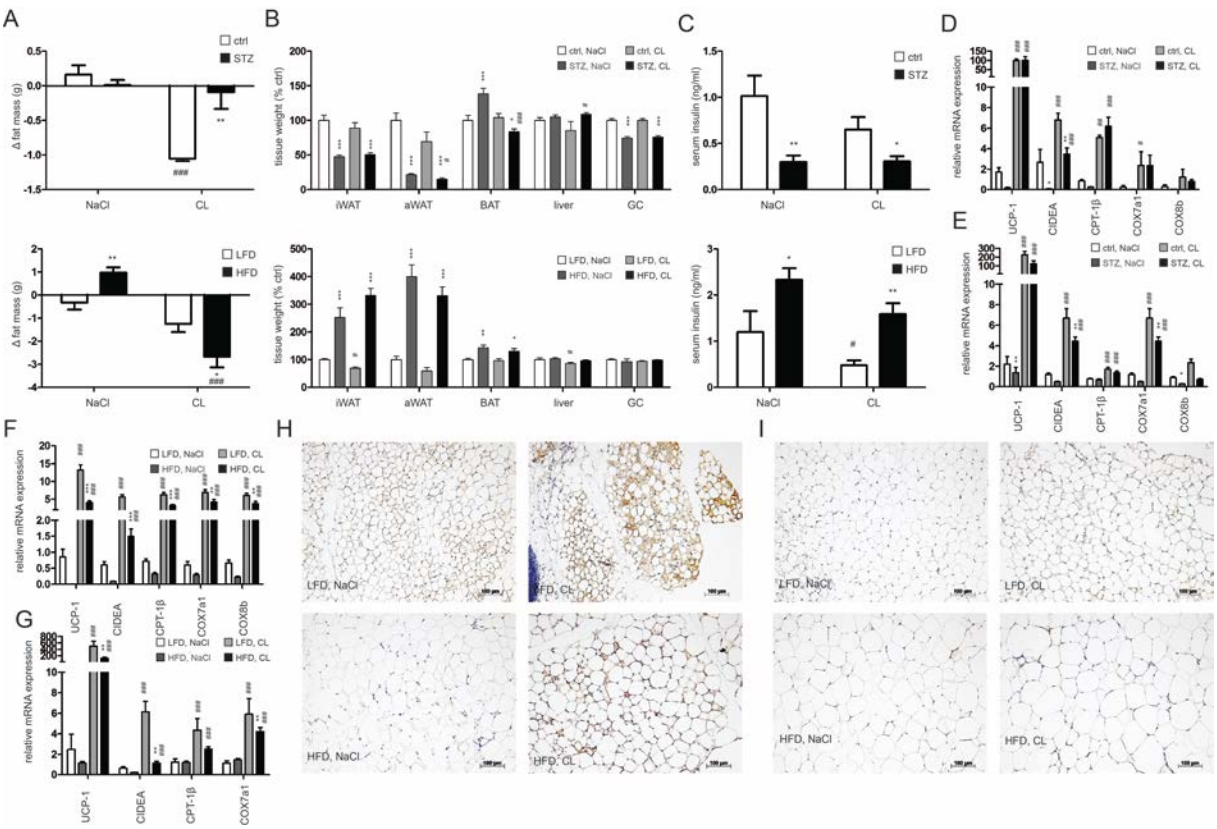

Figure 13. *CL mediated browning occurs largely independant from insulin signalling status. (A) ECHO-MRI body composition analysis, change in fat mass in STZ-injected and control (upper panel) or LFD and HFD-fed (lower panel) mice during the 10 days of CL or control treatment. (B) Tissue weights of iWAT, aWAT, BAT, liver and gastrocnemius skeletal muscle (GC) and (C) random fed serum insulin levels of STZ-injected and control (upper panel) or LFD and HFD-fed (lower panel) mice treated with CL or NaCl for 10 days. (D) mRNA expression of Ucp1, Cidea, Cpt1b, Cox7a1, Cox8 in iWAT and (E) aWAT of STZ-injected and control mice or (F) iWAT and (G) aWAT of LFD and HFD-fed mice treated with CL or NaCl for 10 days. (H) UCP-1 stained iWAT and (I) aWAT slices of mice fed LFD or HFD mice treated with CL or NaCl for 10 days. All values are expressed as means ± SEM, n = 7-10, #p<0.05, ##p<0.01, ###p<0.001 white (NaCL-treatment) vs. brite (CL-treatment), *p<0.05, **p<0.01, ***p<0.001 control vs. STZ and LFD vs. HFD-fed animals.*

Altogether, these findings indicate that while unstimulated WAT depots display lower brite marker expression as a result of aberrant insulin signalling status, β3-adrenergic stimulation still could efficiently induce the browning program. Even if a slightly compromised brite end-state apparently was achieved in the disease models, it is still obvious that recruitment of UCP-1 positive adipocytes within WAT depots can efficiently take place independently of insulin signalling.

Browning of white adipose tissue increases systemic glucose clearance in an insulin-independent manner

After elucidating that the browning mechanism in WAT can take place largely independently of insulin, we prompted the converse question whether brite adipocytes and depots are more insulin sensitive than white. It is established that cold exposure increases glucose uptake of brown adipocytes [78, 110], therefore enhancing the number of UCP-1 positive adipocytes increases the mass of target tissue for stimuli enhancing glucose uptake. It was not clear however, whether brite adipocytes and tissue per se are more sensitive to insulin than white cells. Therefore, primary iWAT SVF-derived adipocyte progenitors were differentiated into white or brite adipocytes as described above and glucose uptake in response to increasing doses of insulin was determined. The cells, whose white or brite identity was confirmed based on their marker gene expression profile in comparison to white or brown primary adipocytes (Figure14.A), were treated for 20 minutes with 0 – 100 nM of insulin in the presence of the radiolabelled non-metabolisable glucose derivative ^{3}H-2-deoxyglucose (^{3}H-2DOG). Brite adipocytes incorporated markedly higher amounts of ^{3}H-2DOG even in the basal (not insulin-treated) state. Upon insulin treatment, ^{3}H-2DOG uptake increased in a dose dependant manner in both cell types (Figure14.B). However normalizing ^{3}H-2DOG uptake in response to any administered dose of insulin to the differential basal levels revealed that the fold increase in response to insulin was the same in brite as in white adipocytes (Figure14.C), indicating that both cell types are equally insulin sensitive. This was also confirmed by Western Blot analysis, detecting a comparable degree of insulin-induced AKT (Protein Kinase B) or GSK3β (Glycogen synthase kinase 3) beta phosphorylation in white or brite differentiated adipocytes (Figure14.D, E).

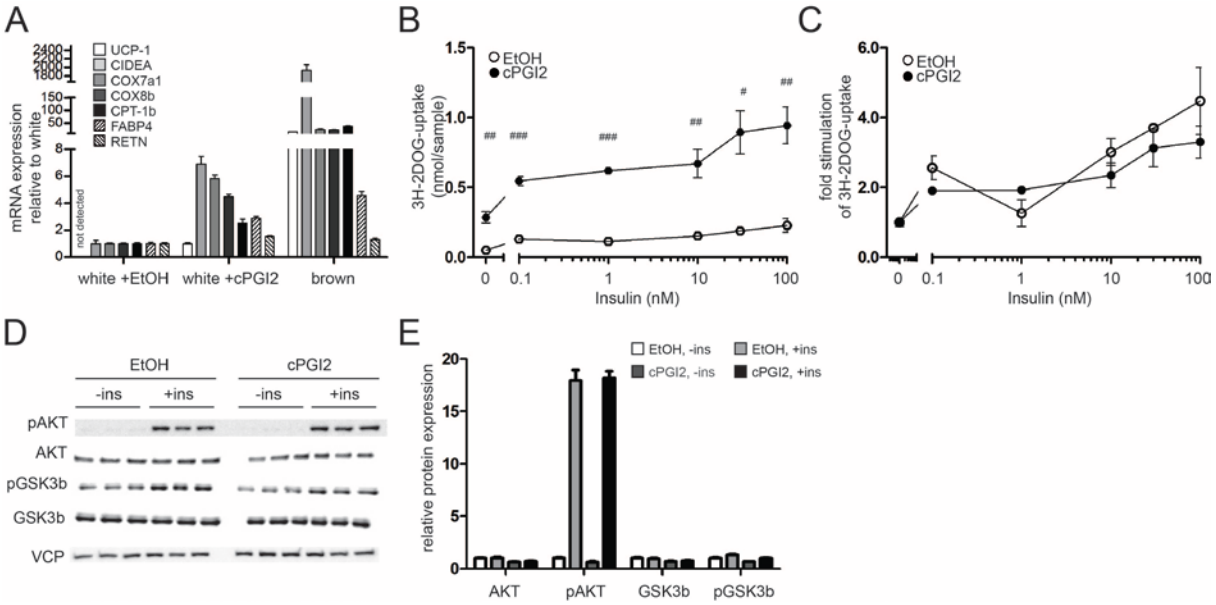

Figure 14. Brite adipocytes are not more insulin sensitive than white despite elevated glucose uptake*. (A) mRNA expression of Ucp1, Cidea, Cpt1b, Cox7a1, Cox8, Fabp4, Retn in primary iWAT SVF-derived adipocyte progenitors differentiated into white (EtOH-treated) or brite (cPGI2-treated) adipocytes or in primary BAT SVF-derived adipocyte progenitors differentiated into adipocytes. Values are shown as relative to expression in white adipocytes, except for Ucp1 which was not detectable in white adipocytes and is expressed as relative to levels in brite adipocytes. (B, C) ^{3}H-2-deoxy-D-glucose (^{3}H-2DOG) uptake by primary iWAT SVF-derived adipocytes (B) absolute or (C) relative to unstimulated basal uptake. Cells stimulated with different doses of Insulin for 20 minutes. (D) Western Blot and (E) corresponding quantification with imageJ (relative to VCP) of iWAT SVF-derived primary adipocyte progenitors differentiated into white (EtOH-treated) or brite (cPGI2-treated) adipocytes and stimulated with 100 nM insulin (ins) for 15 minutes. All values are expressed as means ± SEM, n = 5–15 animals for cell isolation #p<0.05, ##p<0.01, ###p<0.001 white (EtOH-treated) vs. brite (cPGI$_2$ -treated).*

To confirm our results on glucose uptake in an in vivo setting, we induced brite recruitment in female BL6 mice by CL administration via subcutaneous implantation of osmotic pumps as described above. As seen in previous experiments, indicators of CL-induced elevated metabolism could be observed, such as markedly reduced weight gain (Figure15.A), reduced body fat mass (Figure15.B) and WAT weight (Figure15.C) as well as lowered blood glucose levels (Figure15.D) in CL-treated mice (no gene expression analysis could be performed in this experiment due to the radioactive nature of the assay performed and described below). In these animals, we performed an intraperitoneal insulin tolerance test (ITT). The lowered blood glucose level in CL-treated “brite recruited” animals compared to “white” animals was

maintained throughout the assay both in basal and in insulin stimulated conditions (Figure15.E). Normalizing blood glucose levels to non-insulin-treated levels revealed that the relative decrease in blood glucose in response to insulin was comparable between the white and the brite group (Figure15.F). Next, glucose uptake into various tissues was assessed. The enrichment of the ^{3}H-2DOG tracer in blood did not differ between groups, confirming that differences in total blood glucose levels did not dilute the tracer, thus allowing comparison of amounts of tracer incorporated into tissues between groups (Figure15.G). Gererally, both insulin and CL affected tissue glucose uptake as expected, with insulin treatment increasing uptake into WAT and heart and CL-induced browning increasing uptake into WAT, regardless of insulin (Figure15.H). The overall contribution of each depot to systemic glucose utilization per mouse was calculated from the respective uptake rate and weight of each tissue. In the white state, iWAT and aWAT roughly utilize only a third of the amount of glucose taken up by BAT, despite its higher mass. In the brite state, the amount of whole-body glucose uptake attributable to WAT increases to the level contributed by the heart and almost to the level contributed by BAT when treated with insulin (Figure15.J). Notably, while total ^{3}H-2DOG uptake into WAT was substantially elevated upon browning, the relative fold increase glucose uptake as an effect of insulin stimulation did not differ between the two groups (Figure15.I). In summary, our data show that brite recruitment in WAT increases systemic clearance of glucose from the bloodstream. However, the effect could not be attributed to improved insulin sensitivity of adipose tissue after browning.

Browning of white adipose tissue induces GLUT-1 expression

To address the mechanism of the elevated glucose uptake of white adipocytes induced by browning, after ruling out enhanced insulin sensitivity, and upon the observation that glycolysis genes were not differentially regulated (data not shown), insulin-independent glucose-transport via glucose transporter 1 (GLUT-1) was examined. In primary iWAT SVF-derived adipocyte progenitors differentiated into white (EtOH-treated) or brite (cPGI$_2$-treated) adipocytes, browning induced slightly elevated mRNA (Figure16.A) and markedly elevated protein levels (Figure16.B, C) of GLUT-1. To address the physiological relevance of GLUT-1 induction, female BL6 mice were exposed to cold (5 °C). Induction of the thermogenic program was confirmed by elevated UCP-1 levels (Figure16.D), and analogously to in vitro experiments, browning induced strong upregulation of GLUT-1 protein levels (Figure16.D, E). To validate this observation in an independent in vivo setting, we tested GLUT-1 induction upon browning induced by chronical CL-treatment. Whereas Glut-1 mRNA levels were not substantially affected by CL (Figure16.F), immunohistochemical analysis revealed that

multilocular adipocytes arising upon CL-induced browning were GLUT-1 positive, whereas white cells displayed hardly any detectable GLUT-1 staining (Figure16.G).

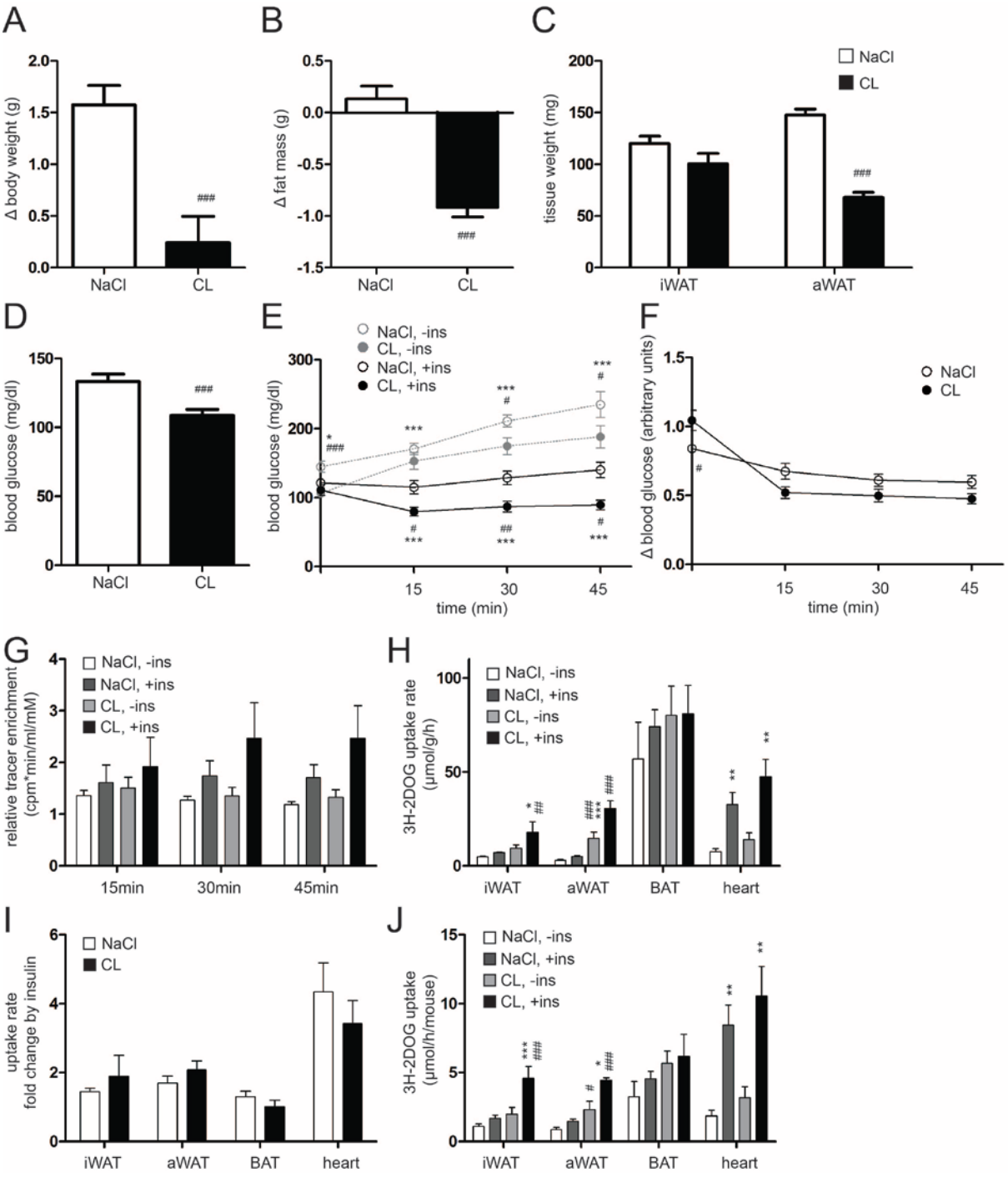

Figure 15. Browning of WAT increases systemic glucose clearance without being attributable to higher insulin sensitivity. *(figure legend continued on next page)*

Figure 15. Browning of WAT increases systemic glucose clearance without being attributable to higher insulin sensitivity. *(figure legend continued from previous page)*

*(A) Change in body weight and (B) fat mass of mice during the 10 days of CL or control treatment. (C) iWAT and aWAT weights at time of sacrifice. (D) Basal blood glucose values upon 10 days of CL or control treatment. (E, F) Intraperitoneal insulin (Ins) tolerance test (ITT) (0.5 U/kg body weight insulin) of mice treated with CL or control for 10 days. (E) Absolute blood glucose levels and (F) levels relative to non-insulin-stimulated are shown. (G) Relative enrichment of the ^{3}H-2-deoxy-D-glucose (^{3}H-2DOG) tracer in blood of mice treated with CL or control for 10 days, over the 45 minutes course of the experiment. (H, I) ^{3}H-2DOG uptake rate into iWAT, aWAT, BAT and heart of the same mice as in A-G. (H) Absolute uptake and (I) uptake relative to non-insulin-stimulated conditions is shown. Uptake rates were measured 45 minutes after intraperitoneal injection of insulin or vehicle. (J) Total ^{3}H-2DOG uptake by each tissue of the mice shown in (F), calculated from the ^{3}H-2DOG uptake rate and from the weight of each tissue. All values are expressed as means ± SEM, n = 6, #p<0.05, ##p<0.01, ###p<0.001 white (NaCL-treatment) vs. brite (CL-treatment), *p<0.05, **p<0.01, ***p<0.001 basal vs. insulin stimulation.*

To demonstrate that the observed increase of GLUT-1 expression is insulin-independent, GLUT-1 induction was investigated in the pathological setting of insulin deficiency caused by β-cell ablation as described above. Consistent with our finding that functional browning occurs despite lack of insulin in the STZ mouse model (Figure13.C upper panel, D, E), we found GLUT-1 protein to be significantly elevated upon CL administration in iWAT of STZ-treated mice (Figure16.H, I).

To functionally validate the role of GLUT-1 in browning-stimulated glucose uptake, GLUT-1-dependent ^{3}H-2DOG uptake by adipocytes was blocked with the specific inhibitor STF-31. GLUT-1 inhibition significantly decreased basal glucose uptake in white adipocytes (Figure16.J). Expectedly, insulin-stimulated glucose uptake was still functional with chemical inhibition of GLUT-1. Notably, also browning almost fully rescued the decrease in ^{3}H-2DOG uptake by GLUT-1 inhibition (Figure16.J), indicating that compensatory mechanisms control elevated glucose uptake during browning in the absence of GLUT-1 activity.

In summary, our data indicate that browning is accompanied by augmentation of GLUT-1 expression, thereby increasing glucose uptake into adipose tissue in an insulin-independent manner. Nevertheless, given that browning was able to compensate for the impaired glucose uptake caused by specific GLUT-1 inhibition, GLUT-1 induction only partially explains the enhanced glucose uptake of brite compared to white adipocytes.

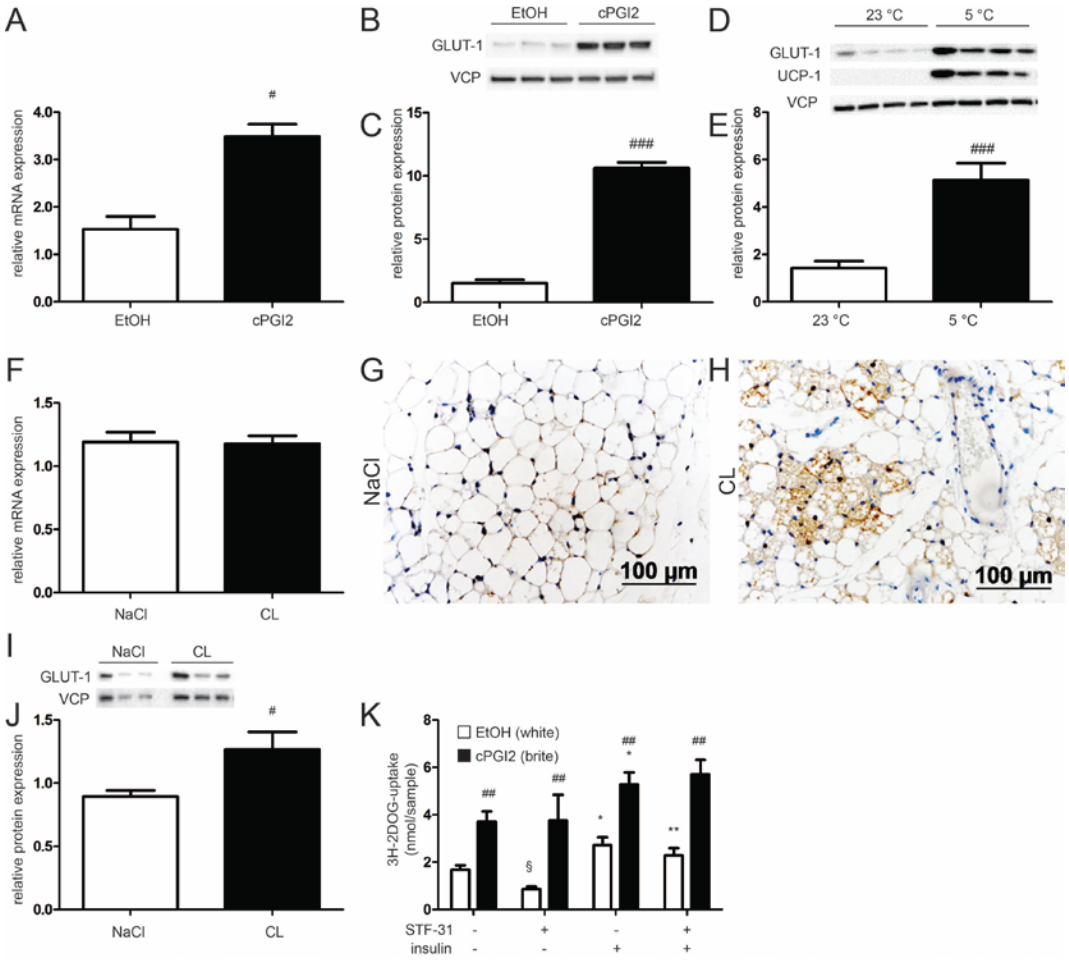

Figure 16. Browning induces GLUT-1 expression which only partially explains elevated glucose uptake. *(A) mRNA expression, (B) Western Blot analysis and (C) corresponding imageJ quantification (relative to VCP) of GLUT-1 in primary iWAT SVF-derived adipocyte progenitors differentiated into white (EtOH-treated) or brite (cPGI$_2$ treated) adipocytes. (D) Representative Western Blot and (E) imageJ quantification (relative to VCP) of GLUT-1 from iWAT of mice housed at 23 °C and 5 °C respectively for 10 days. (F) mRNA expression and (G) immunohistochemic staining of GLUT-1 in iWAT of mice fed LFD upon 10 days of CL or control treatment. (H) Representative immunoblot and (I) imageJ quantification (relative to VCP) of GLUT-1 from iWAT of STZ-injected upon 10 days of CL or control treatment. (J) ^{3}H-2DOG uptake by primary iWAT SVF-derived adipocyte progenitors differentiated into white (EtOH-treated) or brite (cPGI$_2$ treated) adipocytes, ± GLUT-1 inhibitor STF-31 for the last 2 days and stimulated ± 20 nM Insulin for 20 minutes. All values are expressed as means ± SEM, n = 6-10 for in vivo experiments and 10–12 animals for cell isolation, #p<0.05, ##p<0.01, ###p<0.001 white (EtOH treatment in cells, NaCL-treatment or housing at room temperature in mice) vs. brite (cPGI$_2$ treatment in cells, CL-treatment or housing at 5 °C in mice), *p<0.05, **p<0.01, ***p<0.001 basal vs. insulin stimulation, §p<0.05, §§p<0.01, §§§p<0.001 vehicle vs STF-31.*

BROWN ADIPOSE TISSUE IS ONE OF THE CHECKPOINTS FOR THE METABOLIC MASTER-REGULATOR TBLR

Another focus of this project, besides the data presented on the interplay between insulin signalling and white adipose tissue browning, was to untangle what specific role the metabolic master-regulator Transducin (beta)-like 1 X-linked Receptor 1 (TBL1XR1, or also TBLR) plays in brown adipose tissue (BAT) and how this local signal impacts metabolism systemically. Based on its known role in regulating liver [140] and general adipose tissue [139] we hypothesised in BAT, which has very unique functions in contrast to white adipose (WAT) or other tissues, such a regulator would assume distinct tissue-specific roles. To this point we not only studied the role of TBLR in mouse BAT under diverse metabolic challenges, but also employed in vitro and in vivo methods depleting brown adipocytes from TBLR to elucidate its physiological relevance.

TBLR localises to the nucleus in vitro, but to the cytosol in vivo

In the initial phase of our investigations we tested different antibodies to assure that subsequently retained results would be reliable. We did so by generating nuclear and cytosolic lysates of BAT and of differentiated preBAT cells (brown adipocyte progenitors immortalized by SV40 T infection [148] , which were used for all in vitro studies unless indicated otherwise). When incubating fractionated BAT lysates that were either wildtype or deficient of TBLR with the commercial antibodies NB600-270 (Novus), ab24550 (Abcam) or with 1:5 diluted antisera produced by immunizing rabbits with TBLR peptide (done by Pineda) it became apparent that only one of these was suitable to specifically detect TBLR. Antiserum detected a large number of unspecific proteins and ab24550 (Abcam), despite detecting only a small number of proteins, was unable to distinguish between control and knockout (KO) samples (Figure 17.A). Hence both of these antibodies were excluded from former studies. NB600-270 however was able to detect specifically a 50 kDa protein that was absent in TBLR KO BAT (Figure 17.A), therefore this protein was assumed to be TBLR and this antibody was used in all subsequent experiments. Detecting the cytosolic marker protein glycerinaldehyd-3-phosphat-dehydrogenase (GAPDH) and the nuclear marker poly-[ADP-Ribose]-polymerase 1 (PARP1) confirmed successful fractionation of BAT to nuclear and cytosolic lysates, respectively (Figure 17.A). Interestingly, despite being known to be a nuclear receptor co-regulator, we detected TBLR at stronger levels in the cytosol than in nuclei. There was an approximately 70 kDa band detected in the nuclei that seemed to be

present at lower levels in BATKO animals (Figure 17.A). It cannot be excluded that this presents a modified nuclear form of TBLR, despite the fact that phosphatase treatment of TBLR immunuprecipitated from nuclear and cytosolic extracts of wildtype mice did not affect the size of the detected nuclear band (Figure 17.B). Also, CL injection to the animals 2, 4 or 8 hours before tissue collection did not cause any detectable shuttling or changing in band rations (data not shown).

In vitro however, TBLR localised to the nucleus as expected, the identity of the band being confirmed by comparing lysates of control cells to lysates from cells transfected with adenovirus expressing short hairpin RNAs (shRNAs) to knock down TBLR (AV_shTblr), its sequence homologue and interaction partner Transducin (beta)-like 1 X-linked (TBL1X, or also TBL) (AV_shTbl) or both, respectively (Figure 17.C). In cells deficient of TBL, TBLR could to some extent also been found in the cytosol (Figure 17.C). Overall we concluded that NB600-270 is a suitable antibody for TBLR detection in brown fat and that TBLR localises to the nucleus in cells, however to the cytosol in tissue.

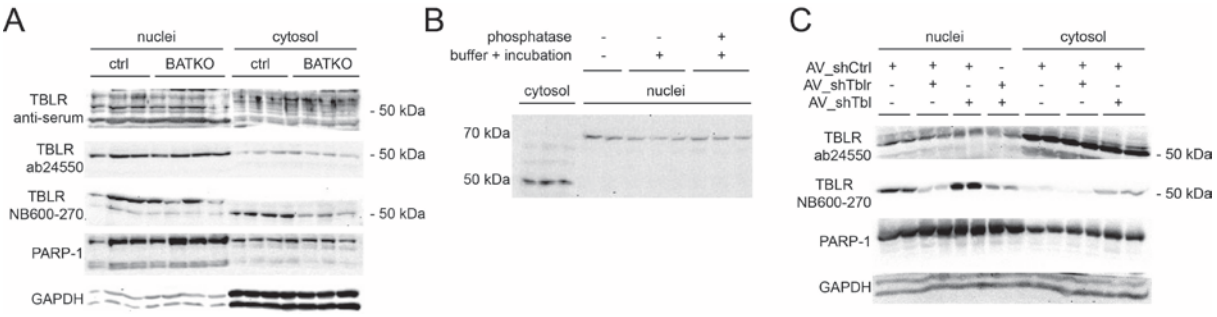

Figure 17. TBLR1 localises to the cytosol in BAT, but to the nucleus in preBAT cells. *(A) Western Blot analyses of cytosolic and nuclear lysates of BAT from Tblr1$^{fl/fl}$Ucp1Cre^{+} or Tblr1$^{fl/fl}$Ucp1Cre^{-} mice injected for 5 consecutive days with 2 mg/mouse/day of tamoxifen (BATKO and ctrl) and incubated with 1:5 diluted serum of rabbits immunized against TBLR, 1:1000 ab24550 (Abcam), 1:1000 NB600-270 (Novus) or antibodies against GAPDH or PARP1. (B) Western Blot analyses of TBLR (detection AB: NB600-270), immuno-precipitated (precipitation AB: NB600-270) from 40 µg nuclear and cytosolic lysates. Precipitate was on-bead treated with 100 units of Lambda Protein Phosphatase or control conditions without enzyme. (C) Western Blot analyses of cytosolic and nuclear lysates of preBAT cells infected with AV_shTblr, AV_shTbl or both and then differentiated for 7 days, incubated with NB600-270 or antibodies against PARP1.*

Tblr expression in BAT is inducible in vitro

To understand its role in brown adipose cells or tissues we next asked the question whether *Tblr* is regulated, and if so, by which pathways. We approached this question first by bioinformatic data already available. Since more experimental annotation data was available for the human sequence of *Tblr*, we chose to display the human sequence, however the identified regulatory regions are conserved in mouse.

Displaying *Tblr* in the UCSC genome browser [149] we first identified a 10 kB region (chr3:176,911,000-176,921,000) with high GC content, which is often indicative of a promoter region since it allows regulation of gene expression via DNA methylation (Hartl, Jones (2005). ISBN 0-7637-1511-5) (Figure 18.A, upper panel shows the whole gene sequence, the peak is highlighted with a blue box and shown in larger view in the lower panel). We then enabled further information on this sequence to be displayed and assuming that DNAse sensitive, interspecies conserved regions with active chromatin [150] were important in its regulation, we identified one major peak (at the transcription start site) and two minor peaks (upstream, intronic) to possess the properties of active chromatin (Figure 18.B, upper panel, the three peaks are highlighted with a blue, red and green box, respectively, and shown in larger view in the lower panels). The track “Transcription Factor ChIP-seq” (161 factors, from ENCODE with Factorbook [151, 152] was activated to display transcription factors (TFs) binding this region (darkness of bars corresponds to TF binding signal intensity) (Figure 18.B).

The set of transcription factors binding the active regions around the *Tblr* gene were compared to hits predicted by other bioinformatics tools, such as generegulator.com or rVISTA (http://rvista.dcode.org). The strongest open chromatin peak is bound by RNA polymerase, confirming it to be the transcription start site (Figure 18.A). Overall, growth promoting factors were the most prominent binding factors, such as E2F, MAX, MYC and AP-1 / AP-2 associated proteins (FOS, JUN, basic leucine zipper transcription factor (BATF)) [153], (Figure 18.A). E2F is known to regulate expansion versus differentiation in early adipogenesis [154-156], and MYC / FOS / JUN have been suggested to play a role in the MAPK pathway [157-159]. However, also RUNX3, a known tumor-suppressor [160], is reported to bind to the *Tblr* promoter region, suggesting the possibility of tissue- or stage-dependent differences in the role of TBLR for growth and differentiation.

Further, factors known to regulate early adipogenesis, such as the forkhead box A1 (FOXA1) interactor GATA binding protein 3 (GATA3) [161], C/EBPβ and E1A binding protein p300

((E)p300) [162] as well as the adipose regulator forkhead box A2 (FOXA2) [163] were standing out (Figure 18.A). Finally, a TF who is associated with type II diabetes risk if mutated, TCF7L2, strongly bound the *Tblr* promotor [164] (Figure 18.A). Overall, based on our predictions a metabolic role of TBLR, possibly by equilibrating growth versus differentiation, seemed likely.

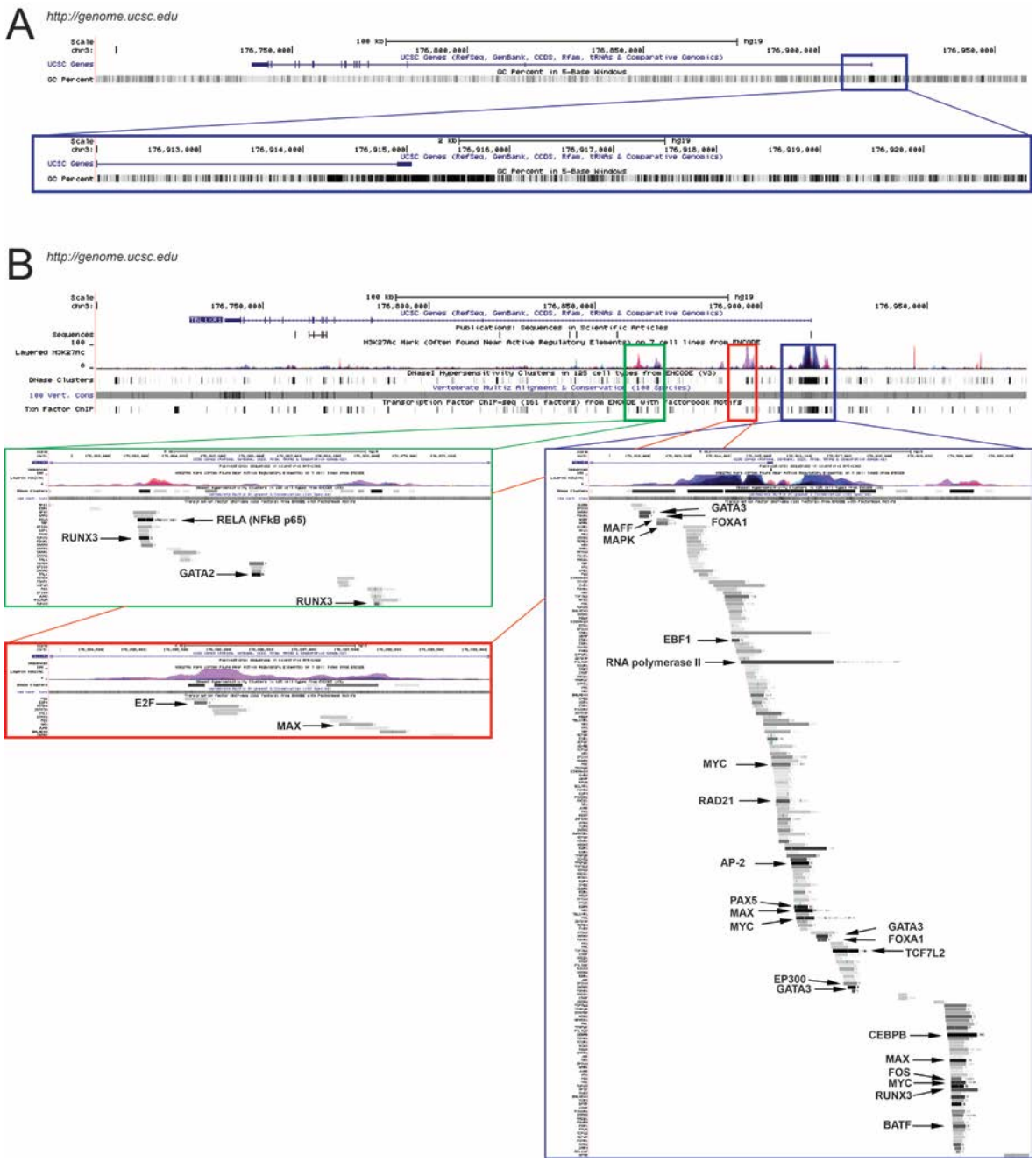

Figure 18. The transcription start site of TBLR is a region of active chromatin regulated by growth and adipogenesis involved transcription factors. *(figure legend continued on next page)*

Figure 18. The transcription start site of TBLR is a region of active chromatin regulated by growth and adipogenesis involved transcription factors. *(figure legend continued from previous page)*

(A) UCSC genome browser view of the human Tblr1x1 gene and regions with high GC content (upper panel). The region highest in GC content is highlighted with a blue box and shown in larger magnification in the lower panel. (B) UCSC genome browser view of the human Tblr1x1 gene aligned with experimental information (upper panel). Shown are sites protected from DNAse digest, conserved between species, comprised of active chromatin in terms of histone modification and bound by transcription factors. The three most active regions are highlighted with a blue, red and green box, respectively and shown in larger magnification in the lower panel, alongside with more detailed information about transcription factor binding data for this region.

Having characterized the *Tblr* promoter region we were interested in its relevance in brown adipocytes. TBLR shares 90% sequence homology with its homologue TBL [128], and while in liver both proteins are required for the transcription of fatty acid oxidation genes [140], in white adipose tissue the absence of TBLR alone is sufficient to cause deregulated metabolism [139]. To compare their roles in brown adipocytes, the expression levels of *Tblr* and *Tbl* were compared both in primary iWAT or BAT SVF-derived adipocyte progenitors and differentiated white, brite or brown adipocytes (as described above). The data is based on microarray analysis with Affymetrix chips and was kindly provided by Alexandros Vegiopoulos. *Tblr* was expressed at lower levels than *Tbl* both in white and in brown adipocyte progenitors, however only *Tblr* but not *Tbl* was higher in brown compared to white cells, indicating a brown-selective role (Figure 19.A). Further, while both mRNA (Figure 19.B) and protein (Figure 19.C) levels of TBLR were slightly but significantly induced during brown adipocyte differentiation, and even stronger during white or brite adipocyte differentiation (Figure 19.D), *Tbl* mRNA decreased both in brown and white or brite differentiating adipocytes (Figure 19.E, F), resulting in final levels of *Tbl* not being elevated anymore over those of *Tblr* (Figure 19.G). We hypothesised that the induction of *Tblr* during differentiation might depend on glucocorticoid signalling as a direct result of the dexamethasone (Dex) present in the medium in the 24 hours following induction of differentiation, and indeed, treatment of mature preBAT adipocytes with Dex lead to elevated *Tblr* mRNA expression (Figure 19.H). However, mice deficient for the glucocorticoid receptor (GR), did not show differential levels of *Tblr* mRNA expression (data not shown). These data show that *Tblr*, but not its homologue *Tbl*, is induced during adipocyte differentiation and is present in higher levels in brown adipocyte progenitors than in white.

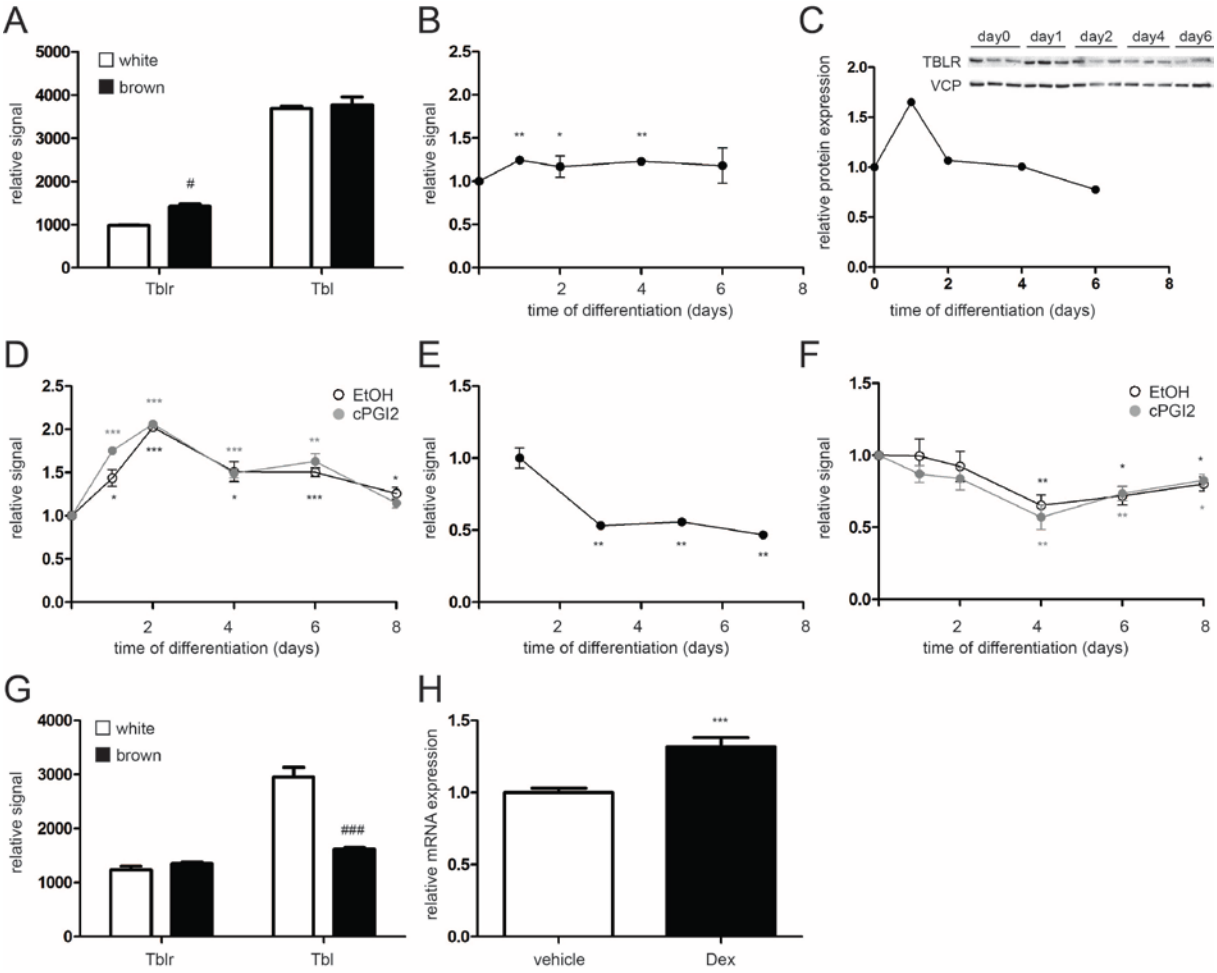

Figure 19. Tblr mRNA expression is induced upon initiation of adipogenic differentiation. *(A) Affymetrix expression signal of Tblr and Tbl in iWAT or BAT SVF-derived adipocyte progenitors at the time of induction of adipogenic differentiation or (G) at day 8 of adipogenic differentiation. (B) Affymetrix expression signal of Tblr during the time of brown adipogenic differentiation. (C) Western Blot analyses (upper panel) and imageJ quantification (lower panel) of TBLR during the time of brown adipogenic differentiation. (D) Affymetrix expression signal of Tblr in primary iWAT SVF-derived adipocyte progenitors differentiated into white (EtOH-treated) or brite ($cPGI_2$ treated) adipocytes. (E) Affymetrix expression signal of Tbl in primary BAR or (F) iWAT SVF-derived adipocyte progenitors differentiated into adipocytes. (H) mRNA expression of Tblr in differentiated preBAT adipocytes treated for 3 hours with 5 µM dexamethasone (Dex). All values are expressed as means ± SEM, n = 3 technical replicates, *p<0.05, **p<0.01, ***p<0.001 day 0 vs. different times (A) or ctrl vs. Dex (E), #p<0.05, ##p<0.01, ###p<0.001 white vs brown*

Besides factors involved in adipogenic differentiation, also MAPK pathway components are predicted regulators of *Tblr*. Since the activation of brown fat by β-adrenergic stimulation leads to PKA-mediated stimulation of the MAPK pathway [88] we hypothesised that in this cell type *Tblr* expression might depend on PKA-MAPK signalling and might be inducible by β-adrenergic stimuli. While treatment of differentiated preBAT cells with the β-adrenergic agonist CL316243 (CL) did induce a time-dependent elevation of *Ucp1* mRNA as expected, *Tblr* mRNA was significantly, but only slightly induced (Figure 20.A), which was not visible on protein level during the short time period of observation (Figure 20.B). However since this weak induction could be consistently observed in our studies with primary BAT-derived adipocytes (data not shown), we assumed that the cell culture medium might contain factors blocking the induction of *Tblr* expression through CL. When cultured in serum- and glucose-free Krebs-Ringer Buffer (KRB), treatment with insulin lowered *Tblr* expression (Figure 20.C), and indeed, when applying CL in KRB instead of medium it did induce *Tblr* expression in differentiated preBAT cells (Figure 20.D). To further prove that this activation is dependent on PKA signalling we applied the PKA inhibitor H-89, which efficiently blocked the CL-induced induction of *Tblr* (Figure 20.E).

These data indicate that *Tblr* expression is induced in the initial phase of adipocyte differentiation and is also regulated in mature brown adipocytes. Insulin blunted and β-adrenergic stimulation-induced *Tblr* expression, the signal being transmitted via the PKA-MAPK pathway and potentially being mediated via promoter region binding of transcription factors linked to this pathway.

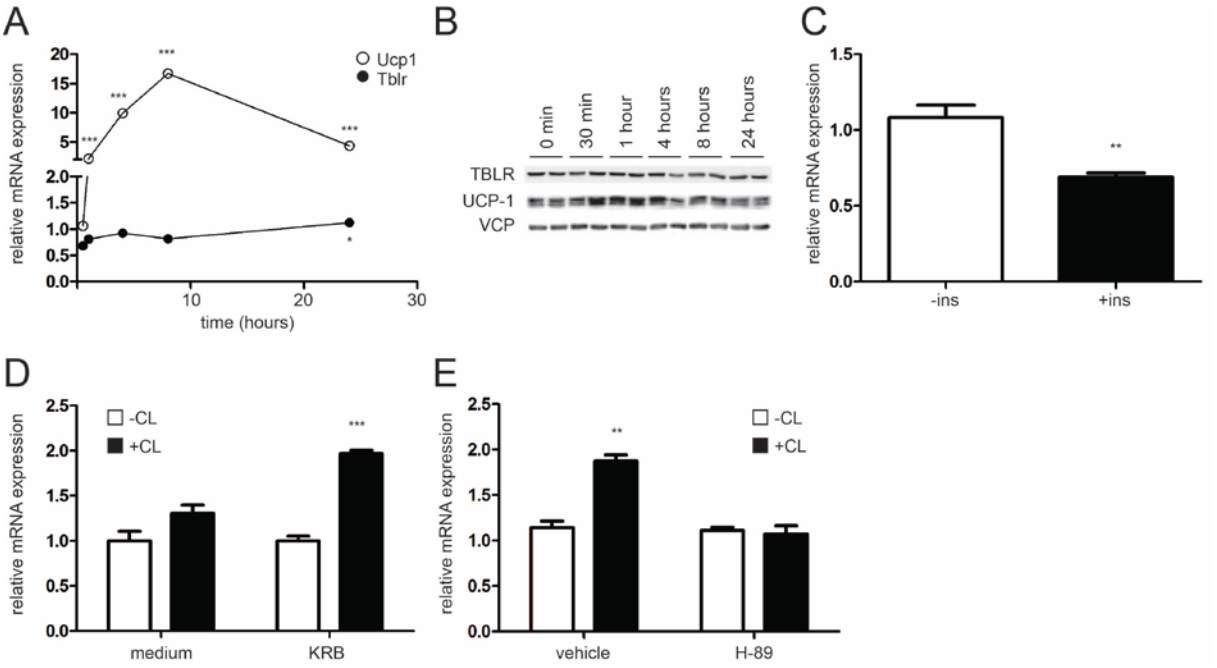

Figure 20. Tblr mRNA expression in adipocytes is induced by β-adrenergic induction of the PKA-MAPK pathway. *(A) mRNA and (B) protein expression of Tblr and Ucp1 in differentiated preBAT adipocytes in medium upon stimulation with 1 µM CL316243 (CL). (C) mRNA expression of Tblr in differentiated preBAT adipocytes upon 3 – 4 hours of treatment with 20 nM insulin (ins), (D) 1 µM CL or (E) 50 µM H-89, cultured in Krebs-Ringer buffer (KRB) unless stated otherwise. All values are expressed as means ± SEM, n = 3 technical replicates, *p<0.05, **p<0.01, ***p<0.001 ctrl vs. treatment.*

Tblr expression in BAT is inducible in vivo

We then posed the question whether *Tblr* expression is regulated in vivo, examining brown adipose tissue (BAT) gene expression under various conditions. The samples were obtained either from previous studies or from studies performed by colleagues (Dasa Medrikova, Jessica Fuhrmeister, Alexandros Vegiopoulos) or collaborators (Pavel Flachs, Jan Kopecky).

Since insulin was shown in vitro to blunt *Tblr* expression (Figure 20.C), we compared expression levels in fasted and refed mice (Figure 21.A) as well as in control and leptin receptor knockout (db/db) mice (Figure 21.B), and observed that in states known to induce high circulating insulin levels, *Tblr* expression was reduced. Interestingly, *Tblr* was up-regulated in BAT of HFD compared to LFD-fed mice (Figure 21.C). Analogously to our in vitro observations, CL stimulation in vivo strongly induced BAT *Tblr* expression. In mice treated for 10 days with daily injection of CL (Figure 21.D) or exposed to cold for 10 days

(Figure 21.E), *Tblr* expression was induced compared to animals injected with vehicle or housed at room temperature (22 °C), respectively. This was also true comparing cold exposed animals to animals housed at thermoneutrality (30 °C) and the regulation was shown to peak acutely upon exposure to the cold stimulus to then decline to relatively lower, but still elevated levels, and in this way behaved differently from *Ucp1*, whose levels continued to rise for an extended period (Figure 21.F). Analogously for the results shown above for adipogenic differentiation, also for acute *Tblr* induction in mature adipocytes we wanted to distinguish between *Tblr* and its homologue *Tbl*. We hypothesised that if *Tbl* is able to fully compensate for the function of *Tblr* in BAT, it should likewise be induced by β-adrenergic stimulation. However *Tbl* mRNA expression was only induced to a minor degree (Figure 21.F), which was also reflected in vitro (data not shown). Further, *Tbl* was not differentially expressed in BAT upon fasting or in db/db mice or in CL injected mice (data not shown).

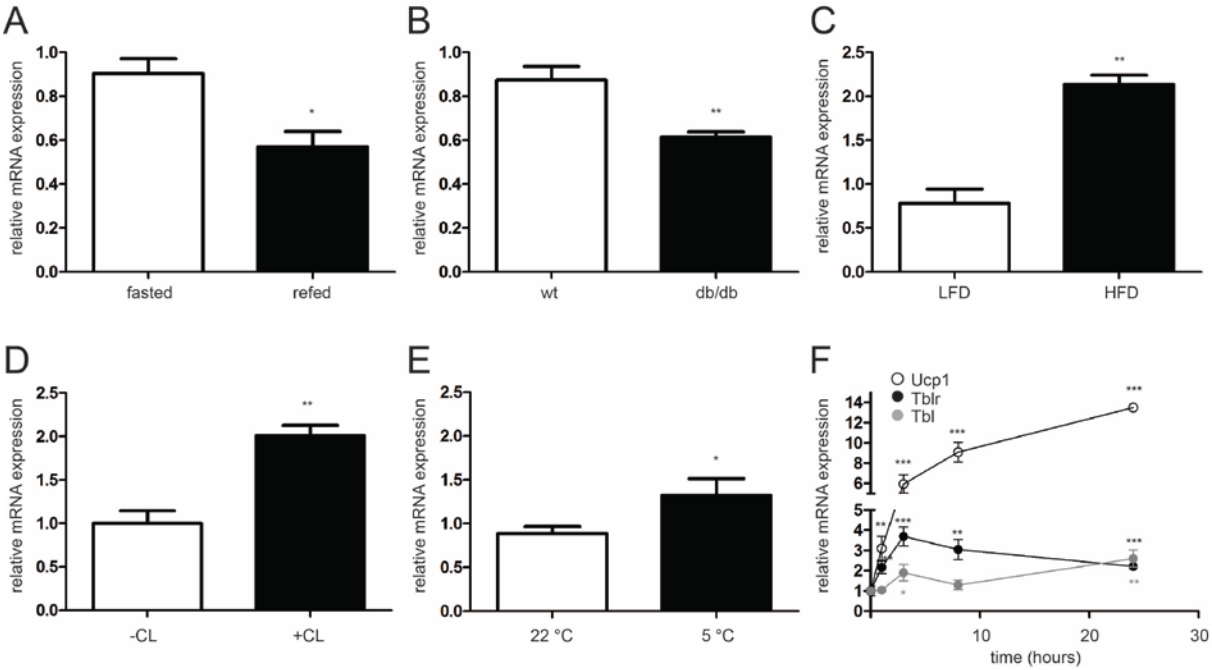

Figure 21 Tblr mRNA expression in BAT is transiently induced by β-adrenergic stimuli. *(A) Tblr mRNA expression in BAT of animals fasted for 24 hours or refed for 6 hours (n=4), (B) of random fed control and db/db animals (n=4), (C) of mice treated for 10 consecutive days with daily i.p. injection of or NaCl or 1 mg/kg body weight CL (n=7), (D) housed at room temperature or 4 °C for 10 days (n=7) or (E) acutely exposed to 4 °C (n=8). All values are expressed as means ± SEM, *p<0.05, **p<0.01, ***p<0.001 fasting vs. refeeding (A), ctrl vs. db/db (B), LFD vs. HFD (C), ctrl vs. CL (D), 22 °C vs. 4 °C (E) or 30 °C vs. 4 °C (F).*

Since the induction of *Tblr* mRNA expression was strongest immediately after stimulation (Figure 21.F) we chose to closer examine the exact site of regulation 8 hours following injection of CL. At this time *Tblr* was induced almost as strongly as *Ucp1* (Figure 22.A), which was not translated into elevated protein levels at this short time period (Figure 22.B). 8 hours after injection we dissected BAT and subjected it to collagenase digestion to fractionate it into (floating) mature adipocyte fraction (AF) and (pelleting) stromal vascular fraction (SVF), containing undifferentiated adipocyte progenitors. We confirmed by qPCR that SVF was enriched in the pre-adipocyte marker *Cd31* (Figure 22.C), while the AF was enriched in the mature adipocyte marker β3-adrenoreceptor (*Adrb3*) (Figure 22.D). However the difference between fractions was only minor and it was found that SVF expressed *Ucp1*, which was further elevated in samples from CL- versus vehicle-treated animals (Figure 22.F). Since adipocyte progenitors do not express the β3-adrenoreceptor [78] and thus also do not react to CL-stimulation, we conclude that brown adipocytes, being lower in fat content than white and thus denser, partly pellet together with the SVF. Because of that no conclusive statement can be made about gene expression in pelleted cells, while floating cells still can be assumed to comprise the differentiated adipocyte fraction of BAT. We observed that AF from 8 hour CL-treated animals expressed strongly elevated mRNA levels of *Tblr* (Figure 22.E). Since TBLR was found to localise to the nucleus in vitro but to the cytoplasm in vivo (Figure 17.A and B) we were interested whether localisation of TBLR might be affected by CL-treatment in vivo. To these regards we injected mice with CL and dissected BAT after various timepoints and fractionated the tissue to cytosol and nuclei. We could detect no difference in the cytosolic to nuclear ratio of TBLR protein (Figure 22.G).

Taken together, we show that, in accordance with in vitro findings, in vivo *Tblr* expression is down-regulated in states with high circulating insulin and induced in a transient manner by β-adrenergic stimulation. This regulation seems to be a feature distinguishing *Tblr* from *Tbl* in BAT. This induction takes place in the mature adipocyte fraction of BAT and does not trigger shuttling of TBLR protein from the cytosol to the nucleus.

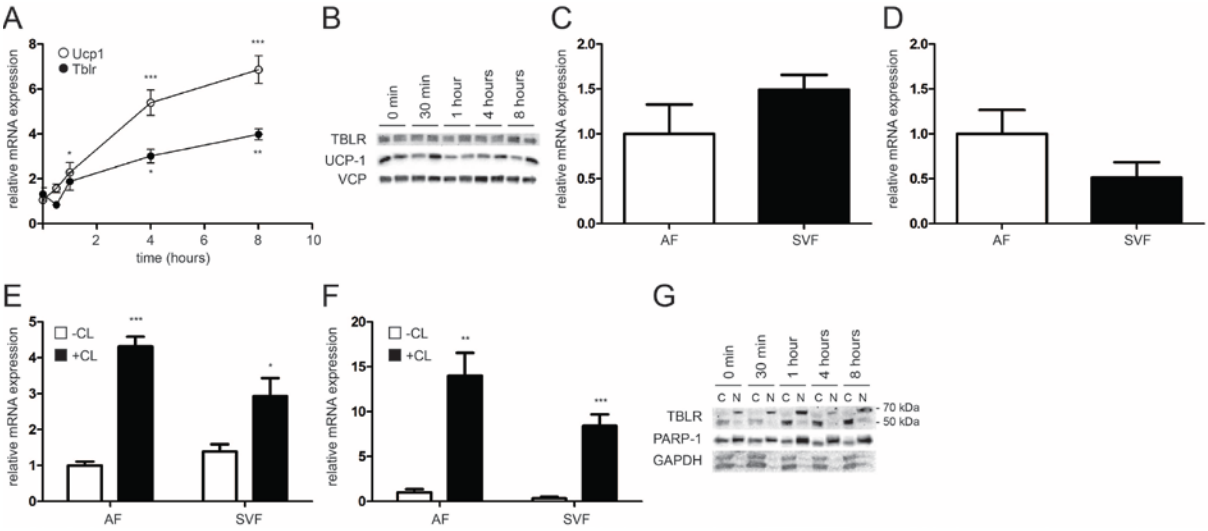

Figure 22. Tblr1 is induced by CL in mature adipocytes without inducing cytoplasmatic to nuclear shuttling. *(A) mRNA and (B) protein expression of Tblr and Ucp1 in BAT of mice injected intraperitoneally with 1 mg/kg BW CL and sacrificed at the indicated timepoints (n=3). (C) CD31 and (D) Adrb3 mRNA expression in the adipocyte fraction (AF) or stromal vascular fraction (SVF) of BAT of mice AF was separated from SVF by collagenase digest followed by centrifugation, the floating fraction being defined as AF, the pelleting cells as SVF (n=5). (E) Tblr and (F) Ucp1 mRNA expression in AF or SVF of BAT of mice injected with NaCl or CL 8 hours before sacrifice (n=5). (G) Western Blot analyses of cytosolic (C) and nuclear (N) lysates of BAT from mice injected with CL and sacrificed at the indicated timepoints (n=3). All values are expressed as means ± SEM, *p<0.05, **p<0.01, ***p<0.001 0 hours vs. indicated time (A), NaCl vs. CL (E, F)*

Tblr1 is involved in the adipogenic program and in mature adipocyte function

TBLR, as a nuclear receptor co-regulator, can bind to regulatory sequences of genes and influence their expression [128, 132]. Having observed that *Tblr* expression is regulated in brown fat upon pro-adipogenic and β3-adrenergic stimulatory conditions we were interested to study the gene expression programs controled by TBLR in brown adipocytes. We thus performed global analysis of TBLR binding to genomic DNA (chromatin immunoprecipitation followed by sequencing, ChIPseq). In order to distinguish between the roles of TBLR during the two states in which it was found to be transcriptionally regulated – upon induction of adipogenic differentiation or in mature adipocytes – analyses were performed preBAT cells harvested at two distinct timepoints, either 24 hours following induction of adipogenic differentiation or 7 days later in the fully differentiated state. First we checked the quality of the obtained material, i.e. chromatin crosslinked with bound proteins, by ChIP with PPAR γ

antibody. From the obtained bound genomic regions we amplified by qPCR positive and negative control sequences for PPAR γ binding [4]. Indeed, the positive control region ("2 kB") was clearly enriched over the negative control regions ("negative", "1 kB", "2.8 kB") (Figure 23.A), confirming sufficient material quality. We next performed ChIP with an antibody against TBLR and subjected the obtained DNA to sequencing after having confirmed by qPCR that TBLR bound to two genomic regions known to be involved in adipogenic differentiation, the Pparg2 promoter and caveolin 2 (Cav2) [4] (Figure 23.B). ChIPseq and data analyses were performed by our collaborator Anne Loft (Susanne Mandrup's lab, Department of Biochemistry and Molecular Biology, University of Southern Denmark).

Table 1 TBLR binds to genes associated with adipocyte differentiation and function.

Unbiased ranking by enrichment of all KEGG pathways with significantly enriched TBLR binding

during differentiation		
KEGG pathway	**p-value**	**fold enrichment**
mmu00062:Fatty acid elongation in mitochondria	5,39E-03	6,11
mmu04710:Circadian rhythm	3,64E-02	3,76
mmu01040:Biosynthesis of unsaturated fatty acids	4,31E-03	3,26
mmu00533:Keratan sulfate biosynthesis	5,90E-02	3,26
mmu05216:Thyroid cancer	6,94E-03	3,03
mmu04920:Adipocytokine signaling pathway	2,43E-05	2,92
mmu05221:Acute myeloid leukemia	1,22E-04	2,92
mmu05212:Pancreatic cancer	2,36E-04	2,58
mmu05210:Colorectal cancer	3,10E-04	2,39
mmu00280:Valine, leucine and isoleucine degradation	1,57E-02	2,34
mmu05220:Chronic myeloid leukemia	1,37E-03	2,32
mmu05213:Endometrial cancer	1,42E-02	2,26
mmu00071:Fatty acid metabolism	3,54E-02	2,17
mmu04910:Insulin signaling pathway	1,07E-04	2,13
in differentiated cells		
KEGG pathway	**p-value**	**fold enrichment**
mmu04621:NOD-like receptor signaling pathway	1,21E-03	10,28
mmu05220:Chronic myeloid leukemia	2,58E-03	8,39
mmu05215:Prostate cancer	4,76E-03	7,08
mmu04730:Long-term depression	1,74E-02	7,08
mmu03320:PPAR signaling pathway	2,22E-02	6,46
mmu04662:B cell receptor signaling pathway	2,29E-02	6,38
mmu05214:Glioma	8,59E-02	5,98
mmu04920:Adipocytokine signaling pathway	9,29E-02	5,71
mmu04660:T cell receptor signaling pathway	1,22E-02	5,40
mmu04620:Toll-like receptor signaling pathway	3,96E-02	5,15
mmu04910:Insulin signaling pathway	8,83E-02	3,70
mmu05200:Pathways in cancer	2,76E-03	3,55
mmu04062:Chemokine signaling pathway	4,96E-02	3,50
mmu04010:MAPK signaling pathway	5,06E-02	2,89

In general, more binding events were observed during the initial phase of differentiation than in differentiated adipocytes, indicating that coordination of the adipogenic program is one of the key functions of TBLR in brown adipocytes. Table 1 lists the results of KEGG pathway analyses performed on the set of genes found to be bound by TBLR (ranked by enrichment). In general, both during differentiation and in mature adipocytes, TBLR binding occurred within gene networks known to regulate growth (cancer) versus differentiation. Those pathways are highlighted in red. During differentiation of preBAT cells, TBLRbinding was enhanced at gene loci associated with pathways involved in adipocyte differentiation and lipid accumulation, such as fatty acid biosynthesis and elongation or adipocytokine and insulin signalling (highlighted in grey). In differentiated adipocytes, in addition to pathways involved in immunity, TBLR was found to bind to genes involved in mature adipocyte function, such as PPAR signalling or adipocytokine and insulin signalling (highlighted in grey).

To combine these data with functionality, i.e. to determine extent and direction of the regulation of the identified pathways, we performed global gene expression analyses of preBAT cells following adenoviral (AV)-mediated shRNA knockdown of *Tblr*. Since TBLR binding to genomic DNA was found to be more intense during adipogenic differentiation, we decided to knock down TBLR prior to induction of adipogenic differentiation, resulting in adipocytes that were deficient of TBLR during differentiation. We confirmed that in all the samples AV mediated KD of gene expression was strong and specific (Figure 23.C) and thus subjected RNA from these cells to microarray analyses. Sample handling and data analyses were performed by our collaborator Carsten Sticht (Medical Faculty, University Mannheim). Table 2 lists all significantly regulated KEGG pathways in preBAT cells transduced with shTblr compared to cells transducted with shCtrl, ranked by enrichment. In general pathways found to be regulated, in accordance with data obtained in ChIPseq analyses, were pathways associated with the balance between growth and differentiation. There was a shift from pro-growth to pro-differentiation in the absence of TBLR, the most strongly de-repressed pathways being the key metabolic pathways in adipocytes, oxidative phosphorylation and the citric acid cycle, while the most strongly depleted pathway involved cancer growth.

Table 2 TBLR KD leads to reduced growth-promoting signature and de-repression of metabolic pathways.

Unbiased ranking by enrichment of all KEGG pathways significantly regulated by TBLR KD. Pathways induced by TBLR (depleted in KD) are indicated in red, pathways repressed by TBLR (de-repressed in KD) are highlighted in green.

KEGG pathway	enrichment score	p-value
Oxidative phosphorylation	2,43	0,00E+00
Citrate cycle (TCA cycle)	2,25	0,00E+00
Pyruvate metabolism	2,14	0,00E+00
Parkinson's disease	2,11	0,00E+00
Propanoate metabolism	2,04	0,00E+00
Non-alcoholic fatty liver disease (NAFLD)	1,97	0,00E+00
Alzheimer's disease	1,91	0,00E+00
Huntington's disease	1,90	0,00E+00
Fatty acid degradation	1,89	0,00E+00
DNA replication	1,82	0,00E+00
Carbon metabolism	1,76	0,00E+00
2-Oxocarboxylic acid metabolism	1,72	4,09E-03
Ribosome	1,65	0,00E+00
Terpenoid backbone biosynthesis	1,55	4,93E-02
Glyoxylate and dicarboxylate metabolism	1,53	3,88E-02
Fatty acid metabolism	1,53	1,76E-02
Proteasome	1,51	3,45E-02
Fatty acid elongation	1,49	4,32E-02
PPAR signaling pathway	1,44	2,95E-02
Cytokine-cytokine receptor interaction	-1,39	8,90E-03
Leishmaniasis	-1,41	5,30E-02
Renin-angiotensin system	-1,42	7,38E-02
Salmonella infection	-1,42	3,70E-02
Glycosaminoglycan degradation	-1,42	6,76E-02
Complement and coagulation cascades	-1,43	1,97E-02
TNF signaling pathway	-1,45	1,95E-02
Chagas disease (American trypanosomiasis)	-1,46	1,14E-02
Amino sugar and nucleotide sugar metabolism	-1,46	3,48E-02
Hematopoietic cell lineage	-1,51	9,54E-03
p53 signaling pathway	-1,51	1,34E-02
Axon guidance	-1,55	1,89E-03
Rheumatoid arthritis	-1,56	3,68E-03
Malaria	-1,77	3,76E-03
MicroRNAs in cancer	-1,99	0,00E+00

Correlating the knowledge gained about TBLR binding and genes found to be de-regulated in TBLR-deficient cells, it was possible to identify some target genes found to be both, strongly bound and regulated by TBLR. Interestingly, the most outstanding candidate was *Ucp1*, being both the most strongly bound target gene in differentiated adipocytes and the most strongly de-repressed target upon TBLR knockdown. Further genes found to be repressed

by TBLR in differentiating adipocytes included players of differentiation, such as Ppargc1a or SMAD family member 6 (*Smad6*), proteins involved in fatty acid synthesis, such as acetyl-coenzyme A carboxylase (*Acc*) as well as regulators of mitochondrial energy metabolism, such as pyruvate dehydrogenase kinase (*Pdk4*), acetyl-Coenzyme A acyltransferase 2 (*Acaa2*), the glycerol transporter aquaporin7 (*Aqp7*) or the components of the repiratory chain, namely subunits of NADH dehydrogenase, cytochrome c oxidase and ATP synthase. On the other hand, mitogen-activated protein kinase (MAPK) pathway components such as mitogen-activated protein kinase kinase kinase kinase (*Map4k*), the jun proto-oncogene, dual specificity phosphatase 6 (*Dusp6*) or the TGF-beta activated kinase *Tab2* appeared to be activated by TBLR binding, since their expression was found to be decreased in KD cells.

The UCSC genome browser was used to visualize examples of genomic regions bound by TBLR. Figure 23 depicts binding to to *Ucp1* (Figure 23.D) and *Dusp6* (Figure 23.E) as compared to a non bound gene (DNA polymerase A1, *pola1*, (Figure 23.F)). Table 3 summerizes ChIPseq binding data (Tag counts per gene) correlated with microarray expression data (fold change by TBLR KD) to the genes mentioned above, Figure 23.F depicting the relative abundance of TBLR regulated genes in preBAT adipocytes.

Overall global analyses confirmed that *Tblr* is not only regulated in brown adipocytes, but also does participate in key metabolic pathways, mainly during adipogenesis and further in mature brown adipocytes. Surprisingly, despite being up-regulated during differentiation, TBLR in this phase seems to promote growth and suppress differentiation and development of brown mitochondria. In mature adipocytes, despite exhibiting lower overall binding behavior and not targeting respiratory chain players anymore, TBLR was found to target regulators of mature brown function, such as *Ucp1* and signalling proteins, indicating that TBLR can play different roles depending on the developmental state of the cells.

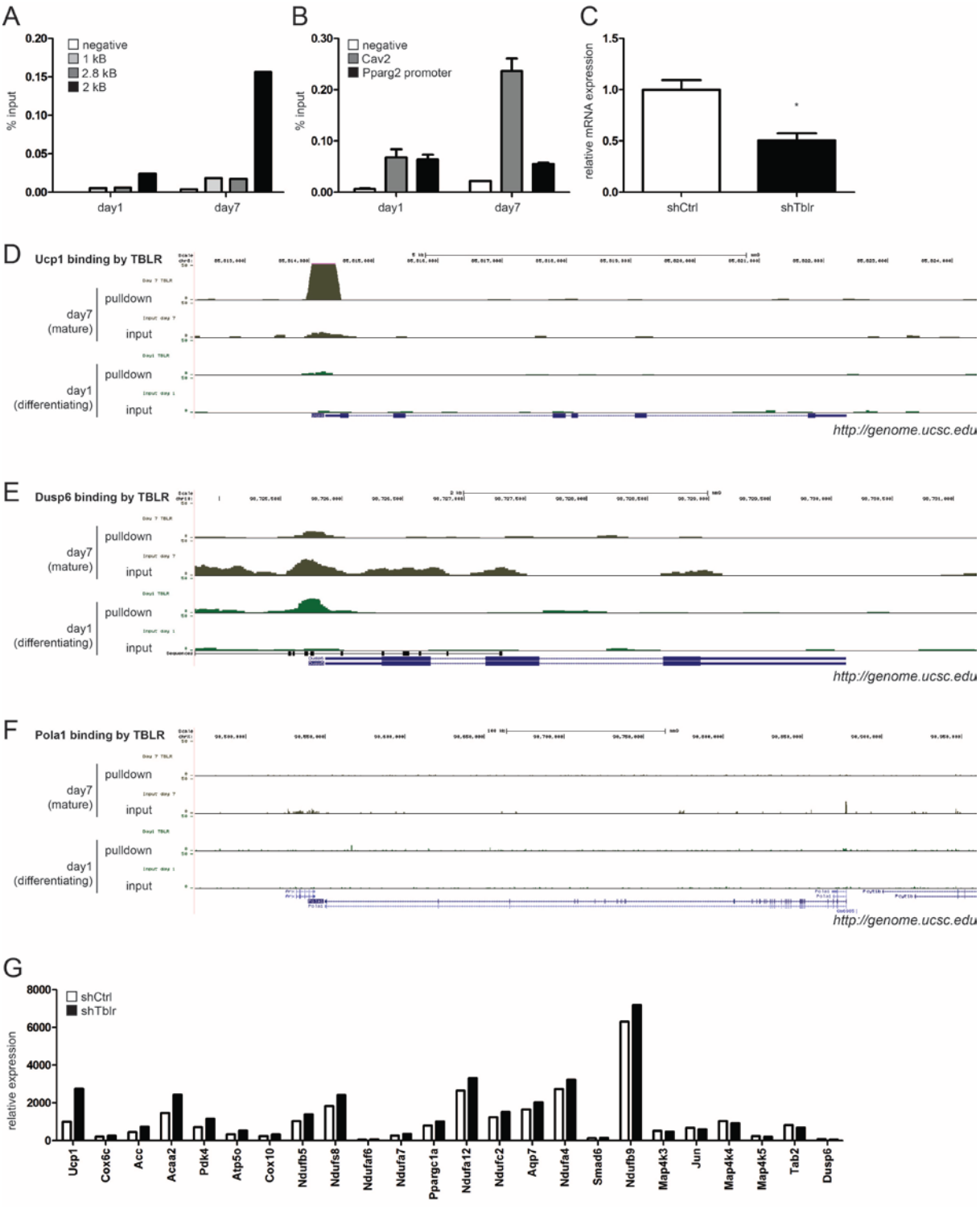

Figure 23. ChIPseq analysis of global TBLR binding and microarray analysis of global geneexpression in the basence of TBLR reveal its involvement in adipogenesis and brown adipocyte functions. *(figure legend continued on next page)*

Figure 23. ChIPseq analysis of global TBLR binding and microarray analysis of global geneexpression in the basence of TBLR reveal ist involvement in adipogenesis and brown adipocyte functions. *(figure legend continued from previous page)*

(A) qPCR amplification of genomic DNA pulled down by PPAR-γ antibody or (B) TBLR antibody from crosslinked chromatin of preBAT cells at day 1 or day 7 of adipogenic differentiation. Values are expressed as % input (chromatin before pulldown), the amplified targets are a general negative control sequence (negative), 2 negative control sequences for PPAR-γ binding (1 kB, 2.8 kB) and a PPAR- γ binding positive control sequence (2 kB) or positive control sequences frequently bound in adipogenic differentiation (Cav2, Pparg2 promoter). [4] (C) Tblr mRNA expression in differentiated preBAT cells transduced before the induction of adipogenic differentiation with AV expressing shCtrl or shTblr with a multiplicity of infection (MOI) of 50. (D-F) ChIPseq for TBLR binding in preBAT cells was performed on day1 and day7 respectively of adipogenic differentiation and results were visualised in the UCSC genome browser, comparing sequence abundance upon

Table 3. TBLR binding represses brown adipocyte metabolic genes and induces proliferative genes.

Ranking by fold-regulation of gene expression in TBLR KD. Genes induced by TBLR (depleted in KD) are indicated in red, genes repressed by TBLR (de-repressed in KD) are highlighted in green.

gene name	TAG count day 1	TAG count day 7	fold change in KD cells	p-value
Ucp1	56,84	446,46	2,74	6,14E-05
Cox6c	190,48	17,25	1,73	3,08E-04
Acc	49,16	47,18	1,64	4,60E-04
Acaa2	49,16	47,18	1,64	4,60E-04
Pdk4	190,48		1,61	2,99E-05
Atp5o	238,11		1,56	4,89E-04
Cox10	30,72		1,37	4,28E-04
Ndufb5	18,43		1,34	3,28E-04
Ndufs8	52,23		1,31	1,71E-03
Ndufaf6	13,83		1,31	2,04E-02
Ndufa7	35,33		1,30	2,56E-02
Ppargc1a	208,93	30,44	1,26	1,99E-02
Ndufa12	18,43		1,25	1,06E-02
Ndufc2	55,3		1,23	1,02E-02
Aqp7		8,62	1,22	2,91E-01
Ndufa4	104,46		1,18	3,74E-03
Smad6	302,62		1,17	2,15E-02
Ndufb9	24,58		1,14	6,91E-03
Map4k3	216,59		0,91	4,79E-02
Jun	89,09	26,38	0,90	1,84E-02
Map4k4	195,09	27,39	0,89	4,52E-02
Map4k5	76,81		0,86	4,87E-02
Tab2	139,8	24,85	0,83	3,98E-02
Dusp6	314,91	51,23	0,73	2,47E-02

Tblr1 ablation in vitro can distinguish between role during differentiation and role in mature adipocytes

Having discovered the regulation of *Tblr* in BAT and its action on gene expression by DNA binding, we continued to elucidate which role TBLR-mediated gene regulation would have on brown adipocytes. In order to investigate both the role TBLR is expected to play during the initial phase of adipogenesis as well as its role in mature adipocytes, we tested knockdown at two timepoints: 2 days prior to induction of adipogenic differentiation ("early KD") and 2 days prior to harvest of mature adipocytes ("late KD"), and in both cases the adipocytes were harvested on day 7 of adipogenic differentiation. We used the adenoviral vectors described above to ablate *Tblr/Tbl* gene expression and chose to use preBAT cells rather than primary BAT SVF-derived adipocyte progenitors for most of the experiments, since we found knock down of TBLR expression was more reproducible in this cell line. We found that upon early KD, mRNA levels of *Tblr* and *Tbl* were still reduced in mature preBAT adipocytes (Figure 24.A), the effect being much more pronounced at the protein level (Figure 24.B). Upon late KD, while mRNA levels were strongly reduced (Figure 24.C), protein levels were diminished but there was not complete deletion of TBLR or TBL (Figure 24.D). Likewise, in primary BAT SVF-derived adipocytes, early KD reduced protein levels more strongly than late KD (Figure 24.E). These findings indicate that TBLR protein is very stable, reacting only with some days of delay to changes in mRNA levels. There was no apparent difference in cell shape or lipid accumulation of mature adipocytes subjected either to early or late KD (Figure 24.F-G), likewise the adipogenic markers *Ppargc1a* and sterol regulatory element-binding protein 1c (*Srebp1c*) were not affected (Figure 24.H-I). In primary BAT SVF-derived adipocytes subjected to early or late KD *Fabp4* expression was assessed and in concordance with the findings showed above were not found to be affected by the treatment (Figure 24.J-K). Also largely unchanged HSL and ATGL protein levels (Figure 25. C) indicate that cells differentiated into mature adipocytes regardless of TBLR and TBL ablation before differentiation. Taken together these results indicate that AV knockdown of TBLR alone or together with TBL is specific and does not generally inhibit the adipogenic program, however TBLR protein is very stable and not immediately removed from the cells upon transduction.

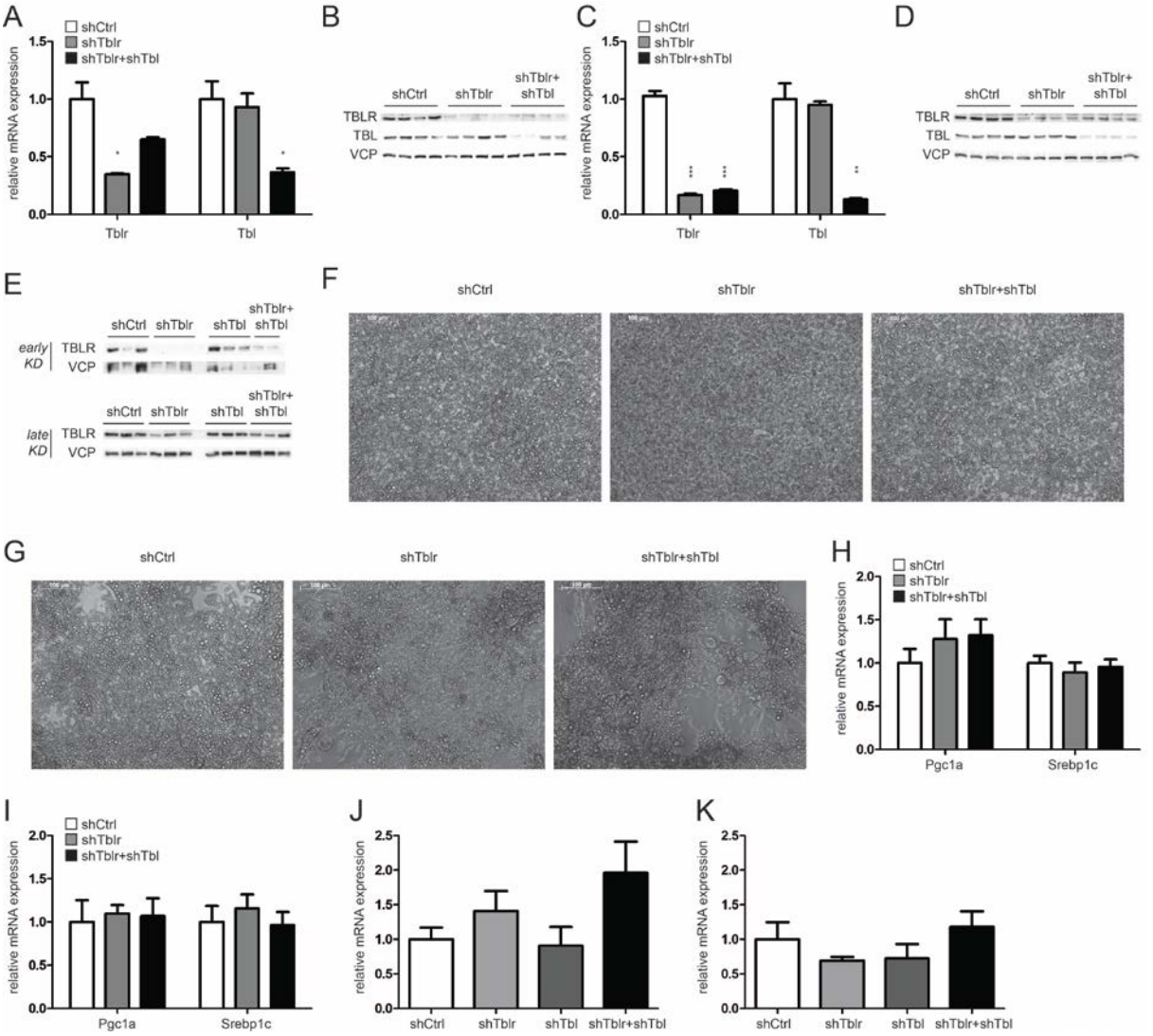

Figure 24. AV mediated KD of Tblr and Tbl is strong and specific without blocking the adipogenic program. *(A) Tblr mRNA and (B) protein expression of preBAT cells subjected to "early KD", i.e. transduction with a multiplicity of infection (MOI) of 50 of AV expressing shCtrl, shTblr and/or shTbl 2 days prior to induction of adipogenic differentiation. (C) Tblr mRNA and (D) protein expression of preBAT cells subjected to "late KD", i.e. transduction with a multiplicity of infection (MOI) of 500 of AV 2 days prior to harvest of mature adipocytes. (E) TBLR protein expression of primary BAT SVF-derived adipocytes subjected to early KD or late KD as described in (A-D). (F) Microscopy of mature preBAT adipocytes previously subjected to early or (G) late KD. (H) mRNA expression of Pgc1a and Srepb1c in mature preBAT adipocytes previously subjected to early or (I) late KD. (J) mRNA expression of Fabp4 in primary BAT SVF-derived adipocytes previously subjected to early or (K) late KD. All values are expressed as means ± SEM, n=3 technical replicates for preBAT cells or n=8-10 mice for primary cells, *p<0.05, **p<0.01, ***p<0.001 ctrl vs. KD*

First, we addressed the role of TBLR during adipogenesis and investigated the metabolic phenotype of preBAT adipocytes upon early KD. Lipolysis, in terms of free fatty acids and glycerol released into the medium in the basal state or upon stimulation with the general β-adrenergic agonist isoproterenol (Iso), was mainly maintained functional also in TBLR or TBLR/TBL-deficient adipocytes (Figure 25. A). There was a trend to lowered lipolysis upon KD of both factors, and this effect was reproduced in primary BAT SVF-derived adipocytes, however still being marginal (Figure 25. B). In accordance with these findings, the expression of the 2 major lipases, HSL and ATGL, as well as phosphorylation of HSL upon Iso stimulation, was largely unaffected by TBLR KD alone and slightly decreased by double KD (Figure 25. C). The uptake of isotope-labelled non metabolisable glucose analogue ^{3}H-2-deoxy-D-glucose (^{3}H-2-DOG) was significantly lower in cells lacking TBLR and TBL during differentiation, both basally or in the insulin stimulated state (Figure 25. D), which was also observed in primary brown adipocytes and was found to depend more on TBL than on TBLR (Figure 25. E). In accordance with this, also glucose metabolism in terms of retention of metabolisable ^{14}C-D-glucose was lowered particularly in the absence of both factors (Figure 25. F), and less of this glucose was converted into lipids in the basal state, which could be overcome by insulin treatment (Figure 25. G). Further, these cells exhibited de-regulated gene expression, as the brown fat markers *Ucp1* and *Cpt1b* were induced upon early KD (Figure 25. H), which could be observed also in primary cells and was true both in the basal as well as in the β-adrenergic stimulated state (Figure 25. I). Taken together, early KD of both TBLR and TBL leads to less active adipocytes with a lower lipid from glucose production rate and a deregulated profile of brown fat marker genes.

Analogously, preBAT adipocytes subjected to late KD were assessed for their metabolic phenotype. In these cells, in which TBLR and TBL were present during differentiation but depleted in mature cells, albeit only partially, due to technical limitations (Figure 24.D), lipolysis was unaffected (Figure 26.A), although double KD tended to decrease lipase protein levels (Figure 26.B) similar to what was observed upon early KD. ^{3}H-2-DOG uptake (Figure 26.C), retention of ^{14}C-D-glucose (Figure 26.D) and subsequent conversion to lipids (Figure 26.E) were unaffected by the viral treatment, regardless of the presence of insulin. Different from cells deficient of TBLR and TBL during differentiation, ablation in mature cells decreased rather than increased *Ucp1* mRNA expression (Figure 26.F). Overall, partial depletion of TBLR and TBL from mature adipocytes decreased their expression of thermogenic genes but allowed them to maintain their metabolic competence.

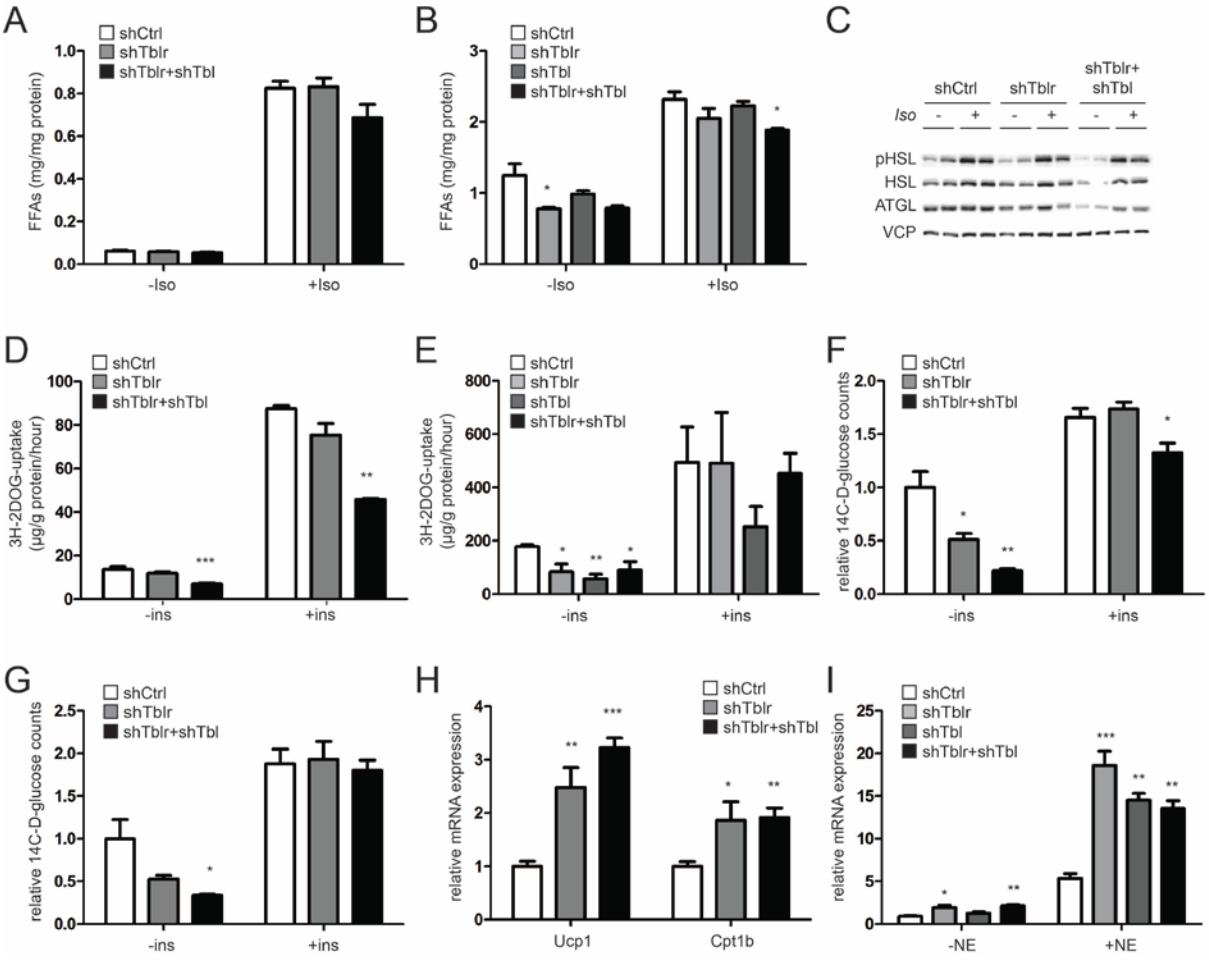

Figure 25. Early KD of TBLR and TBL leads to less active adipocytes with de-regulated brown gene expression profile. *preBAT cells were subjected to early KD of TBLR alone or TBLR and TBL together by transduction with a MOI of 50 of adenovirus 2 days prior to induction of adipogenic differentiation. Cells were then differentiated to mature adipocytes until day 7 and used for assays. For primary SVF-derived adipocyte progenitors, a MOI of 10 was used. (A) Release of free fatty acids (FAA) as indicator of triglyceride hydrolysis in preBAT adipocytes or (B) primary brown adipocytes 3 hours after treatment with 1 µM isoproterenol (Iso) or vehicle. (C) Western Blot analyses of lipase expression and phosphorylation in preBAT adipocytes upon 15 minutes treatment with 1 µM Iso or vehicle. (D) ^{3}H-2-DOG incorporation to preBAT adipocytes or (E) primary brown adipocytes in the basal or 20 nM insulin stimulated (ins) state during the course of 20 minutes. (F) ^{14}C-D-glucose accumulation and (G) conversion to lipids in preBAT adipocytes in the basal or 20 nM ins stimulated state during the course of 20 minutes. (H) mRNA expression of Ucp1 and Cpt1b in preBAT adipocytes and (I) Ucp1 mRNA expression in primary adipocytes stimulated for 3 hours with 1 µM NE or vehicle. All values are expressed as means ± SEM, n = 3 technical replicates for preBAT cells, n= 8 mice for primary cells, *p<0.05, **p<0.01, ***p<0.001 ctrl vs. KD.*

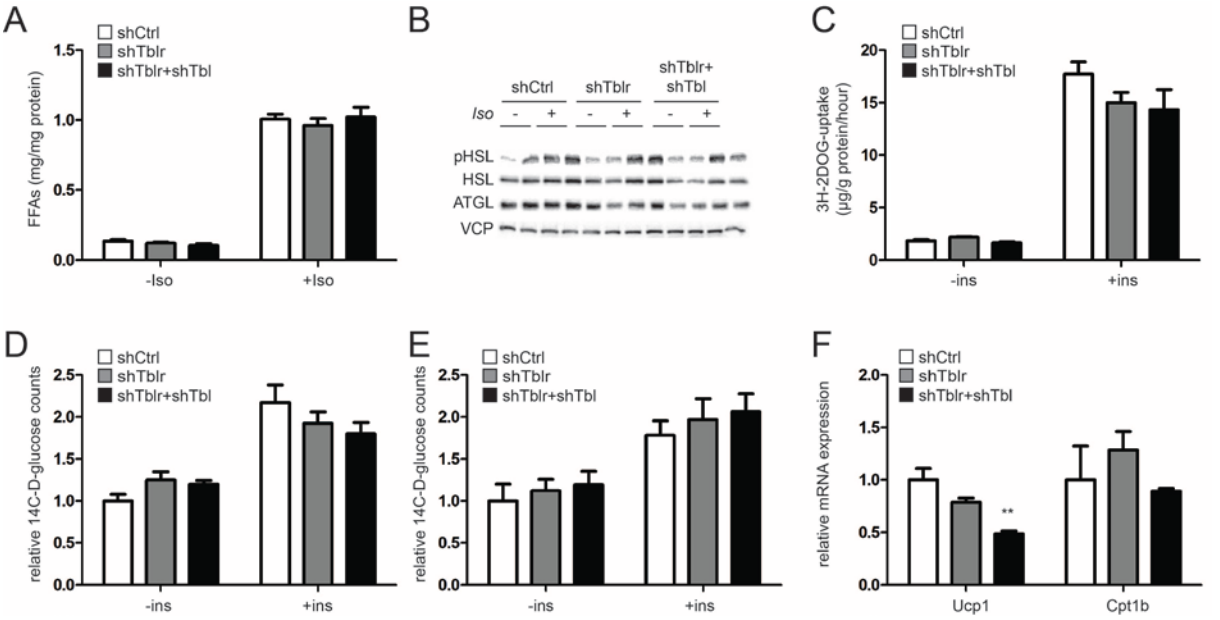

Figure 26. Late KD of TBLR and TBL leads to adipocytes with lower Ucp1 and normal metablic competence. *preBAT cells were differentiated to mature adipocyte and subjected to late KD of TBLR alone or TBLR and TBL together by transduction with a MOI of 500 of adenovirus 2 days prior to assays. (A) Release of free fatty acids (FAA) as indicator of triglyceride hydrolysis in preBAT adipocytes 3 hours after treatment with 1 µM isoproterenol (Iso) or vehicle. (B) Western Blot analyses of lipase expression and phosphorylation in preBAT adipocytes upon 15 minutes treatment with 1 µM Iso or vehicle. (C) ^{3}H-2-DOG incorporation to preBAT adipocytes in the basal or 20 nM insulin stimulated state during the course of 20 minutes. (F) ^{14}C-D-glucose accumulation and (G) conversion to lipids in preBAT adipocytes in the basal or 20 nM insulin stimulated state during the course of 20 minutes. (H) mRNA expression of Ucp1 and Cpt1b in preBAT adipocytes stimulated for 3 hours with 1 µM NE or vehicle. All values are expressed as means ± SEM, n = 3 technical replicates, *p<0.05, **p<0.01, ***p<0.001 ctrl vs. KD.*

To further understand the metabolic status of adipocytes deficient of TBLR or TBL we performed extracellular flow bioanalysis on a Seahorse XF96 analyser. By this method, living cells can be automatically treated with diverse substances and their reaction in terms of oxygen consumption and glycolytic activity can be observed in real time.

In the experiments shown above, early KD affected both glucose metabolism and lipogenesis stronger than late KD and *Ucp1* expression was regulated in the opposite direction in these two settings (Figure 25.F-H and Figure 26.D-F). Extracellular flow bioanalysis, however, showed very similar effects in both cases. The absence of TBLR and TBL in adipocytes lead to them being less metabolically active, exhibiting both a lower oxygen consumption rate

(OCR) (Figure 27.A) and glycolytic activity, assessed in terms of extracellular acidification rate (ECAR) (Figure 27.B). The same observation was true in primary cells (Figure 27.C). Consequently, there was no shift from oxidative phosphorylation to glycolysis, regardless whether glucose was present in the medium (Figure 27.D).

Since we showed that KD of TBLR alone or together with TBL compromises basal glucose uptake, which can be rescued by the addition of insulin (Figure 25.F,G), we were interested in the glycolytic capacity of these metabolically less active adipocytes. Thus, glucose and insulin were added, subsequently, to the cells. Addition of glucose could not rescue the defect in basal glycolysis in either early KD (Figure 27.E) or late KD (Figure 27.F) cells. In fact, the relative response in terms of delta AUC was even lower in cells deficient for TBLR or TBL (statistical AUC analysis was performed using the seahorse software) (data not shown). The addition of insulin, however, could rescue the defect and bring the ECAR of cells subjected to early or late KD back to the level of control cells (Figure 27.E-F).

Since the mitochondrial uncoupling protein *Ucp1* was not only identified as a target of TBLR by ChIPseq analysis (Figure 23.D), but also was found to be dysregulated upon early or late KD of TBLR alone or TBLR/TBL, we speculated that deficient cells might exhibit altered uncoupling. We assayed the performance of the mitochondrial respiration of these cells by treating them with different compounds, observing the effect on oxygen consumption (OCR). Addition of the ATP synthase inhibitor oligomycine lowered OCR and the degree of this reduction reflects respiration caused by ATP production (coupled respiration), while all oxygen still consumed is caused by proton leak. We found that preBAT cells subjected to late KD reduced their OCR, and the remaining respiration (proton leak) was still lower in KD cells, demonstrating that they are not more uncoupled (Figure 27.G). Still, subtracting OCR of oligomycin-treated cells from their basal OCR (reflecting the rate of ATP production) revealed that also this rate was significantly lower in KD cells (Figure 27.H).

In the normal brown adipocyte setting, uncoupling mainly takes place via fatty acid-mediated UCP-1 activation [4, 95]. We thus speculated that by applying Iso, which is thought to allow fatty acid-mediated uncoupling via UCP-1 by inducing lipolysis [101], we would be able to assay lipolysis and fatty acid-dependent brown adipocyte respiration. Indeed, Iso could induce uncoupling of respiration in the absence, but not in the presence of the fatty acid scavenger BSA, indicative of the dependence of the respiration-stimulatory effect of Iso on free fatty acids (Figure 27.I) [165]. In preBAT adipocytes subjected to late KD, Iso could not fully rescue the defect in respiration (Figure 27.J). Anaologously, in primary adipocytes

deficient of TBLR, TBL or both, NE failed to fully rescue respiration (Figure 27.K). However, addition of the ion carrier carbonyl cyanide 4-(trifluoromethoxy)phenylhydrazone (FCCP), that uncouples respiration from ATP production by dissipating the H^+ gradient over the mitochondrial membrane, even lead to higher maximal thermogenic capacity (that is, OCR induction over baseline respiration) in knockdown preBAT or primary adipocytes (Figure 27.L-M).

Taken together, these data demonstrate that in the absence of TBLR/TBL adipocytes are less metabolically active, and both their coupled and uncoupled respiration rates are lower. Both insulin and chemical uncoupling via FCCP rescued the effect, in accordance with the observation that *Ucp1* and respiratory chain elements are expressed more abundantly upon TBLR KD (Figure 23.G, Table 3), while fatty acid dependent respiration was still deficient. Consequently, we wanted to know whether the knockdown adipocytes were capable of normal β-oxidation.

We found that the direct addition of fatty acids in the form of BSA-conjugated palmitate, but not of BSA alone, did enhance respiration over baseline in preBAT cells subjected to early KD (Figure 27.N) or late KD (Figure 27.O). However, cells lacking TBLR alone or TBLR/TBL during differentiation, responded less to the substrate stimulus (Figure 27.N), which to a lesser degree was also true for cells in which knockdown was achieved after differentiation (Figure 27.O). To assess to which degree this induction is dependent on a defect in β-oxidation (rather than on, for example, less fatty acid-induced uncoupling [99, 100, 166] due to less available substrate), an inhibitor of mitochondrial fatty acid-import, Etomoxir, was applied and the decrease in OCR was calculated. There was a trend for β-oxidation to be lower in cells deficient of TBLR alone or TBLR/TBL (Figure 27.P).

Overall, our in vitro findings demonstrate that adipocytes need TBLR and TBL to be present, mainly during differentiation but to a lower degree also in the differentiated state, in order to act as fully metabolically competent adipocytes. In the absence of the factors, adipocytes exhibit lower metabolic rates, such as glycolysis, glucose uptake, respiration and lipogenesis, unless stimulated. However, mitochondrial function per see seemes to be intact, since stimulators of nutrient uptake (insulin) or chemical uncouplers (FCCP) rescued these defects.

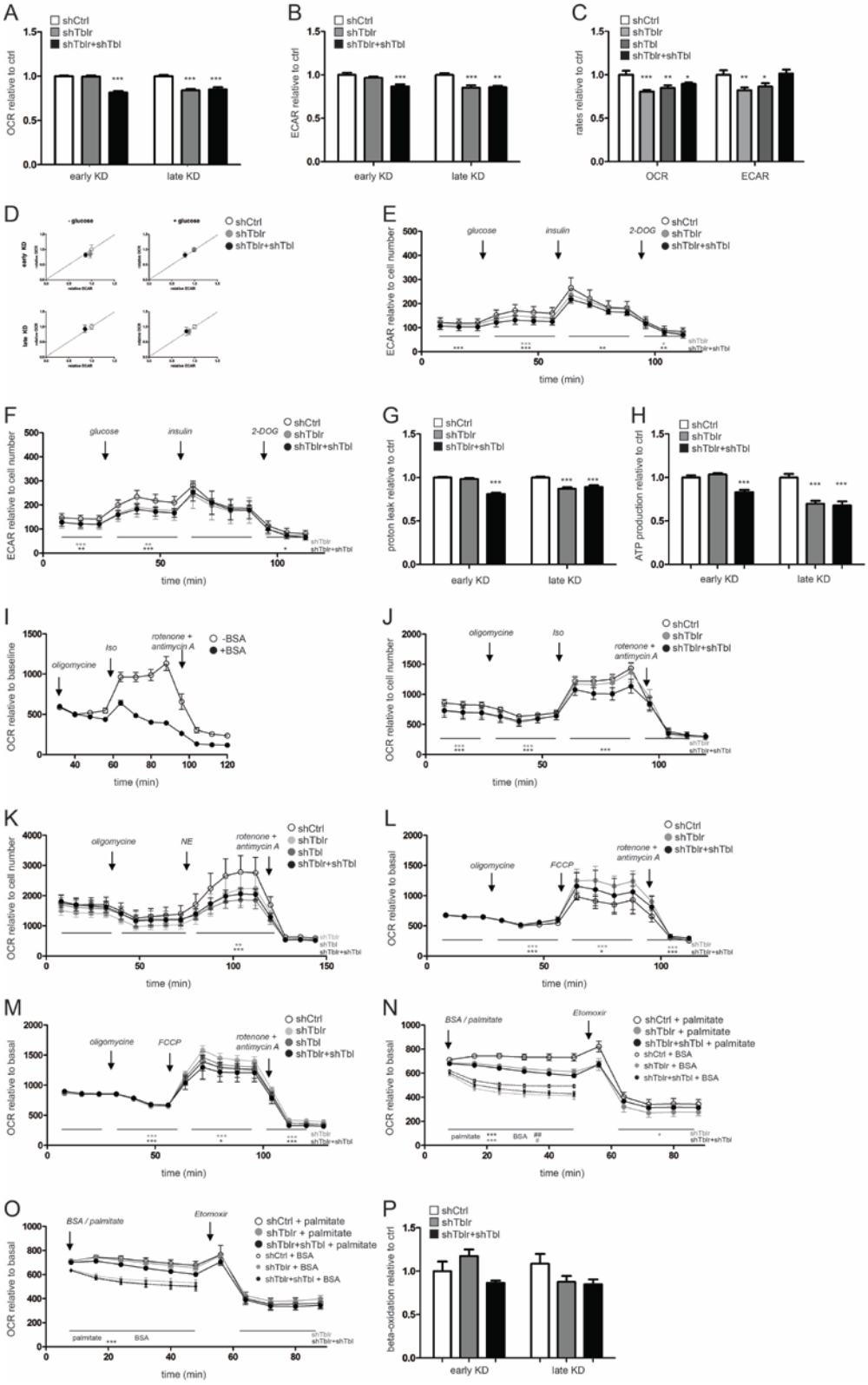

Figure 27. TBLR and TBL deficient adipocytes are less metabolically active in the unstimulated state. *(figure legend continued on next page)*

Figure 27. TBLR and TBL deficient adipocytes are less metabolically active in the unstimulated state. *(figure legend continued from previous page)*

*preBAT cells or primary brown SVF dedived adipocytes were subjected to early or late KD and analysed on a Seahrose extracellular flux analyser. (A) preBAT adipocyte oxygen consumption rate (OCR) as indicator for oxidative phosphorylation or (B) extracellular acidification rate (ECAR) as indicator for glycolytic activity, both displayed relative to shCtrl transducted cells. (C) OCR and ECAR in primary brown SVF dedived adipocytes. (D) AUC over 30 minutes of OCR versus ECAR of preBAT adipocytes assayed with or without glucose in the medium. (E) ECAR of early KD and (F) late KD preBAT adipocytes subjected to a glycolysis stress assay, subsequently adding 10 mM glucose, 20 nM insulin and 100 mM 2-DOG. (G) Proton leak in early and late KD preBAT cells, defined as AUC over 30 minutes of OCR upon treatment with 2 µM oligomycine, displayed relative to shCtrl transducted cells. (H) ATP production in early and late KD preBAT cells, defined as the difference in average AUC over 30 minutes of cells before ("basal") and after ("coupled") treatment with 2 µM oligomycine, displayed relative to shCtrl transducted cells. (I) Changes in OCR relative to baseline in control preBAT cells treated with 1 µM isoproterenol (Iso) in the presence or absence of 0.1 % bovine serum albumin (BSA). (J) OCR of late KD preBAT adipocytes and (K) early KD primary brown adipocytes subjected to a mitochondrial stress assay, subsequently adding 2 µM oligomycine, 1 µM isoproterenol or 1 µM norepinephrine (NE) and 1 µM each of rotenone and antimycin A. (L) Changes in OCR relative to baseline in late KD preBAT adipocytes and (M) early KD primary brown adipocytes, subsequently adding 2 µM oligomycine, 0.5 µM FCCP and 1 µM each of rotenone and antimycin A. (N) OCR of early KD and (O) late KD preBAT adipocytes subjected to a fatty acid oxidation assay, subsequently adding 200 µM palmitate-BSA conjugate or BSA alone and 1 mM etomoxir. (P) β-oxidation in early and late KD preBAT cells, defined as the difference in average AUC over 40 minutes of cells in the presence of 200 µM palmitate-BSA conjugate before and after treatment with 1 mM etomoxir, displayed relative to shCtrl transducted cells. Statistical ANOVA analysis was performed using the Seahorse analysis software based on the AUC of OCR or ECAR over all measurements performed at the respective condition. n = 4-32 wells per condition, *p<0.05, **p<0.01, ***p<0.001 ctrl vs. KD.*

BAT-specific TBLR ablation in vivo is strong and specific

With the data above we have established that TBLR is regulated specifically under conditions that activate brown adipose tissue, that in brown adipocytes it regulates gene expression programs connected to adipogenesis and mature adipocyte function and that its ablation in vitro during or after adipogenic differentiation, especially when eliminating also its homologue TBL, leads to metabolically impaired adipocytes. We hypothesised that TBLR, being a metabolic master regulator with known functions in liver and adipose tissue, can exert its actions in a tissue-specific way and that thus brown adipose tissue-specific knockout of TBLR will impact the whole organism. To address this hypothesis we crossbred Tblr floxed mice [139] with mice expressing tamoxifen-inducible Cre recombinase under the control of the *Ucp1* promoter [167]. By this method we obtained Tblr1$^{fl/fl}$Ucp1Cre^{+} and Tblr$^{fl/fl}$Ucp1Cre^{-} mice, the former of which become knockout for the *Tblr* gene in all *Ucp1* expressing cells upon tamoxifen injection ("BATKO" mice).

Female BATKO mice showed strongly decreased *Tblr* mRNA levels in BAT while other tissues such as inguinal or abdominal white adipose tissue (iWAT, aWAT), skeletal muscle (gastrocnemius, GC) or liver expressed normal *Tblr* levels (Figure 28.A). The same was true in male animals (data not shown). The knockout was stable also upon up to 3 week long exposure to thermoneutrality (30 °C) or cold (4 °C) at both the level of mRNA (Figure 28.B) and protein (Figure 28.C). Since in this animal model only *Ucp1*-expressing cells are targeted by the knockout and BAT is comprised of both UCP-1^{+} adipocytes and UCP-1^{-} stromal vascular cells, it was not surprising that TBLR was still to some degree detectable in BAT lysates. Further, TBLR knockout was conserved at the level of mRNA (Figure 28.D) and protein (Figure 28.E) even following 2 months of high fat diet feeding. Finally we tested whether this genetic mouse model technically allows the induction of knockout in brite adipocytes. To show this we injected Tblr1$^{fl/fl}$Ucp1Cre^{+} and Tblr$^{fl/fl}$Ucp1Cre^{-} mice with tamoxifen to render them BATKO and control mice, respectively. Following a three week adaptation phase, we acclimatised them to 4 °C for 3 weeks and then divided them into 3 groups. While cre^{-} control animals and one cre^{+} BATKO group were injected with another dose of tamoxifen, the other group of cre^{+} BATKO mice received only vehicle. Interestingly, while both BATKO groups maintained strong *Tblr* knockout in BAT, the group re-injected with tamoxifen after cold-induced recruitment of UCP-1^{+}adipocytes in WAT exhibited reduced *Tblr* levels in WAT (Figure 28.F). We hereby showed that this is a strong, stable and specific genetic mouse model for inducible BAT- (and brite-) specific knockout of TBLR.

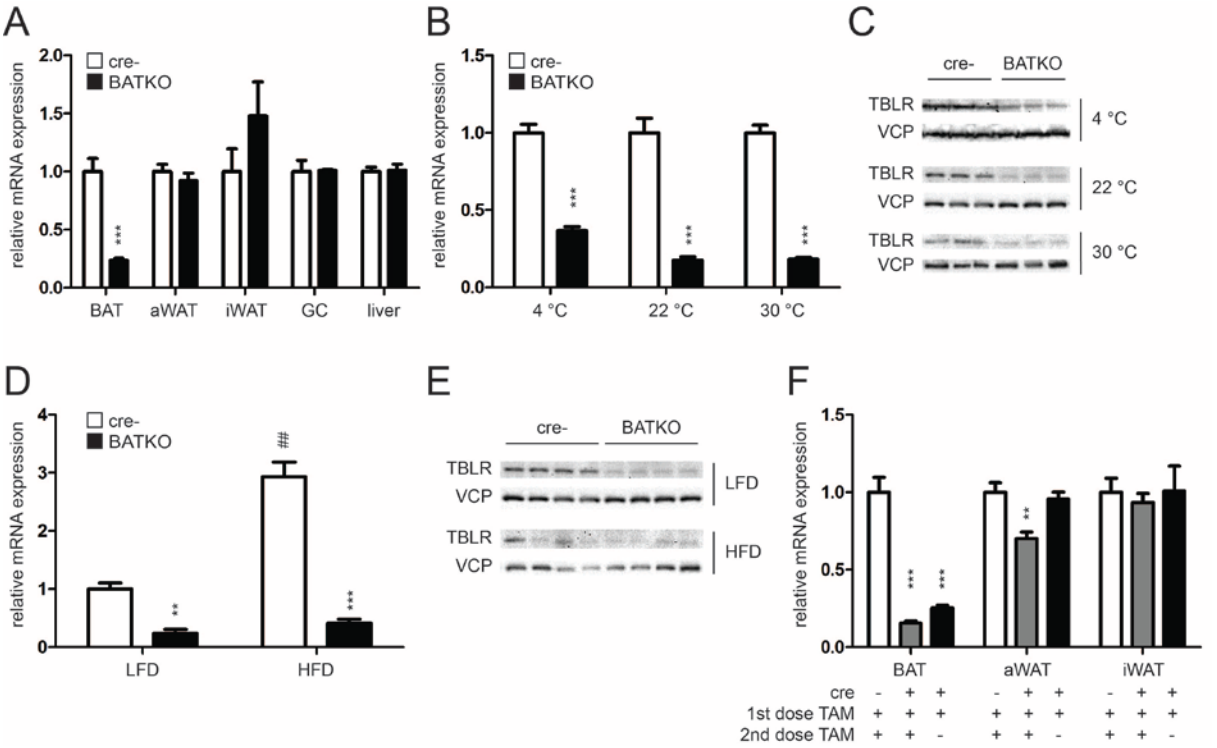

Figure 28. Tamoxifen induced TBLR knockout in BATKO mice is strong, stable and specific. *(A) Tblr mRNA levels in BAT, aWAT, iWAT, GC and liver of female BATKO and cre- control mice (n=3-4). (B) Tblr mRNA and (C) protein levels in BAT of BATKO and control mice housed for 3 weeks at 30 ° C, 22 ° C or 4 ° C (n=3-10). (D) Tblr mRNA and (E) protein levels in BAT of BATKO and control mice fed a HFD or LFD for 2 months at 22 ° C (n=6-7). (F) Tblr mRNA levels in BAT, iWAT and aWAT of BATKO and cre- control mice all injected with tamoxifen, then exposed to 4 ° C for 3 weeks, then injected again with either tamoxifen or sunflower oil as vehicle. All values are expressed as means ± SEM, *p<0.05, **p<0.01, ***p<0.001 ctrl vs. BATKO, #p<0.05, ##p<0.01, ###p<0.001 LFD vs. HFD*

TBLR ablation in vivo hardly affects BAT gene expression

Analogous to our in vitro studies we were interested in the impact of TBLR deletion on BAT gene expression. We first analysed the expression of selected individual targets and then performed microarray analysis on RNA obtained from BAT that was control or knockout, respectively, for TBLR. We analysed BAT of animals housed at room temperature or exposed to 4 °C for 2 days. The expression of *Ucp1*, the main player in brown adipose tissue thermogenic function, was not differentially regulated in BATKO mice, despite the fact that it was identified as the most strongly bound target in mature preBAT adipocytes and to be dysregulated upon in vitro KD of TBLR (Figure 29.A and B). Neither did KO of TBLR lead to

compensatory up-regulation of *Tbl* (Figure 29.C). Differently from in vitro results, where TBLR ablation before induction of differentiation enhanced expression of mitochondrial respiratory chain components, upon in vivo knock out of TBLR in mature adipocytes we found a modest tendency for mitochondrial markers and the β3-adrenergic receptor to be reduced (*Cox7a1*, *Cox8b*, succinate dehydrogenase complex subunit B and C (*Sdhb*, *Sdhc*), ATP synthase subunit O (*Atp5o*) and *Adrb3*), although the differences were not statistically significant (Figure 29.D). Analysis of global gene expression in BAT revealed that BATKO mice showed a very similar profile to control mice both at room temperature (Figure 29.E) and at 4 °C (data not shown).

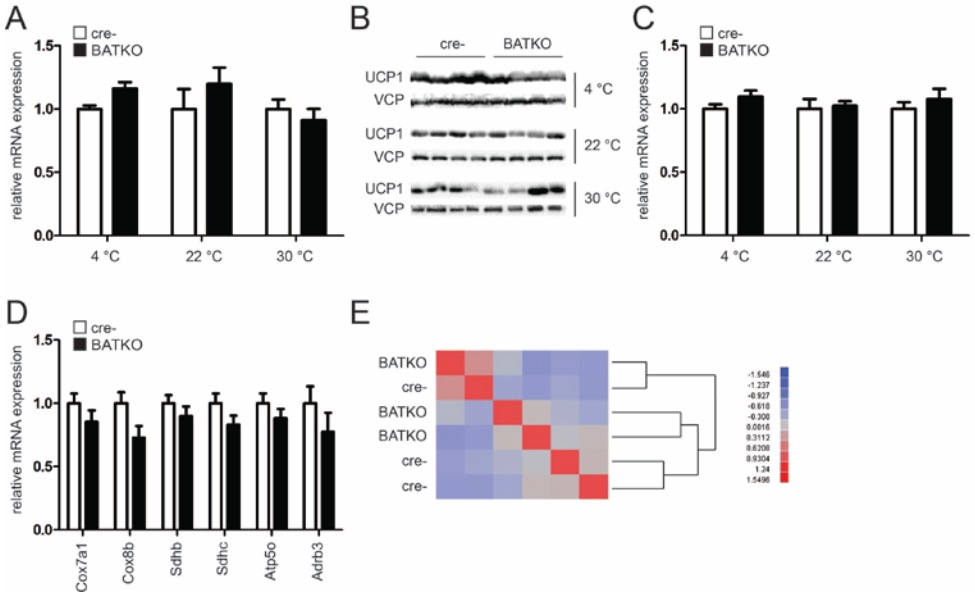

Figure 29. TBLR deficient BAT shows only marginally affected gene expression patterns. *Gene expression was analysed in BAT of female BATKO and cre- control mice. (A) Ucp1 mRNA and (B) protein levels. (C) mRNA levels of Tbl and (D) mitochondrial and adipocyte markers. (E) Heatmap showing differential mRNA expression between BAT of BATKO and cre- ctrl mice housed at 22 ° C. Higher and lower expression is displayed in red and blue, respectively. All values are expressed as means ± SEM, n = 5-10, *p<0.05, **p<0.01, ***p<0.001 ctrl vs. BATKO.*

KEGG pathway analyses did not give overlapping results between BAT of mice housed at 22 °C or 4 °C, and in general yielded low enrichment scores (Table 4), the highest enriched pathway scoring ± 0.7, as compared to ± 2.5 in the in vitro study shown in Table 2. This further indicates that there was little specific influence of TBLR deletion in mature brown adipocyte or BAT global gene expression programs.

Table 4. Regulation of KEGG pathways by TBLR knockout is weak and not reproducible in different temperature settings.

KEGG pathways significantly regulated by TBLR KO ranked by enrichment.

suppressed by TBLR (enriched in KO BAT)		
22 °C		
KEGG pathway	**enrichment score**	**p-value**
Asthma	0,69	5,38E-03
Glycosaminoglycane degradation	0,65	1,83E-02
Glycosphingolipid biosynthesis	0,62	7,71E-03
Thyroid cancer	0,62	9,17E-03
Leishmaniasis	0,60	0,00E+00
4 °C		
KEGG pathway	**enrichment score**	**p-value**
Hypertrophic cardiomyopathy	0,64	0,00E+00
Dilated cardiomyopathy	0,63	0,00E+00
Cardiac muscle contraction	0,63	0,00E+00
Tight junction	0,61	0,00E+00
Arrhythmogenic right ventricular cardiomyopathy	0,58	0,00E+00

induced by TBLR (enriched in WT BAT)		
22 °C		
KEGG pathway	**enrichment score**	**p-value**
Steroid biosynthesis	-0,74	0,00E+00
Aminoacyl T-RNA synthesis	-0,63	0,00E+00
Butanoate metabolism	-0,61	2,31E-03
Basal transcription factors	-0,57	4,12E-03
Proteasome	-0,56	0,00E+00
4 °C		
KEGG pathway	**enrichment score**	**p-value**
Steroid biosynthesis	-0,73	0,00E+00
Antigen processing and degradation	-0,56	0,00E+00
Glycosphingolipid biosynthesis	-0,53	9,03E-02
Glycosylphosphoinositol (GPI)-anchor biosynthesis	-0,52	3,39E-02
Dorso-ventral axis formation	-0,51	6,24E-02

Of all significantly regulated genes, neither of them was changed by more than 70 % (at 4 °C) or 30 % (at room temperature), respectively, and a higher number of genes was up- rather than down-regulated upon TBLR knockout in both settings, indicating that in BAT TBLR acts more often as a co-repressor than as a co-activator. For analysis, only genes expressed differentially by at least 10% and with a p-value smaller than 0.05 were considered. The complete list of genes matching these criteria is shown below (Table 5).

At 22 °C, the most strongly reduced gene in TBLR-deficient BAT was elongation of long-chain fatty acids family member 6 (*Elovl6*). Further, the highly expressed adipokine complement factor D (*Cfd*, also known ad adipsin), which is known to be regulated in obesity and to stimulate glucose transport and fatty acid re-esterification [168], was found to be

expressed at lower levels in TBLR deficient BAT. This gene is reported to inhibit lipolysis, as is another target found to be down-regulated, Apolipoprotein C3 (*Apoc3*), which is an inhibitor of LPL [169]. Also the glucose transporter *Slc2a12* (solute carrier family 2 member 12) was down-regulated in TBLR-deficient BAT.

There was no clear redundance or common pattern of changes in BAT gene regulation in response to TBLR KO comparing samples from animals housed at 4 °C or at 22 °C, respectively. Interestingly, many muscle associated genes were de-repressed. In the set of genes decreased in expression in TBLR-deficient BAT, the LDL receptor (*Ldlr*) stood out.

Table 5. TBLR deficient BAT shows only marginal changes in gene expression.

Ranking by fold-regulation of gene expression in TBLR KO. Genes induced by TBLR (depleted in KO) are indicated in red, genes repressed by TBLR (de-repressed in KD) are highlighted in green.

22 °C		
gene name	fold change in KO BAT	p-value
Gldn	1,28	8,86E-03
Nek6	1,24	1,88E-02
Dmrt2	1,21	2,29E-02
2410066E13Rik	1,18	2,94E-05
Cdsn	1,17	4,11E-02
Apol6	1,16	2,63E-02
Ccnd1	1,16	2,68E-02
Slc6a13	1,15	3,06E-02
Col12a1	1,15	3,41E-02
Pkp2	1,14	3,17E-02
H2-T23	1,14	3,76E-02
Fscn1	1,13	2,03E-02
Gp49a	1,13	3,88E-02
Il2rg	1,13	1,46E-02
Tnc	1,13	2,01E-03
Lbp	1,12	2,05E-02
Stk10	1,12	1,15E-02
Lctl	1,12	6,25E-04
1300014I06Rik	1,11	4,62E-02
Sh3tc1	1,11	3,44E-02
Hist2h3c1	0,91	2,75E-02
Slc2a12	0,91	8,96E-03
A830018L16Rik	0,89	2,36E-05
Pcdhga1	0,89	6,44E-03
Tst	0,89	2,40E-02
Apoc3	0,88	2,90E-03
Ifi27l2a	0,87	5,97E-03
Cfd	0,87	3,57E-02
Orm3	0,85	1,61E-02
Elovl3	0,83	3,39E-02

4 °C		
Spalte1	fold change in KO BAT	p-value
Atp2a1	1,67	9,21E-03
Myh4	1,67	3,42E-03
Pygm	1,40	8,04E-03
Actn3	1,40	2,28E-03
Mybpc2	1,25	8,21E-03
Eno3	1,23	8,16E-03
Myoz1	1,19	9,38E-03
Nrap	1,13	8,46E-03
Cacna1s	1,11	9,73E-03
Glis3	1,10	7,69E-04
Npas2	1,10	1,25E-04
Myom1	1,10	7,40E-03
Ldlr	0,92	7,64E-03
Tubb6	0,91	6,26E-03
Hsph1	0,89	7,58E-03
Pcdhgb8	0,87	1,14E-03

Overall, in terms of gene expression, TBLR-deficient BAT largely resembled wildtype, with muscule-like signatures being enriched in the cold, while KO at room temperature resulted in a reduction of genes associated with lipogenesis-induction and lipolysis-suppression.

TBLR ablation does not affect adiposity in HFD feeding

Since Rohm et al found that adipose-specific deletion of TBLR induces overweight [139] we were interested whether selective brown fat-specific knockout would show the same phenotype. However, BATKO mice did not gain more weight on HFD or LFD (Figure 30.A) and their food intake was not changed (Figure 30.B). Since with conventional methods only LFD intake can be quantified reliably (whereas the lipid-rich HFD crumbles too much for weighing), we made use of Phenomaster cages (TSE Systems), that, among other parameters, are able to track food intake. We found that the feeding behaviour of BATKO and control mice was equal at all light cycle phases during normal chow diet feeding as well as HFD re-feeding after an overnight fast (Figure 30.C) (average of light and dark phase shown). In accordance with body weight, magnetic resonance analysis of body composition proved that fat and lean mass did not differ between genotypes (Figure 30.D-E). After 6 weeks of HFD feeding, weight loss and re-gain during fasting and re-feeding respectively was determined, and also in this regard BATKO and control mice were found to be equal (Figure 30.F). In line with these findings, the weight of individual organs was not significantly affected at 22 °C, however WAT depots tended to be smaller (Figure 30.G). Since brown fat weight was found to be slightly reduced upon KO of TBLR in individual cohorts, while it was not affected in biological replicates in the same settings, all available data was compared. Overall, there was no significant difference in BAT weight at any housing temperature (Figure 30.H). Since it is known that TBLR-deficient white adipocytes accumulate more lipids due to a defect in lipolysis [139], we hypothesised that despite unaltered adiposity in brown fat-specific TBLR deficiency, the lipid content of BAT might be different between genotypes, however we found also BAT triglycerides not to be affected by TBLR knockout at any temperature (Figure 30.I).

Overall BATKO mice were not more obese than controls, and the same observations made on female mice were found in male BATKO and control animals (data not shown). Thus BATKO mice do not reproduce the previously described phenotype of whole fat-specific ATKO mice [139].

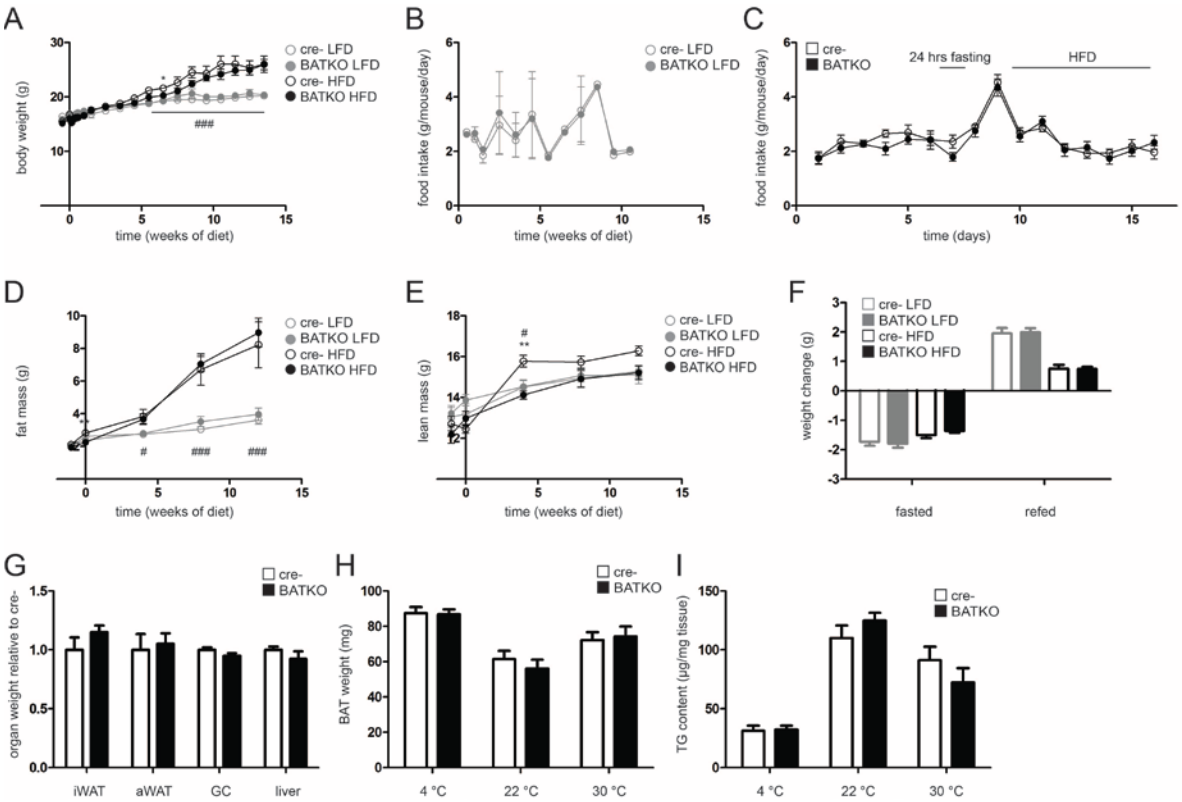

Figure 30. The adiposity of BATKO mice does not differ from controls. *(A) Body weight and (B) food intake of BATKO and control mice fed a high fat diet (HFD) or low fat diet (LFD) for 14 weeks (n=4-7). (C) Food intake of BATKO and control mice housed at 30 ° C in phenomaster cages and presented, subsequently, with normal chow, no food, or HFD (as indicated) (n=9-10). (D-E) ECHO-MRI body composition analysis of BATKO ant control mice fed a HFD or LFD, fat mass (D) and lean mass (E) were determined every 4 weeks (n=4-7). (F) Changes in body weight of the mice shown in (A), (B) and (D) upon 16 hours fasting and 6 hours of refeeding of the respective diet. (G) Organ weights of BATKO and control mice housed at 22 ° C (n=3-4). (H) BAT weight of BATKO and control mice housed at the indicated temperatures (n=17-33). (I) Triglyceride content in BAT of BATKO and control mice housed at the indicated temperatures (n=3-10). All values are expressed as means ± SEM, n = 4-10, *p<0.05, **p<0.01, ***p<0.001 ctrl vs. BATKO, #p<0.05, ##p<0.01, ###p<0.001 LFD vs. HFD*

Absence of TBLR in BAT does not affect systemic glucose handling

Since in vitro data indicated that brown adipocytes deficient in TBLR exhibit reduced glucose metabolism (Figure 25.D-F), that *Tblr* expression is repressed by insulin (Figure 20.C) and since ChIPseq analysis in preBAT cells indicated that components of the insulin signalling pathway were regulated by TBLR (Table 1), we hypothesised, that despite their unaltered adiposity, BATKO mice might exhibit differential glucose handling properties. However determination of random fed blood glucose of mice housed at different temperatures (Figure 31.A) as well as in fasted or refed state at room temperature (Figure 31.B) illustrated that systemic blood glucose was independent from the presence of TBLR in BAT. BATKO and control mice fed on a HFD or LFD were subjected to monthly glucose tolerance tests (GTTs). Neither blood glucose levels (Figure 31.C) nor corresponding serum insulin levels (Figure 31.D) were found to be different between genotypes for the first 8 weeks of feeding the respective diet. After 12 weeks of HFD feeding, when mice started to exhibit signs of the onset of insulin resistance such as elevated serum insulin levels compared to LFD-fed animals (Figure 31.D, right panel), HFD-fed BATKO mice tended to clear less glucose from the blood (Figure 31.C, right panel). We hypothesised that TBLR-deficient BAT, analogously to in vitro findings, would take up less glucose. To address this question, we housed mice at 22 °C or at 4 °C for 3 weeks in order to compare BAT in different levels of activation. The uptake rate of intraperitoneally injected ^{3}H-2DOG tracer into WAT, BAT, heart or brain of BATKO or control mice was determined (Figure 31.E), and the relevance to systemic glucose clearance was estimated by expressing tissue contribution as the product of the uptake rate and the respective tissue weight as described in the first section (Figure 31.F). While BATKO mice tended to deposit more glucose to the heart and less to brain, adipose tissues behaved equally in both genotypes. There was a tendency for BAT to take up less glucose in the cold, however technical variation in these experimental settings is high and thus more data would be required to confirm this observation. Overall, depletion of TBLR from mature, UCP-1-expressing brown adipocytes in vivo did not lead to an impairment of glucose uptake, consistent with observations in cells in which TBLR was absent during adipogenic differentiation (Figure 25.D-F), indicating that the role of TBLR in the regulation of glucose metabolism of brown adipocytes is probably more pronounced during the course of adipogenesis. Further, in vivo other factors such as the presence of TBL might compensate the deficiency of TBLR.

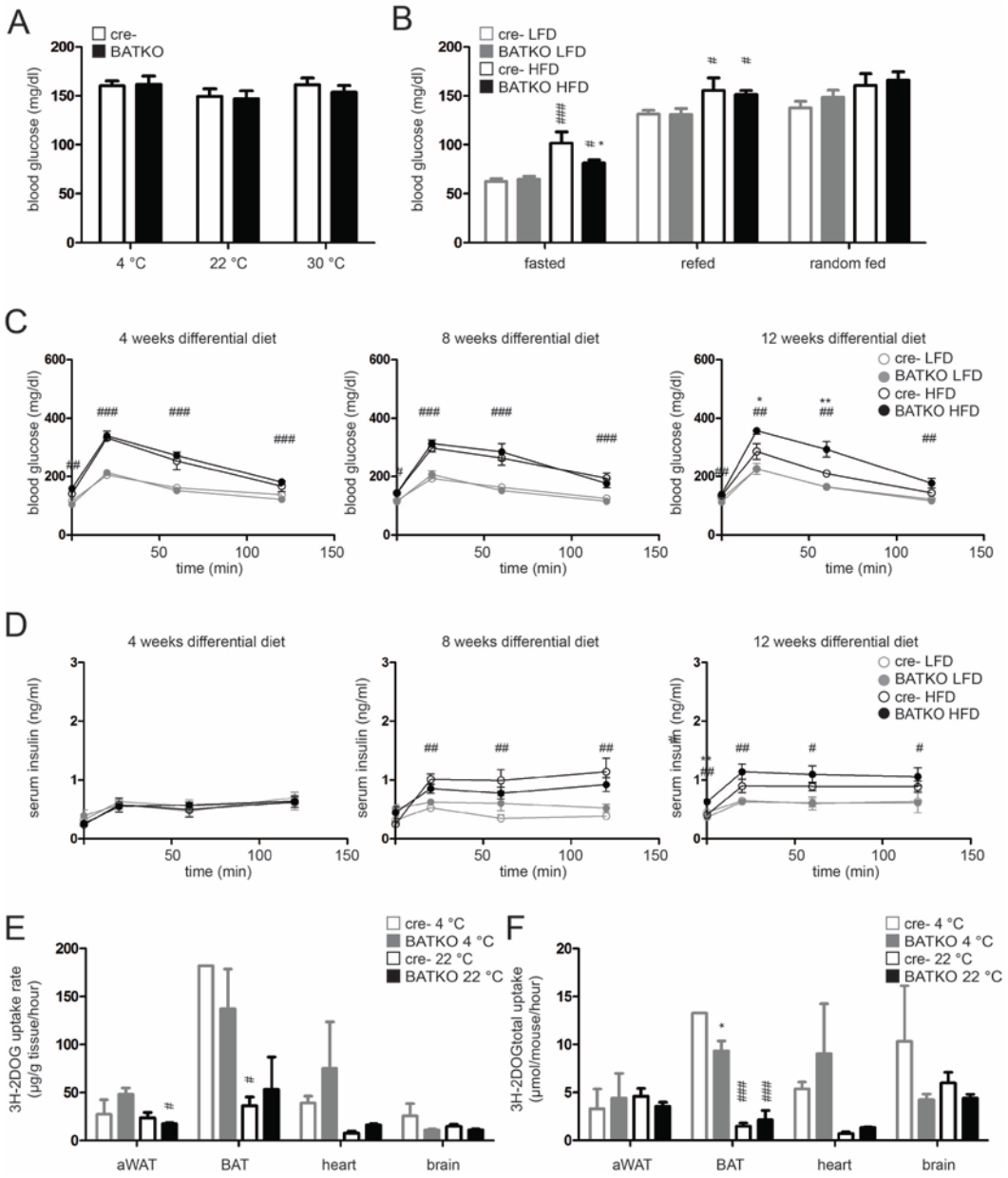

Figure 31. Absence of TBLR in BAT does not affect systemic glucose handling. *(A) Random fed blood glucose levels of mice housed at the indicated temperatures (n=3-10) or (B) random fed, 16 hour fasted or 6 hour refed blood glucose levels of BATKO and control mice fed a HFD or LFD for 12 weeks (n=4-7). (C) Blood glucose and (D) serum insulin levels of 6 hour fasted BATKO or control mice fed a HFD or LFD for 4 weeks, 8 weeks or 12 weeks, respectively, upon i.p. injection of 1 g/kg body weight glucose (n=4-7). (E) ^{3}H-2DOG uptake rate into aWAT, BAT, heart and brain of mice housed at 22 ° C or 4 ° C for 3 weeks (n=3-4). (F) Total ^{3}H-2DOG uptake by each tissue of the mice shown in (E), calculated from the ^{3}H-2DOG uptake rate and from the weight of each tissue. All values are expressed as means ± SEM, *p<0.05, **p<0.01, ***p<0.001 ctrl vs. BATKO, #p<0.05, ##p<0.01, ###p<0.001 LFD vs. HFD (A-D) or 4 ° C vs. 22 ° C (E-F)*

TBLR-deficient BAT is capable of normal lipolysis

Albeit previous studies on the effect of TBLR KO in whole adipose tissue [139] suggested impaired lipolytic capacity of TBLR-deficient adipose tissue, in vitro studies of specifically brown adipocytes suggested that lipolysis is largely unaffected by the deletion of TBLR (Figure 25.A-C). We wanted to exclude the possibility that in vitro knockdown was simply not strong enough to mediate effects as observed in vivo previously, so BAT from BATKO and control mice was dissected and subjected to a lipolysis assay. Although the efficient deletion of *Tblr* expression could be confirmed (Figure 32.A), neither lipolysis (Figure 32.B) nor glucose metabolism (Figure 32.C) or lipogenesis (Figure 32.D) were found to be different in BAT from BATKO mice. In line with these findings, the analysis of protein levels in BAT of BATKO and control mice revealed that BATKO mice at 30 °C tended to express reduced levels of HSL (Figure 32.E). However, in mice housed in the cold or at thermoneutrality, neither PKA signalling nor HSL phosphorylation were affected by the knockout of TBLR, indicating that activation of lipolysis is not impaired in BATKO mice (Figure 32. E).

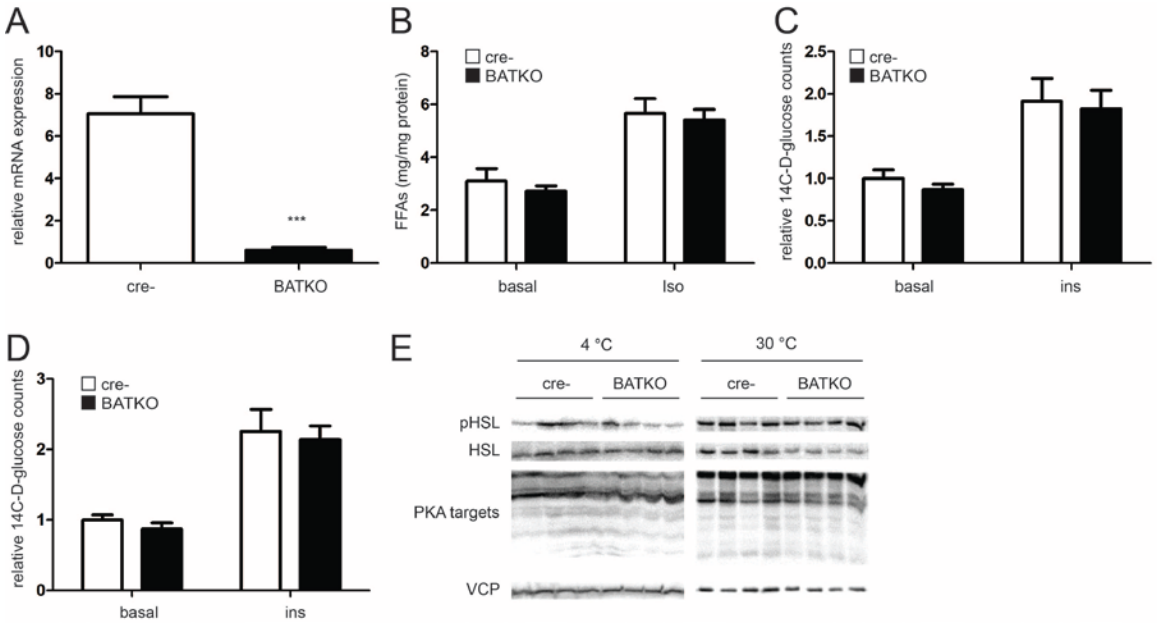

Figure 32. TBLR deficient BAT shows normal lipolysis. *(A-D) BAT of BATKO or control mice was dissected and subjected to lipolysis or lipogenesis assays. (n=5-7) (A) Tblr mRNA levels, (B) release of free fatty acids (FAA) as indicator of triglyceride hydrolysis 3 hours after treatment with 1 µM isoproterenol (Iso) or vehicle, (C) ^{14}C-D-glucose accumulation and (D) conversion to lipids in the basal or 20 nM insulin (ins) stimulated state during the course of 20 minutes. (E) Western Blot analysis of BAT of BATKO and control mice housed at 4 ° C or 30 ° C (n=6-10). All values are expressed as means ± SEM, *p<0.05, **p<0.01, ***p<0.001 ctrl vs. BATKO.*

Similar to the previously shown findings that a defect in glucose uptake following TBLR KD in vitro did not translate to a glucose-metabolism defect in BATKO mice in vivo, we show that the same is the case for TBLR-mediated regulation of lipolysis. Thus, TBLR-mediated regulation of lipid and glucose handling in brown fat is probably indirect by affecting basal metabolic settings as a result of dysregulated gene programs during adipogenesis.

Acute stimulation reveals a defect in maximal capacity of TBLR KO BAT

We so far have established by in vitro experiments that TBLR deficiency has more severe adverse effects on adipocytes when manifested already during adipogenesis (Figure 17 compared to Figure 18), and accordingly in vivo did not observe differential lipolysis or glucose metabolism in BATKO mice (in which TBLR is absent only from mature, UCP-1 expressing adipocytes). However TBLR was found to be required also in mature adipocytes, since knockdown both before and after differentiation into mature adipocytes similarly compromised metabolism (Figure 27). Thus we hypothesised that in BATKO mice, the respiratory capacity of BAT in response to β3-adrenergic stimulation would be compromised.

We made use of phenomaster cages in which not only the ambient temperature can be regulated, but also a multitude of metabolic parameters are assessed, such as oxygen (O_2) consumption and carbon dioxide (CO_2) production and the resulting respiratory exchange ratio (RER), or movement and conversely the resting metabolic rate (RMR) of non-moving animals. The RER is an indicator of fuel use, where pure carbohydrate consumption leads to a ratio of volume of consumed oxygen (VO_2) to volume of produced carbon dioxide (VCO_2) of nearly 1, whereas pure lipid oxidation results in an RER of 0.7; RMR is the oxygen consumption corrected for consumption caused by physical activity and thus represents movement-independent metabolism, including thermogenesis. Observing BATKO and control mice subjected to a subsequent change of ambient temperature from 30 °C to 22 °C and then to 4 °C, we found that neither VO_2 (Figure 33.A) nor VCO_2 (data not shown) and thus neither RER was affected by the KO of TBLR in BAT (Figure 33.B). Further, physical activity did not differ between genotypes (data not shown), thus RMR was equal between BATKO and control mice (Figure 33.C). Also assessing these parameters separately for the active dark or the inactive light phase did not reveal differences between genotypes (data not shown).

In order to assess the ability of the mice to defend their body temperature in various ambient temperatures, they were implanted with subcutaneous transponder thermometers prior to phenotyping. While at thermoneutrality body temperature was 0.5 °C higher in BATKO

animals, putting the mice to 4 °C lead to a drop in body temperature of 2 °C in both groups, equalizing the difference (Figure 33.D). Also upon prolonged adaptation to 4 °C, body temperature was maintained at 35° in both groups, with no difference between BATKO and control animals (Figure 33.E).

Since it is believed that not only temperature but also dietary challenges can induce thermogenesis [104, 170, 171], a study was performed to observe the acute metabolic response to fasting, refeeding and subsequently feeding of HFD. The measurements were done at thermoneutrality, thus allowing us to determine thermogenesis independently of requirements for thermoregulation. The phenomaster cages were able to detect the general consequences of these dietary cues, body weight dropped during fasting, was re-gained in refeeding and started to rise continuously immediately upon changing the diet from chow to HFD, however there was no difference between BATKO and control mice (Figure 33.F). Fuel use was adapted to the feeding situation as expected. The RER was around 0.9 on chow diet, dropped to 0.8 during the fasting-induced switch from the use of carbohydrate to lipid stores, rose to almost 1 upon re-feeding (where lipid reserves are replenished and carbohydrates are oxidised) and dropped as low as 0.8 when feeding a HFD, indicating that the high fat content of the diet forces a switch to higher lipid oxidation. However, BATKO mice and controls adapted their metabolism to the corresponding situation in the same way, indicating that TBLR is dispensable for these functions (Figure 33.G). VO_2 and RMR were found to rise in response to HFD, indicating diet-induced thermogenesis (Figure 33.H). RMR on HFD tended to be lower in BATKO animals, implying that the diet-induced induction of thermogenesis depends on the action of TBLR in mature BAT, however this difference was not significant.

Overall, BATKO mice were able to adapt as well as their wildtype counterparts to thermogenic challenges caused by ambient temperature or diet.

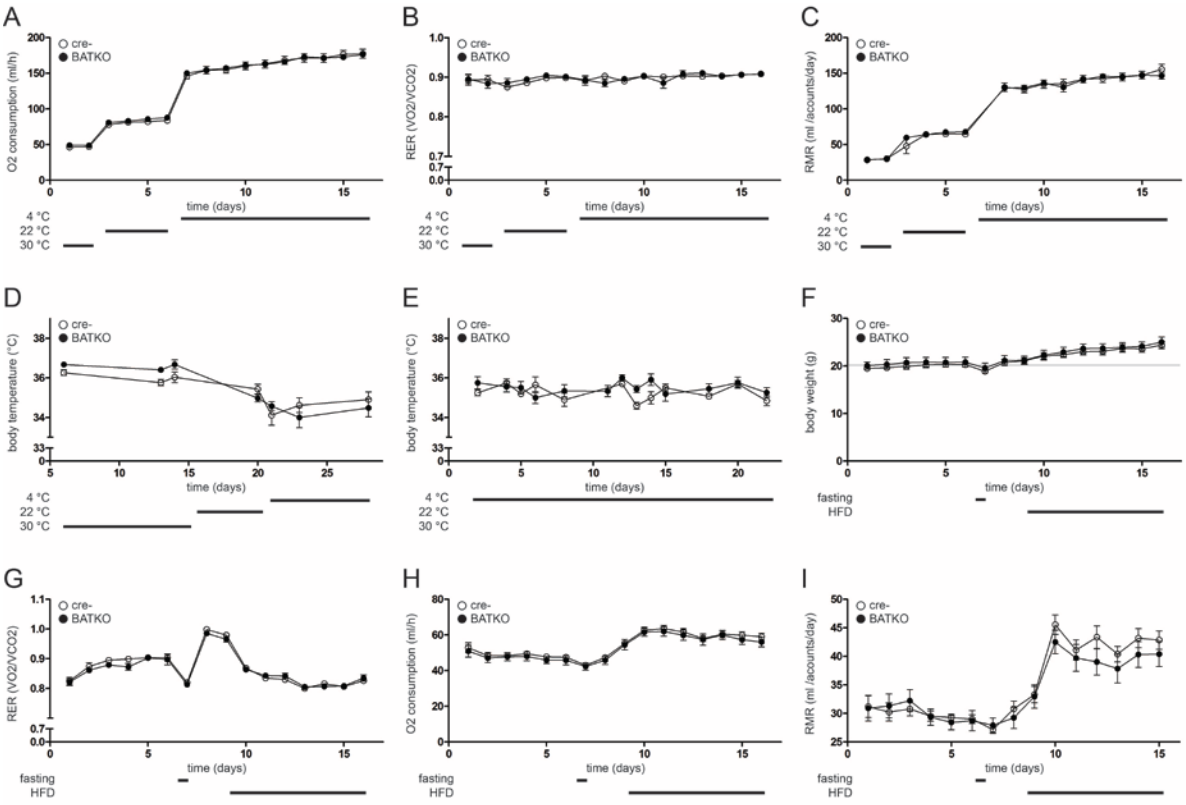

Figure 33. In both BATKO and control mice, metabolism adapts to changes in temperature and diet. *(A-D) BATKO and control mice were implanted with subcutaneous transponder thermometers and housed individually in phenomaster cages where the ambient temperature was set to be 30 ° C for 3 days, 22 ° C for other 3 days and finally 4 ° C for 10 days (n=6-7). (A) Oxygen consumption (VO_2), (B) respiratory exchange ratio (RER) of VO_2/VCO_2, (C) resting metabolic rate (RMR) and (D) body temperature in BATKO and control animals at the indicated temperatures. (E) Body temperature in BATKO and control mice subjected to prolonged cold exposure (n=4-7). (F-H) BATKO and control mice housed individually in phenomaster cages at 30 ° C were fed a chow diet for 6 days, fasted for 16 hours, then re-fed with chow for 2 days and subsequently fed a HFD for the rest of the duration of the experiment (n=9-10). (F) Body weight, (G) RER, (H) VO_2 and (I) RMR in BATKO and control mice being fed the indicated diets. All values are expressed as means ± SEM, *p<0.05, **p<0.01, ***p<0.001 ctrl vs. BATKO*

Since we observed earlier that cold exposure leads to an acute but transient induction of *Tblr* expression (Figure 21.F), we hypothesised that the role of TBLR in the thermogenic response in mature adipocytes might only serve a very acute purpose, and that subsequent recruitment of factors and mechanisms might allow for compensation of TBLR knockout over time. Based on these observations we decided to assess the acute maximal BAT capacity by

injecting the animals with the β3-adrenergic agonist CL and determining the immediate oxygen consumption-response. Since this agent also reduced physical activity, we corrected the data for movement, resulting in VO_2 caused by BAT activity. Strikingly, we found that BATKO mice housed at thermoneutrality exhibited a blunted maximal BAT capacity, being 15 % lower compared to controls (Figure34.A). Subsequent acclimatisation of the same animals to 4 °C and repetition of the measurement after 1 week (Figure34.B) and 3 weeks (Figure34.C) respectively of cold adaptation (always measuring at 30 °C though, to inactivate the sympathic tone), revealed that although the general the capacity of cold-adapted BAT to react to acute stimuli was increased, BATKO mice always demonstrated a dampened oxygen consumption-response compared to controls (Figure34.D). These findings demonstrate that mature BAT is dependent on TBLR to acutely respond to thermogenic stimuli, but that its role is transient and that compensatory mechanisms can be activated.

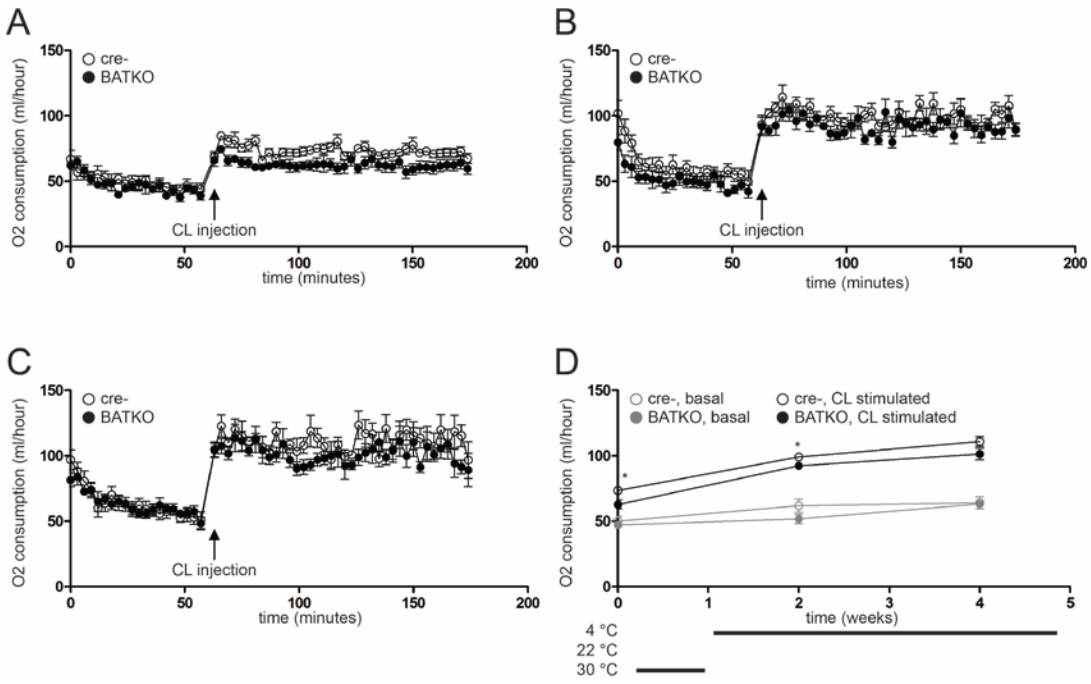

Figure 34. TBLR is required for immediate reaction of BAT to thermogenic stimuli. *BATKO and control mice were acclimatised to 30 ° C, injected intraperitoneally with 1 mg/kg body weight CL and respiration at 30 ° C was assessed in phenomaster cages. Subsequently, the animals were transferred to 4 ° C for another 3 weeks, the measurement being repeated 2 more times at 30 ° C (n=10). Correction for physical activity was performed. (A) VO_2 at 30 ° C, (B) after 1 week and (C) 3 weeks of housing at 4° C. (D) Average VO_2 per condition at the indicated times and temperatures. All values are expressed as means ± SEM, *p<0.05, **p<0.01, ***p<0.001 ctrl vs. BATKO (comparing the avereage rate per condition).*

BATKO mice have reduced serum VLDL at different temperatures

Interestingly, despite unaltered adiposity, glucose handling and BAT lipolysis in BATKO mice, we found that serum triglyceride (TG) levels in these animals were lower, not only at 4 °C where BAT is highly active, but also at room temperature (22 °C) and thermoneutrality (30 °C) (Figure 35.A). This was specific for TGs, while there was no difference in serum levels of free fatty acids (Figure 35.B) or cholesterol (Figure 35.C). Also when challenging fasted mice with oral administration of a defined dose of olive oil (oral lipid tolerance test, OLTT), serum TG levels were maintained at lower levels in BATKO mice compared to controls (Figure 35D). Fast-protein liquid chromatography (FPLC) analysis revealed that in the serum of mice housed at 4 °C (Figure 35.E) or 30 °C (Figure 35.F) the fraction corresponding to very low density lipoprotein (VLDL) was reduced in TG (AUC of protein signal during FPLC, being 50 % reduced at 4 °C and 20 % reduced at 30 °C), with cholesterol levels not greatly being affected (2 % more signal in BATKO at both temperatures) (Figure 35.G-H).

This phenotype is very interesting, since BATKO mice exhibit diminished thermogenesis upon acute activation and thus are expected to oxidize less rather than more nutrients. However we cannot outrule that vice versa the altered lipid profile is the primary defect in BATKO mice that in turn leads to comprised thermogenic flexibility in situations with increased fuel demand.

To address the question of how BAT-specific knockout of TBLR can affect systemic serum VLDL levels despite not being metabolically more or less active in terms of glucose uptake (Figure 31.E-F), lipolysis or lipogenesis (Figure 32.B-E), we hypothesised that BAT, being known to have the potential to function as an endocrine organ [172, 173], might signal to other organs, thus affecting systemic lipid handling. We thus individually dissected the routes in which lipids systemically are distributed and used. Hypothetically, lower serum lipid levels can be the result of a multitude of different settings. The amount of TGs being taken up into the system via feeding might be lowered by hypophagia [174] or increased loss of energy to feces [175, 176]. Alternatively, hepatic output of VLDL or on the other hand lipid clearance from the blood might be disturbed [177-179].

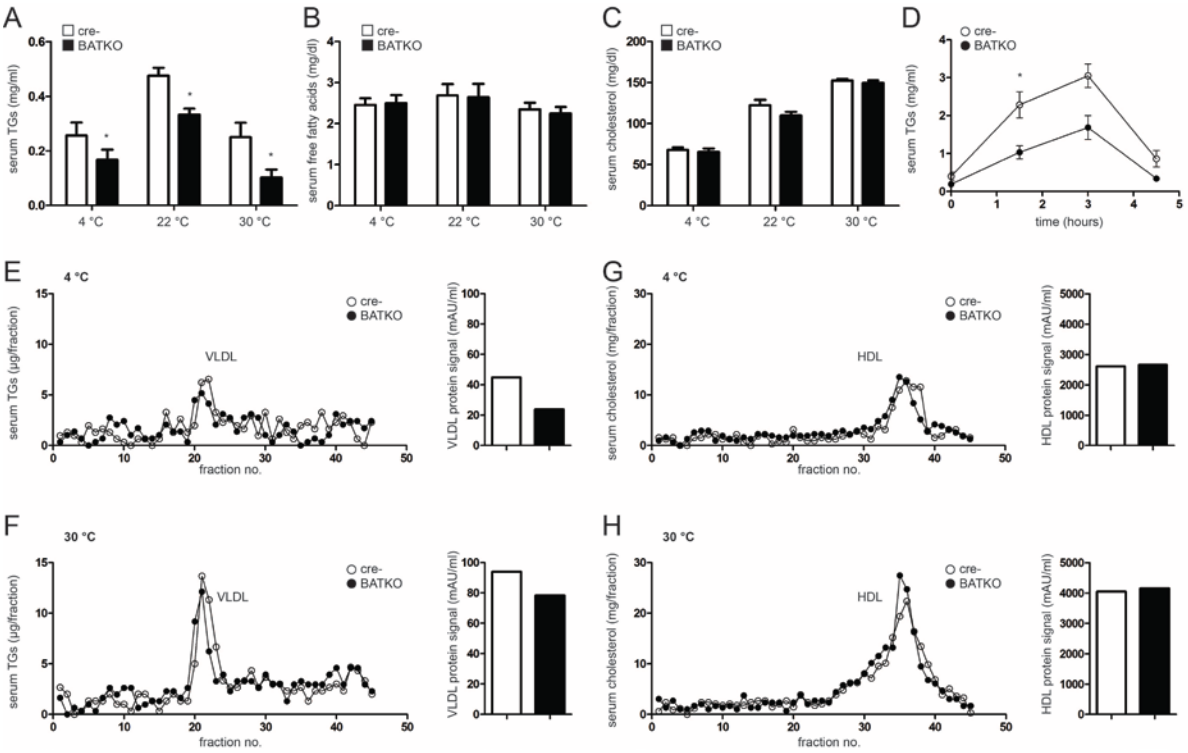

Figure 35. BATKO mice have lower serum VLDL levels. *Serum levels of BATKO and control mice housed at the indicated temperatures of (A) triglycerides (TGs), (B) free fatty acids or (C) cholesterol (n=3-10). (D) Oral lipid tolerance test (OLTT) in BATKO and control mice housed at 22 °C. Mice were fasted over night and an oral dose of 100 µl olive oil was gavaged, followed by blood sampling every 90 minutes and serum triglyceride determination (n=7-8). (E-H) Fast - protein liquid chromatography (FPLC) was performed from pooled serum of BATKO or control mice housed at 4 ° C or 30 ° C, pooling the serum of 6 mice per group and eluting 1 fraction of 0.5ml per minute. UV absorption signal was used to determine location and intensity of lipoprotein peaks and subsequently triglyceride and cholesterol concentration of the individual fractions were determined. (E-F) Triglyceride levels of BATKO and control mice housed at 4 ° C (E) and 30 ° C (F) respectively and corresponding protein intensity for VLDL peaks; and (G-H) cholesterol levels of BATKO and control mice housed at 4 ° C (G) and 30 ° C (H) respectively and corresponding protein intensity for HDL peaks. Values for (A-D) are expressed as means ± SEM, n = 3-10, *p<0.05, **p<0.01, ***p<0.001 ctrl vs. BATKO*

Food intake as assessed by weighing of food (Figure 30.B) had shown not to be affected by BAT-specific KO of TBLR, however we made use of the ability of phenomaster cages to more closely observe the behaviour of individual mice in response to acute metabolic challenges. We made the observation that the increase in food intake induced in mice by lowering the ambient temperature to 4 °C was blunted in BATKO mice (Figure36.A). This difference in feeding behaviour was found to disappear quickly when raising the temperature back to 30 °C (Figure36.B) or allowing the animals to acclimatise to 4 °C for 3 weeks before determining their food intake (Figure36.C). In accordance with that, food intake during re-feeding after over-night fasting was lowered in BATKO mice but then normalized quickly (Figure36.D). While these findings may partially explain altered serum lipid profiles in mice shortly after being challenged with cold stress, it is likely that also other factors contribute and thus allow the phenotype to be conserved in different temperature settings. We next determined fecal energy content and could prove that BATKO mice did not differ in terms of energy absorption from food (Figure 36.E).

We next turned our attention to the liver, being active in lipogenesis and being the responsible organ for VLDL output [180]. We could not detect increased phosphorylation of Acetyl-CoA carboxylase (ACC) as an indicator of lowered liponeogenesis (Figure 36.F). Likewise, at room temperature liver mRNA expressions of genes involved in lioponeogenesis and lipid homeostasis, like sterol regulatory element-binding protein (*Srebp1c*), stearoyl-CoA desaturase-1 (*Scd1*), sirtuin-1 (*Sirt1*) and angiopoietin-like 3 (*Angptl3*), were mainly unaffected by BAT-specific TBLR deficiency, even if, interestingly, there was a trend for angiopoietin-like 4 (*Angptl4*) to be up-regulated in BATKO livers. (*Figure 36.G*). As a final proof to outrule decreased hepatic VLDL production as the cause of the lowered plasma TG levels observed in BATKO mice we subjected animals housed at room temperature to a hepatic output assay. Mice were fasted for 16 hours to eliminate intestinal lipid absorption and chylomicron production, thus TGs accumulating in the serum can be attributed to hepatic production. To outrule plasma lipolytic activity and subsequent lipid clearance to tissues, tyloxapol was administered intravenously, allowing the observation of serum TG-accumulation. As expected, BATKO and control mice did not differ in terms of hepatic output (Figure 36.H).

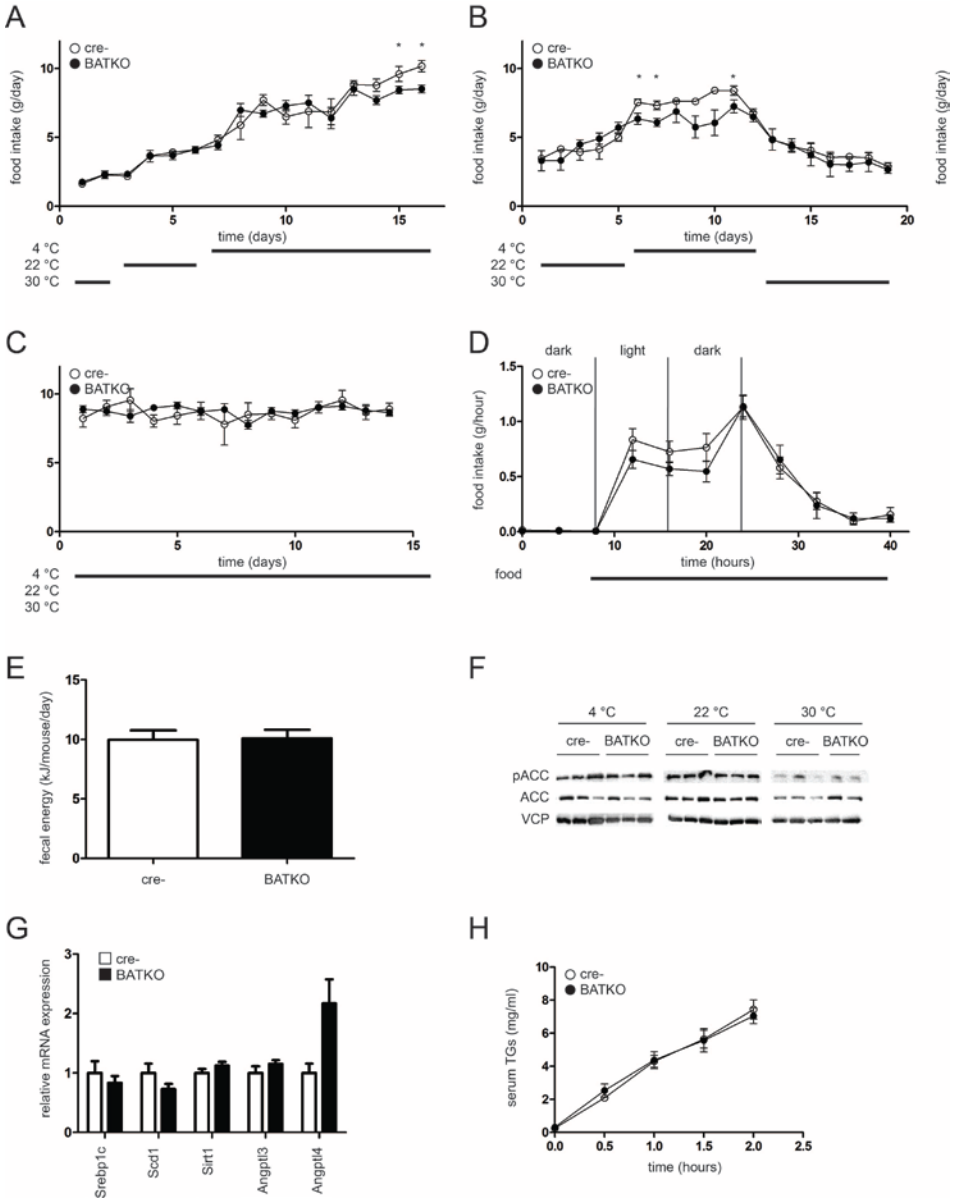

Figure 36. While hypophagic in acute cold stress, BATKO mice show no difference in fecal ilpid excretion or hepatic production. *(A) Food intake of BATKO and control mice housed individually in phenomaster cages where the ambient temperature was set to be 30 ° C for 3 days, 22 ° C for 3 days and 4 ° C for 10 days (n=6-7) or (B) 22 ° C for 6 days, 4 ° C for 7 days and 30 ° C for 7 days (n=3-4) or (C) were cold acclimatised for 3 weeks before measuring food intake for another 2 weeks (n=4-7). (D) Food intake of BATKO and control mice housed individually in phenomaster cages at 30 ° C, fasted for 16 hours, then re-fed with chow (n=9-10). (E) Fecal energy content in BATKO and control mice housed at room temperature was assessed by bomb calorimetry and total fecal energy content was calculated based on the fecal mass produced over the course of 24 hours (n=7).*

(figure legend continued on next page)

Figure 36. While hypophagic in acute cold stress, BATKO mice show no difference in fecal ilpid excretion or hepatic production. *(figure legend continued from previous page)*

*(F) ACC protein expression and phosphorylation in the liver of BATKO and control mice housed at the indicated temperatures (n=3-10). (G) mRNA expression of Srebp1c, Scd1, Sirt1, Angptl3 and Angptl4 in the liver of BATKO and control mice housed at 22 ° C (n=3-4). (H) Hepatic output of VLDL in BATKO and control mice fasted for 16 hours and i.v. injected with 500 mg/kg tyloxapol, determining serum triglyceride levels every 30 minutes (n = 7). All values are expressed as means ± SEM, *p<0.05, **p<0.01, ***p<0.001 ctrl vs. BATKO (comparing the avereage rate per condition).*

Since lipids were not lost to feces and were neither differentially produced by the liver, we assumed that the observed difference in serum TG levels in BATKO mice is caused by dysregulated clearance of TGs to peripheral tissues. We speculated that since, based on the respiration measurements shown above, enhanced thermogenic oxidation in BAT is unlikely to account for lowered serum TG levels, that the observed enhanced TG clearance in BATKO mice might rather be mediated by an endocrine BAT factor acting on peripheral tissues. Meta-analysis of all available data on tissue weights of BATKO and control mice at different housing temperatures was performed, compiling relative organ weights between genotypes across several independent studies. Interestingly we could reveal that WAT tends to be heavier in BATKO mice, which reached significance at 4 °C and 22 °C (Figure 37.A, 4 °C, Figure 37.B, 22 °C, Figure 37.C, 30 °C). In line with these findings, WAT, but not BAT or liver tended to exhibit higher TG concentrations in BATKO mice housed at 22 °C (Figure 37.D, BAT, Figure 37.E, WAT, Figure 37.F, liver).

To address the question, if and how BATKO mice differ from controls in regard to their TG clearance, we performed an oral lipid tolerance test (OLTT). Gavaging fasted animals housed at 22 °C with a defined volume of olive oil traced with ^{3}H-triolein allowed us to assess tracer accumulation in tissues after a defined period of time. First, accumulation of the administered tracer in the blood was followed over the time of the experiment, as well as the total TG levels. We found that while the absorption of ^{3}H-triolein was comparable between groups, even tending to be higher in BATKO compared to control mice (Figure37.G), total serum TG levels did not rise as drastically (Figure 37.H), indicative of higher clearance in the knockout animals. When measuring tracer accumulation in diverse tissues, we found that in general, BAT showed the highest TG uptake rate of all assayed tissues, followed by liver and then WAT and muscle. While BAT and liver TG uptake rates did not differ between genotypes, we could observe that in BATKO mice white adipose tissue had an 80 %

elevated TG uptake rate, and also the heart of these animals cleared TGs at a 30 % higher rate (Figure 37.I). In order to estimate the physiological relevance of these observations, we calculated total TG uptake by each tissue by factoring the respective depot size into their uptake rates (Figure 37.J). While it becomes evident that white adipose tissue in general is only a side player in lipid clearance compared to liver and BAT, it is still reasonable to assume that the enhanced deposit of TG into WAT of BATKO mice contributes to their lower serum TG levels.

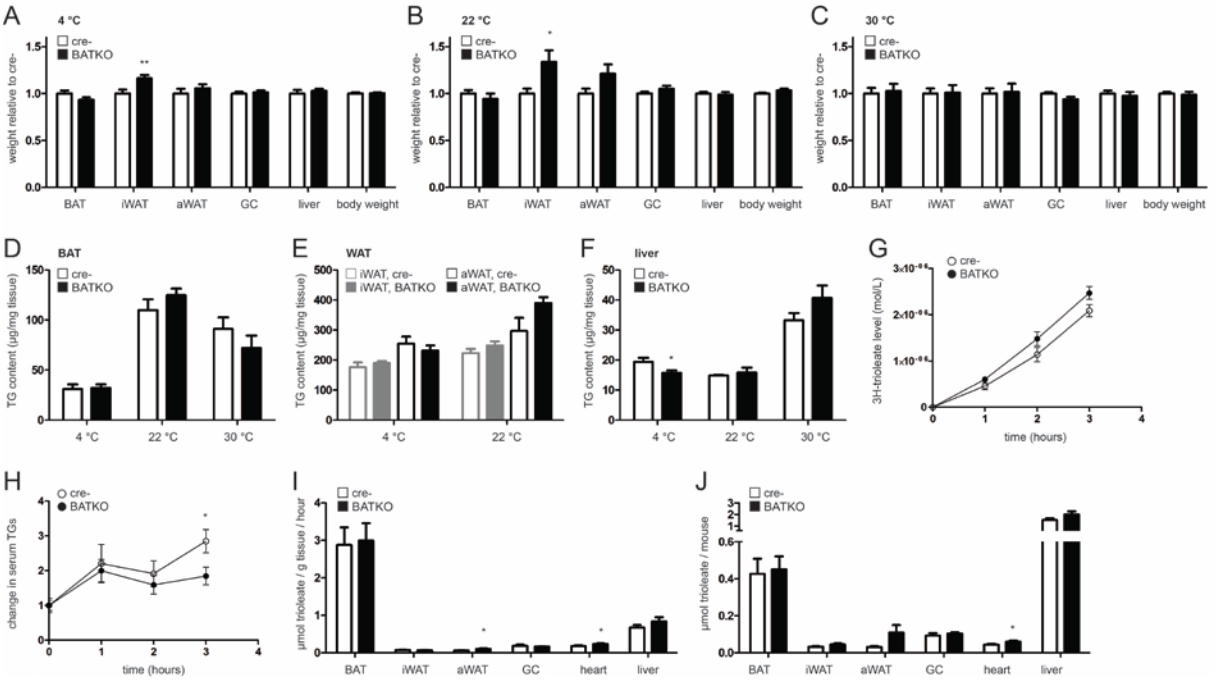

Figure 37. BATKO mice clear more triglycerides from their blood, which accumulate in WAT. *(A-C) Meta-analysis of organ (BAT, iWAT, aWAT, liver, GC) and body weights across all performed experiments, calculating the ratio of BATKO over cre- for all parameters and compiling data of mice housed at equal temperatures and diets for comparable time periods (n=17-33). Shown are mice housed at (A) 4 ° C, (B) 22 ° C or (C) 30 ° C. (D-F) Triglyceride (TG) content of (D) BAT, (E) WAT or (F) liver of BATKO or control animals at the indicated temperatures (n=3-10). (G-J) Oral lipid tolerance test. BATKO and control mice housed at 22 ° C were fasted for 16 hours and orally gavaged with 100 µl olive oil traced with 10 µCi/mouse 9,10-^{3}H(N)-triolein. Serum was collected every hour and the mice were sacrificed 3 hours after tracer administration (n=8). (G) ^{3}H(N)-triolein accumulation and (H) total TG concentration in the serum. (I) TG accumulation rate in BAT, iWAT, aWAT, GC, heart and liver. (J) Whole body accumulation was calculated multiplying each tissue's accumulation rate with its respective weight. All values are expressed as means ± SEM, n = 6-10, *p<0.05, **p<0.01, ***p<0.001 ctrl vs. BATKO*

Overall, we could observe that BATKO mice, albeit being genetically modified only in their brown adipose tissue, exhibit a systemic phenotype in the form of lowered serum VLDL levels, which is indicative of a signalling function of BAT to peripheral tissues. General energy loss to feces, or altered liver metabolism, were outruled as causative contributors to the phenotype. We did however observe that BATKO mice were hypophagic during acute cold stress and that they deposit more TGs to WAT compared to control animals, both of which presumably leads to loss of lipids from the circulation.

TBLR-deficient BAT differentially expresses secreted proteins

Having shown that TBLR-deficient BAT can cause systemic effects in mice we aimed to identify candidate proteins differentially secreted from BAT in the absence of TBLR. Among the targets most strongly regulated in BAT genome-wide expression analysis (see Table 5.), the regulation of *Ldlr* and *Apoc3* in BATKO mice stood out, both being known to regulate lipid clearance, the former enhancing it by mediating LDL internalization [181, 182], the latter dampening it by inhibiting lipoprotein lipase (LPL) [169]. Further, angiopoietin-like 3 (*Angptl3*), another inhibitor if LPL [183, 184], was found to be significantly down-regulated in KO BAT (albeit only to a small degree, thus not showing up in Table 5.). Further, ChIPseq data from preBAT cells as described earlier suggested TBLR binding to the *Lpl* gene as well as to several members of the angiopoietin-like family, such as angiopoietin-like 4 (Angptl4) (Figure38.A-B), a known inhibitor of LPL [185-187]. We thus investigated the expression of some of these secreted factors and found that while Angptl4 expression was not differentially regulated in BAT of BATKO mice, *Angptl3* expression was strongly reduced in TBLR-deficient BAT (Figure38.C). Interestingly, also other tissues, such as iWAT, aWAT and liver of BATKO mice at 4 °C expressed lower Angptl3 levels (Figure38.D), indicating that Angptl3 may not be a direct TBLR target in BAT but rather be affected downstream of TBLR regulated factors secreted by BAT. Other BAT secreted factors with known metabolic roles are, for example, fibroblast growth factor 21 (*Fgf21*) [188], *Leptin* [189, 190] or neuregulin 4 (*Nrg4*) [172], thus we profiled their expression. While there was no differential Nrg4 or Leptin expression in BAT of BATKO mice, there were lower levels of *Fgf21* at 4 °C, a state in which BAT mRNA expression is known to be induced and is supposedly mediating thermogenic response [191] (Figure38.E-F). Analyses of serum revealed that lowered Angptl3 expression was, at least in the cold, also reflected in the serum of BATKO mice, there was only a non-significant trend for serum FGF21 levels to be lower in the serum of BATKO mice at any housing temperature (Figure38.G).

Overall these data indicate that, directly or indirectly, TBLR ablation in BAT leads to systemically lower *Angptl3* expression, which we hypothesise may contribute to de-inhibition of LPL and subsequently to enhanced lipid import from the serum to WAT.

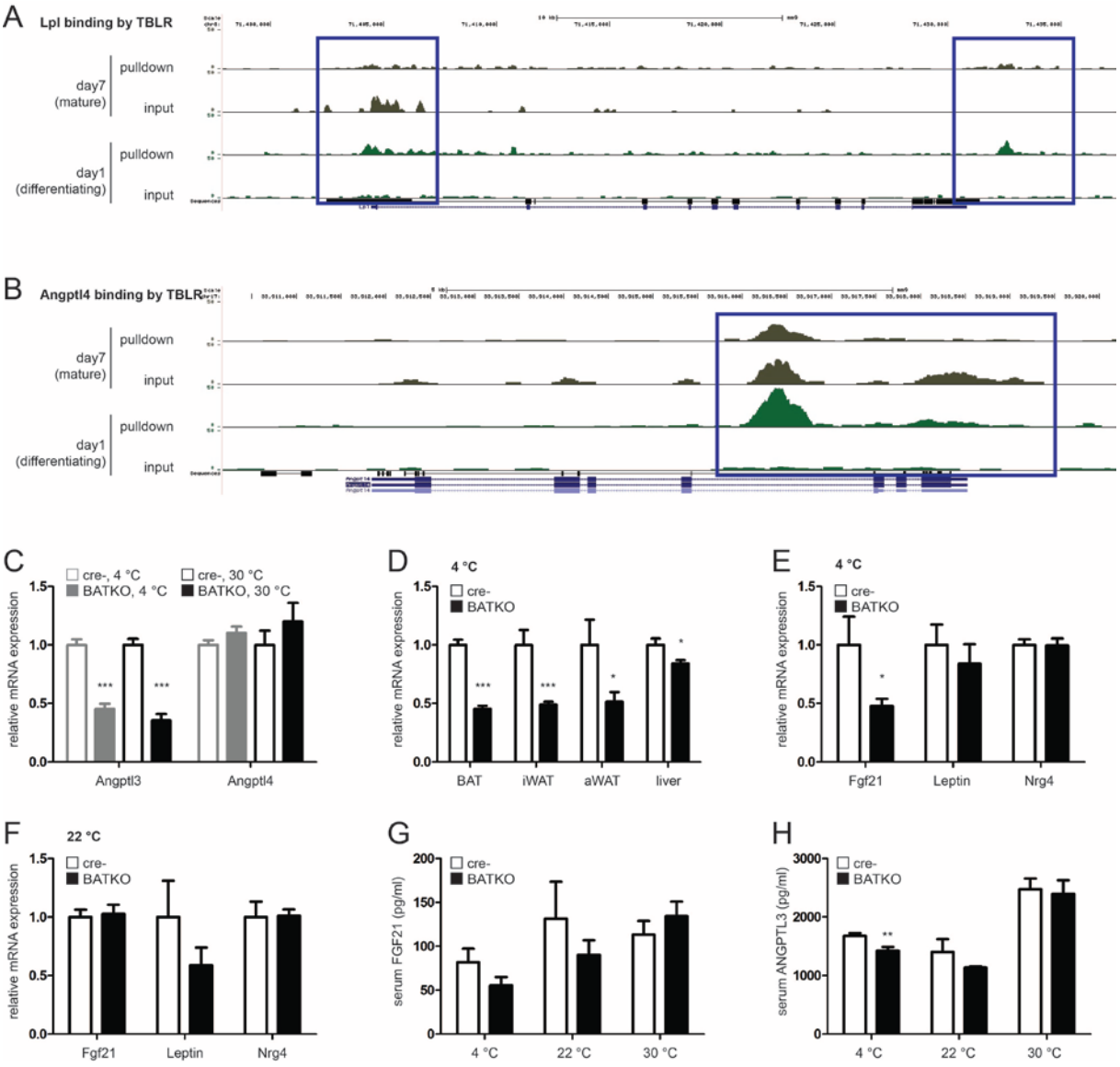

Figure 38. TBLR deficient BAT differentially expresses secreted proteins. *(A-B) ChIPseq for TBLR binding in preBAT cells was performed on day1 and day7 respectively of adipogenic differentiation and results were visualised in the UCSC genome browser, comparing sequence abundance upon TBLR-pulldown to chromatin input Control. (A) Ldl (A) and Angptl4 (B) binding are shown, blue boxes highlighting TBLR hotspots. (C) Angptl3 and Angptl4 mRNA expression in BAT of BATKO and control mice housed at the indicated temperatures (n=6-10).*

(figure legend continued on next page)

Figure 38. TBLR deficient BAT differentially expresses secreted proteins. *(figure legend continued from previous page)*

*(D) Angptl3 mRNA expression in BAT, aWAT or liver of BATKO and control mice housed at 4 ° C (n=4-7). (E) Fgf21, Leptin and Nrg4 mRNA expression in BAT of BATKO and control mice housed at 4 ° C (n=6-7) or (F) 22 ° C (n=5). (G) Cirulating FGF21 and (H) ANGPTL3 levels in serum of mice housed at the indicated temperatures were determined via enzyme-linked immunosorbent assay (ELISA) (n=4-10). All values are expressed as means ± SEM, n = 4-10, *p<0.05, **p<0.01, ***p<0.001 ctrl vs. BATKO*

iWAT browning and TBL potentially compensate for TBLO KO

In the study presented here we show that TBLR, being a transcriptional regulator known to be implicated in liver and white adipose tissue metabolism, not only needs to be present for proper differentiation of brown adipocytes, but also integrates non-thermogenic as well as acutely thermogenic rules in mature BAT. However, considering the striking phenotype of TBLR deficiency in WAT [139], BATKO mice were remarkably capable of adapting their metabolism regardless of the presence of TBLR, unless acutely challenged.

In vivo complex interlocked networks guarantee backup mechanisms in the case of defects in individual players of a regulatory network, thus it is challenging to experimentally demonstrate the specific role of individual players by depleting them. One of these backup mechanisms, in the case of brown fat, is the ability of white adipose tissue to adapt brown adipocyte features in order to back up the defect in BAT function [192]. We thus hypothesised that in BATKO mice one of the factors compensating for the absence of TBLR in BAT, particularly in the presence of thermogenic stimuli, might be white adipose tissue browning. At room temperature, iWAT of BATKO mice (albeit itself expressing normal levels of *Tblr*) demonstrated slightly elevated expression of brown marker genes (Figure39.A). Also at 4 °C, where iWAT browning is part of the normal cold adaptation process, iWAT of BATKO mice on top of that expressed higher levels of *Ucp1* (Figure39.B), even if morphology of BATKO iWAT largely resembled that of control animals (Figure39.C). Overall these findings indicate indicate that iWAT browning is part of the compensatory mechanism rescuing BATKO mice from the absence of TBLR.

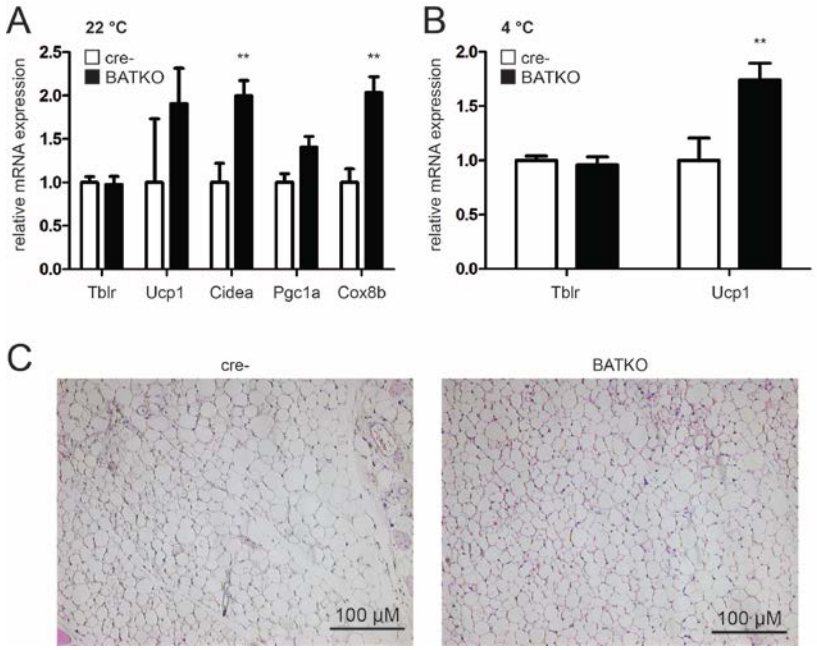

Figure 39. iWAT of BATKO mice shows compensatory browning. *(A) mRNA expression of Tblr and of the brown marker genes Ucp1, Cidea, Pgc-1α and Cox8b in iWAT of BATKO and control mice housed at 22 ° C (n=3-4). (B) mRNA expression of Tblr and Ucp1 in iWAT or (C) hematoxylin and eosin staining of iWAT slices of BATKO and control mice housed at 4 ° C for 3 weeks (n=10). All values are expressed as means ± SEM, *p<0.05, **p<0.01, ***p<0.001 ctrl vs. BATKO*

However the most likely factor capable of compensation for the deletion of TBLR is its homologue TBL. Analogously to in vitro studies, in which double knock down of TBLR together with TBL exacerbated the observed phenotype (Figures 17-19), we expect the ablation of TBL in BATKO mice to allow the observation of a more pronounced phenotype. To address this problem we designed a BAT-specific adeno-associated viral (AAV) vector expressing a microRNA targeting *Tbl*, aiming to achieve *Tbl* knockdown in vivo upon intravenous injection of the virus. To achieve expression of the miR-Tbl specifically in BAT, it was necessary to set it under the control of the BAT specific *Ucp1* promoter. However the *Ucp1* promoter region in its original form is too long to allow packaging of the final construct to a double stranded AAV. Thus a shortened version was generated by amplifying the two minimal elements identified as to being crucial for the promoter's function ("220bp element" and "cre4pro element") by Kozak et al [193], with their kind permission to use the constructs described in this publication and with the primers listed in Table 9. The described elements were inserted into the pGL3-Basic Vector (Figure 40).

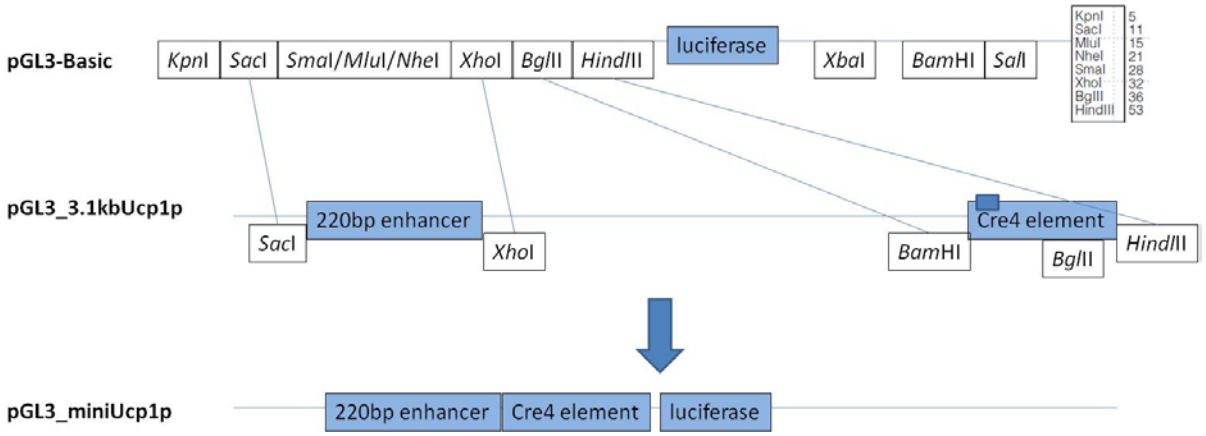

Figure 40. The Ucp1 mini promoter was generated by insertion of 2 crucial elements to a pGL3-Basic Vector. *From the template vector pGL3_3.1kbUcp1p (citation), the desired sequences were amplified using PCR primers adding the restriction sites necessary for subsequent addition to a luciferase reporter vector.*

Functionality and specificity of the mini-promoter was confirmed by luciferase assays performed by Eva Gröter, showing that it is responsive to rosiglitazone or forskolin in a brown adipocyte-specific way as compared to in non-adipocyte cells (data not shown). Thus, the *Ucp1* mini-promoter was amplified and subcloned to a double stranded AAV construct expressing a microRNA targeting *Tbl*, replacing the present LP-1 promoter (pdsAAV-LP1-GFPmut-miR-Tbl1).

Since systemic application of AAV is expected to lead to large amounts of the virus being deposited to the liver, it is possible that even with a tissue-specific promoter some leaking of the *Tbl* microRNA expression might affect expression of liver *Tbl*. Therefore, a target site for the liver-specific miR-122 was inserted, resulting in an AAV construct that, when expressed in an off target manner in hepatocytes, would be degraded (pdsAAV-GFPmut-miR122site-miR-Tbl1) (Figure 41, Figure 42). Analogously, vectors expressing miR-NC or miR-Tblr1 were produced.

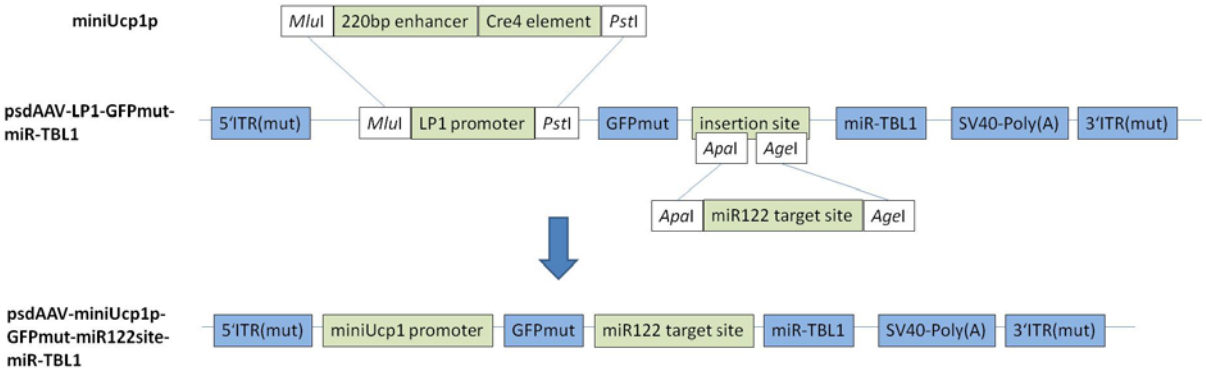

Figure 41. The Ucp1 mini promoter and a miR-122 binding site were inserted to an AAV miR-Tbl expression vector*. Using the available double stranded AAV vector expressing miR-Tbl1 (pdsAAV-LP1-GFPmit-miR-Tbl1), a BAT specific version was created by replacing the present LP1 promoter with the newly generated Ucp1 mini promoter and by inserting a target site for miR-122 mediated degradation of the expressed product in the liver.*

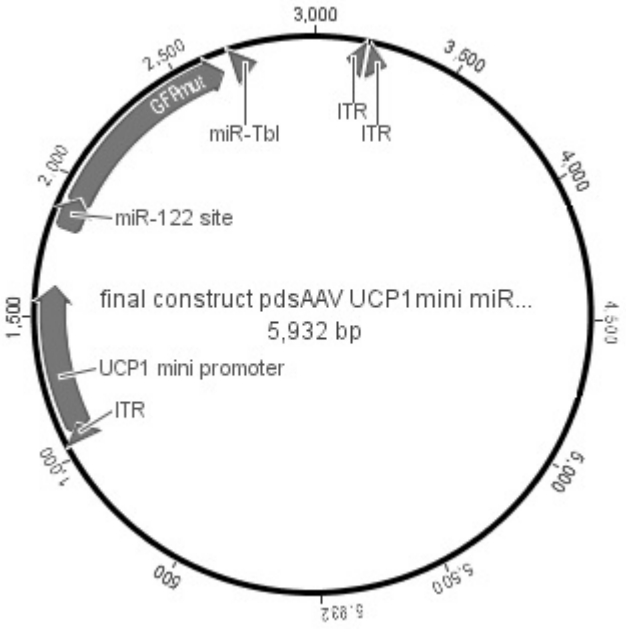

Figure 42. Final construct pdsAAV-GFPmut-miR122site-miR-Tbl1*. An illustration of the he final construct cloned as described above was created using the Genious software.*

DISCUSSION

The presented work is casting light on mechanisms controlling the regulation of browning of white adipose tissue as well as on the function of classical brown adipose tissue. Uncoupling of the respiratory chain may emerge as a promising strategy to treat obesity [194]. While potent chemical activators are available, their use or application is limited by toxicity [195], thus understanding the physiological regulatory mechanisms controlling BAT recruitment and activation is crucial for safe therapy.

The first part of this thesis elucidates the interplay between insulin signaling and the recruitment of brite adipocytes in white depots. While it was known before that obesity correlates with reduced brite capacity [196, 197], it was not clear whether this correlation is based on a causative connection. We published our findings on this topic, outlining two hypotheses on how insulin signalling and brite capacity might be co-dependant [198]. On the one hand it is known that insulin is crucial for general adipogenic development [199], raising the possibility that the recruitment of brite cells might depend on functional insulin signalling and that upon the onset of insulin resistance in obesity this in turn leads to a lesser degree of browning of WAT. Adressing the problem from the opposite angle, our alternative hypothesis on the correlation of obesity and lower BAT activity is that lower brite recruitment establishes before the onset of obesity, eventually causing weight gain by lowering insulin tolerance. It is known that BAT has the potential to systemically clear glucose, thereby improving insulin sensitivity in humans [42, 43], however if brite cells and tissues per se are more responsive to insulin remained unressolved.

Surprisingly, we discovered that β3-adrenergic stimulation was able to fully recover brite activation, allowing mice either deficient of insulin or insulin resistant to normally induce the browning program in WAT. These findings are in line with a recent study on classical BAT that demonstrated that insulin/IGF-1 signalling are dispensable for activation of the BAT thermogenic program [143].

When tackling insulin sensitivity in the brite recruited state, we postulated that previous studies neglected to distinguish between systemic and cell- or tissue-specific insulin sensitivity. We show that brite cells exhibit strongly elevated basal glucose uptake, irregardless of the presence of insulin. Further, stimulating either brite cells or brite recruited mice with insulin does result in higher glucose uptake to cells and clearance from the system than in the white state, however the relative response of the system compared to the non insulin-stimulated state is unchanged. Thus, it is the presence of brite tissue, not its

sensitivity to insulin, that is promoting the beneficial effects on glucose homeostasis described in previous studies. Higher presence of brite WAT translates to higher target tissue abundance for insulin. However, while in terms of the whole organism thus the brite state allows for increased glucose clearance upon insulin stimulation and can be described as more insulin sensitive, this is not based on cell-specific sensitivity.

The mechanism allowing brite cells taking up elevated amounts of glucose independently from insulin may in part be due to the expression of the insulin-independent glucose transporter GLUT-1, which we, for the first time, reported to be markedly increased upon browning. This is in line with the fact that while GLUT-1 is known to only play a minor role in WAT [200], but is expressed in high abundance in BAT [201]. What still remains to be understood is the upstream regulatory cascade leading to induction of GLUT-1 in brown and brite adipocytes. Partially this may be mediated by FGF-21, which is elevated two-fold in brite compared to white adipocytes (data not shown) and is known to elevate GLUT-1 expression [202]. However, we showed that high fat diet fed mice, which are reported to be FGF-21 resistant [202], are able to upregulate GLUT-1 in response to browning, thus additional mechanisms may contribute to this effect. Also, GLUT-1 induction does not seem to be the only mechanism aumenting glucose uptake in brite adipocytes, since we show that browning can overcome the reduction in glucose uptake observed upon specific GLUT-1 inhibition.

Overall, we showed that the brite state did prove beneficial for systemic glucose homeostasis and could circumvent insulin resistance. This was due to the fact that regardless of functional insulin signalling, brite recruitment could take place. Further, brite cells and tissues had the capacity for higher glucose uptake, likely through a multilayer network involving elevated expression of the insulin-independent glucose transporter GLUT-1. Thus, even in the insulin resistant state, recruitment of brite adipose tissue promises to counteract hyperglycemia in diabetic patients.

The second part of this thesis was investigating the regulation and role in brown adipose tissue of the transcriptional co-regulator TBLR, which acts together with its homologue TBL in multi-protein complexes regulating global gene expression. TBLR is well described in different disease settings like mental disabilities [133-135] or cancer, where depending on tissue type it can act as pro-tumorigenic [137] or anti-tumorigenic [136]. Our group identified the role of TBL and TBLR as metabolic players, preventing hepatosteatosis and hypertriglyceridemia in the liver by promoting fatty acid oxidation [132], and preventing obesity by regulating lipolysis in WAT [139].

Using brown adipocyte cell lines as well as brown fat-specific TBLR knockout mice, numerous findings have been presented here casting light on TBLR-dependent brown adipose mechanisms. This study focussed mainly on TBLR rather than TBL for the following reasons: (1) in WAT, TBLR alone was sufficient to mediate effects on lipolysis independent of TBL [139], (2) we found *Tblr* to be regulated stronger than *Tbl* in response to the signal that activates BAT, β-adrenergic stimulation, and (3) while for the in vivo deletion of *Tblr* we had a mouse model available, *Tbl*, located on the X chromosome, could currently not be deleted in mice. However it should be kept in mind that the actions of TBLR and TBL are likely interdependent, since it is known that these factors often have additive effects and manipulating one of them can, by disrupting their interaction, impacts the actions of the other [132].

The data presented make it clear that when describing the role of genetic regulators in adipose tissue, it has to be distinguished between the phase of adipogenesis where cells shift from growth to differentiation, and the specific metabolic function of mature, differentiated cells.

We show that upon induction of adipogenic differentiation, the expression of *Tblr* was up-regulated, while that of *Tbl* was reduced. Since in silico analyses identified hotspots in the *Tblr* promoter that in human are reported to be bound by factors involved in adipogenesis, such as C/EBPβ , (E)p300, FOXA1, FOXA2 or GATA3, it can be assumed that the observed regulation of *Tblr* is part of the physiological adipogenic program. The same can be assumed for the observed regulation of *Tbl*, which similary in humans is targeted by C/EBPβ and PPARα (data is publically available on https://genome.ucsc.edu). The possibility remains that the observed regulation was an artefact of cell culture, since we showed that one of the agents used to induce differentiation, dexamethasone, was able to directly induce *Tblr* expression in already differentiated adipocytes.

Still, we demonstrated that TBLR is an active player in adipogenesis, which was not only regulated transcriptionally, but also targeted genes involved in the differentiation of adipocytes by direct DNA binding. Interestingly we observed that immediately upon induction of differentiation, pathways over-abundantly targeted by TBLR binding were found to be both, pathways regulating cancer and growth and pathways regulating metabolic functions such as adipocytokine and insulin signalling and lipogenesis. TBLR can, depending on interaction partners and targets, act either by mediating gene suppression [130] or activation [132]. Thus the observation that its targets are involved in opposing pathways indicates that TBLR containing complexes have the potential to serve as a common platform for the cell to switch between pro- and anti-proliferative pathways.

Surprisingly, despite being up-regulated during differentiation, we did not observe a general impairment of adipogenesis upon TBLR depletion in terms of morphology or general adipocyte marker gene expression. Further, by linking binding data obtained by ChIPseq to global gene expression analyses, we showed that brown adipocyte-specific gene sets, specifically components of the mitochondrial respiration chain and the key BAT gene *Ucp1*, were repressed by *Tblr* during differentiation. Considering that we showed *Tblr* expression to be elevated more strongly during white than during brown adipogenesis it is possible that *Tblr* promotes white rather than brown adipogenesis. This inference is supported by the fact that it targets and represses *Ppargc1a* and *Ppargc1b*, which cause a switch from white to brown adipogenesis [127].

Interestingly, two of the most strongly bound targets of TBLR were found to be *Tblr* itself and *Tbl* (data not shown), which might indicate that upon initial induction there is a feedback loop bringing *Tblr* expression back down to normal levels. However TBLR is unlikely the only causative factor for the observed down-regulation of *Tbl* during adipogenesis, since we never observed strong *Tbl* up-regulation in TBLR-deficient cells (data not shown).

Despite expressing higher levels of *Ucp1* and mitochondrial markers, brown adipocytes lacking TBLR during their differentiation did not exhibit an elevated oxygen consumption rate. On the contrary, basal respiration as well as glycolytic rate were found to be reduced in this setting. However, treatment with the chemical uncoupler FCCP not only rescued the phenotype, but allowed even higher respiration than in control cells, which was to be expected considering the higher content of mitochondrial genes. Since we also observed impaired import of glucose in adipocytes lacking TBLR during differentiation, it is conceivable that the lowered metabolic rates in knockdown cells depend on limited substrate availability,

which is an assumption strengthened by the observation that insulin treatment was able to rescue the defect. Further, there was no shift between respiration and glycolysis, as would be expected if one of those pathways was selectively affected by the absence of TBLR. And finally, norepinephrine treatment, known to stimulate UCP-1-mediated uncoupling via generating fatty acids as substrate and activators [82, 99], was not able to cause higher respiration in knockdown cells, despite higher *Ucp1* expression, further indicating that these cells lack available substrate.

It has to be considered, that lower glucose import to adipocytes, which also translated to lower lipid generation, was only clearly pronounced if both TBLR and TBL were ablated at the same time. Still, in both settings, respiration and glycolysis were impaired. Therefore, it is likely that other factors contribute to decreased basal metabolism despite higher mitochondrial capacity.

The presented data clearly establish a role of TBLR during adipogenesis. We propose the following model, as outlined in Figure 43. *Tblr* expression is induced by adipogenic activators. TBLR as part of the NCoR complex, targets either pro- or anti-proliferative pathways, depending on the nuclear environment such as available binding partners. In an adipogenic setting it targets pathways involved in the regulation of white versus brown differentiation, lipid and glucose handling, facilitating cells to mature to functional adipocytes.

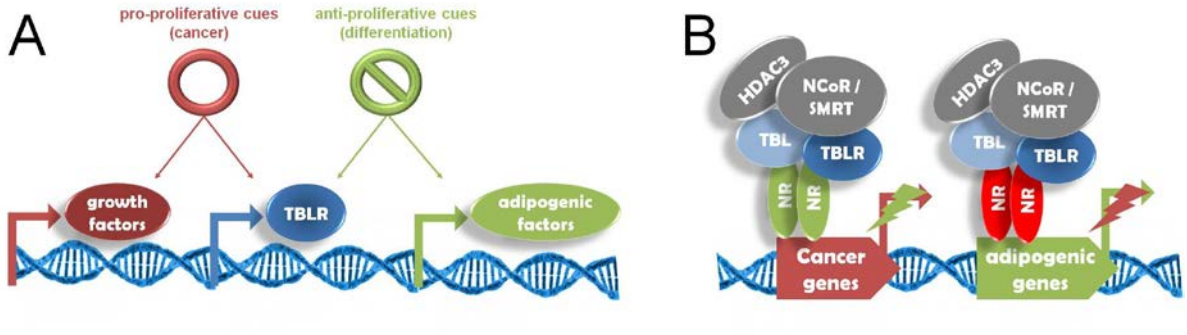

Figure 43. TBLR serves as a common platform to balance pro- and anti-proliferative cues. *(A) TBLR expression is under the control of growth promoting cues (E2F, MAX, MYC, FOS, JUN), but also adipogenic cues (C/EBPβ, (E)p300, FOXA1, FOXA2 or GATA3). (B) Binding partners and mediated response of TBLR in the co-regulator complex depend on the environment (pro-growth or pro-adipogenic setting).*

The actions of TBLR, once mature brown adipocytes have formed, seem to have less impact. Overall we observed lower TBLR to DNA binding frequency in fully differentiated brown adipocytes compared to differentiating cells. This correlated with the observation that

knockdown of TBLR in mature cells did not reproduce the defects in glucose import or basal lipolysis found in cells lacking TBLR during differentiation. This may be partly attributed to technical limitations, since due to high protein stability of TBLR, its levels remain stable for days after administration of shTblr expressing AV, hence knockdown in mature adipocytes was weaker compared to earlier KD (Figure 24.B and D). Still, in vivo results were in accordance with in vitro findings, global gene expression analysis in TBLR-deficient BAT revealed that there was hardly any alteration in expression patterns. Interestingly, despite being the most strongly bound gene in mature adipocyte cells, and to having been shown to being the most strongly de-repressed gene upon TBLR depletion during brown adipocyte differentiation, *Ucp1* was not found to be repressed by TBLR in mature brown adipocytes. On the contrary, in cell culture, upon double knockdown of *Tblr* and *Tbl*, *Ucp1* expression was even decreased.

Mature adipocytes differ from pre-adipocytes as they switch from β1- to β3-adrenergic receptor (β1/3-AR) expression [85]. Downstream of the β3-AR, the MAPK pathway mediates the thermogenic response in acute cold stimulation [78]. TBLR, whose promoter is predicted to be targeted by components that are under the control of the MAPK pathway, such as MYC, FOS and JUN [157-159], was found to also target the MAPK signalling pathway by binding to its components, when performing ChIPseq analysis of mature brown adipocytes. It can thus be assumed that the role of TBLR differs from its actions during differentiation once this signalling pathway regulating the key brown adipogenic function of thermogenesis is established. In line with our expectations that in mature BAT TBLR would be involved in the regulation of the thermogenic program, *Tblr* expression was found to be strongly induced both in cell culture and in vivo upon treatment with β3-adrenergic agonists. This induction was much stronger in the mature adipocyte fraction compared to the undifferentiated stromal vascular fraction of BAT, and was dependent on cAMP signalling, since applying a PKA inhibitor blunted the response. Further, insulin signalling also regulated *Tblr* expression, as treatment of mature adipocytes with insulin or re-feeding in fasted mice decreased *Tblr* expression. In HFD-fed mice, which are known to be insulin resistant [147], *Tblr* levels in BAT were elevated. It is not clear by which mechanism insulin affects *Tblr* levels. Since insulin is known to disrupt β3- adrenergic signals to PKA [203], its inhibition of *Tblr* expression might be indirect, via blocking the MAPK pathway dependant induction described above.

It is known that ablation of TBLR from all adipose tissues impairs lipolysis and causes obesity [139]. However the brown fat-specific TBLR deficiency of BATKO mice did not result in the same phenotype. Neither in adipocytes in which TBLR was knocked down after

differentiation into mature cells, nor in BAT explants from BATKO mice, we observed comprised fatty acid release or lipase phosphorylation. Further, BATKO animals did not differ from controls in terms of body weight, body composition, glucose tolerance or glucose clearance to tissues.

We thus postulate that TBLR in BAT, being shown to be under the control of brown fat-specific signalling cascades, fulfils divergent roles than that in white adipose tissues.

The absence of long term effects and the transiency of *Tblr* induction upon β3-adrenergic stimulation prompted us to hypothesise that a role of TBLR in BAT lies in the mediation of the acute thermogenic response. In fact, while in both cold and warm settings BATKO mice showed normal respiration and body temperature, challenging mice acclimatised to thermoneutrality with an acute β3-adrenergic stimulus [204] revealed a defect in maximal thermogenic capacity in BATKO mice. This confirmes TBLR is an indispensable player in mediating acute thermogenic activation in response to β3-adrenergic stimulation. The mechanisms that are responsible for the ability of BAT to compensate for the absence of TBLR upon prolonged cold exposure are not yet clear. It can be speculated, based on the fact that TBLR in mature brown adipocytes was shown to bind to components of the MAPK pathway, that TBLR deficiency in BAT results in dysbalanced levels of players of this pathway, hampering its ability to mediate the acute β3-adrenergic response. This hypothesis is outlined in Figure 44.

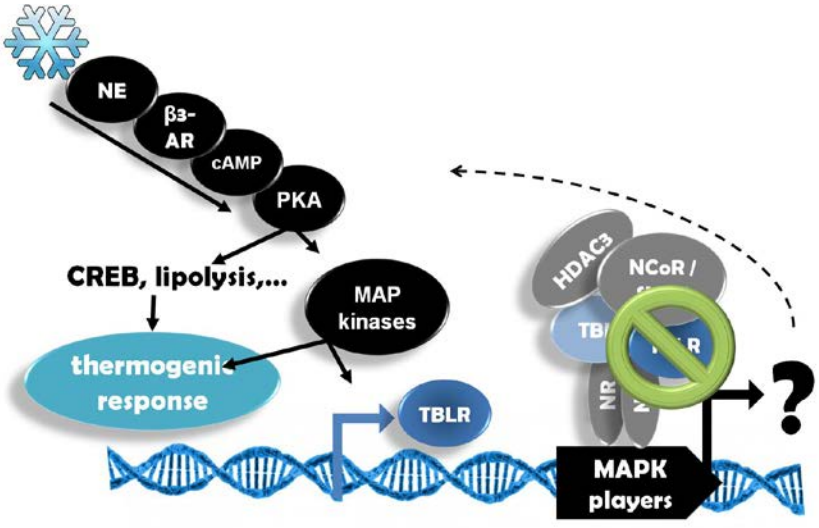

Figure 44. TBLR balances players required for the acute activation of BAT. *TBLR binds and regulates players of the MAPK pathway, the canonical route of acute activation of BAT. This may explain why TBLR deletion hampers the ability of BAT to react to acute β3-adrenergic stimulation.*

Unexpectedly, we found that despite robust compensation for the knockout of TBLR in BAT in most settings, BATKO mice maintained lower serum TG levels, not only in the cold, but also at room temperature and at thermoneutrality. Since KO BAT was found to have either impaired or unaltered metabolic capacity, this phenotype cannot be explained by altered BAT lipid oxidation. Since lipid uptake into BAT was not increased, nor did lipid content or histology indicate elevated uptake into BAT, it becomes evident that the TGs must be lost via a different route. The emerging understanding that BAT has the capacity to act as an endocrine organ [172, 173] lead us to the assumption that the KO of TBLR in BAT disrupts signalling to other organs, which in turn induces the observed decrease in serum TG levels. Since FPLC analyses revealed that the depleted triglycerides correspond to the VLDL fraction, we initially assumed that hepatic VLDL output might be decreased in BATKO mice. The liver is a known target of BAT endocrine signals [172] and the responsible organ for VLDL production [205]. However we did neither observe differential VLDL output in BATKO mice nor lipid accumulation in the liver of KO animals as would be expected in the case of diminished TG excretion [206]. Further, there was no differential loss of energy to feces and feeding behaviour was largely normal. Curiously, BATKO mice tended to be hypophagic during the initial phase of cold challenge, however since they quickly recovered, this behaviour is unlikely to explain the markedly lower serum TG levels observed at different housing temperatures.

We observed however, that WAT of BATKO mice tended to be heavier and have higher lipid content compared to control animals. Indeed, the uptake of labelled triglycerides to white adipose tissue was found to be slightly but significantly elevated in BATKO mice.

Lipid uptake to adipose tissue is mainly mediated by LPL [207], which leads to VLDL clearance from the serum [208]. Thus, if there is a factor secreted by BAT increasing TG deposit to other tissues, we hypothesised this would be a factor influencing LPL activity. We found TBLR-deficient BAT to express lower levels of *Fgf21* at 4 °C, a secreted hormone mediating glucose and lipid metabolism and being under thermogenic control in BAT [191]. However levels of circulating FGF-21 were not altered in BATKO mice compared to controls. While we thus exclude FGF-21 to being the responsible hormone for the observed systemic effects, it is still very well possible that FGF-21 regulation in TBLR-deficient BAT might contribute to the metabolic capacity of BATKO mice. Recent reviews suggest that FGF-21 also acts in an autocrine manner [209], and by targeting factors like PGC-1α [210] might influence BAT function independent from circulating protein levels.

ChIPseq analysis suggested that in brown adipocytes, besides *Lpl*, *Angptl4*, a known secreted inhibitor of LPL [211], was targeted by TBLR. *Angptl4* expression was not found to be different in BATKO mice, however, strikingly, the expression of a related LPL inhibitor, *Angptl3* [211], was reduced not only in BAT, but also in WAT, muscle and to some extent in liver, both in the cold or at thermoneutrality. Even circulating ANGPTL-3 levels were found to be reduced at 4 °C. Since it is known that *Angptl3* KO leads to lower serum TG levels [183], its downregulation in BATKO mice might partly be responsible for the lower TG levels observed, potentially by inhibiting WAT associated LPL. However it is not clear whether LPL de-inhibition can by itself suffices to explain the reduced serum TG levels, since studies on adipose-specific knockout of LPL or studies tracing TG uptake showed that it is rather BAT than WAT being responsible for TG clearance from the serum [111, 212]. We did however not observe increased lipid uptake or accumulation in BAT.

While ANGPTL-3 may not be the only responsible mediator of the observed systemic response, it is still noteworthy that BAT-specific knockout of TBLR induced robust systemic changes in gene expression. *Angptl3* expression is known to be suppressed by insulin and leptin [213], however BATKO mice did not express higher levels of leptin and also serum insulin levels were never found to be altered (Figure 31.D). We hypothesise, since *Angptl3* is reported to being regulated by hormones such as thyroid hormone [214] or ligands of the liver X rexeptor (LXR) [215, 216], that BATKO mice differently secrete hormones that in turn alter gene expression and lipid handling in peripheral tissues. The classical hormone known to be secreted by BAT is thyroid hormone (triiodothyronine, T_3) [173, 217, 218], so we hypothesise that TBLR in mature BAT regulates the expression of hormones that act on peripheral tissues, altering their capacity for lipid clearance. (Figure 45). This hypothesis remains to be experimentally tested.

We can only speculate on the necessity of BAT to up- or down-regulate peripheral lipid clearance. We suggest that BAT, being an organ known to clear circulating lipid levels [111, 219], may depend on sufficient TG supply when challenged with acute cold exposure. This might be an additional or even alternative explanation for our findings that BATKO mice exhibit a defect in the acute induction of the thermogenic response, potentially just lacking fuel, before compensatory mechanisms such as WAT lipolysis [96-98] are triggered.

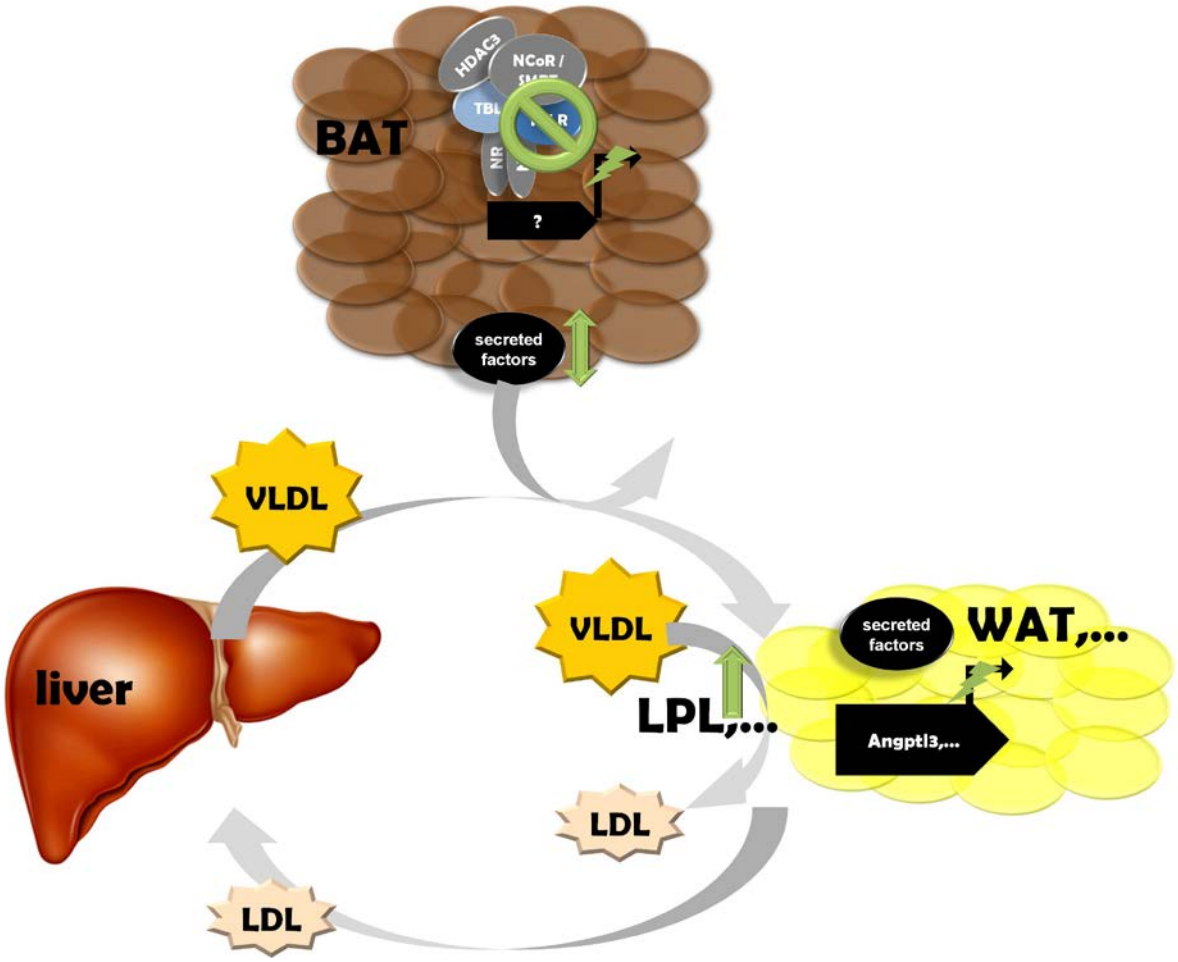

Figure 45. TBLR KO in BAT changes systemic gene expression and lipid clearance. *BATKO mice are hypotriglyceridemic and express lower levels of Angptl3 in WAT and muscle. This may lead to LPL de-inhibition and enhanced lipid deposit to peripheral tissues.*

As a side-note it is worthy to mention that the estrogen antagonist tamoxifen, the drug we used in this model to induce TBLR knockout, was shown to modulate serum lipid levels in human. Some reports found a decrease in VLDL [220], others an increase [221]. While the inducible Cre-lox system uses a mutated form of the ER to control Cre recombinase expression, thus excluding its activation by endogenous estrogen, tamoxifen-induced toxicity and side-effects are still possible [222]. In our model cre$^-$ control animals were treated with the same dose of tamoxifen to account for unspecific side effects. However, the TBL/TBLR co-regulator complex is reported to regulate, among others, the actions of the estrogen receptor (ER) [3]. Thus, some possibility remains that upon the onset of TBLR deficiency, ER-mediated signals caused by tamoxifen are processed differently, potentially altering metabolism. Whether this would have to be considered a side-effect of tamoxifen or rather a phenotype of TBLR deficiency can be debated.

A last consideration has to be made to conclude our findings, and also generally when working with tissue-specific knockout models, namely the validity of promoter-usage in knockout models. This study uses the *Ucp1* promoter to control the expression of the Cre recombinase, triggering TBLR KO supposedly only in fully differentiated brown adipocytes. However, *Ucp1* expression is activated already during the process of adipogenic differentiation. In cell culture, we found *Ucp1* mRNA to be undetectable in pre-adipocytes, however as early as 1 day after induction of differentiation, mRNA levels increase gradually, reaching 300-fold higher *Ucp1* mRNA levels 1 week later (data not shown). It is thus possible that when treating mice with tamoxifen, a part of the SVF pool is targeted together with the mature adipocyte fraction. Still, having chosen an inducible knockout model, we limit this possibility compared to constitutive models, in which the Cre recombinase is not only activated upon stimulation, but can mediate knockout whenever its promoter is activated. The presented study could not reproduce some findings showed previously on constitutive TBLR knockout under the control of the promoter of aP-2 (adipocyte protein 2, also known as fatty acid binding protein 4, FABP4) [139]. While the main reason for this discrepancy seems to be differential action of TBLR in white versus brown adipose tissue as outlined above, it still needs to be considered that the models differ in terms of what cells are targeted and when. Constitutive KO driven by the *Fabp4* promoter leads to TBLR deletion in cells as soon as *Fabp4* starts to be expressed during adipogenesis. This is rather early, and there are even subpopulations of pre-adipocytes expressing aP-2 [223]. On the other hand tamoxifen-induced KO driven by the *Ucp1* promoter allows adipocytes to differentiate fully before the deletion is triggered. Thus, the reason that the study on whole fat-specific TBLR KO observed a markedly stronger phenotype may be partly attributed to the fact that TBLR knockout is, at least partially, present during differentiation of adipocytes, which also in brown adipocytes would be expected to cause more severe effects, based on the data presented above. Further, the *Fabp4* promoter, while widely used for adipocyte-specific KO models, it was recently shown that it may be of limited use for this purpose, since it also drives gene expression in other tissues, such as the developing central nervous system [224].

A further advantage of using inducible KO systems in particular when utilizing the *Ucp1* promoter is that this way not only brown but also brite adipocytes can be targeted. We showed that while tamoxifen administration did not induce KO in white adipose tissue, administration of a second dose after cold administration did reduce TBLR levels by 30% (Figure 28.F), which is less than in brown and probably reflects the fraction of browned adipocytes now having activated the *Ucp1* promoter. Thus, this mouse model is an interesting tool for studies on white adipose tissue browning.

CONCLUSION AND OUTLOOK

The study presented here helps to understand tissue and stage dependence and specificity of general regulatory machineries of gene transcription networks, using the transcriptional co-regulator TBLR as an example. It became clear that the master-regulator TBLR, for which a role in the regulation of lipid and white fat metabolism recently was established, serves as a common platform to mediate very distinct responses, probably depending on its environment and interaction partners. During adipogenesis, TBLR regulates the players of this cascade, helping cells to differentiate into adipocytes fully competent of substrate import and usage, and supposedly suppressing brown in favour of white fate determination. In differentiated adipocytes we showed TBLR to mediate brown fat-specific roles, not only being regulated by the same cues that activate the MAPK signalling cascade, but also targeting the same signalling pathway. Its depletion specifically in BAT leads to animals not fully flexible when challenged with acute β3-adrenergic stress. Finally, our findings that the absence of TBLR in BAT leads to changes in gene expression in other tissues and to hypotriglyceridemia make it probable that one of the BAT functions dependent on TBLR regulation is the endocrine secretion of hormones.

It will be extremely interesting to understand the route by which TBLR in BAT affects peripheral tissues. This involves, firstly, the BAT inherent mechanism of TBLR leading to the observed effects. Since we hypothesised that TBLR can act as a common platform with different actions depending on its interaction partners, these partners will need to be characterised. A possible approach would be co-immunoprecipitation of TBLR in order to detect its associated proteins, potentially in different settings, stages of differentiation or tissues.

Further, levels of BAT secreted hormones such as T3 might cast light on the players mediating the described systemic effect on circulating lipid levels. It is however not certain that the unknown secreted factor is already well characterised, thus this approach bears the risk of remaining in the dark. Comparative secretome analyses, while not trivial, might be a more sensitive and, importantly, an unbiased method to identify differentially secreted proteins from TBLR-deficient compared to control BAT. Further, the actual events in target tissues remain unclear. Different analyses promise help elucidate if and how WAT, muscle, liver or other tissues are affected by the ablation of TBLR in BAT, whether it be via global gene or protein expression analyses or by determination of the activity of key metabolic enzymes. A promising candidate enzyme, based on the data presented here, would be LPL, which is inhibited by ANGPTL-3 and thus may exhibit higher activity in the periphery.

Finally, since TBLR and TBL are described as functionally redundant [128], it would be very interesting to see if presented findings are true in the setting of both TBL and TBLR ablation. We generated an AAV vector expressing an shRNA targeting *Tbl* under the control of a truncated form of the *Ucp1* promoter. Since we also inserted a liver-specific micro-RNA target site to the expression product of this vector, it is expected that it will prove as a useful tool to mediate brown fat-specific gene knock down upon systemic administration, without leakage to the liver.

METHODS

Molecular and Biochemical Methods

Determination of Nucleic Acid Concentration

DNA or RNA concentration was determined subjecting 1.2 µl of nucleic acid to a NanoDrop ND-1000 Spectrophotometer (Peqlab Biotechnology) and measuring absorbance at 260 nM.

RNA Isolation and Quantitative RT-PCR

Cells and tissues were harvested in QIAzol (QIAGEN), tissues were additionally lysed in a tissuelyser (QIAGEN). RNA was isolated using the RNeasy Micro- and -Mini Kit (QIAGEN) for cells and tissues, respectively, performing on-column DNAse digest. 100 to 1000 ng RNA were reverse transcribed with the SuperScript II Kit (Invitrogen) and Oligo(dT) primers (Fermentas), then cDNA was diluted to a final concentration of 1 ng input RNA per µl cDNA and 5 µl were used for RT-PCR. Detection of gene expression was performed using the Taqman system with Taqman Gene Expression Master Mix and specific Gene Expression Assays and an ABI StepOnePlus sequence detector (Applied Biosystems). mRNA levels relative to TBP expression were calculated by the delta Ct method.

Microarray Analysis

$Lin^{-}Sca1^{+}$ adipocyte progenitor cells were isolated and cultured to confluency as described below. Then adipogenic differentiation with 1 µM carbaprostacyclin ($cPGI_2$) (Biozol) or ethanol was induced with or without the presence of 1 µg/ml insulin (Sigma). After 24 h cells were harvested, RNA was isolated as described and subjected to gene expression analysis using mouse430.2 arrays (Affymetrix), the group size was 3 arrays per condition. cDNA was synthesized and hybridized according to the manufacturer's recommendations. Annotation of the arrays was performed with a CustomCDF (Version 14) with Entrez based gene definitions. The Raw fluorescence intensity values were normalized by quantile normalization. Differential gene expression was analysed based on loglinear mixed model ANOVA [29], [30] with a commercial software package (SAS JMP7 Genomics, version 4) (SAS Institute, Cary, NC, USA). Significance was assumed based on a false positive rate of $p = 0.05$ with FDR correction.

Chromatin Immunoprecipitation DNA-Sequencing

preBAT cells were differentiated into mature adipocytes in 15 cm dishes (Falcon). Medium was replaced with phosphate buffered saline (PBS) (Life Technologies) containing 2mM

disuccinimidyl glutarate (DSG crosslinker) (Proteochem) and 0.4% DMSO and cells were incubated for 45 minutes at RT. Then cells were crosslinked for 10 minutes at RT with PBS containing 1 % formaldehyde (Baker), subsequently glycine (Sigma) was added to a final concentration of 0.125 M. After 2 PBS washes, cells were harvested in Chip Lysis Buffer (20mM Tris (Sigma), 0.15 M sodium chloride (NaCl) (Sigma), 1 mM ethylenediaminetetraacetic acid (EDTA) (Sigma), 0.1 % Sodium dodecyl sulfate (SDS) (Sigma), 1 % Triton-X100 (Applichem), pH 8). The chromatin was subjected to 16 on/off cycles of sonication (30 seconds, maximal intensity) with a Bioruptor (Diagenode) followed by 10 minutes centrufugation at 13,000 rpm and 4 °C. Aliquots of the supernatant were used for chromatin immunoprecipitation or stored for subsequent input control. Up to 1.5 ml Chromatin was diluted 3-fold in Chip Lysis Buffer and antibody (anti-PPARg H100 (sc-7196, Santa Cruz) or anti-TBL1XR1 (NB600-270, Novus)) and bovine serum albumin (BSA) (Sigma) were added to a final concentration of 6.7 µg/ml and 1 µg/µl, respectively. After 3 hours of rotation at 4 °C, 1/3 volume of 1:5 diluted protein A/G agarose beads (sc-2003) (pre-blocked with 1 µg/µl BSA for 2 hours) were added and the samples were being rotated over night at 4 °C.

Then the beads were washed twice with Wash Buffer 1 (20mM Tris, 0.15 M NaCl, 1 mM EDTA, 0.1 % SDS, 1 % Triton-X100, 0.1 % sodium deoxycholate (NaDOC) (Sigma), pH 8), once with Wash Buffer 2 (20mM Tris, 0. 5 M NaCl, 1 mM EDTA, 0.1 % SDS, 1 % Triton-X100, 0.1 % NaDOC, pH 8), once with Wash Buffer 3 (20mM Tris, 1 mM EDTA, 0.5 % NaDOC, 0.5 % NP-40 (Sigma), 0.25 M lithium chloride (LiCl) (Roth), pH 8) and twice with Wash Buffer 4 (20mM Tris, 1 mM EDTA, pH 8), each washing step consisting of 5 minutes of rotation at 4 °C and 5 minutes of centrifugation at 2,700 rpm and 4 °C. One original chromatin volume of Elution Buffer (1% SDS, 0.1 M sodium hydrogen carbonate ($NaHCO_3$) (AppliChem)) was added to the beads and chromatin was eluted rotating 20 minutes at RT. After centrifugations, supernatants and input controls were de-crosslinked by adding NaCl to a final concentration of 200mM and incubating for 4 hours at 65 °C.

Bound DNA was recovered by phenol chloroform extraction, mixing it with 1 volume of phenol chloroform isoamylalcohol (PCI) (Roth), incubating for 5 minutes followed by 5 minutes of centrifugation at 13,000 rpm and RT, collecting the upper liquid phase, mixing it with 1 volume of chloroform (VWR) and incubating and spinning like previously. DNA was precipitated from the liquid phase by adding 80 µg/ml glycogen, 0.3 M sodium acetate (NaAc) (Applichem) and 2.5 volumes of ethanol followed by 1 hour incubation at -20 °C. Samples were centrifuged for 25 minutes at 13,000 rpm and 4 °C, washed with 70% ethanol, dried and dissolved in water.

DNA concentration was determined using the Qubit dsDNA HS Assay Kit (Life Technoligies). For determination of binding to individual targets, DNA was diluted 10-fold and used for quantitative real time PCR as described above. ChIP sequencing and data analysis were performed by Anne Loft et al as described in their prior publications [225]. Binding was visualized using the UCSC genome browser.

RNA-Sequencing

preBAT cells were cultured and differentiated as described below. 2 to 3 days before RNA harvest, cells were transducted with adenovirus expressing short hairpin RNAs against TBLR1 or TBL1 as described below, using a MOI of 10 for adipocyte progenitors and a MOI of 100 for adipocytes. Cells were harvested on day1 and day7, respectively, of adipogenic differentiation and RNA was isolated as described above. RNA sequencing and data analysis were performed by Anne Loft et al as described in their prior publications.

Cloning

Restriction digest

Plasmid DNA restriction was performed for 4-6 hours at 37 °C using 20-50 U of restriction enzyme and corresponding buffer (used enzymes are listed in Table 13). When performing single enzyme digest, 10 U Calf Intestinal Phosphatase (CIP, New England Biolabs) was added. Subsequently, the DNA was supplemented with loading dye (final concentration of 1.7 mM EDTA, 11.7 % glycerol, trace amounts of Orange G (Sigma)), subjected to gelelectrophoresis on 1% agarose (Applichem) / TBE gels (10 mM Tris, 0.1 mM EDTA, 9 mM boric acid (Sigma), pH 8) containing 1µg/ml ethidiumbromide (EtBr, Roth), bands of the appropriate size were identified using a Gel Imager (Intas) and UV light (254 nM), cut and DNA was purified from gel pieces with the Qiaquick Gel Extraction Kit (Qiagen).

Insert generation

Insert DNA was generated either by annealing artificial oligonucleotides (denaturated at 95 °C followed by slow cooling to RT, sequences listed in Table 7), or by restriction digest from existing constructs as described above, or by Polymerase Chain Reaction (PCR) for 35 cycles (10 seconds denaturation at 98 °C, 30 seconds annealing and elongation at 72 °C) using a PTC-200 thermocycler (Biozyme), Phusion High-Fidelity DNA-Polymerase and according buffer (Thermo Scientific), dNTPs (Life Technologies) and 5µM of primers listed in Table 9, followed by purification of the DNA using the QIAquick PCR Purification Kit (Qiagen).

Ligation

100 ng plasmid DNA were ligated with either double stranded insert DNA generated by PCR or restriction digest (at a molar ratio of 1/3 mols of plasmid DNA) or with 10 - 100 picomoles of annealed artificial oligonucleotide, using T4 Ligase (New England Biolabs) and corresponding buffers for 2 hours at RT followed by o.n. incubation at 4 °C.

Transformation

25 µl One Shot TOP10 Chemically Competent *E. coli* (Life Technologies) were supplemented with 2.5 µl of ligation reaction, incubated for 30 minutes at 4 °C, heat shocked for 30 sec at 42 °C, supplemented with 250 µl S.O.C. medium (Life Technologies), incubated for 60 minutes at 37 °C, shaking, and plated to LB agar plates (Roth) and 50 mg/L ampicillin (Sigma). Following o.n. incubation at 37 °C, colonies were picked and cultured in 4 mL LB medium + 50 mg/L ampicillin, shaking o.n.

Plasmid purification

Plasmid DNA was isolated using the QIAprep Plasmid Miniprep Kit (Qaigen) and 10µl of 100 ng/µl DNA were supplemented with 5µl of 5 µM sequencing primers listed in Table 8 (sequencing was performed by LGC genomics and results were analysed using the CLC sequence viewer 7 or the genious software).

Cloning strategy

The “220bp element” and “cre4pro element” described by Kozak et al [193] were inserted into the pGL3-Basic Vector (Promega) using *Sac*I and *Xho*I for the 220bp element and *Bam*HI and *Hind*III for the cre4pro enhancer element (whereby the *Bam*HI site attached to the cre4pro element is compatible with the *Bgl*II site in the pGL3-Basic Vector). The *Ucp1* mini-promoter was amplified and subcloned to the pdsAAV-LP1-GFPmut-miR-Tbl1 construct (based on [226], using *Mlu*I and *Pst*I, replacing the LP1 promoter. Subsequently, ologonucleotides containing 3 repeats of a binding site for the liver-specific miR-122 were annealed as described above and inserted to the AAV construct using *Apa*I and *Age*I. This resulted in the construct pdsAAV-GFPmut-miR122site-miR-Tbl1. Analogously, vectors expressing miR-NC or miR-Tblr1 were produced.

Luciferase assays

For luciferase assays, cells were transfected with luciferase reporter plasmids (firefly luciferase pGL3 construct plus 1/20 amount renilla luciferase pRL-TATA-luc) as described below. 30 hours after transfection, cells were stimulated for 16 hours with 10µM Forskolin (Forsk), 2.5µM Rosiglitazone (Rosi) or 1µM Norepinephrine (NE). Cell lysis and determination of luciferase activity were performed using the Dual-Luciferase Reporter Assay

System (Promega), a Mithras Microplate Reader (Berthold) and the MicroWin software (Siemens), following the manufacturer's instructions.

Protein Analysis

Generation of total protein lysates

Cells were harvested in protein extraction buffer (PEB) consisting of 25 mM Tris-HCl (pH 7.4), 100 mM NaCl, 1 mM EDTA, 0.5% Triton-X100, 0.5% NP-40, 1x protease inhibitor cocktail (PIC) (Sigma), 1x phosphatase inhibitor cocktail (Sigma), 0.5 mM sodium orthovanadate (Na_3VO_4) (Sigma), 10 mM sodium fluoride (NaF) (Sigma) and 10 mM glycerol-2-phosphate (G2P) (Sigma). Nuclear and cytosolic extracts were generated using the NE-PER Nuclear and Cytoplasmic Extraction Kit (Thermo Scientific).

Tissue protein lysates were generated by homogenising pre-pulverized tissue in a tissuelyser with protein lysis buffer, rotation for 1 hour at 4 °C and subsequent centrifugation for 10 minutes at 4 °C and 13,000 rpm and harvest of the supernatants.

Separation of nuclear and cytosolic protein extracts

Nuclear and cytosolic extracts were generated by sacrificing female C57Bl6 mice up to 8 hours after injection of 1 mg/kg bodyweight of CL316243 (CL) (Tocris Bioscience) and dissecting brown adipose tissue (BAT) as described below. 1ml of Tissue Fractionation Buffer A (50 mM Tris, 250 mM sucrose (Sigma), 10mM potassium chloride (KCl) (Roth), 1 mM EDTA, 10 mM NaF, 2 mM Na_3VO_4 , 1 mM dithiothreitol (DTT) (Roth), 1 x PIC, pH 7.2) was added and whole tissue biopsies were homogenized by subjecting them to 15 strokes in a dounce homogenizer. After 30 minutes of rotation at 4 °C, lysates were centrifuged for 10 minutes at 3,200 rpm and 30 °C, supernatants were defined as cytosolic extracts. Pelles were lysed in 500 µl of Tissue Fractionation Buffer B (50 mM Tris, 25% glycerol (Sigma), 420 mM NaCl, 1.5 mM $MgCl_2$ (Sigma), 10 mM NaF, 1 mM DTT, 1 x PIC, 0.1% SDS, 1% NP-40, pH 7.2), rotated 30 minutes at 4 °C, centrifuged for 30 minutes at 10,000 rpm and supernatants were defined as nuclear extracts.

Separation of stromal vascular and adipocyte fraction for protein extracts

Stromal vascular fraction (SVF) and adipocyte fraction (AF) of BAT were generated by sacrificing female C57Bl6 mice up to 8 hours after injection of 1 mg/kg bodyweight of CL and dissecting BAT as described below. The tissue was subjected to collagenase digest and centrifugation as described below. 500 µl of the floating adipocytes were referred to as AF, mixed with 1 ml Qiazol and frozen. The cell pellet was referred to as SVF, resuspended in 1 ml Qiazol and frozen. RNA was extracted and analysed as described above.

Western Blot

Protein concentration was quantified using the BCA Protein Assay (Thermo Scientific) or the 2D-Quant kit (GE Healthcare) and 20-50 µg of protein were loaded to 12% SDS-polyacrylamide gels (collection gel consisting of 5% acrylamide/bisacrylamide 37.5:1 (Roth), 125mM Tris, 0.1% SDS, 0.1% ammonium persulfate (APS) (Roth), 0.1% N,N,N',N'-tetramethylethane-1,2-diamine (TEMED) (Roth), pH 6.8; and separation gel consisting of collection gel consisting of 12% acrylamide/bisacrylamide 37.5:1, 375mM Tris, 0.1% SDS, 0.1% APS, 0.04% TEMED, pH 8.8). Separation was performed at 80 – 120 volts in Running Buffer (200mM glycine, 25mM Tris, 0.1% SDS). Subsequently, separated proteins were blotted to nitrocellulose membranes (GE Healthcare) for 90 minutes at 80 volts in Transfert Buffer (150mM glycine, 20mM Tris, 20% methanol), blocked for 1 hour at RT with 5% milk (Gerbu) in tris buffered saline with tween (TBS-T) (50 mM Tris, 150 mM NaCl, 0.1% Tween 20 (Sigma), pH 7.6) and incubated over night at 4 °C with 1:1000 diluted primary antibodies in 5% milk / TBS-T. For the detection of phospho-proteins, BSA (Biomol) was used instead of milk. Blots were washed 3 x 10 minutes in TBS-T, incubated for 1 hour at RT with 1:5000 secondary antibody in 5% milk / TBS-T, washed 3 x 10 minutes in TBS-T and protein bands were detected using the ECL Western Blotting Substrate (Thermo Scientific) and a ChemiDoc XRS Blot imager (Biorad). Band identity was confirmed by comparing to PageRuler Prestained Protein Ladder (Thermo Scientific). The antibodies used for Western Blot are listed in Table 12. Quantification was performed using the Image Lab software.

Phosphatase digest of protein lysates

40µl of cytosolic or nuclear protein lysates were diluted to equal volumes, incubated over night with 1:500 antibody against TBLR (NB600-270, Novus) and protein A/G agarose beads (sc-2003), washed 3 times with TBS-T and treated with 100 units of Lambda Protein Phosphatase (Lambda PP, New England Biolabs) according to the manufacturer's instructions. Control samples were treated with the same buffers and temperatures without the enzyme present.

Immunohistochemistry

Tissues were subjected to 24 h fixation in 4% paraformaldehyde (Histofix) (Roth), washed for 2 h in running tap water and stored in 70% ethanol for up to several weeks until paraffine-embedding, then tissues were sliced and dried. For staining, slices were stepwise de-paraffinated by incubating them for 5 minutes in xylene (Merck), 100% ethanol, 96% ethanol, 90% ethanol, 80% ethanol, 70% ethanol, H_2O and PBS. For antigen retrieval, slides were boiled in 10 mM citrate buffer (10 mM sodium citrate (Sigma), 0.05% Tween 20, pH 6.0), blocked for 1 h with 1% BSA (Biomol) and stained with 1:50 anti-UCP-1 (ab23841, Abcam)

antibody over night at 4 °C. After 3 x 10 minutes washing in PBS, 1 hour incubation at RT with secondary antibody (172–1019, BioRad) and another 3 x 10 minutes of washing with PBS, slides were subjected to 3,3′-diaminobenzidine (DAB) (Sigma) staining and hematoxylin (Sigma) – eosin (Roth) counterstaining. After re-hydration (2 minutes incubation in the ethanol solutions previously used, increasing concentration) slides were mounted with Eukitt quick-hardening mounting medium (Sigma) and examined by light microscopy (Zeiss).

Quanification of Mouse Serum Metabolites

Serum insulin, FGF21 and ANGPTL3 were quantified using a mouse insulin ELISA (Alpco), mouse FGF21 ELISA (R&D) and mouse ANGPTL3 ELISA (R&D), respectively, following the manufacturer's instructions. Serum lipids were quantified using commercial kits for the detection of non-esterified fatty acids (NEFAs) (WAKO), glycerol and triglycerides (TGs) (Sigma) and cholesterol (Randox). For all measurements, 4 µl of serum were measured in duplicates.

Cholorimetric absorption was measured with the Mithras Microplate Reader (Berthold) and analysed using the MicroWin software.

Quantification of Tissue Triglyceride Levels

10 – 20 mg tissue powder were homogenised using a tissuelyser and 1 ml of 2:1 chloroform:methanol (Sigma). Samples were rotated for 20 minutes at RT and centrifuged for 10 minutes at 4,000 rpm and RT. The aqueous phase was mixed with 1 volume 0.9% NaCl and centrifuged for 5 minutes at 2,000 rpm. 100 µl of the lower organic phase were mixed with 10 µl of 1:1 Chloroform:Triton-X100, dried o.n. under the fumehood and dissolved in 50 µl H_2O. TG content was measured as described above and normalized to material weight.

Fast-protein liquid chromatography

Serum from a specified number of mice per experimental group was pooled and subjected to fast-protein liquid chromatography (FPLC). 0.3 ml of pooled plasma were loaded onto a Superose 6B 10/300 column (GE Healthcare) and eluted with a constant flow of PBS. 1 fraction per minute (corresponding to a volume of 0.5 ml) was collected and TG and cholesterol content were determined as described above. Values were calculated as µg of triglyceride or cholesterol per ml.

Bomb calorimetry of feces

Feces of mice individually housed on chow diet and at room temperature were collected over the period of 24 hours. A defined aliquot was subjected to lyophilization and subsequent

bomb calorimetry using a calorimeter (IKA). The determined energy content in Joules per dry weight, the water content based on weight pre and post lyophilization and the total fecal mass during 24 hours were used to calculate the total fecal output per mouse.

Cell Biology

Cell Cultivation

Eucaryotic cells were cultivated under sterile conditions at 37 °C, 5 % CO_2 and 95 % humidity. Media and supplements were purchased from Life Technologies (Invitrogen) and DMEM with 4.5 g/l glucose was used unless stated otherwise.

1 ml frozen cell aliquots containing 10% DMSO and stored in liquid nitrogen (N_2) were thawed at 37 °C, washed in 9 ml of the respective medium, centrifuged for 3 minutes at 3,000 rpm and RT and distributed to a 15 cm dish in 20 ml medium. 24 hours later medium was exchanged to new medium, cells were cultivated to 80 % confluency and propagated by 3 minutes incubation at 37 °C with 3 ml trypsin (Life Technologies), washing with 9 ml medium, centrifugation for 3 minutes at 3,000 rpm and RT and redistribution to 15 cm dishes in 1:10 to 1:80 dilutions.

Human embryonic kidney cells (HEK293 [227]) were cultivated in DMEM + 10% fetal calf serum (FCS) + 100 U/ml (1%) penicillin / streptomycine (P/S). When using HEK293A, containing sequences necessary to faciliate adenovirus production, 1% non-essential-amino-acids (NAA) were added. Immortalized hibernoma cells (HIB1B [228]) and 3T3-L1 preadipocyte cells [229] were cultivated in DMEM + 10% FCS + 1%P/S. Brown adipocyte progenitors immortalized by SV40 T infection (PreBAT cells, [148]) were cultivated to confluency in maturation medium (DMEM, 20% FBS, 1% P/S, 20 nM insulin (Sigma) and 1nM 3,3′,5-Triiodo-L-thyronine sodium salt (T3) (Sigma)). Primary adipocyte progenitors were cultivated to confluency in laminin (Santa Cruz) coated cell culture plates in DMEM, 10% FBS, 1% P/S), and 10 ng/ml murine basic fibroblast growth factor (bFGF) (R&D Systems).

In vitro differentiation

In 3T3-L1 cells, differentiation was induced by exchanging the medium to induction medium (DMEM, 10% FBS, 1% P/S, 172 nM insulin, 0.25 µM dexamethasone (Dex) (Sigma), 0.5 mM 3-isobutyl-1-methylxanthin (IBMX) (Sigma), 0.125mM indometacine (Sigma), 250 µM L-ascorbat (Sigma), 17 µM pantothenat (Sigma), 1 µM D-biotin (Sigma)). 2 days later fresh induction medium was applied, another 2 days later medium was replaced by induction medium without Dex and IBMX, another 2 days later by normal culture medium. Cells were

harvested on day 8. In preBAT cells, differentiation was induced by exchanging the medium to induction medium (DMEM, 20% FBS, 1% P/S, 5 µM Dex, 0.5 mM IBMX, 0.125mM indometacine, 20 nM insulin and 1nM T3). After 24 hours the medium was replaced with maturation medium and after day 3 of differentiation medium was exchanged daily. Cells were harvested on day 7. In primary adipocyte progenitors differentiation was induced by exchanging the medium to DMEM, 10% FBS, 1% P/S, 500 nM Dex, 172 nM insulin and 3 nM T3 ("day 0"). To induce brite differentiation 1 µM $cPGI_2$ or ethanol as vehicle control was added during the duration of the differentiation process as described previously [230]. After 2 days the medium was replaced by DMEM, 5% FBS, 172 nM, 3 nM T3 and 1 µM $cPGI_2$ or ethanol. The medium was exchanged every day. Cells were harvested on day 8.

Cell stimulation for mRNA expression analysis

For the study of effects on mRNA expression, the respective cells were treated for 3 hours with 1 µM CL, 1 µM NE, 100 nM insulin, 10 µM GW7647 (Ppar-α agonist), 1 µM GW501516 (Ppar-βδ agonist), 2.5 µM Rosi (Ppar-γ agonist) or 5 µM Dex. For co-application of the PKA inhibitor H-89 (Calbiochem), cells were washed with PBS, pre-incubated for 1 hour without stimuli and with or without 50 µM H-89, and subsequently incubated for 3 hours with or without CL and H-89. For harvest, cells were washed with PBS, homogenised in 1 ml Trizol, and mRNA was prepared as described above.

Progenitor Isolation and Cell Culture

All antibodies were obtained from eBioscience. Primary SVF-derived Lin^-Sca1^+ adipocyte progenitor cells [144] were isolated from inguinal white adipose tissue of male C57Bl6 mice (Charles River) at age 6–8 weeks. Progenitor isolation has been approved by the DKFZ ethical committee (DKFZ252) and was performed previously in our lab [139]. Tissues were minced, digested with 1.5 mg/ml collagenase type II (Sigma) in DMEM (4.5 g/l glucose) supplemented with 0.5% BSA (Sigma), 15 mM HEPES (Life Technologies), 3.2 mM $CaCl_2$, 10% FBS and 0.05 mg/ml DNase I (Roche) for 30 to 50 minutes shaking at 37 °C. The cell suspension was strained through a 300 µM nylon mesh (Neolab), collected by centrifugation at 900 rpm for 10 minutes, washed in BSA-buffer (1x PBS supplemented with 0.5% BSA and 1 mM EDTA) and strained again through a 70 µM cell strainer (BD biosciences). Subsequently cells were incubated on ice for 10 minutes with anti-CD16/32, then for 30 minutes additionally with Lin (anti-CD31-biotin, anti-CD45-biotin and anti-Ter119-biotin), washed twice with BSA buffer and incubated on ice for 15 minutes with streptavidin microbeads (Miltenyi Biotech). After washing with BSA-buffer, cells were separated using MS columns and the Octo MACS Separator Starter Kit (Miltenyi Biotech), collecting the Lin^- cell

fraction by pelleting the cells of the flow through at 900 rpm for 10 minutes. Those cells were incubated on ice for 15 minutes with anti-Sca1 microbeads (Miltenyi Biotech). Then cells were subjected to the separation columns again, discarding the flow through and eluting the Lin^-Sca1^+ fraction by removal of the magnet. Cells were counted, seeded at 10^4 cells/well and cultivated as described above.

Transfection

Transfection of plasmid DNA

Depending on the cell line, different transfection reagents and protocols were applied. Generally, cells were cultured as described below and 16,000 cells / well were seeded to 48-well-plates in normal culture medium. 24 hours after seeding, cells were transfected after allowing plasmid DNA and transfection reagents to form complexes for 15 minutes at room temperature. 24 hours post transfection, medium was exchanged to fresh medium.

For HIB1B cells, 4.5 µl/µg DNA of Attractene (Qiagen) were applied together with 150 ng vector DNA (plus 7 ng renilla luciferase ctrl vector in luciferase assays) per well. Culture medium of cells was replaced with 1/2 volume of fresh medium, then 1/2 volume of DNA + Attractene were added.

For Hepa-1-6 cells, 2 µl/µg DNA of Lipofectamine 2000 (Life Technologies) were applied together with 200 ng vector DNA (plus 10 ng ctrl vector in luciferase assays) per well. Culture medium of cells was replaced with 9/10 volume of fresh medium, then 1/10 volume of DNA + Lipofectamine were added.

For HEK293A cells, Polyethylenimin (PEI) (Sigma) at 1/6 final volume of medium on the cells was applied together with 250 ng vector DNA (plus 12.5 ng ctrl vector in luciferase assays) per well. Culture medium of cells was replaced with 1/2 volume of fresh medium, then 1/2 volume of DNA + Lipofectamine were added.

Transfection of siRNA

Primary iWAT SVF-derived Lin^-Sca1^+ adipocyte progenitor cells were isolated and plated as described above and transfected with 50 nM siRNA 2 days prior to induction of differentiation, using Mm_Slc2a1_5 FlexiTube siRNA or Allstars Negative Control siRNA (Qiagen). Nucleic acids were pre-incubated with DharmaFECT 1 siRNA Transfection Reagent (Dharmacon) for 20 minutes before adding them to the cells.

Adenoviral Transduction

The adenoviral (AV) constructs used in this study were already present in the lab and were generated based on the BLOCKiT Adenoviral RNAi Expression System (Life Technologies) and expressed shRNAs against murine Tblr1, Tbl1 or scrambled control shRNA.

Virus production

For virus production, the helper cell line HEK293A, expressing the viral antigens E1 and E3 necessary for production of viral particles, was utilised. Per construct 20 confluent 15 cm dishes were transduced with 1 µl/dish adenovirus. Once ~ 80% of cells detached, they were harvested by rinsing and centrifugation for 10 minutes at 2,000rpm in a Super T21 centrifuge (Heraeus). The cell pellet was re-suspended in 20 ml PBS-TOSH (30.8 mM NaCl, 120.7 mM KCl, 8.1 mM sodium hydrogen phosphate (Na_2HPO_4) (Neolab), 1.46 mM potassium dihydrogen phosphate (KH_2PO_4) (Roth), 10 mM $MgCl_2$, pH 7.2) and frozen in liquid nitrogen (N_2).

CsCl fractionation

After subjecting the crude lysate to 3 freeze / thaw cycles and 5 minutes centrifugation at 2,000 rpm in a Biofuge Prime (Heraeus), a cesium chloride (CsCl) (Roth) gradient was performed to purify virus particles. The CsCl solutions contained 10 mM HEPES and were adjusted to a pH of 7.2. First, a gradient was poured consisting of 9 ml of 4 M CsCl solution, topped by 9 ml of 2.2 M CsCl solution. The virus lysate was administered on top and ultracentrifugation was carried out for 2 hours at 24,000 rpm and 4 °C. The virus band was extracted using a syringe, mixed with 1 volume of a saturated CsCl solution and placed on the bottom of a centrifuge tube. Then a gradient was created by adding first 1/2 volume of a 4 M CsCl solution and then 1/2 volume of a 2.2 M CsCl solution on top. Ultracentrifugation was carried out for 3 hours at 35,000 rpm and 4 °C. The virus band was extracted with a syringe and sealed in a dialysis tube (Roth). O.n. dialysis was carried out in dialysis buffer (1 x PBS, 10% glycerol, pH 7.2) before adding 10% glycerol and storing the virus at -80 °C.

Virus titer determination using the Tissue Culture Infectious Dose 50 ($TCID_{50}$) method

To assess the titer of the virus in terms of plaque forming units (pfu) per ml, HEK293A cells were seeded at a density of 10^4 cells / well to a 96 well plate. 2 hours after seeding, an equal volume of virus solution of decreasing concentration was added, infecting 10 wells per dilution up to a 10^{-12} dilution of original the virus solution. After 12 days of incubation at 37 °C, plaques were counted using the following formula:

$$s = \frac{number\ of\ wells\ positive\ for\ plaques}{10}$$

$$\text{titer} = 10\ x\ 10^{1+(s-0.5)}\ \text{pfu/ml}$$

Transduction [231]

For adenoviral transduction cells were incubated for 24 hours in antibiotic free medium. Then adenovirus was added in 1/4 of culture media volume at a multiplicity of infection (MOI) of 10 (for adipocyte progenitors, applied 2 days prior to induction of adipogenic differentiation) to 100 (for adipocytes, applied on day 5 of adipogenic differentiation) in DMEM containing 0.5 µg/ml poly-L-lysine (Sigma). After 90 minutes incubation, DMEM supplemented with FCS and P/S was added, reaching a final concentration of 10% and 1%, respectively.

GLUT-1 Inhibition

Primary iWAT SVF-derived $Lin^{-}Sca1^{+}$ adipocyte progenitor cells were isolated and plated and differentiated as described above. For the last 2 days the glucose transporter inhibitor III STF-31 (Calbiochem) was added to the medium at a concentration of 1 µM according to previous reports [232].

Lipolysis Assay

Differentiated adipocytes prior transduced with adenoviral knockdown constructs as described above were washed with PBS and incubated for 2 hours at 37 °C with Krebs Ringer Buffer (KRB) (115 mM NaCl, 5.9 mM KCl,1.2 mM $MgCl_2$, 1.2 mM sodium dihydrogen phosphate (NaH_2PO_4) (Applichem), 1.2 mM sodium sulfate (Na_2SO_4) (Applichem), 2.5 mM $CaCl_2$, 25 mM $NaHCO_3$, pH 7.4). Subsequently, cells were incubated for 3 hours with stimulation medium (KRB containing 5mM glucose (Applichem), 5% BSA (fatty acid free, Sigma), 25 mM HEPES) with or without 1 µM of isoproterenol (Iso). Supernatants were harvested and NEFA and glycerol levels were determined as described above. Results were normalized to protein content by harvesting the cells in Tx protein lysis buffer (150mM NaCl, 0.05% Triton-X100, 10mM Tris, pH 8) and performing a BCA assay according to the manufacturer's instruction.

Lipogenesis Assay

In differentiated adipocytes prior transduced with adenoviral knockdown constructs as described above, 24 h before the assay the medium was replaced with low glucose DMEM (1 g/l glucose) supplemented with 0.5% BSA. Then, cells were washed with KRB and incubated for 2 hours at 37 °C with stimulation medium (KRB containing 5mM glucose (Applichem), 0.5% BSA, 20 mM HEPES, 1 µCi/ml glucose D-[^{14}C(U)] (Perkin Elmer)) with or without 20 nM of insulin. Cells were lysed in 0.5 M sodium hydroxide (NaOH) (Sigma). Protein concentration was determined using the BCA assay. 1/3 volume of cell lysate was used for scintillation counting to determine glucose metabolisation, 1/2 volume was used for lipid extraction to determine lipogenesis in terms of ^{14}C incorporation to lipids. For this, 1.3

volumes of 3:1 chloroform:methanol were added, samples were mixed, incubated for 2 minutes at room temperature and centrifuged for 2 minutes at 13,000 rpm. Equal volumes of the lower lipid phase were transferred to scintillation tubes (VWR) and organic solvent was evaporated over night. Scintillation counting was performed by adding 4 ml of Rotiscint scintillation liquid (Roth) and counts per minute (CPM) were measured on a liquid scintillation counter (Tri-Carb® 2100TR or 2900TR) (Perkin Elmer). Relative glucose metabolisation and lipogenesis were calculated compared no samples without insulin.

In Vitro Glucose Uptake Assay

In differentiated adipocytes prior transduced with adenoviral knockdown constructs as described above, 24 h before the assay the medium was replaced with low glucose DMEM (1 g/l glucose) supplemented with 0.5% BSA ± cPGI2 and ± STF-31. Cells were incubated for 1 hour at 37 °C with basal medium (KRB containing 5mM glucose, 0.1% BSA, 10 mM HEPES, 8mM mannitol (Sigma), 2 mM pyruvate (Life Technologies), 1 mM NAA) and then stimulated with stimulation medium (glucose free basal medium spiked with 1mM 2-Deoxy-D-glucose (2DOG) (Sigma), 0.3 µCi/ml ^{3}H-Deoxy-D-glucose, 2-[1,2-^{3}H (N)] (^{3}H-2DOG) (Perkin Elmer) and 0.2 µCi/ml ^{14}C-Mannitol, D-[1-^{14}C] (Perkin Elmer)) with or without insulin (20 nM if not stated otherwise) or 25 µM cytochalasin B (Sigma). After 20 minutes at 37 °C the reaction was stopped by adding ice cold basal medium supplemented with 25 mM glucose followed by a PBS wash. Cells were lysed in protein extraction buffer using a tissue lyser. Protein concentration was determined using the BCA assay and glucose uptake by measuring scintillation counting of a defined volume as described above. Since dual counting was performed, disintegrations per minute (DPM) rather than CPM were determined in order to minimize overlap of spectra.

Calculation of Glucose uptake

To calculate glucose uptake, ^{3}H counts were measured for glucose and ^{14}C counts for mannitol. By comparison to counts measured in a defined volume of original stimulation medium, the volume of medium taken up can be calculated and thereby the known amount of non-radioactive glucose present in this volume. To refine the data, counts were corrected for unspecific extracellular volume remaining on the cells after washing. This was done considering ^{14}C counts, since mannitol is not taken up by the cells. Finally, values were normalized to protein content per well and duration of the assay to result in the glucose uptake rate.

Seahorse Metabolic Flux Analysis

Using a Seahorse XF96 extracellular flow bioanalyser (Seahorse Biosciences), living cells were monitored in real time for their respiration (in terms of oxygen consumption rate, OCR) and glycolysis (in terms of extracellular acidification rate, ECAR) in response to various stimuli.

preBAT cells were differentiated in 15 cm dishes and transduced with adenovirus to knock down Tblr1 alone or together with Tbl in adipocyte progenitors or adipocytes as described above. On day 7 of differentiation, 16 hours prior to measurement, adipocytes were trypsinized, counted and seeded to XF96 polystyrene (PS) cell culture microplates at a density of 70,000 living cells per well. Primary BAT SVF-derived $Lin^{-}Sca1^{+}$ adipocyte progenitor cells were isolated and plated as described above directly in laminin coated XF96 PS microplates. 2 days prior to induction of adipogenic differentiation, they were transduced with adenovirus as described above and subsequently differentiated until day 7, when the measurement was performed.

Following the manufacturer's instructions, cells were washed and pre-incubated with unbuffered (sodium bicarbonate free) minimal DMEM supplemented with 2 mM L-glutamine (Life Technologies) carefully adjusted to pH 7.4. For measuring respiration, medium was further supplemented with 1 mM pyruvate and 5 mM glucose. For fatty acid challenge, instead of DMEM low buffered KRB (110 mM NaCl, 4.7 mM KCl, 2 mM $MgSO_4$, 1.2 mM Na_2HPO_4, pH 7.4) was used, supplemented with 2.5 mM glucose and 0.5 mM L-carnitine (Sigma). Cells were stimulated with chemicals provided by the commercially available XF Cell Mito Stress Test Kit and XF Glycolysis Stress Test Kit (Seahorse Bioscience): 2 µM oligomycine, 0.5 µM carbonyl cyanide 4-(trifluoromethoxy)phenylhydrazone (FCCP), 1 µM rotenone, 1 µM antimycin A, 10 mM glucose or 100 mM 2DOG. Further, cells were stimulated with chemicals available in the lab, such as 10 µM isoproterenol, 1 µM NE, 20 nM insulin. For fatty acid challenge, a conjugate solution of 170 µM BSA and 1 mM sodium palmitate (Sigma) was generated by heating palmitate dissolved in a 150 mMNaCl solution to 70 °C, adding it to 1 volume of a 37 °C 340 µM BSA solution, stirring for 1 hour and adjusting the pH to 7.4. Cells were stimulated with BSA alone or with 200 µM palmitate, followed by blocking of FA oxidation with 1 mM (+)-Etomoxir sodium salt hydrate (Etomoxir) [233] (Sigma).

For quantification of cell density for normalization of data, cells were fixed for 1 hour at -20 °C in 100 µl 95% ethanol and 5% acetic acid (Sigma) and subsequently washed with water and stained for 30 minutes with 50µl of a 0.4% solution of sulforhodamine B (Sigma) in 1% acetic

acid. Following 4 washing steps with 1% acetic acid, the stain was eluted by shaking for 10 minutes in 100 µl 10 mM Tris pH 10, measured with the Mithras Microplate Reader (Berthold) at 540 nm and analysed using the MicroWin software.

For data analysis and calculation of statistics for areas under the curve (AUCs), the Seahorse XF 96software was used.

Animals

For the studies on insulin and brightening, male C57Bl6 mice were purchased from Charles River Laboratories (CRL) at age 6–8 weeks, while for the project focusing on the role of TBLR1 female mice were used (see genetic models below). 129S6/SvEvTac mice were purchased from Taconic. Organs and serum were collected, washed in PBS, snap-frozen in liquid nitrogen and stored at −80 °C. Intra-abdominal visceral white adipose tissue (aWAT) was dissected from the abdominal cavity, inguinal WAT (iWAT) (equivalent to subcutaneous WAT) was dissected from the layer under the skin and outside of the abdominal cavity at the hips. Brown adipose tissue (BAT) was dissected from the interscapular region. All lymph nodes, as well as adjacent WAT in BAT, were removed prior to further processing. Blood serum was obtained by centrifuging blood for 30 minutes at 4 °C and 5,000 rpm.

Obesity Models

For the ablation of pancreatic β-cells 13-week old mice were i.p.-injected daily with 60 µg/g body weight streptozotocin (STZ) (Axxora) or 0.05 M sodium citrate as vehicle control for 6 consecutive days. Random fed and 16 h fasted blood glucose levels were determined 3 weeks later using an automatic glucose monitor (Accu-Chek Performa, Roche) and compared to random fed blood glucose levels before the STZ injections to verify the diabetic state. For diet studies 8-week old mice were fed with low fat diet (LFD) (10% calories from fat) or high fat diet (HFD) (60% calories from fat) (Research Diets) for 12 weeks. Total body fat mass was determined by magnetic resonance imaging on an EchoMRI-100 quantitative NMR body composition analyser (Echo Medical Systems).

Genetic Models

As a model for whole fat knockout of TBLR1 on a C57Bl6 background, the adipose tissue knockout (“ATKO”) mice generated and described by Rohm et al [139] were used.

For brown fat-specific knockout of TBLR1, mice homozygous for floxed allele 5 of the Tblr1 gene were used, as generated by TaconicArtemis (Cologne, Germany) and described by Rohm et al [139]. These mice were bred with mice heterozygously expressing a tamoxifen-inducible variant of the Cre recombinase under the control of the *Ucp1* promotor, as

generated and described by Rosenwald et al [167], resulting in Tblr1$^{fl/fl}$Ucp1Cre^{+} and Tblr1$^{fl/fl}$Ucp1Cre^{-} mice, the former of which, upon tamoxifen injection, become knockout for the *Tblr* gene in all UCP-1 expressing cells ("BATKO" mice).

Tamoxifen injections

5 week old Tblr1$^{fl/fl}$Ucp1Cre^{+} and Tblr1$^{fl/fl}$Ucp1Cre^{-} mice were intraperitoneally (i.p.) injected with 2 mg/mouse/day of tamoxifen (Sigma), dissolved in 5/6 volume sunflower oil (Sigma) and 1/6 volume ethanol (EtOH), twice daily for 5 consecutive days. Mice were used only 3 weeks after the last injection to minimize unspecific side effects of tamoxifen.

CL316243 injections

For acute β-adrenergic stimulation, animals were i.p.-injected with 1 mg/kg body weight CL. For chronic injections to induce browning, this procedure was repeated once daily for 10 consecutive days.

Osmotic Pumps

For chronic β-adrenergic stimulation to induce browning of white adipose tissue, CL in 0.9% NaCl or vehicle was administered at continuous rates at a dose of 1 µg/g body weight/day by subcutaneous implantation of an osmotic pump (ALZET model 1002). After 10 days mice were sacrificed.

Glucose Tolerance Test

BATKO and control mice were fasted for 6 hours and basal blood glucose was recorded using an automatic glucose monitor as described above. Then they were i.p.-injected with 1 g/kg body weight glucose and blood glucose levels were determined 20 minutes, 60 minutes and 120 minutes after injection.

ITT and in Vivo Glucose Uptake Assay

8-week old male C57Bl6 mice were implanted with osmotic pumps containing CL or vehicle and body fat mass was determined by magnetic resonance imaging as described above. 10 days later, on the day of the experiment, the initial blood glucose value was determined, then animals were i.p.-injected with 240 µCi/kg body weight ^{3}H-2DOG (Perkin Elmer) and with 0.5 U/kg body weight huminsulin 100 (Lilly) or vehicle, all in 0.1 mM 2DOG. Every 15 min, blood glucose was determined and 25 µl of blood were collected. After 45 minutes the animals were sacrificed and organs and serum were collected, washed in PBS, snap-frozen in liquid nitrogen and stored at −80 °C. For analysis tissue weights were recorded and tissue was homogenised with a Mikro-Dismembrator S (Sartorius) in 1 ml tissue lysis buffer consisting of

50 mM Tris, 1 mM EDTA, 10 mM NaF, 2 mM NOV, 1 mM DTT, 150 mM NaCl and 1% NP-40 (Sigma), pH 7.5. Lysates were centrifuged at 6,500 rpm for 20 minutes at 4 °C and part of this supernatant (S1) was supplemented with 1/4 volume of 0.3 M barium hydroxide solution ($Ba(OH)_2$) (Sigma) and 1/4 volume of 0.3 M zinc sulfate solution ($ZnSO_2$) (Sigma) to derivatize and precipitate phosphorylated ^{3}H-2DOG. Following a centrifugation 6,500 rpm for 20 minutes at 4 °C this supernatant (S2) was saved for determination of not taken up (underivatised) tracer. S1 and S2 were subjected to scintillation counting as described above. Also blood was supplemented with 0.3 M $Ba(OH)_2$ and 0.3 M $ZnSO_4$, centrifuged and the supernatant was used for scintillation counting. For standard activity measurement to normalize the data the injected insulin/^{3}H-2DOG/2DOG solution was used.

Calculation of glucose uptake

Calculations were adapted from known publications [234-236]. For tracer activity in blood an AUC over the course of the 45 minutes duration of the experiment was calculated from background and volume corrected cpm. These calculations are illustrated in Figure 44. It was assumed that from t_0 (time of injection) to t_{15} (first measurement point) blood concentration of tracer is increasing (Figure 44.A and B), and subsequently linearly decreasing (Figure 44.C and D). Values retrieved from tissue samples were corrected for background measurement, tissue weight and dilution and then further corrected for tissue perfusion by subtracting the volume of non-phosphorylated and thus not taken up tracer (calculated from S2) from tracer volume in tissue (calculated from S1). Together with the activity measured in blood and the mean blood glucose values that were determined during the experiment the glucose uptake into the various tissues could be determined.

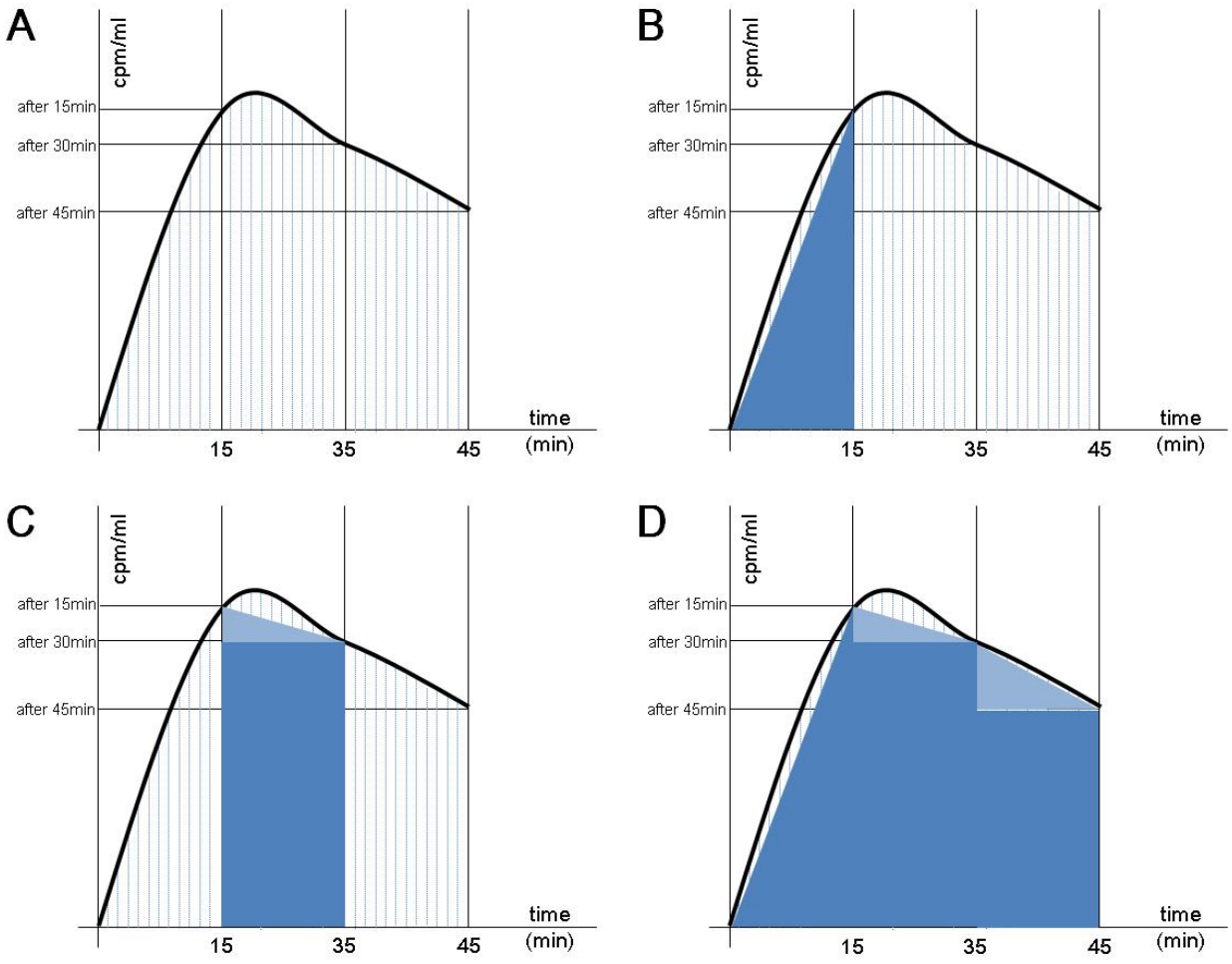

Figure 44. The area under the curve of blood glucose during the experiment was approximated. (A) Blood glucose upon injection was assumed to start decreasing after an initial rise. (B) During the period of increase, AUC was approximated by assuming half the measured activity at t_{15} over the time of 15 minutes. (C) AUC between two timepoints was approximated by multiplying the counts of the later time point with the passed time and adding half the measured difference of the two time points over the passed time. (D) Total AUC was assumed as the sum of individual AUCs.

Oral Lipid Tolerance and Trioleate Uptake Test

The method and calculations were adapted from known publications [111]. BATKO and control mice were fasted for 16 hours. A 50 µl blood sample was collected prior to assay, then animals were gavaged with 100 µl olive oil (Sigma) and further blood samples were collected after 1.5 hours, 3 hours and 4.5 hours. The blood samples were centrifuged for 5 minutes at 5,000 rpm and serum was subjected to triglyceride measurement as described above. For Trioleate Uptake Test, the oil was traced with 10 µCi/mouse triolein [9,10-3H(N)]

(Hartmann) and further blood samples were collected after 1 hour, 2 hours and at the end of the assay. Animals were sacrificed after 3 hours and blood and organs were collected (iWAT, aWAT, BAT, liver, gastrocnemius skeletal muscle (GC), heart, intestine). For BAT, liver, ~ 100 mg of tissue was weighed and homogenized in 1 ml Solvable (Perkin Elmer) using a tissue lyser. For the other organs, whole samples were homogenized in 1 ml Solvable. 400 µl of homogenates, 5 µl of serum and 50 µl of original traced olive oil were subjected to scintillation counting as described above.

Calculation of triolein uptake

Counts (cpm) of tissues were corrected for background measurement, tissue weight and dilution. Based on the specific activity measured in an aliquot of the traced olive oil that was administered to the mice (cpm/mol of triolein), as well as the assay duration, the tissue uptake rate (µmol/g tissue/hr) could be determined. Taking into account the original tissue weight, the contribution of each tissue to whole body triolein uptake could be determined.

Hepatic output assay

An hepatic output assay was performed based on established protocols [237]. BATKO and control mice were housed 22 °C and fasted for 16 hours to eliminate intestinal lipid absorption and chylomicron production. To block plasma lipolytic activity and subsequent lipid clearance to tissues, 500 mg/kg BW Tyloxapol (Sigma) as a 10 % w/v solution in sterile 0.9 % NaCl was administered intravenously. 50 µl blood sample was drawn before injection and every 30 minutes after injection, after 2 hours the animals were sacrificed. The blood samples were centrifuged for 5 minutes at 5,000 rpm and serum was subjected to triglyceride measurement as described above.

Metabolic Phenotyping in the TSE System

BATKO and control mice were housed at 4 °C, 22 °C or 30 °C in PhenoMaster cages (TSE Systems) on a 12 h light-dark cycle for up to 3 weeks. For the measurement of acute changes in VO_2 in response to CL injection, mini chambers were used to minimize movement and accelerate rate at which data points can be recorded.

Detection of body temperature

For non-invasive measurement of body temperature, mice were implanted with lPTT-300 transponder thermometers (BioMedic Data Systems), allowing wireless signal detection using the DAS-7006/7s handheld reader system for wireless temperature detection (BioMedic Data Systems).

Calorimetry and assessment of further metabolic parameters

For indirect calorimetry PhenoMaster cages were used. Oxygen consumption (VO_2), carbon dioxide consumption (VCO_2), physical activity, feeding, drinking and body weight were recorded. Respiratory exchange ratio (RER) resulted from VO_2 and VCO_2 and expresses an indicator of fuel use (values are expected to be between 0.7 at pure lipid use and 1 at pure carbohydrate use). The resting metabolic rate (RMR) is metabolism corrected for VO_2 caused by activity and was calculated as previously described [238].

Adipose Tissue Explants

For in vitro culture of adipose tissue, BAT from female C57Bl6 mice was dissected as previously described and cut to 12 equally sized pieces per animal. For technical replicates of each condition, a tissue piece of a different mouse was used. 1 piece per well was weighed and transferred to 24 well plates and assays were performed analogously to cell assays in terms of buffer composition, incubation times and supernatant collection. In radioactive assays, tissue pieces were homogenized in protein extraction buffer with a tissue lyser and specific volumes were used for scintillation counting as described above.

Ethics Statement

All animal handling procedures were performed in accordance with the European Union directives and the German animal welfare act and have been approved by local authorities (Regierungspräsidium Karlsruhe, Az. 35-9185.81/G-82/12).

Adipocyte progenitor isolation has been approved by the DKFZ ethical committee (DKFZ252).

Statistical Analysis

The results are shown as means ± standard error of the mean (SEM). Statistical analysis was performed by two-tailed student's t test, For RT-PCR data this was calculated on log10-transformed data, significance was assumed at $p<0.05$. For pairwise multiple comparison procedures an ANOVA analysis based on the Student-Newman-Keuls Method was performed.

MATERIAL

Buffers

Table 6. Buffers

Buffer name	Composition
Citrate Buffer (Histology)	10 mM sodium citrate, 0.05% Tween 20, pH 6.0
Dialysis Buffer (adenovirus production)	1 x PBS, 10% glycerol, pH to 7.2
DNA Loading Dye 6x	10 mM EDTA, 70 % glycerol, trace amounts of Orange G
Elution Buffer (ChIP)	1% SDS, 0.1 M NaHCO3
Krebs-Ringer Buffer (KRB)	115 mM NaCl, 5.9 mM KCl,1.2 mM MgCl2, 1.2 mM NaH2PO4, 1.2 mM Na2SO4, 2.5 mM CaCl2, 25 mM NaHCO3, pH 7.4
low buffered KRB (Seahorse)	110 mM NaCl, 4.7 mM KCl, 2 mM MgSO4, 1.2 mM Na2HPO4, pH 7.4
Lysis Buffer (ChIP)	20mM Tris, 0.15 M NaCl, 1 mM EDTA, 0.1 % SDS, 1 % Triton-X100, pH 8
PBS-TOSH (adenovirus production)	30.8 mM NaCl, 120.7 mM KCl, 8.1 mM Na2HPO4, 1.46 mM KH2PO4, 10 mM MgCl2, pH 7.2
Protein Extraction Buffer (PEB)	25 mM Tris-HCl, 100 mM NaCl, 1 mM EDTA, 0.5% Triton-X100, 0.5% NP-40, 1x PIC, 1x phosphatase inhibitor cocktail, 0.5 mM Na3VO4, 10 mM NaF, 10 mM G2P, pH 7.4
Running Buffer (Western Blotting)	200mM glycine, 25mM Tris, 0.1% SDS
SDS sample buffer 5x	250 mM Tris, 10% SDS, 50% glycerol, 0.5 mM DTT, 0.01% bromphenol blue, pH 6.8
Tissue Fractionation Buffer A	50 mM Tris, 250 mM sucrose, 10mM, 1 mM EDTA, 10 mM NaF, 2 mM Na3VO4 , 1 mM DTT, 1 x PIC, pH 7.2
Tissue Fractionation Buffer B	50 mM Tris, 25% glycerol, 420 mM NaCl, 1.5 mM MgCl2, 10 mM NaF, 1 mM DTT, 1 x PIC, 0.1% SDS, 1% NP-40, pH 7.2
Tissue Lysis Buffer (Glucose Uptake Assay)	50 mM Tris, 1 mM EDTA, 10 mM NaF, 2 mM Na3VO4, 1 mM DTT, 150 mM NaCl, 1% NP40, pH 7.5
Transfert Buffer (Western Blotting)	150mM glycine, 20mM Tris, 20% methanol
Tris Buffered Saline with Tween-20 (TBS-T)	50 mM Tris, 150 mM NaCl, 0.1% Tween 20, pH 7.6
Tris-Borate-EDTA Buffer (TBE)	10 mM Tris, 0.1 mM EDTA, 9 mM boric acid, pH 8
Tx Protein Lysis Buffer	150mM NaCl, 0.05% Triton-X100, 10mM Tris, pH 8
Wash Buffer 1 (ChIP)	20mM Tris, 0.15 M NaCl, 1 mM EDTA, 0.1 % SDS, 1 % Triton-X100, 0.1 % NaDOC, pH 8
Wash Buffer 2 (ChIP)	20mM Tris, 0. 5 M NaCl, 1 mM EDTA, 0.1 % SDS, 1 % Triton-X100, 0.1 % NaDOC, pH 8
Wash Buffer 3 (ChIP)	20mM Tris, 1 mM EDTA, 0.5 % NaDOC, 0.5 % NP-40 (Sigma), 0.25 M LiCl, pH 8
Wash Buffer 4 (ChIP)	20mM Tris, 1 mM EDTA, pH 8

Oligonucleotides

Oligonucleotides for annealing of double stranded insert

Overlapping oligonucleotides containing 3 repeats of the miR-122 target sequence (underlined) as according to www.mirbase.org were designed to create overlaps matching the *Apa*I and *Age*I restriction sites present in the vector (bold).

Table 7. Oligonucleotides for annealing of double stranded insert

Designed primer sequence	Description
5'C**CAAACACCATTGTCACACTCCA**GTATACA**CAAACACCATTGTCACACTCCA**GATA**TCACAAACACCATTGTCACACTCCA**	miR-122 Target Site, fwd
5'CCGG**TGGAGTGTGACAATGGTGTTTG**TGATATC**TGGAGTGTGACAATGGTGTTTG**TGTATAC**TGGAGTGTGACAATGGTGTTTG**GGGCC	miR-122 Target Site, rev

Oligonucleotidess for sequencing

To confirm successful cloning of the *Ucp1* mini promoter in the pGL3 vector, the commercial primer GL3 (LGC standards) was used, while to confirm subcloning to pdsAAV vector, sequencing primers were designed ("Ucp1mini subcloning"). Further, sequencing primers were designed to confirm the identity of expressed miRNA ("miR-ID") or the successful insertion of the miR-122 target site (miR-122 insertion).

Table 8. Oligonucleotides for sequencing

Designed primer sequence	Description
5'TTTGTATTCAGCCCATATCG	GL3
5'ATGATTGACATGCTAGTTTTACGA	Ucp1mini subcloning, fwd
5' TCGGCATGGACGAGCTGTACAAGT	Ucp1mini subcloning, rev
5'TCCACTTTGCCTTTCTCTCC	miR-122 site insertion, fwd
5'CGTTGTGGCTGTTGTAGTTG	miR-122 site insertion, rev
5'ACTTCAAGATCCGCCACAAC	miR-ID, fwd
5'CCTCAGATCAATTCCCGCCT	miR-ID, rev

Oligonucleotides for PCR in cloning

To amplify the two key elements for the generation of the *Ucp1* mini promoter, PCR primers were used to amplify the "220 bp element", adding restriction sites for *Sac*I and *Xho*I (underlined) and the "Cre4pro enhancer element", adding restriction sites for *Bam*HI and *Hind*III (underlined) as described by Kozak et al [193]. Subsequently, the *Ucp1* mini promoter was amplified for subcloning to the pdsAAV vector using PCR primers adding restriction sites for *Mlu*I and *Pst*I (underlined).

Table 9. Oligonucleotides for PCR in cloning

Designed primer sequence	Description
5'GGGGAGCTCCTCTACAGCGTCACAGAGG	220 bp, fwd + *Sac*I
5'GGGCTCGAGAGTCTGAGGAAAGGGTTGA	220 bp, rev + *Xho*I
5'GGGGATCCGAGTGACGCGCGGCTGGG	Cre4, fwd + *Bam*HI
5'GGGAAGCTTGGGCTAGGTAGTGCCAG	Cre4, rev + *Hind*III
5'GGGACGCGTGGTACCGAGCTCCT	Ucp1mini, fwd + *Mlu*I
5'GGGCTGCAGAAGCTTGGGCTAGG	Ucp1mini, rev + *Pst*I

Oligonucleotides for quantitative real-time PCR

For positive and negative control PCRs to assess ChIP material quality, primers designed and ordered via Eurofins MWG Operon were used.

Table 10. Oligonucleotides for quantitative real-time PCR

Designed primer sequence	Description
5'CTCAGAAAAGGCAGGGAA	Cav2, fwd (adipogenesis positive control 2)
5'CCCAGTCATGACAACACC	Cav2, rev (adipogenesis positive control 2)
5'TGGTAGCCTCAGGAGCTTGC	General ChIP negative control, fwd
5'ATCCAAGATGGGACCAAGCTG	General ChIP negative control, fwd
5'GTGAATGTGTGGGTCACTGG	Pparg2 promoter -300 bp, fwd (adipogenesis positive control 1)
5'TAATGCTGTCTGCTGCTTTGG	Pparg2 promoter -300 bp, rev (adipogenesis positive control 1)
5'AGCAAACCCGTCTGACACAAGC	Taldo+1kB, fwd (PPAR-γ binding negative control 1)
5'TGGAGCATGTTTTTCCAGCATCCA	Taldo+1kB, fwd (PPAR-γ binding negative control 2)
5'GCCGGTAAACTCTGCACTACACACA	Taldo+1kB, rev (PPAR-γ binding negative control 1)
5'CCCTATAAAAGCCGATGTGCAGTCA	Taldo+1kB, rev (PPAR-γ binding negative control 2)
5'ATACACCCTTTGCCCCGTTT	Taldo+2kB, fwd (PPAR-γ binding positive control)
5' GTGGCTCGTTCTGCTGTCTT	Taldo+2kB, rev (PPAR-γ binding positive control)

For gene expression analysis, either TaqMan probes or primers designed and ordered via Eurofins MWG Operon were used.

Designed mouse primer sequence	Description
5'AAAGCCAAGAAGTCGGTGGAC	Cebpa_for
5'CGAGTACCGGGTACGGCGGGAAC	Cebpa_probe
5'CTTTATCTCGGCTCTTGCGC	Cebpa_rev
5'AATATGTCTACCTCCGAAGCAGGA	Cpt1b_for
5'CAACTATTATGCCATGGATTTTGTGCTTATTAAGA	Cpt1b_probe
5'CGTGAACGGCATTGCCTAG	Cpt1b_rev
5'GATGGCACGCAGCCCTAT	Ppargc1a_for
5'CATTGTTCGATGTGTCGCCTTCTTGCT	Ppargc1a_probe
5'CTCGACACGGAGAGTTAAAGGAA	Ppargc1a_rev
5'GGAGCCATGGATTGCACATT	Srebp1c_for
5'CAGCTCATCAACAACCAAGACAGTGACTTCC	Srebp1c_probe
5'CCTGTCTCACCCCCAGCATA	Srebp1c_rev
5'ACGAGGTGAACTTTCTGGTATATCG	Tbl1_for
5'ATCAGGTTTTTCCCACTCTGCCTTCACG	Tbl1_probe
5'GGACTGGCTAATGTGACTTTCGA	Tbl1_rev

5‘AATGGTGCCCTGGTTCCA	Tblr1_for
5‘CCGCTGCACTCATCTCTATCATCCAGAAA	Tblr1_probe
5‘AGGTGCCATCCTCATTTATGCTA	Tblr1_rev
5‘TTGACCTAAAGACCATTTGCACTT	Tbp_for
5‘TGCAAGAATGCTGAATATAATCCCAAGCG	Tbp_probe
5‘TTCTCATGATGACTGCAGCAAA	Tbp_rev
5‘CCTTCCCGCTGGACACTG	Ucp1_for
5‘CAAAGTCCGCCTTCAGATCCAAGGTG	Ucp1_probe
5‘CCTAGGACACCTTTATACCTAATGGT	Ucp1_rev
Mouse TaqMan probe ID	**Description**
Mm02524224_s1	Adrb2 (inv)
Mm02601819	Adrb3
Mm00803820_m1	Angptl3
Mm00480431_m1	Angptl4
Mm01611862_g1	Atp5o
Mm00432554_m1	Cidea
Mm00438297_g1	Cox7a1
Mm00432648_m1	Cox8b
Mm00662319_m1	Fasn
Mm00433278_m1	Fgf21
Mm00434759_m1	Leptin
Mm00495359_m1	Lipe (Hsl)
Mm00503040_m1	Pnpla2 (ATGL)
Mm00440945_m1	PPARgamma
Mm00445641_m1	Retn
Mm00772290_m1	Scd1
Mm00458268_m1	Sdhb
Mm00481172_m1	Sdhc
Mm00490758_m1	Sirt1
Mm00441480_m1	Slc2a1 (Glut1)

Plasmids

Table 11. Plasmids

Plasmid name	Description	Source
pGL3/3.1kbUcp1p	Luciferase reporter vector containing full length Ucp1 promoter	kindly provided by the Kozak lab (based on pGL3-Basic, Promega)
pdsAAV-LP.1-GFPmut-miR-NC	Double stranded AAV vector expressing control miRNA under the control of LP1 promoter	kindly provided by the Herzig lab (generated by Tessa Walcher)
pdsAAV-LP1-GFPmut-miR-TBL1	Double stranded AAV vector expressing Tbl1 miRNA under the control of LP1 promoter	kindly provided by the Herzig lab (generated by Tessa Walcher)
pdsAAV-LP1-GFPmut-miR-TBLR1	Double stranded AAV vector expressing Tblr1 miRNA under the control of LP1 promoter	kindly provided by the Herzig lab (generated by Tessa Walcher)

Antibodies

Table 12. Antibodies

Mus Musculus Target Protein	Source
Acetyl Coenzyme A Carboxylase (ACC)	3662, Cell Signalling
Adipose Triglyceride Lipase (ATGL)	4126, Cell Signalling
Anti-mouse IgG-HRP (goat)	170-6516, Biorad
Anti-rabbit IgG-HRP (goat)	172-1019, Biorad
CD16/32 (FcBlock)	14-0161-82, ebioscience/Natutec
CD31-biotin	13-0311-81, ebioscience/Natutec
CD45-biotin	13-0451-81, ebioscience/Natutec
Glucose Transporter 1 (GLUT-1)	ab32551, Abcam
Glycerinaldehyd-3-Phosphat-Dehydrogenase (GAPDH)	sc-166545, Santa Cruz
Glycogen synthase kinase 3 beta (GSK3β)	9315 Cell Signalling
Hormone-Sensitive Lipase (HSL)	AB3525, Chemicon
Peroxisome proliferator-activated receptor gamma (PPARg) H100	sc-7196, Santa Cruz
Phosphorylated Acetyl Coenzyme A Carboxylase (p-ACC)	3661, Cell Signalling
phosphorylated Glycogen synthase kinase 3 beta (p-GSK3β)	9336 Cell Signalling
Phosphorylated Hormone-Sensitive Lipase (p-HSL)	4126, Cell Signalling
Phosphorylated PKA substrate (RRXS/T)	9624, Cell Signalling
Phosphorylated Protein Kinase B (p-AKT)	9271, Cell Signalling
Poly [ADP-Ribose] Polymerase 1 (PARP-1)	9542, Cell Signalling
Protein Kinase B (AKT)	9272, Cell Signalling
Ter119-biotin	13-5921-81, ebioscience/Natutec
Transducin (beta)-Like 1 X-Linked Receptor 1 (TBL1XR1)	NB600-270, Novus
Transducin (beta)-Like 1 X-Linked Receptor 1 (TBL1XR1) [only during testing]	ab24550, Abcam
Transducin (beta)-Like 1X-Linked (TBL1X)	ab24548, Abcam
Uncoupling Protein 1 (UCP1)	ab23841, Abcam
Valosin-Containing Protein (VCP)	ab11433, Abcam

Enzymes

Table 13. Enzymes

Restriction endonuclease	Source	Catalogue number
*Age*I	New England Biolabs	R0552
*Apa*I	New England Biolabs	R0114
*Bam*HI	Thermo Fischer Scientific (Fermentas)	ER0051
*Bgl*II	Thermo Fischer Scientific (Fermentas)	ER0082
*Hind*III	Thermo Fischer Scientific (Fermentas)	FD0504
*Mlu*I	Thermo Fischer Scientific (Fermentas)	ER0561
*Not*I	New England Biolabs	R0189
*Pst*I	New England Biolabs	R0140S
*Sac*I	New England Biolabs	R0156S
*Sal*I	New England Biolabs	R0138S
*Xho*I	New England Biolabs	R0146S
Cloning Enzyme	Source	Catalogue number
T4 DNA Ligase	New England Biolabs	M0202L

Calf Intestinal Phosphatase (CIP)	New England Biolabs	M0290L
Phusion High-Fidelity DNA-Polymerase	Thermo Scientific	F-530L
General Enzyme	**Source**	**Catalogue number**
Collagenase Type II	Sigma	C6885
DNase I	Roche	11 284 932 001
Lambda Protein Phosphatase (Lambda PP)	New England Biolabs	P0753S

Instruments

Table 14. Instruments

Instrument	Source
0.5-10µl single-channel pipette (ErgoOne)	Starlab
100-1000µl single-channel pipette (ErgoOne)	Starlab
20-200µl single-channel pipette (ErgoOne)	Starlab
2-20µl single-channel pipette (ErgoOne)	Starlab
Analytical scales (M-Power)	Sartorius
Automated cell counter (Countess)	Life Technologies (Invitrogen)
Automatic glucose monitor (Accu-Chek Performa)	Roche
Bacterial incubator (Function Line)	Thermo Scientific (Heraeus)
Bacterial shaker	Infors AG
Bacterial shaker / incubator (Multitron Standard)	Infors HT
Benchtop centrifuge (Microfuge Heraeus Pico)	Thermo Scientific (Heraeus)
Benchtop centrifuge, cooling (Microfuge Heraeus Fresco)	Thermo Scientific (Heraeus)
Blot imager (ChemiDoc XRS)	Biorad
Bunsen Burner	Campingaz
Calorimeter (IKA C7000)	IKA
Centrifuge (Biofuge Prime) (cell culture)	Thermo Scientific (Heraeus)
Centrifuge (Labofuge 400R)	Thermo Scientific (Heraeus)
Centrifuge (Mikro 22R) (cell culture)	Hettich
Centrifuge (Multifuge X3R)	Thermo Scientific (Heraeus)
Centrifuge (Super T21)	Thermo Scientific (Heraeus)
CO2 incubator	Sanyo
Electrophoresis chamber	Steinbrenner
Electrophoresis power supply (PowerPac™ Basic)	Biorad
Electrophoresis power supply (PowerPac™ HC)	Biorad
Extracellular flow bioanalyser (Seahorse XF96)	Seahorse Bioscience
FPLC system (ÄKTA purifier)	GE Healthcare Life Sciences
Freeze dryer (Alpha 1-2)	Martin Christ
Freezer -20 °C (comfort / med line)	Liebherr
Freezer -80 °C (Herafreeze)	Thermo Scientific (Heraeus)
Fridge 4 °C (comfort / med line)	Liebherr
Fumehood (Airflow RXC 90.1)	WALDNER Laboreinrichtungen
Gel imager (IX)	Intas
Handheld Reader System for Wireless temperature detection (model DAS-7006/7s)	BioMedic Data Systems
Hotplate stirrer (Model 375)	VWR
Labcoat	Bierbaum Proenen
Liquid nitrogen cryogenic tank	Thermo Electron

Liquid scintillation counter (Tri-Carb® 2100TR or 2900TR)	Perkin Elmer
Manual pipetting system (Liquidator 96)	Mettler Toledo
Micro dismembrator S	Sartorius
Microplate reader (Mithras LB 940)	Berthold
Microplatereader SPECTROstar Omega	BMG Labtech
Microscope (Axio Imager.M2) (histology)	Zeiss
Microscope (Axiovert 40 CFL) (cell culture)	Zeiss
Microwave	Bosch
Mini Trans-Blot® cell (buffer tank, lid, cassettes, electrodes)	Biorad
Mini-PROTEAN Tetra cell (buffer tank, lid, running module)	Biorad
Mini-PROTEAN® Tetra handcast systems (casting module, plates, combs)	Biorad
Multichannel pipette reference 8- and 12-channel variable	Eppendorf
Multistep pipette (Multipette Plus)	Eppendorf
pH meter (GMH350)	GHM electronics, Greisinger
PhenoMaster cages	TSE Systems
Photometer (NanoDrop ND-1000)	Peqlab Biotechnology
Pipette controller (accu-jet® pro)	Brandtech Scientific
Real-Time PCR system (StepOnePlus)	Life Technologies (Applied Biosystems)
Rocking platform (Duomax 1030)	Heidolph
Rotating wheel	Neolab
Rotating wheel (model 2-1184)	Neolab
Scales (EG 2200-2NM)	Kern & Sohn Gmbh
Sonicator (Bioruptor)	Diagenode
Sterile biosafety cabinet (e3 Class II Type A/B)	SterilGARD
Tabletop centrifuge (Mini Spin Plus)	Eppendorf
Thermomixer comfort Heatblock	Eppendorf
Timer (TR 118)	Oregon Scientific
TissueLyser II	Qiagen
Ultracentrifuge (XL 70)	Beckman
Vacuum pump	Neolab

Software

Table 15. Software

Software	Source
CLC Sequence Viewer 7	CLCbio
CustomCDF (version 14)	Brainarray
Geneious Pro 5.3.4	Genious
GraphPad Prism 5	GraphPad
Illustrator	Adobe
Image Lab	Biorad
Intas-Capture-Software	Intas
MARS data analysis software	Omega
ND-1000	Nanodrop
Office	Microsoft
SAS JMP7 Genomics (version 4)	SAS Institute
Photoshop	Adobe
Reader Control	Omega
Seahorse XF 96	Seahorse Bioscience

SigmaPlot 12.0	SigmaPlot
STEP 7 MicroWIN	Siemens
StepOne	Life Technologies (Applied Biosystems)
UCSC Genome Browser	http://genome.ucsc.edu

Kits

Table 16. Kits

Kit	Source	Catalogue number
2-D Quant Kit	GE healthcare	80-6483-56
BCA Protein Assay Kit	Thermo Scientific (Pierce)	23225
BLOCK-iT™ Adenoviral RNAi Expression System	Life Technologies	K4941-00
Cholesterol (liquid) assay	Randox	CH200
Cholesterol Standard Solution	Randox	2147CH
Dual-Luciferase Reporter Assay System	Promega	E1960
ECL Western Blotting Substrate	Thermo Scientific (Pierce)	32106
Glycerol Standard Solution	Sigma	G7793
Mouse Angiopoietin-like 3 Immunoassay, Quantikine ELISA	R&D Systems	MANL30
Mouse/Rat FGF-21 Immunoassay, Quantikine ELISA	R&D Systems	MF2100
Mouse Insulin ELISA	Alpco	80-INSMS-E01
NEFA Standard Solution	Wako	276-76491
NEFA-HR Reagent 1	Wako	434-91795
NEFA-HR Reagent 2	Wako	436-91995
NE-PER Nuclear and Cytoplasmic Extraction Kit	Thermo Scientific (Pierce)	78833
Plasmid Maxi Kit	Qiagen	12163
QIAprep Spin Miniprep Kit	Qiagen	27106
QIAquick Gel Extraction Kit	Qiagen	28704
QIAquick PCR Purification Kit	Qiagen	28104
Qubit dsDNA HS Assay Kit	Life Technologies (Thermo)	Q32851
RNeasy Micro kit	Qiagen	74004
RNeasy Mini kit	Qiagen	74104
Serum Triglyceride Determination Kit	Sigma	TR0100
SuperScript II reverse transcriptase	Life Technologies	18064014
XF Calibrant Solution	Seahorse Bioscience	100840-000
XF Cell Mito Stress Test Kit	Seahorse Bioscience	103015-100
XF Glycolysis Stress Test Kit	Seahorse Bioscience	102194-100

Chemicals

Table 17. Chemicals

Chemical	Source	Catalogue number
(+)-sodium L-ascorbate	Sigma	A4034
14C glucose D-[14C(U)]	Perkin Elmer	NEC042X250UC
14C-Mannitol, D-[1-14C]	Perkin Elmer	NEC314050UC
2-Deoxy-D-glucose	Sigma	D8375
3,3′,5-Triiodo-L-thyronine sodium salt (T3)	Sigma	T6397
3,3′-Diaminobenzidine (DAB)	Sigma	32741
30% Acrylamide/Bisacrylamide 37.5:1 (Rotiphorese Gel 30)	Carl Roth	3029.1

3H-Deoxy-D-glucose, 2-[1,2-3H (N)]	Perkin Elmer	NET328001MC
Acetic acid	Sigma	45731
Agarose	Applichem	A8963
Ammonium persulfate (APS)	Roth	9592.3
Ampicillin	Sigma	A9518
Anti-Sca-1 MicroBead Kit (FITC), mouse	Miltenyi Biotec	130-092-529
Attractene Transfection Reagent	Qiagen	301005
Barium hydroxide solution 0.3 N (Ba(OH)2)	Sigma	B4059
Biotin	Sigma	B4639
Boric acid	Sigma	31146
BSA FA free (for ChIP and lipid assays)	Sigma	A8806
BSA fraction V (for WB)	Biomol	1400
BSA in solution (for cell culture)	Sigma	A9576
Calcium chloride (CaCl2)	Carl Roth	CN93.1
Carbaprostacyclin (cPGI2)	Biozol (Cayman)	69552-46-1
Cesium chloride	Carl Roth	7878.2
Chloroform	VWR	22.711.290
Cytochalasin B	Sigma	C6762
D-(+)-Glucose anhydrous	Applichem	A0883
Dexamethasone (Dex)	Sigma	D-8893
Dexamethasone water soluable (Dex)	Sigma	D2915
Dimethyl sulfoxide (DMSO)	Sigma	D2650
Disuccinimidyl glutarate (DSG crosslinker)	Proteochem	c1104
Dithiothreitol (DTT)	Carl Roth	6908.2
D-Mannitol	Sigma	M4125-100G
DMEM, high glucose, pyruvate	Life Technologies (Gibco)	11965-092
DMEM, low glucose, pyruvate	Life Technologies (Gibco)	31885-023
DMEM, no glucose	Life Technologies (Gibco)	11966-025
DMEM, no glucose,/pyruvate/L-glutamine,/phenol red/sodium bicarbonate, powder	Sigma	D5030
DNase / RNase free water	Life Technologies (Gibco)	10977023
dNTPs (10 mM)	Life Technologies	R0191
D-pantothenic acid hemicalcium salt	Sigma	P5710
Dulbecco's phosphate buffered saline (PBS)	Life Technologies (Gibco)	14190094
Eosin G	Carl Roth	7089.1
Ethanol 99%	DKFZ	
Ethanol absolute for analysis	Sigma	32205
Ethidium bromide (EtBr)	Carl Roth	2218.2
Ethylenediaminetetraacetic acid (EDTA)	Sigma	E5134
(+)-Etomoxir sodium salt hydrate (Etomoxir)	Sigma	E1905
Eukitt quick-hardening mounting medium	Sigma	3989
Fetal calf serum (FCS)	Life Technologies (Invitrogen)	10091-148
Formaldehyde solution 37%	J. T. Baker	7040
Forskolin	Sigma	F3917
Gene Ruler 1kb DNA Ladder	Thermo Scientific	SM0314
Glucose Transporter Inhibitor III, STF-31	Calbiochem	351801
Glycerol 2-phosphate disodium salt hydrate (G2P)	Sigma	G6251
Glycerol, 99%	Sigma	15523
Glycine	Sigma	33226

GW501516 (Ppar-α agonist)	Sigma	43732
GW7647 (Ppar-α agonist)	Sigma	G6793
H-89 (PKA Inhibitor)	Calbiochem	371962
Hematoxylin solution Gill No. 2	Sigma	GHS232
HEPES 1M	Life Technologies (Invitrogen)	15630-056
Histofix 4% Formaldehyde Solution for Histology	Carl Roth	P087.5
Huminsulin, 100 U/mL	Lilly	A10AB01
Hydrochloric acid 37% (12.1 M)	Sigma	30721
IBMX (3-Isobutyl-1-methylxanthin	Sigma	I5879-1G
Indomethacine	Sigma	I7378
Insulin human	Sigma	I2643
Isopropanol	Sigma	190764
Isoproterenol hydrochloride	Merck (Calbiochem)	420355
L-(-)-norepinephrine bitartrate (NE)	Sigma	A9512
Laminin	Santa Cruz	sc-29012
LB agar	Carl Roth	X969.1
LB Medium	Carl Roth	X968.1
L-Carnitine	Sigma	C0158
L-glutamine	Life Technoligies (Invitrogen)	25030-081
Lipofectamine 2000 Transfection Reagent	Life Technologies (Thermo)	11668027
Lithium Chloride (LiCl)	Carl Roth	3739.1
Magnesium chloride hexahydrate (MgCl2 *6H2O)	Sigma	M927
MEM Non-Essential Amino Acids Solution (NAA)	Life Technologies	11140
Methanol	Sigma	32213
N,N,N',N'-tetramethylethane-1,2-diamine (TEMED)	Carl Roth	2367.3
NP-40 (IGEPAL)	Sigma	56741
Oligo(dT)18 Primer	Thermo Scientific	SO132
Olive oil	Sigma	75357
One Shot TOP10 Chemically Competent E. coli	Life Technologies (Invitrogen)	C4040
Orange G	Sigma	O3756
PageRuler Prestained Protein Ladder	Thermo Scientific	26616
Penicillin-Streptomycin (10,000 U/mL)	Life Technologies	15140-122
Phenol/Chloroform/Isoamyl alcohol (25:24:1)	Carl Roth	A156.2
Phosphatase Inhibitor Cocktail 2	Sigma	P5726
Polyethylenimin (PEI)	Sigma	764647
Poly-L-lysine	Sigma	P9155
Potassium chloride (KCl)	Carl Roth	6781.1
Potassium dihydrogen phosphate (KH2PO4)	Carl Roth	3904.1
Protease Inhibitor Cocktail	Sigma	P8849
QIAzol lysis reagent	Qiagen	79306
Recombinant Mouse FGF basic (bFGF)	R&D Systems	3139-FB-025
Recombinant Ribonuclease Inhibitor (RNaseOUT)	Life Technologies (Invitrogen)	10777-019
Rosiglitazone	Cayman Chemicals	71740
Rotiszint scintillation liquid	Carl Roth	0016.3
S.O.C. medium	Life Technologies (Invitrogen)	15544-034
Skim milk powder extra grade	Gerbu	1602
Sodium acetate (NaAc)	Applichem	A1522
Sodium chloride (NaCl)	Sigma	31434
Sodium deoxycholate (NaDOC)	Sigma	D6750

Sodium dihydrogen phosphate (NaH2PO4)	Applichem	A3559
Sodium dodecyl sulfate (SDS)	Sigma	62862
Sodium fluoride	Sigma	S1504
Sodium hydrogen carbonate (NaHCO3)	AppliChem	A0384
Sodium hydrogen phosphate (Na2HPO4)	Neolab	4066
Sodium hydroxide standard solution 8 mol/l	Sigma	35255
Sodium orthovanadate (Na3VO4)	Sigma	S6508
Sodium palmitate	Sigma	P9767
Sodium pyruvate	Life Technologies	11360070
sodium sulfate (Na2SO4)	Applichem	A3487
Solvable	Perkin Elmer	6NE9100
Streptavidin MicroBeads	Miltenyi Biotec	130-048-102
Streptozotocin	Axxora	LKT-S7870
Sucrose	Sigma	S1888
Sulforhodamine B sodium salt	Sigma	S9012
Sunflower seed oil from Helianthus annuus	Sigma	S5007
Tamoxifen	Sigma	T-5648
TaqMan Gene Expression Master Mix	Life Technologies	4369016
Triolein [9,10-3H(N)]	Hartmann	ART 0199
Tris base	Sigma	T1503
tri-Sodium citrate dihydrate	Sigma	71405
Triton-X100	AppliChem	A1388
Trypsin-EDTA solution	Life Technologies (Invitrogen)	25200072
Tween 20	Sigma	P9416
Tyloxapol	Sigma	T0307
Xylene	Merck	1.08681.2500
Zinc sulfate solution 0.3 N Zn(SO)4	Sigma	Z2876

Consumables

Table 18. Consumables

Consumable	Source	Catalogue number
10µl graduated tips	Starlab	S1111-3800
1000µl blue graduated tips	Starlab	S1111-2821
10ml Disposable Polystyrene Serological Pipet	Corning (Falcon)	356551
15ml tube PP, sterile (cellstar)	Greiner Bio One	188271
200µl yellow tips	Starlab	S1111-0806
250mL Vacuum Filter/Storage Bottle System, 0.22µm Pore	Sigma (Corning)	430756
25ml Disposable Polystyrene Serological Pipet	Corning (Falcon)	356535
300 µM nylon mesh (Polyamid Monofil)	Neolab	4-1411
50ml Disposable Polystyrene Serological Pipet	Corning (Falcon)	356550
50 ml syringe	BD Biosciences (Falcon)	1404297
50ml tube PP, sterile (cellstar)	Greiner Bio One	227261
5ml Disposable Polystyrene Serological Pipet	Corning (Falcon)	356543
70µM cell strainer nylon	BD Biosciences (Falcon)	352350
96 Well Black with Clear Flat Bottom	Corning (Falcon)	353219
96-Well Microplates, clear, flat bottom (MicroWell)	Thermo Scientific (Nunc)	95029780
Bench liner (Labmat)	VWR	246750000

Cell counting chamber slides (Countess)	Life Technologies (Invitrogen)	C10228
Cell Culture Dishes 100x20 mm	Corning (Falcon)	353003
Cell Culture Dishes 150x25 mm	Corning (Falcon)	353025
Cell Scrapers	Sigma (Corning)	CLS3010
Combitips advanced, 10 mL	Eppendorf	30089464
Combitips advanced, 5 mL	Eppendorf	30089456
Cover Slips	Carl Roth	H878.2
Cryo Cardboard Box, White	Neolab	Feb 01
Cryogenic vials, 1.8ml	Starlab	E3110-6122
Delicate Task Wipes	Kimberley Clark	7216
Dialysis tubing Cellulose Ester	Spectrum Laboratories	131270
Disposable Scalpels	Feather	EF7281 (2975-10)
Disposal bags (Sekuroka)	Carl Roth	E706.1
FPLC column (Superose 6, 10/300 GL)	GE Healthcare Life Sciences	17-5172-01
Gas cartridge	Campingaz	Z00059581
Gloves, Powder Free Textured Latex Exam	blossom	BM 11226-PF-AV
Glucose test strips (Acco-Chek Inform II)	Roche	473360
Grid insert for cryoboxes, 10x10	Neolab	Feb 03
Histology Mega-Cassette System (Tissue-Tek)	Sakura	4173
Insulin syringes (Micro-fine 1ml U-40, 0.33 mm x 12.7 mm)	Becton Dickinson	320801
large volume centrifuge tubes (500ml)	Sigma (Corning)	CLS431123
Liquidator96 LTS tips	Steinbrenner	SL-LT-L20
Micro haematocrit tubes	Brand	7493 11
MicroAmp® Fast Optical 96-Well Reaction Plate	Life Technologies	4346906
MicroAmp® Optical 8-Cap Strips	Life Technologies	4323032
MicroAmp® Optical Adhesive Film	Life Technologies	4311971
Micro-osmotic pump (model 1002)	Alzet	4317
Microscopy Slides	Carl Roth	0656.1
Mouse Genome 430 2.0 Array (GeneChip)	Affymetrix	900496
MS Columns	Miltenyi Biotec	130-042-201
needles (Neolus 27G,40 x 20 mm)	Terumo	NN-2719R
Nitril Gloves, Safeskin Purple	Kimberley Clark	52001M
Nitrocellulose membrane (Protran 0.45 N)	GE healthcare (Amersham)	10600002
Nuclease free SafeSeal Tubes (Multi)	Carl Roth	7080.1
Octo MACS Separator Starter Kit	Miltenyi Biotec	130-042-108
Paper towels comfort	Wepa	277200
Parafilm M	Sigma	P7793
Pasteur capillary pipetts long	Brand	747720
Petri dishes, 94x16 mm	Greiner Bio One	632 180
Pre-Separation Filters	Miltenyi Biotec	130-041-407
Prot/Elec Tips (gel loading)	Biorad	223-9916
Rodent Diet with 10% kcal% fat (low fat diet, LFD)	Research Diets	D12450J
Rodent Diet with 60% kcal% fat (low fat diet, LFD)	Research Diets	D12492
Round Bottom Polypropylene Tube with snap cap 14ml	BD Biosciences (Falcon)	352059
Safe-Lock Tubes 1.5 mL	Eppendorf	22363204
Safe-Lock Tubes 2.0 mL	Eppendorf	22363352
Safe-Lock Tubes, 1.5 ml	Eppendorf	0030 120.086
Safe-Lock Tubes, 2.0 ml	Eppendorf	0030 120.094
scintillation tubes, 5ml PP tube, PE cap	VWR	720-0495

Scintillation vials mini with screwcap	Carl Roth	5404.1
Soft-Ject Disposable Syringes 1ml	Henke Sass Wolf	5010.200V0
Syringe Filter Unit, 0.45 µm (Millex-HV)	Millipore	SLHV033RS
TipOne graduated filtertips, 10µl	Starlab	S1121-3810
TipOne graduated filtertips, 100µl	Starlab	S1120-1840
TipOne graduated filtertips, 1000µl	Starlab	S1126-7810
TipOne graduated filtertips, 20µl	Starlab	S1120-1810
TipOne graduated filtertips, 200µl	Starlab	S1120-8810
Tissue Culture Plates 24 well	Corning (Falcon)	353047
Tissue Culture Plates 48 well	Corning (Falcon)	353078
Tissue Culture Plates 96 well	Corning (Falcon)	353077
Transponder (implantable thermometer) (model IPTT-300)	BioMedic Data Systems	
Whatman cellulose blotting paper	Sigma (Whatman)	Z763187
XF96 FluxPak	Seahorse Bioscience	102310-001
XF96 Polystyrene Cell Culture Microplates	Seahorse Bioscience	101085-004

APPENDIX

Adenovirus Sequences

After cloning, the following AAV constructs were retrieved:

pdsAAV-Ucp1p-GFPmut-miR122site-miR-Tbl1:

- highlighted in yellow: Ucp1 mini promoter (*MluI* and *PstI* sites used for insertion underlined)
- highlighted in grey: miR-122 target site (*ApaI* and *AgeI* sites used for insertion underlined, repeats of miR-122 recognition sequence in bold)
- highlighted in blue: miR-Tbl1 hairpin
- highlighted in dark blue: ITR regions (internal repeat)

CAGCAGCTGGCGTAATAGCGAAGAGGCCCGCACCGATCGCCCTTCCCAACAGTTGCGCAGCCTGAATGGCGAATGGAATTCCAGACGATTGAGCGTCAAAATGTAGG
TATTTCCATGAGCGTTTTTCCTGTTGCAATGGCTGGCGGTAATATTGTTCTGGATATTACCAGCAAGGCCGATAGTTTGAGTTCTTCTACTCAGGCAAGTGATGTTATTA
CTAATCAAAGAAGTATTGCGACAACGGTTAATTTGCGTGATGGACAGACTCTTTTACTCGGTGGCCTCACTGATTATAAAACACTTCTCAGGATTCTGGCGTACCGTTC
CTGTCTAAAATCCCTTTAATCGGCCTCCTGTTTAGCTCCCGCTCTGATTCTAACGAGGAAAGCACGTTATACGTGCTCGTCAAAGCAACCATAGTACGCGCCCTGTAGC
GGCGCATTAAGCGCGGCGGGTGTGGTGGTTACGCGCAGCGTGACCGCTACACTTGCCAGCGCCCTAGCGCCCGCTCCTTTCGCTTTCTTCCCTTCCTTTCTCGCCAC
GTTCGCCGGCTTTCCCCGTCAAGCTCTAAATCGGGGGCTCCCTTTAGGGTTCCGATTTAGTGCTTTACGGCACCTCGACCCCAAAAAACTTGATTAGGGTGATGGTTC
ACGTAGTGGGCCATCGCCCTGATAGACGGTTTTTCGCCCTTTGACGTTGGAGTCCACGTTCTTTAATAGTGGACTCTTGTTCCAAACTGGAACAACACTCAACCCTATC
TCGGTCTATTCTTTTGATTTATAAGGGATTTTGCCGATTTCGGCCTATTGGTTAAAAAATGAGCTGATTTAACAAAAATTTAACGCGAATTTTAACAAAATATTAACGTTTA
CAATTTAAATATTTGCTTATACAATCTTCCTGTTTTTGGGGCTTTTCTGATTATCAACCGGGGTACATATGATTGACATGCTAGTTTTACGATTACCGTTCATCGCCCTGC
GCGCTCGCTCGCTCACTGAGGCCGCCCGGGCAAAGCCCGGGCGTCGGGCGACCTTTGGTCGCCCGGCCTCAGTGAGCGAGCGAGCGCGCAGAGAGGGAGTGGAA
TTCACGCGTGGTACCGAGCTCCTCTACAGCGTCACAGAGGGTCAGCAGTCACCCTTGACCACACTGAACTAGTCGTCACCTTTCCACTCTTCCTGCCAGAAGAGCAGA
AATCAGACTCTCTGGGGATATCAGCCTCACCCCTACTGCTCTCTCCATTATGAGGCAAACTTTCTTTCACTTCCCAGAGGCTCTGGGGGCAGCAAGGTCAACCCTTTCC
TCAGACTCTCGAGATCCGAGTGACGCGCGGCTGGGAGGCTTGCGCACCCAAGGCACGCCCCTGCCAAGTCCCACTAGCAGCTCTTTGGAGACCTGGGCCGGCTCAG
CCACTTCCCCCAGTCCCTCCTCCAGCAAGGGGCTATATAGATCTCCCAGGTCAGGGCGCAGAAGTGCCGGGCAATCTGGGCTTAACGGGTCCTCCCTGCCCGAGCAA
GAGGAAGGGACGCTCACCTTTGAGCTGCTCCACAGCGCCGCCTCTGCACTGGCACTACCTAGCCCAAGCTTCTGCAGAAGTTGGTCGTGAGGCACTGGGCAGGTAA
GTATCAAGGTTACAAGACAGGTTTAAGGAGACCAATAGAAACTGGGCTTGTCGAGACAGAGAAGACTCTTGCGTTTCTGATAGGCACCTATTGGTCTTACTGACATCCA
CTTTGCCTTTCTCTCCACAGGTGTCCACTCCCAGTTCAATTACAGCTCTTAAGGCTAGAGTACTTAATACGACTCACTATAGGCTAGCCTCGACGGTACCGCGGGCCCG
GGACACCATTGTCACACTCCAGTATACACAAACACCATTGTCACACTCCAGATATCACAAACACCATTGTCACACTCCAACCGGTCGCCACTGTAGAAGGGCGAGGAGC
TGTGAACCGGGGTGGTGCCTATCCTGGTCGAGCTGGACGGCGACGTATACGGCCACAAGTTCAGCGTGTCCGGCGAGGGCGAGGGCGATGCCACCTACGGCAAGC
TGACCCTGAAGTTCATCTGCACCACCGGCAAGCTGCCCGTGCCCTGGCCCACCCTCGTGACCACCCTGACCTACGGCGTGCAGTGCTTCAGCCGCTACCCCGACCA
CATGAAGCAGCACGACTTCTTCAAGTCCGCCATGCCCGAAGGCTACGTCCAGGAGCGCACCATCTTCTTCAAGGACGACGGCAACTACAAGACCCGCGCCGAGGTGA
AGTTCGAGGGCGACACCCTGGTGAACCGCATCGAGCTGAAGGGCATCGACTTCAAGGAGGACGGCAACATCCTGGGGCACAAGCTGGAGTACAACTACAACAGCCA
CAACGTCTATATCATGGCCGACAAGCAGAAGAACGGCATCAAGGTGAACTTCAAGATCCGCCACAACATCGAGGACGGCAGCGTGCAGCTCGCCGACCACTACCAGC
AGAACACCCCCATCGGCGACGGCCCCGTGCTGCTGCCCGACAACCACTACCTGAGCACCCAGTCCGCCCTGAGCAAAGACCCCAACGAGAAGCGCGATCACATGGT
CCTGCTGGAGTTCGTGACCGCCGCCGGGATCACTCTCGGCATGGACGAGCTGTACAAGTAAAGCGGCCGCGGGAGGTAGTGAGTCGACCAGTGGATCCTGGAGGCT
TGCTGAAGGCTGTATGCTGAAATGAAGCACTTGCTAACATGTTTTGGCCACTGACTGACATGTTAGCGTGCTTCATTTCAGGACACAAGGCCTGTTACTAGCACTCACA
TGGAACAAATGGCCCAGATCTGGCCGCACTCGAGATATCTAGAGCGGCCGCGACTCTAGATCATAATCAGCCATACCACATTTGTAGAGGTTTTACTTGCTTTAAAAAA
CCTCCCACACCTCCCCCTGAACCTGAAACATAAAATGAATGCAATTGTTGTTGTTAACTTGTTTATTGCAGCTTATAATGGTTACAAATAAAGCAATAGCATCACAAATTT
CACAAATAAAGCATTTTTTTCACTGCATTCTAGTTGTGGTTTGTCCAAACTCATCAATGTATCTTAAGGCGGGAATTGATCTGAGGAACCCTAGTGATGGAGTTGGCCAC
TCCCTCTCTGCGCGCTCGCTCGCTCACTGAGGCCGCCCGGGCAAAGCCCGGGCGTCGGGCGACCTTTGGTCGCCCGGCCTCAGTGAGCGAGCGAGCGCGCAGAGA
GGGAGTGGCCAACCCCCCCCCCCCCCCCCGGCGATTCTCTTGTTTGCTCCAGACTCTCAGGCAATGACCTGATAGCCTTTGTAGAGACCTCTCAAAAATAGCTACCC
TCTCCGGCATGAATTTATCAGCTAGAACGGTTGAATATCATATTGATGGTGATTTGACTGTCTCCGGCCTTTCTCACCCGTTTGAATCTTTACCTACACATTACTCAGGC
ATTGCATTTAAAATATATGAGGGTTCTAAAAATTTTTATCCTTGCGTTGAAATAAAGGCTTCTCCCGCAAAAGTATTACAGGGTCATAATGTTTTTGGTACAACCGATTTAG
CTTTATGCTCTGAGGCTTTATTGCTTAATTTTGCTAATTCTTTGCCTTGCCTGTATGATTTATTGGATGTTGGAATTCCTGATGCGGTATTTTCTCCTTACGCATCTGTGCG
GTATTTCACACCGCATATGGTGCACTCTCAGTACAATCTGCTCTGATGCCGCATAGTTAAGCCAGCCCCGACACCCGCCAACACCCGCTGACGCGCCCTGACGGGCTT
GTCTGCTCCCGGCATCCGCTTACAGACAAGCTGTGACCGTCTCCGGGAGCTGCATGTGTCAGAGGTTTTCACCGTCATCACCGAAACGCGCGAGACGAAAGGGCCTC
GTGATACGCCTATTTTTATAGGTTAATGTCATGATAATAATGGTTTCTTAGACGTCAGGTGGCACTTTTCGGGGAAATGTGCGCGGAACCCCTATTTGTTTATTTTTCTAA
ATACATTCAAATATGTATCCGCTCATGAGACAATAACCCTGATAAATGCTTCAATAATATTGAAAAGGAAGAGTATGAGTATTCAACATTTCCGTGTCGCCCTTATTCCC
TTTTTTGCGGCATTTTGCCTTCCTGTTTTTGCTCACCCAGAAACGCTGGTGAAAGTAAAAGATGCTGAAGATCAGTTGGGTGCACGAGTGGGTTACATCGAACTGGATC
TCAACAGCGGTAAGATCCTTGAGAGTTTTCGCCCCGAAGAACGTTTTCCAATGATGAGCACTTTTAAAGTTCTGCTATGTGGCGCGGTATTATCCCGTATTGACGCCGG
GCAAGAGCAACTCGGTCGCCGCATACACTATTCTCAGAATGACTTGGTTGAGTACTCACCAGTCACAGAAAAGCATCTTACGGATGGCATGACAGTAAGAGAATTATGC
AGTGCTGCCATAACCATGAGTGATAACACTGCGGCCAACTTACTTCTGACAACGATCGGAGGACCGAAGGAGCTAACCGCTTTTTTGCACAACATGGGGGATCATGTA

ACTCGCCTTGATCGTTGGGAACCGGAGCTGAATGAAGCCATACCAAACGACGAGCGTGACACCACGATGCCTGTAGCAATGGCAACAACGTTGCGCAAACTATTAACT
GGCGAACTACTTACTCTAGCTTCCCGGCAACAATTAATAGACTGGATGGAGGCGGATAAAGTTGCAGGACCACTTCTGCGCTCGGCCCTTCCGGCTGGCTGGTTTATT
GCTGATAAATCTGGAGCCGGTGAGCGTGGGTCTCGCGGTATCATTGCAGCACTGGGGCCAGATGGTAAGCCCTCCCGTATCGTAGTTATCTACACGACGGGGAGTCA
GGCAACTATGGATGAACGAAATAGACAGATCGCTGAGATAGGTGCCTCACTGATTAAGCATTGGTAACTGTCAGACCAAGTTTACTCATATATACTTTAGATTGATTTAA
AACTTCATTTTTAATTTAAAAGGATCTAGGTGAAGATCCTTTTTGATAATCTCATGACCAAAATCCCTTAACGTGAGTTTTCGTTCCACTGAGCGTCAGACCCCGTAGAAA
AGATCAAAGGATCTTCTTGAGATCCTTTTTTTCTGCGCGTAATCTGCTGCTTGCAAACAAAAAAACCACCGCTACCAGCGGTGGTTTGTTTGCCGGATCAAGAGCTACC
AACTCTTTTTCCGAAGGTAACTGGCTTCAGCAGAGCGCAGATACCAAATACTGTCCTTCTAGTGTAGCCGTAGTTAGGCCACCACTTCAAGAACTCTGTAGCACCGCCT
ACATACCTCGCTCTGCTAATCCTGTTACCAGTGGCTGCTGCCAGTGGCGATAAGTCGTGTCTTACCGGGTTGGACTCAAGACGATAGTTACCGGATAAGGCGCAGCGG
TCGGGCTGAACGGGGGGTTCGTGCACACAGCCCAGCTTGGAGCGAACGACCTACACCGAACTGAGATACCTACAGCGTGAGCTATGAGAAAGCGCCACGCTTCCCG
AAGGGAGAAAGGCGGACAGGTATCCGGTAAGCGGCAGGGTCGGAACAGGAGAGCGCACGAGGGAGCTTCCAGGGGGAAACGCCTGGTATCTTTATAGTCCTGTCG
GGTTTCGCCACCTCTGACTTGAGCGTCGATTTTTGTGATGCTCGTCAGGGGGGCGGAGCCTATGGAAAAACGCCAGCAACGCGGCCTTTTTACGGTTCCTGGCCTTTT
GCTGGCCTTTTGCTCACATGTTCTTTCCTGCGTTATCCCCTGATTCTGTGGATAACCGTATTACCGCCTTTGAGTGAGCTGATACCGCTCGCCGCAGCCGAACGACCGA
GCGCAGCGAGTCAGTGAGCGAGGAAGCGGAAGAGCGCCCAATACGCAAACCGCCTCTCCCCGCGCGTTGGCCGATTCATTAATG

For miR-Tblr1 and miR-NC constructs, sequence was identical apart from the expressed micro RNA:

pdsAAV-Ucp1p-GFPmut-miR122site-miR-Tblr1:

TGTTCACTATTCCAATCTAGAGAGTTTTGGCCACTGACTGACTCTCTAGAGGAATAGTGAA

pdsAAV-Ucp1p-GFPmut-miR122site-miR-NC:

TGAAATGTACTGCGCGTGGAGACGTTTTGGCCACTGACTGACGTCTCCACGCAGTACATTT

Glossary

(E)p300 (E1A binding protein p300)
^{2}DOG (deoxy-D-glucose)
^{3}H-2DOG (^{3}H-2-Deoxy-D-glucose)
AAV (adeno-associated virus)
Acaa2 (acetyl-Coenzyme A acyltransferase 2)
ACC (acetyl-coenzyme A carboxylase)
Acsl5 (acyl-CoA synthetase long-chain family member 5)
ADP (adenosine diphosphate)
Adrb3, β3-AR (β3-adrenoreceptor)
AF (adipocyte fraction)
AKT (protein Kinase B)
Angptl3 (angiopoietin-like 3)
Angptl4 (angiopoietin-like 4)
aP-2 (adipocyte protein 2, also fatty acid binding protein 4, FABP4)
Apoc3 (apolipoprotein 3)
APS (ammonium persulfate)
Aqp7 (aquaporin7)
AR (androgen receptor)
ATKO mice (adipose tissue knockout mice)
ATP (adenosine triphosphate)
Atp5o (ATP synthase subunit O)
AUC (Area under the curve)
AV (adenovirus)
aWAT (intra-abdominal / visceral WAT)
$Ba(OH)_2$ (Barium hydroxide)
BAT (brown adipose tissue)
BATF (basic leucine zipper transcription factor)
BATKO (brown adipose tissue-specific TBLR1 knockout mice)
bFGF (basic fibroblast growth factor)
BL6 (C57Bl6 mice)
BMI (body mass index)
BMPs (bone morphogenic proteins)
brite (brown in white)
BSA (bovine serum albumin)
C/EBPα, C/EBPβ, C/EBPδ (CCAAT/enhancer-binding protein alpha, beta, delta)
cAMP (cyclic adenosin monophosphate)
Cav2 (caveolin 2)
Cfd (complement factor D, also known ad adipsin)
ChIP (chromatin immune-precipitation)
ChIPseq (chromatin immune-precipitation sequencing)
Cidea (cell death-inducing DNA fragmentation factor, alpha subunit-like effector A)
CIP (calf intestinal phosphatase)
CL (CL316243)
CO_2 (carbon dioxide)
Cox7a1 (cytochrome c oxidase subunit VIIa 1)
Cox8b (cytochrome c oxidase subunit VIIIb)
$cPGI_2$ (carbaprostacyclin)
CPM (counts per minute)
Cpt1b) (carnitine palmitoyltransferase 1b)
CREB (cAMP responsive element binding)
CsCl (cesium chloride)
Dex (dexamethasone)
DMEM (Dulbecco's Modified Eagle Medium)
DPM (disintegrations per minute)
DSG (disuccinimidyl glutarate)
DTT (dithiothreitol)
Dusp10 (dual specificity protein phosphatase 10)
Dusp6 (dual specificity phosphatase 6)
early KD (knockdown 2 days prior to induction of adipogenic differentiation)
EDTA (ethylenediaminetetraacetic acid)
ELISA (enzyme-linked immunosorbent assay)
Elovl6 (elongation of long-chain fatty acids family member 6)
ER (estrogen receptor)
EtBr (ethidiumbromide)
EtOH (ethanol)
Fabp4 (fatty acid binding protein 4)
FABP4 (fatty acid binding protein 4, also adipocyte protein 2, aP-2)
FAs, FFAs (fatty acids, free fatty acids)
FCCP (carbonyl cyanide 4-(trifluoromethoxy)phenylhydrazone)
FCS (fetal calf serum)
Fgf21 (fibroblast growth factor 21)
Forsk (forskolin)
FOXA1, 2 (forkhead box A1, 2)
FPLC (fast-protein liquid chromatography)
G_2P (glycerol-2-phosphate)
GAPDH (glycerinaldehyd-3-phosphat-dehydrogenase)
GATA3 (GATA binding protein 3)
GC (gastrocnemius skeletal muscle)
Glut1 (glucose transporter 1)
GPCR (G-protein coupled receptor)
GR) (glucocorticoid receptor)
GSK3 (Glycogen synthase kinase 3)
GTT (glucose tolerance test)
H^+ (proton)
HDACs (histone-deacetylases)
HDL (high density lipoprotein)
HFD (high fat diet)
i.p. (intraperitoneally)
IBMX (3-isobutyl-1-methylxanthin)
IGF-1 (insulin-like growth factor)
Iso (isoproterenol)
ITT (insulin tolerance test)
iWAT (inguinal WAT)
kb (kilobasepairs)
KCl (potassium chloride)
KD (knockdown)
kg (kilograms)
KH_2PO_4 (Potassium dihydrogen phosphate)
KO (knockout)
KRB (Krebs Ringer Buffer)
late KD (knockdown 2 days prior to harvest of mature adipocytes)
Ldlr (LDL receptor)
LFD (low fat diet)
LiCl (lithium chloride)
LPL (lipoprotein lipase)

LXR (liver X rexeptor)
MAP kinase (p38 mitogen-activated protein kinase)
Map4k (mitogen-activated protein kinase kinase kinase kinase)
MAPK (mitogen-activated protein kinase)
MOI (multiplicity of infection)
MRI (magnetic resonance imaging)
MSCs (mesodermal stem cells)
Myf5 (myogenic factor 5)
N_2 (Nitrogen)
Na_2HPO_4 (disodium phosphate)
Na_3VO_4 (sodium orthovanadate)
NAA (non-essential-amino-acids)
NaAc (sodium acetate)
NaCl (sodium chloride)
NaDOC (sodium deoxycholate)
NaF (sodium fluoride)
NaH_2PO_4 (sodium dihydrogen phosphate)
$NaHCO_3$ (sodium hydrogen carbonate)
NaOH (sodium hydroxide)
NCoR (nuclear receptor co-repressor)
NE (norepinephrine)
NEFAs (non-esterified fatty acids)
NF-κB (nuclear factor κB)
Nrg4 (neuregulin 4)
NRs (nuclear receptors)
o.n. (over night)
O_2 (oxygen)
P/S (penicillin / streptomycine)
PARP1 (poly-[ADP-Ribose]-polymerase 1)
PBS (phosphate buffered saline)
PCI (phenol chloroform isoamylalcohol)
PCR (polymerase chain reaction)
Pdk4 (pyruvate dehydrogenase kinase)
PEB (protein extraction buffer)
PEI (polyethylenimin)
pfu (plaque forming units)
PGC-1α (peroxisome proliferator-activated receptor gamma coactivator 1-alpha)
P_i (inorganic phosphate)
PIC (protease inhibitor cocktail)
PKA (protein kinase A)
PKCδ (protein kinase C-δ)
pola1 (DNA polymerase A1)
Ppara, Pparg / PPARα, PPARγ (peroxisome proliferator activated receptor alpha, gamma)
PRDM16 (PRD1-BF1-RIZ1 homologous domain containing 16)
PS (polystyrene)
qRT-PCR (quantitative real-time polymerase chain reaction)
RER (respiratory exchange ratio)
Res (response elements)
Retn (resistin)
RMR (resting metabolic rate)
RNAseq (RNA sequencing)
Rosi (rosiglitazone)
RXRα (retinoid X receptor alpha)
Scd1 (stearoyl-CoA desaturase-1)
Sdhb, Sdhc (succinate dehydrogenase complex subunit B, C)
SDS (sodium dodecyl sulfate)
SEM (standard error of the mean)
shRNA (short hairpin RNA)
Sirt1 (sirtuin-1)
Smad6 (SMAD family member 6)
SMRT (silencing mediator of retinoid and thyroid receptors)
Srebp1c (sterol regulatory element-binding protein 1c)
STZ (streptozotocin)
SV129 (129S6/SvEvTac mice)
SVF (stromal vascular fraction)
T_3 (thyroid hormone, 3,3′,5-triiodothyronine)
TBE (tris-borate-EDTA)
TBL (transducin (beta)-like 1 X-linked, also TBL1X)
TBLR (transducin (beta)-like 1 X-linked receptor 1, also TBL1XR1)
TBS-T (tris buffered saline with tween)
TEMED (N,N,N',N'-tetramethylethane-1,2-diamine)
TF (transcription factor)
TGs (triglycerides)
TNFα (tumor necrosis factor alpha)
UCP-1 (uncoupling protein 1, also thermogenin)
VCO_2 (carbon dioxide consumption)
VLDL (very low density lipoprotein)
VO_2 (oxygen consumption)
WAT (white adipose tissue)
$ZnSO_2$ (zinc sulfate)

LITERATURE

1. Tam, C.S., V. Lecoultre, and E. Ravussin, *Brown adipose tissue: mechanisms and potential therapeutic targets.* Circulation, 2012. **125**(22): p. 2782-91.
2. Cinti, S., *Between brown and white: novel aspects of adipocyte differentiation.* Ann Med, 2011. **43**(2): p. 104-15.
3. Perissi, V., et al., *TBL1 and TBLR1 phosphorylation on regulated gene promoters overcomes dual CtBP and NCoR/SMRT transcriptional repression checkpoints.* Mol Cell, 2008. **29**(6): p. 755-66.
4. Siersbaek, R., et al., *Extensive chromatin remodelling and establishment of transcription factor 'hotspots' during early adipogenesis.* EMBO J, 2011. **30**(8): p. 1459-72.
5. Lazar, M.A., *Nuclear receptor corepressors.* Nucl Recept Signal, 2003. **1**: p. e001.
6. Bourguet, W., P. Germain, and H. Gronemeyer, *Nuclear receptor ligand-binding domains: three-dimensional structures, molecular interactions and pharmacological implications.* Trends Pharmacol Sci, 2000. **21**(10): p. 381-8.
7. Vidal-Puig, A.J., *Uncoupling expectations.* Nat Genet, 2000. **26**(4): p. 387-8.
8. Harms, M. and P. Seale, *Brown and beige fat: development, function and therapeutic potential.* Nat Med, 2013. **19**(10): p. 1252-63.
9. Nedergaard, J., T. Bengtsson, and B. Cannon, *Unexpected evidence for active brown adipose tissue in adult humans.* Am J Physiol Endocrinol Metab, 2007. **293**(2): p. E444-52.
10. Jeffery, R.W., et al., *Socioeconomic status differences in health behaviors related to obesity: the Healthy Worker Project.* Int J Obes, 1991. **15**(10): p. 689-96.
11. Sorensen, T.I., *Socio-economic aspects of obesity: causes or effects?* Int J Obes Relat Metab Disord, 1995. **19 Suppl 6**: p. S6-8.
12. Choquet, H. and D. Meyre, *Genetics of Obesity: What have we Learned?* Curr Genomics, 2011. **12**(3): p. 169-79.
13. Walley, A.J., A.I. Blakemore, and P. Froguel, *Genetics of obesity and the prediction of risk for health.* Hum Mol Genet, 2006. **15 Spec No 2**: p. R124-30.
14. Eckel, R.H., S.M. Grundy, and P.Z. Zimmet, *The metabolic syndrome.* Lancet, 2005. **365**(9468): p. 1415-28.
15. Muoio, D.M. and C.B. Newgard, *Mechanisms of disease:Molecular and metabolic mechanisms of insulin resistance and beta-cell failure in type 2 diabetes.* Nat Rev Mol Cell Biol, 2008. **9**(3): p. 193-205.
16. Eckel, R.H., *Lipoprotein lipase. A multifunctional enzyme relevant to common metabolic diseases.* N Engl J Med, 1989. **320**(16): p. 1060-8.
17. Kim, Y.B., G.I. Shulman, and B.B. Kahn, *Fatty acid infusion selectively impairs insulin action on Akt1 and protein kinase C lambda /zeta but not on glycogen synthase kinase-3.* J Biol Chem, 2002. **277**(36): p. 32915-22.
18. Chavez, J.A., et al., *A role for ceramide, but not diacylglycerol, in the antagonism of insulin signal transduction by saturated fatty acids.* J Biol Chem, 2003. **278**(12): p. 10297-303.

19. Samuel, V.T., et al., *Mechanism of hepatic insulin resistance in non-alcoholic fatty liver disease.* J Biol Chem, 2004. **279**(31): p. 32345-53.
20. Strissel, K.J., et al., *Adipocyte death, adipose tissue remodeling, and obesity complications.* Diabetes, 2007. **56**(12): p. 2910-8.
21. Xu, H., et al., *Chronic inflammation in fat plays a crucial role in the development of obesity-related insulin resistance.* J Clin Invest, 2003. **112**(12): p. 1821-30.
22. Lewis, G.F., et al., *Interaction between free fatty acids and insulin in the acute control of very low density lipoprotein production in humans.* J Clin Invest, 1995. **95**(1): p. 158-66.
23. Gordon, T., et al., *High density lipoprotein as a protective factor against coronary heart disease. The Framingham Study.* Am J Med, 1977. **62**(5): p. 707-14.
24. Kwiterovich, P.O., Jr., *The metabolic pathways of high-density lipoprotein, low-density lipoprotein, and triglycerides: a current review.* Am J Cardiol, 2000. **86**(12A): p. 5L-10L.
25. Hanson, R.L., et al., *Components of the "metabolic syndrome" and incidence of type 2 diabetes.* Diabetes, 2002. **51**(10): p. 3120-7.
26. Laaksonen, D.E., et al., *Metabolic syndrome and development of diabetes mellitus: application and validation of recently suggested definitions of the metabolic syndrome in a prospective cohort study.* Am J Epidemiol, 2002. **156**(11): p. 1070-7.
27. Gesta, S., Y.H. Tseng, and C.R. Kahn, *Developmental origin of fat: tracking obesity to its source.* Cell, 2007. **131**(2): p. 242-56.
28. Berry, D.C., et al., *The developmental origins of adipose tissue.* Development, 2013. **140**(19): p. 3939-49.
29. Kissebah, A.H. and G.R. Krakower, *Regional adiposity and morbidity.* Physiol Rev, 1994. **74**(4): p. 761-811.
30. Fain, J.N., et al., *Comparison of the release of adipokines by adipose tissue, adipose tissue matrix, and adipocytes from visceral and subcutaneous abdominal adipose tissues of obese humans.* Endocrinology, 2004. **145**(5): p. 2273-82.
31. Kershaw, E.E. and J.S. Flier, *Adipose tissue as an endocrine organ.* J Clin Endocrinol Metab, 2004. **89**(6): p. 2548-56.
32. Bourin, P., et al., *Stromal cells from the adipose tissue-derived stromal vascular fraction and culture expanded adipose tissue-derived stromal/stem cells: a joint statement of the International Federation for Adipose Therapeutics and Science (IFATS) and the International Society for Cellular Therapy (ISCT).* Cytotherapy, 2013. **15**(6): p. 641-8.
33. Hirsch, J. and B. Batchelor, *Adipose tissue cellularity in human obesity.* Clin Endocrinol Metab, 1976. **5**(2): p. 299-311.
34. Nicholls, D.G., V.S. Bernson, and G.M. Heaton, *The identification of the component in the inner membrane of brown adipose tissue mitochondria responsible for regulating energy dissipation.* Experientia Suppl, 1978. **32**: p. 89-93.
35. Virtanen, K.A., et al., *Functional brown adipose tissue in healthy adults.* N Engl J Med, 2009. **360**(15): p. 1518-25.

36. van Marken Lichtenbelt, W.D., et al., *Cold-activated brown adipose tissue in healthy men.* N Engl J Med, 2009. **360**(15): p. 1500-8.
37. Cypess, A.M., et al., *Identification and importance of brown adipose tissue in adult humans.* N Engl J Med, 2009. **360**(15): p. 1509-17.
38. Bray, G.A. and L.A. Tartaglia, *Medicinal strategies in the treatment of obesity.* Nature, 2000. **404**(6778): p. 672-7.
39. Moitra, J., et al., *Life without white fat: a transgenic mouse.* Genes Dev, 1998. **12**(20): p. 3168-81.
40. Ross, S.R., R.A. Graves, and B.M. Spiegelman, *Targeted expression of a toxin gene to adipose tissue: transgenic mice resistant to obesity.* Genes Dev, 1993. **7**(7B): p. 1318-24.
41. Peirce, V. and A. Vidal-Puig, *Regulation of glucose homoeostasis by brown adipose tissue.* Lancet Diabetes Endocrinol, 2013. **1**(4): p. 353-60.
42. Orava, J., et al., *Different metabolic responses of human brown adipose tissue to activation by cold and insulin.* Cell Metab, 2011. **14**(2): p. 272-9.
43. Enerback, S., *Human brown adipose tissue.* Cell Metab, 2010. **11**(4): p. 248-52.
44. Cinti, S., *Adipocyte differentiation and transdifferentiation: plasticity of the adipose organ.* J Endocrinol Invest, 2002. **25**(10): p. 823-35.
45. Tonello, C., et al., *Role of sympathetic activity in controlling the expression of vascular endothelial growth factor in brown fat cells of lean and genetically obese rats.* FEBS Lett, 1999. **442**(2-3): p. 167-72.
46. Nedergaard, J., D. Ricquier, and L.P. Kozak, *Uncoupling proteins: current status and therapeutic prospects.* EMBO Rep, 2005. **6**(10): p. 917-21.
47. Golozoubova, V., et al., *Only UCP1 can mediate adaptive nonshivering thermogenesis in the cold.* FASEB J, 2001. **15**(11): p. 2048-50.
48. Nedergaard, J., et al., *UCP1: the only protein able to mediate adaptive non-shivering thermogenesis and metabolic inefficiency.* Biochim Biophys Acta, 2001. **1504**(1): p. 82-106.
49. Farmer, S.R., *Brown fat and skeletal muscle: unlikely cousins?* Cell, 2008. **134**(5): p. 726-7.
50. Wang, E.A., et al., *Bone morphogenetic protein-2 causes commitment and differentiation in C3H10T1/2 and 3T3 cells.* Growth Factors, 1993. **9**(1): p. 57-71.
51. Huang, H., et al., *BMP signaling pathway is required for commitment of C3H10T1/2 pluripotent stem cells to the adipocyte lineage.* Proc Natl Acad Sci U S A, 2009. **106**(31): p. 12670-5.
52. Suh, J.M., et al., *Hedgehog signaling plays a conserved role in inhibiting fat formation.* Cell Metab, 2006. **3**(1): p. 25-34.
53. Arango, N.A., et al., *Conditional deletion of beta-catenin in the mesenchyme of the developing mouse uterus results in a switch to adipogenesis in the myometrium.* Dev Biol, 2005. **288**(1): p. 276-83.
54. Kennell, J.A. and O.A. MacDougald, *Wnt signaling inhibits adipogenesis through beta-catenin-dependent and -independent mechanisms.* J Biol Chem, 2005. **280**(25): p. 24004-10.
55. Tang, Q.Q., T.C. Otto, and M.D. Lane, *CCAAT/enhancer-binding protein beta is required for mitotic clonal expansion during adipogenesis.* Proc Natl Acad Sci U S A, 2003. **100**(3): p. 850-5.

56. Zhang, J.W., et al., *Role of CREB in transcriptional regulation of CCAAT/enhancer-binding protein beta gene during adipogenesis.* J Biol Chem, 2004. **279**(6): p. 4471-8.
57. Cao, Z., R.M. Umek, and S.L. McKnight, *Regulated expression of three C/EBP isoforms during adipose conversion of 3T3-L1 cells.* Genes Dev, 1991. **5**(9): p. 1538-52.
58. Yeh, W.C., et al., *Cascade regulation of terminal adipocyte differentiation by three members of the C/EBP family of leucine zipper proteins.* Genes Dev, 1995. **9**(2): p. 168-81.
59. Tontonoz, P., E. Hu, and B.M. Spiegelman, *Stimulation of adipogenesis in fibroblasts by PPAR gamma 2, a lipid-activated transcription factor.* Cell, 1994. **79**(7): p. 1147-56.
60. Rosen, E.D., et al., *C/EBPalpha induces adipogenesis through PPARgamma: a unified pathway.* Genes Dev, 2002. **16**(1): p. 22-6.
61. Wu, Z., N.L. Bucher, and S.R. Farmer, *Induction of peroxisome proliferator-activated receptor gamma during the conversion of 3T3 fibroblasts into adipocytes is mediated by C/EBPbeta, C/EBPdelta, and glucocorticoids.* Mol Cell Biol, 1996. **16**(8): p. 4128-36.
62. Wu, Z., et al., *Conditional ectopic expression of C/EBP beta in NIH-3T3 cells induces PPAR gamma and stimulates adipogenesis.* Genes Dev, 1995. **9**(19): p. 2350-63.
63. Seale, P., et al., *PRDM16 controls a brown fat/skeletal muscle switch.* Nature, 2008. **454**(7207): p. 961-7.
64. Seale, P., et al., *Transcriptional control of brown fat determination by PRDM16.* Cell Metab, 2007. **6**(1): p. 38-54.
65. Ashwell, M., et al., *Effect of acclimation temperature on the concentration of the mitochondrial 'uncoupling' protein measured by radioimmunoassay in mouse brown adipose tissue.* FEBS Lett, 1983. **161**(1): p. 108-12.
66. Huttunen, P., J. Hirvonen, and V. Kinnula, *The occurrence of brown adipose tissue in outdoor workers.* Eur J Appl Physiol Occup Physiol, 1981. **46**(4): p. 339-45.
67. Guerra, C., et al., *Emergence of brown adipocytes in white fat in mice is under genetic control. Effects on body weight and adiposity.* J Clin Invest, 1998. **102**(2): p. 412-20.
68. Cousin, B., et al., *Occurrence of brown adipocytes in rat white adipose tissue: molecular and morphological characterization.* J Cell Sci, 1992. **103 (Pt 4)**: p. 931-42.
69. Goudenege, S., et al., *Enhancement of myogenic and muscle repair capacities of human adipose-derived stem cells with forced expression of MyoD.* Mol Ther, 2009. **17**(6): p. 1064-72.
70. Timmons, J.A., et al., *Myogenic gene expression signature establishes that brown and white adipocytes originate from distinct cell lineages.* Proc Natl Acad Sci U S A, 2007. **104**(11): p. 4401-6.
71. Kopecky, J., et al., *Synthesis of mitochondrial uncoupling protein in brown adipocytes differentiated in cell culture.* J Biol Chem, 1990. **265**(36): p. 22204-9.
72. Lee, Y.H., et al., *In vivo identification of bipotential adipocyte progenitors recruited by beta3-adrenoceptor activation and high-fat feeding.* Cell Metab, 2012. **15**(4): p. 480-91.
73. Wang, Q.A., et al., *Tracking adipogenesis during white adipose tissue development, expansion and regeneration.* Nat Med, 2013. **19**(10): p. 1338-44.

74. Granneman, J.G., et al., *Metabolic and cellular plasticity in white adipose tissue I: effects of beta3-adrenergic receptor activation.* Am J Physiol Endocrinol Metab, 2005. **289**(4): p. E608-16.
75. Himms-Hagen, J., et al., *Multilocular fat cells in WAT of CL-316243-treated rats derive directly from white adipocytes.* Am J Physiol Cell Physiol, 2000. **279**(3): p. C670-81.
76. Barbatelli, G., et al., *The emergence of cold-induced brown adipocytes in mouse white fat depots is determined predominantly by white to brown adipocyte transdifferentiation.* Am J Physiol Endocrinol Metab, 2010. **298**(6): p. E1244-53.
77. Cinti, S., *Transdifferentiation properties of adipocytes in the adipose organ.* Am J Physiol Endocrinol Metab, 2009. **297**(5): p. E977-86.
78. Cannon, B. and J. Nedergaard, *Brown adipose tissue: function and physiological significance.* Physiol Rev, 2004. **84**(1): p. 277-359.
79. Rosen, E.D. and B.M. Spiegelman, *Adipocytes as regulators of energy balance and glucose homeostasis.* Nature, 2006. **444**(7121): p. 847-53.
80. Schultz, B.E. and S.I. Chan, *Structures and proton-pumping strategies of mitochondrial respiratory enzymes.* Annu Rev Biophys Biomol Struct, 2001. **30**: p. 23-65.
81. Rousset, S., et al., *The biology of mitochondrial uncoupling proteins.* Diabetes, 2004. **53 Suppl 1**: p. S130-5.
82. Klingenberg, M. and K.S. Echtay, *Uncoupling proteins: the issues from a biochemist point of view.* Biochim Biophys Acta, 2001. **1504**(1): p. 128-43.
83. Garofalo, M.A., et al., *Effect of acute cold exposure on norepinephrine turnover rates in rat white adipose tissue.* J Auton Nerv Syst, 1996. **60**(3): p. 206-8.
84. Evans, B.A., et al., *Ligand-directed signalling at beta-adrenoceptors.* Br J Pharmacol, 2010. **159**(5): p. 1022-38.
85. Bronnikov, G., et al., *beta1 to beta3 switch in control of cyclic adenosine monophosphate during brown adipocyte development explains distinct beta-adrenoceptor subtype mediation of proliferation and differentiation.* Endocrinology, 1999. **140**(9): p. 4185-97.
86. Sprang, S.R., *Cell signalling: Binding the receptor at both ends.* Nature, 2011. **469**(7329): p. 172-3.
87. Hansen, J.B. and K. Kristiansen, *Regulatory circuits controlling white versus brown adipocyte differentiation.* Biochem J, 2006. **398**(2): p. 153-68.
88. Collins, S., W. Cao, and J. Robidoux, *Learning new tricks from old dogs: beta-adrenergic receptors teach new lessons on firing up adipose tissue metabolism.* Mol Endocrinol, 2004. **18**(9): p. 2123-31.
89. Gonzalez, G.A. and M.R. Montminy, *Cyclic AMP stimulates somatostatin gene transcription by phosphorylation of CREB at serine 133.* Cell, 1989. **59**(4): p. 675-80.
90. Thonberg, H., et al., *A novel pathway for adrenergic stimulation of cAMP-response-element-binding protein (CREB) phosphorylation: mediation via alpha1-adrenoceptors and protein kinase C activation.* Biochem J, 2002. **364**(Pt 1): p. 73-9.
91. Zhou, Z., et al., *Cidea-deficient mice have lean phenotype and are resistant to obesity.* Nat Genet, 2003. **35**(1): p. 49-56.

92. Cao, W., et al., *p38 mitogen-activated protein kinase is the central regulator of cyclic AMP-dependent transcription of the brown fat uncoupling protein 1 gene.* Mol Cell Biol, 2004. **24**(7): p. 3057-67.
93. Herzig, S., et al., *CREB regulates hepatic gluconeogenesis through the coactivator PGC-1.* Nature, 2001. **413**(6852): p. 179-83.
94. Sears, I.B., et al., *Differentiation-dependent expression of the brown adipocyte uncoupling protein gene: regulation by peroxisome proliferator-activated receptor gamma.* Mol Cell Biol, 1996. **16**(7): p. 3410-9.
95. Shabalina, I.G., et al., *Native UCP1 displays simple competitive kinetics between the regulators purine nucleotides and fatty acids.* J Biol Chem, 2004. **279**(37): p. 38236-48.
96. Djouder, N., et al., *PKA phosphorylates and inactivates AMPKalpha to promote efficient lipolysis.* EMBO J, 2010. **29**(2): p. 469-81.
97. Carmen, G.Y. and S.M. Victor, *Signalling mechanisms regulating lipolysis.* Cell Signal, 2006. **18**(4): p. 401-8.
98. Egan, J.J., et al., *Mechanism of hormone-stimulated lipolysis in adipocytes: translocation of hormone-sensitive lipase to the lipid storage droplet.* Proc Natl Acad Sci U S A, 1992. **89**(18): p. 8537-41.
99. Prusiner, S.B., B. Cannon, and O. Lindberg, *Oxidative metabolism in cells isolated from brown adipose tissue. 1. Catecholamine and fatty acid stimulation of respiration.* Eur J Biochem, 1968. **6**(1): p. 15-22.
100. Wojtczak, L. and P. Schonfeld, *Effect of fatty acids on energy coupling processes in mitochondria.* Biochim Biophys Acta, 1993. **1183**(1): p. 41-57.
101. Matthias, A., et al., *Thermogenic responses in brown fat cells are fully UCP1-dependent. UCP2 or UCP3 do not substitute for UCP1 in adrenergically or fatty scid-induced thermogenesis.* J Biol Chem, 2000. **275**(33): p. 25073-81.
102. Shabalina, I.G., et al., *Within brown-fat cells, UCP1-mediated fatty acid-induced uncoupling is independent of fatty acid metabolism.* Biochim Biophys Acta, 2008. **1777**(7-8): p. 642-50.
103. Stock, M.J., *Gluttony and thermogenesis revisited.* Int J Obes Relat Metab Disord, 1999. **23**(11): p. 1105-17.
104. Rothwell, N.J. and M.J. Stock, *A role for brown adipose tissue in diet-induced thermogenesis.* Nature, 1979. **281**(5726): p. 31-5.
105. Mercer, S.W. and P. Trayhurn, *Effect of high fat diets on energy balance and thermogenesis in brown adipose tissue of lean and genetically obese ob/ob mice.* J Nutr, 1987. **117**(12): p. 2147-53.
106. Lowell, B.B., et al., *Development of obesity in transgenic mice after genetic ablation of brown adipose tissue.* Nature, 1993. **366**(6457): p. 740-2.
107. Enerback, S., et al., *Mice lacking mitochondrial uncoupling protein are cold-sensitive but not obese.* Nature, 1997. **387**(6628): p. 90-4.
108. Oberkofler, H., et al., *Uncoupling protein gene: quantification of expression levels in adipose tissues of obese and non-obese humans.* J Lipid Res, 1997. **38**(10): p. 2125-33.

109. Stock, M.J. and N.J. Rothwell, *Role of brown adipose tissue thermogenesis in overfeeding: a review.* J R Soc Med, 1983. **76**(1): p. 71-3.

110. Greco-Perotto, R., et al., *Stimulatory effect of cold adaptation on glucose utilization by brown adipose tissue. Relationship with changes in the glucose transporter system.* J Biol Chem, 1987. **262**(16): p. 7732-6.

111. Bartelt, A., et al., *Brown adipose tissue activity controls triglyceride clearance.* Nat Med, 2011. **17**(2): p. 200-5.

112. McKenna, N.J. and B.W. O'Malley, *Combinatorial control of gene expression by nuclear receptors and coregulators.* Cell, 2002. **108**(4): p. 465-74.

113. Olefsky, J.M., *Nuclear receptor minireview series.* J Biol Chem, 2001. **276**(40): p. 36863-4.

114. Evans, R.M., *The steroid and thyroid hormone receptor superfamily.* Science, 1988. **240**(4854): p. 889-95.

115. Mangelsdorf, D.J., et al., *The nuclear receptor superfamily: the second decade.* Cell, 1995. **83**(6): p. 835-9.

116. McKenna, N.J., R.B. Lanz, and B.W. O'Malley, *Nuclear receptor coregulators: cellular and molecular biology.* Endocr Rev, 1999. **20**(3): p. 321-44.

117. Horlein, A.J., et al., *Ligand-independent repression by the thyroid hormone receptor mediated by a nuclear receptor co-repressor.* Nature, 1995. **377**(6548): p. 397-404.

118. Chen, J.D. and R.M. Evans, *A transcriptional co-repressor that interacts with nuclear hormone receptors.* Nature, 1995. **377**(6548): p. 454-7.

119. Seol, W., et al., *Two receptor interacting domains in the nuclear hormone receptor corepressor RIP13/N-CoR.* Mol Endocrinol, 1996. **10**(12): p. 1646-55.

120. Hollenberg, A.N., et al., *Function of nuclear co-repressor protein on thyroid hormone response elements is regulated by the receptor A/B domain.* J Biol Chem, 1996. **271**(45): p. 28516-20.

121. Guenther, M.G., et al., *A core SMRT corepressor complex containing HDAC3 and TBL1, a WD40-repeat protein linked to deafness.* Genes Dev, 2000. **14**(9): p. 1048-57.

122. Li, J., et al., *Both corepressor proteins SMRT and N-CoR exist in large protein complexes containing HDAC3.* EMBO J, 2000. **19**(16): p. 4342-50.

123. Zhang, J., et al., *The N-CoR-HDAC3 nuclear receptor corepressor complex inhibits the JNK pathway through the integral subunit GPS2.* Mol Cell, 2002. **9**(3): p. 611-23.

124. Hong, S.H. and M.L. Privalsky, *The SMRT corepressor is regulated by a MEK-1 kinase pathway: inhibition of corepressor function is associated with SMRT phosphorylation and nuclear export.* Mol Cell Biol, 2000. **20**(17): p. 6612-25.

125. Chen, H., et al., *Regulation of hormone-induced histone hyperacetylation and gene activation via acetylation of an acetylase.* Cell, 1999. **98**(5): p. 675-86.

126. Lonard, D.M., et al., *The 26S proteasome is required for estrogen receptor-alpha and coactivator turnover and for efficient estrogen receptor-alpha transactivation.* Mol Cell, 2000. **5**(6): p. 939-48.

127. Puigserver, P., et al., *A cold-inducible coactivator of nuclear receptors linked to adaptive thermogenesis.* Cell, 1998. **92**(6): p. 829-39.

128. Yoon, H.G., et al., *Purification and functional characterization of the human N-CoR complex: the roles of HDAC3, TBL1 and TBLR1.* EMBO J, 2003. **22**(6): p. 1336-46.

129. Ishizuka, T. and M.A. Lazar, *The nuclear receptor corepressor deacetylase activating domain is essential for repression by thyroid hormone receptor.* Mol Endocrinol, 2005. **19**(6): p. 1443-51.

130. Yoon, H.G., et al., *Reading and function of a histone code involved in targeting corepressor complexes for repression.* Mol Cell Biol, 2005. **25**(1): p. 324-35.

131. Kipreos, E.T. and M. Pagano, *The F-box protein family.* Genome Biol, 2000. **1**(5): p. REVIEWS3002.

132. Perissi, V., et al., *A corepressor/coactivator exchange complex required for transcriptional activation by nuclear receptors and other regulated transcription factors.* Cell, 2004. **116**(4): p. 511-26.

133. Tabet, A.C., et al., *De novo deletion of TBL1XR1 in a child with non-specific developmental delay supports its implication in intellectual disability.* Am J Med Genet A, 2014. **164A**(9): p. 2335-7.

134. Saitsu, H., et al., *A girl with West syndrome and autistic features harboring a de novo TBL1XR1 mutation.* J Hum Genet, 2014. **59**(10): p. 581-3.

135. Pons, L., et al., *A new syndrome of intellectual disability with dysmorphism due to TBL1XR1 deletion.* Am J Med Genet A, 2015. **167A**(1): p. 164-8.

136. Daniels, G., et al., *TBLR1 as an androgen receptor (AR) coactivator selectively activates AR target genes to inhibit prostate cancer growth.* Endocr Relat Cancer, 2014. **21**(1): p. 127-42.

137. Wang, J., et al., *TBLR1 is a novel prognostic marker and promotes epithelial-mesenchymal transition in cervical cancer.* Br J Cancer, 2014. **111**(1): p. 112-24.

138. Ramadoss, S., et al., *Transducin beta-like protein 1 recruits nuclear factor kappaB to the target gene promoter for transcriptional activation.* Mol Cell Biol, 2011. **31**(5): p. 924-34.

139. Rohm, M., et al., *Transcriptional cofactor TBLR1 controls lipid mobilization in white adipose tissue.* Cell Metab, 2013. **17**(4): p. 575-85.

140. Kulozik, P., et al., *Hepatic deficiency in transcriptional cofactor TBL1 promotes liver steatosis and hypertriglyceridemia.* Cell Metab, 2011. **13**(4): p. 389-400.

141. MacDougald, O.A. and M.D. Lane, *Transcriptional regulation of gene expression during adipocyte differentiation.* Annu Rev Biochem, 1995. **64**: p. 345-73.

142. Boucher, J., Y.H. Tseng, and C.R. Kahn, *Insulin and insulin-like growth factor-1 receptors act as ligand-specific amplitude modulators of a common pathway regulating gene transcription.* J Biol Chem, 2010. **285**(22): p. 17235-45.

143. Boucher, J., et al., *Impaired thermogenesis and adipose tissue development in mice with fat-specific disruption of insulin and IGF-1 signalling.* Nat Commun, 2012. **3**: p. 902.

144. Rodeheffer, M.S., K. Birsoy, and J.M. Friedman, *Identification of white adipocyte progenitor cells in vivo.* Cell, 2008. **135**(2): p. 240-9.

145. Saladin, R., et al., *Differential regulation of peroxisome proliferator activated receptor gamma1 (PPARgamma1) and PPARgamma2 messenger RNA expression in the early stages of adipogenesis.* Cell Growth Differ, 1999. **10**(1): p. 43-8.

146. Rossini, A.A., et al., *Studies of streptozotocin-induced insulitis and diabetes.* Proc Natl Acad Sci U S A, 1977. **74**(6): p. 2485-9.

147. Winzell, M.S. and B. Ahren, *The high-fat diet-fed mouse: a model for studying mechanisms and treatment of impaired glucose tolerance and type 2 diabetes.* Diabetes, 2004. **53 Suppl 3**: p. S215-9.

148. Klein, J., et al., *beta(3)-adrenergic stimulation differentially inhibits insulin signaling and decreases insulin-induced glucose uptake in brown adipocytes.* J Biol Chem, 1999. **274**(49): p. 34795-802.

149. Kent, W.J., et al., *The human genome browser at UCSC.* Genome Res, 2002. **12**(6): p. 996-1006.

150. Creyghton, M.P., et al., *Histone H3K27ac separates active from poised enhancers and predicts developmental state.* Proc Natl Acad Sci U S A, 2010. **107**(50): p. 21931-6.

151. Wang, J., et al., *Factorbook.org: a Wiki-based database for transcription factor-binding data generated by the ENCODE consortium.* Nucleic Acids Res, 2013. **41**(Database issue): p. D171-6.

152. Gerstein, M.B., et al., *Architecture of the human regulatory network derived from ENCODE data.* Nature, 2012. **489**(7414): p. 91-100.

153. Dorsey, M.J., et al., *B-ATF: a novel human bZIP protein that associates with members of the AP-1 transcription factor family.* Oncogene, 1995. **11**(11): p. 2255-65.

154. Blanchet, E., et al., *E2F transcription factor-1 regulates oxidative metabolism.* Nat Cell Biol, 2011. **13**(9): p. 1146-52.

155. Porse, B.T., et al., *E2F repression by C/EBPalpha is required for adipogenesis and granulopoiesis in vivo.* Cell, 2001. **107**(2): p. 247-58.

156. Fajas, L., et al., *E2Fs regulate adipocyte differentiation.* Dev Cell, 2002. **3**(1): p. 39-49.

157. Gupta, S. and R.J. Davis, *MAP kinase binds to the NH2-terminal activation domain of c-Myc.* FEBS Lett, 1994. **353**(3): p. 281-5.

158. Noguchi, K., et al., *Regulation of c-Myc through phosphorylation at Ser-62 and Ser-71 by c-Jun N-terminal kinase.* J Biol Chem, 1999. **274**(46): p. 32580-7.

159. Tournier, C., et al., *Mitogen-activated protein kinase kinase 7 is an activator of the c-Jun NH2-terminal kinase.* Proc Natl Acad Sci U S A, 1997. **94**(14): p. 7337-42.

160. Li, Q.L., et al., *Causal relationship between the loss of RUNX3 expression and gastric cancer.* Cell, 2002. **109**(1): p. 113-24.

161. Tong, Q., et al., *Function of GATA transcription factors in preadipocyte-adipocyte transition.* Science, 2000. **290**(5489): p. 134-8.

162. Steger, D.J., et al., *Propagation of adipogenic signals through an epigenomic transition state.* Genes Dev, 2010. **24**(10): p. 1035-44.

163. Wolfrum, C., et al., *Role of Foxa-2 in adipocyte metabolism and differentiation.* J Clin Invest, 2003. **112**(3): p. 345-56.

164. Florez, J.C., *The new type 2 diabetes gene TCF7L2.* Curr Opin Clin Nutr Metab Care, 2007. **10**(4): p. 391-6.

165. Li, Y., et al., *Taking control over intracellular fatty acid levels is essential for the analysis of thermogenic function in cultured primary brown and brite/beige adipocytes.* EMBO Rep, 2014. **15**(10): p. 1069-76.

166. Reed, N. and J.N. Fain, *Potassium-dependent stimulation of respiration in brown fat cells by fatty acids and lipolytic agents.* J Biol Chem, 1968. **243**(23): p. 6077-83.

167. Rosenwald, M., et al., *Bi-directional interconversion of brite and white adipocytes.* Nat Cell Biol, 2013. **15**(6): p. 659-67.

168. Ronti, T., G. Lupattelli, and E. Mannarino, *The endocrine function of adipose tissue: an update.* Clin Endocrinol (Oxf), 2006. **64**(4): p. 355-65.

169. Larsson, M., et al., *Apolipoproteins C-I and C-III inhibit lipoprotein lipase activity by displacement of the enzyme from lipid droplets.* J Biol Chem, 2013. **288**(47): p. 33997-4008.

170. Westerterp, K.R., *Diet induced thermogenesis.* Nutr Metab (Lond), 2004. **1**(1): p. 5.

171. Westerterp, K.R., S.A. Wilson, and V. Rolland, *Diet induced thermogenesis measured over 24h in a respiration chamber: effect of diet composition.* Int J Obes Relat Metab Disord, 1999. **23**(3): p. 287-92.

172. Wang, G.X., et al., *The brown fat-enriched secreted factor Nrg4 preserves metabolic homeostasis through attenuation of hepatic lipogenesis.* Nat Med, 2014. **20**(12): p. 1436-43.

173. Villarroya, J., R. Cereijo, and F. Villarroya, *An endocrine role for brown adipose tissue?* Am J Physiol Endocrinol Metab, 2013. **305**(5): p. E567-72.

174. Pimentel, G.D., et al., *High-fat diets rich in soy or fish oil distinctly alter hypothalamic insulin signaling in rats.* J Nutr Biochem, 2012. **23**(7): p. 822-8.

175. Buchowski, M.S., et al., *Effect of dairy and non-dairy calcium on fecal fat excretion in lactose digester and maldigester obese adults.* Int J Obes (Lond), 2010. **34**(1): p. 127-35.

176. Heymsfield, S.B., et al., *Energy malabsorption: measurement and nutritional consequences.* Am J Clin Nutr, 1981. **34**(9): p. 1954-60.

177. Santamarina-Fojo, S., *The familial chylomicronemia syndrome.* Endocrinol Metab Clin North Am, 1998. **27**(3): p. 551-67, viii.

178. Feingold, K.R., et al., *Endotoxin rapidly induces changes in lipid metabolism that produce hypertriglyceridemia: low doses stimulate hepatic triglyceride production while high doses inhibit clearance.* J Lipid Res, 1992. **33**(12): p. 1765-76.

179. Jones, A., et al., *TSC22D4 is a molecular output of hepatic wasting metabolism.* EMBO Mol Med, 2013. **5**(2): p. 294-308.

180. Kamagate, A., et al., *FoxO1 mediates insulin-dependent regulation of hepatic VLDL production in mice.* J Clin Invest, 2008. **118**(6): p. 2347-64.

181. Schneider, W.J., *The low density lipoprotein receptor.* Biochim Biophys Acta, 1989. **988**(2): p. 303-17.

182. Brown, M.S. and J.L. Goldstein, *Receptor-mediated endocytosis: insights from the lipoprotein receptor system.* Proc Natl Acad Sci U S A, 1979. **76**(7): p. 3330-7.

183. Koishi, R., et al., *Angptl3 regulates lipid metabolism in mice.* Nat Genet, 2002. **30**(2): p. 151-7.

184. Koster, A., et al., *Transgenic angiopoietin-like (angptl)4 overexpression and targeted disruption of angptl4 and angptl3: regulation of triglyceride metabolism.* Endocrinology, 2005. **146**(11): p. 4943-50.

185. Georgiadi, A., et al., *Overexpression of angiopoietin-like protein 4 protects against atherosclerosis development.* Arterioscler Thromb Vasc Biol, 2013. **33**(7): p. 1529-37.

186. Lafferty, M.J., et al., *Angiopoietin-like protein 4 inhibition of lipoprotein lipase: evidence for reversible complex formation.* J Biol Chem, 2013. **288**(40): p. 28524-34.

187. Sukonina, V., et al., *Angiopoietin-like protein 4 converts lipoprotein lipase to inactive monomers and modulates lipase activity in adipose tissue.* Proc Natl Acad Sci U S A, 2006. **103**(46): p. 17450-5.

188. Lee, P., et al., *Irisin and FGF21 are cold-induced endocrine activators of brown fat function in humans.* Cell Metab, 2014. **19**(2): p. 302-9.

189. Buyse, M., et al., *Insulin and glucocorticoids differentially regulate leptin transcription and secretion in brown adipocytes.* FASEB J, 2001. **15**(8): p. 1357-66.

190. Kraus, D., et al., *Leptin secretion and negative autocrine crosstalk with insulin in brown adipocytes.* J Endocrinol, 2002. **175**(1): p. 185-91.

191. Chartoumpekis, D.V., et al., *Brown adipose tissue responds to cold and adrenergic stimulation by induction of FGF21.* Mol Med, 2011. **17**(7-8): p. 736-40.

192. Schulz, T.J., et al., *Brown-fat paucity due to impaired BMP signalling induces compensatory browning of white fat.* Nature, 2013. **495**(7441): p. 379-83.

193. Rim, J.S. and L.P. Kozak, *Regulatory motifs for CREB-binding protein and Nfe2l2 transcription factors in the upstream enhancer of the mitochondrial uncoupling protein 1 gene.* J Biol Chem, 2002. **277**(37): p. 34589-600.

194. Harper, J.A., K. Dickinson, and M.D. Brand, *Mitochondrial uncoupling as a target for drug development for the treatment of obesity.* Obes Rev, 2001. **2**(4): p. 255-65.

195. Goldgof, M., et al., *The chemical uncoupler 2,4-dinitrophenol (DNP) protects against diet-induced obesity and improves energy homeostasis in mice at thermoneutrality.* J Biol Chem, 2014. **289**(28): p. 19341-50.

196. Ouellet, V., et al., *Outdoor temperature, age, sex, body mass index, and diabetic status determine the prevalence, mass, and glucose-uptake activity of 18F-FDG-detected BAT in humans.* J Clin Endocrinol Metab, 2011. **96**(1): p. 192-9.

197. Pace, L., et al., *Determinants of physiologic 18F-FDG uptake in brown adipose tissue in sequential PET/CT examinations.* Mol Imaging Biol, 2011. **13**(5): p. 1029-35.

198. Mossenbock, K., et al., *Browning of white adipose tissue uncouples glucose uptake from insulin signaling.* PLoS One, 2014. **9**(10): p. e110428.

199. Haas, B., et al., *Protein kinase G controls brown fat cell differentiation and mitochondrial biogenesis.* Sci Signal, 2009. **2**(99): p. ra78.

200. Mueckler, M. and B. Thorens, *The SLC2 (GLUT) family of membrane transporters.* Mol Aspects Med, 2013. **34**(2-3): p. 121-38.

201. Dallner, O.S., et al., *Beta3-adrenergic receptors stimulate glucose uptake in brown adipocytes by two mechanisms independently of glucose transporter 4 translocation.* Endocrinology, 2006. **147**(12): p. 5730-9.

202. Ge, X., et al., *Fibroblast growth factor 21 induces glucose transporter-1 expression through activation of the serum response factor/Ets-like protein-1 in adipocytes.* J Biol Chem, 2011. **286**(40): p. 34533-41.

203. Zhang, J., et al., *Insulin disrupts beta-adrenergic signalling to protein kinase A in adipocytes.* Nature, 2005. **437**(7058): p. 569-73.

204. Virtue, S. and A. Vidal-Puig, *Assessment of brown adipose tissue function.* Front Physiol, 2013. **4**: p. 128.

205. Gibbons, G.F., et al., *Synthesis and function of hepatic very-low-density lipoprotein.* Biochem Soc Trans, 2004. **32**(Pt 1): p. 59-64.

206. Cohen, J.C., J.D. Horton, and H.H. Hobbs, *Human fatty liver disease: old questions and new insights.* Science, 2011. **332**(6037): p. 1519-23.

207. Mead, J.R., S.A. Irvine, and D.P. Ramji, *Lipoprotein lipase: structure, function, regulation, and role in disease.* J Mol Med (Berl), 2002. **80**(12): p. 753-69.

208. Wang, H. and R.H. Eckel, *Lipoprotein lipase: from gene to obesity.* Am J Physiol Endocrinol Metab, 2009. **297**(2): p. E271-88.

209. Kharitonenkov, A. and P. Larsen, *FGF21 reloaded: challenges of a rapidly growing field.* Trends Endocrinol Metab, 2011. **22**(3): p. 81-6.

210. Potthoff, M.J., et al., *FGF21 induces PGC-1alpha and regulates carbohydrate and fatty acid metabolism during the adaptive starvation response.* Proc Natl Acad Sci U S A, 2009. **106**(26): p. 10853-8.

211. Li, C., *Genetics and regulation of angiopoietin-like proteins 3 and 4.* Curr Opin Lipidol, 2006. **17**(2): p. 152-6.

212. Garcia-Arcos, I., et al., *Adipose-specific lipoprotein lipase deficiency more profoundly affects brown than white fat biology.* J Biol Chem, 2013. **288**(20): p. 14046-58.

213. Shimamura, M., et al., *Leptin and insulin down-regulate angiopoietin-like protein 3, a plasma triglyceride-increasing factor.* Biochem Biophys Res Commun, 2004. **322**(3): p. 1080-5.

214. Fugier, C., et al., *The lipoprotein lipase inhibitor ANGPTL3 is negatively regulated by thyroid hormone.* J Biol Chem, 2006. **281**(17): p. 11553-9.

215. Inaba, T., et al., *Angiopoietin-like protein 3 mediates hypertriglyceridemia induced by the liver X receptor.* J Biol Chem, 2003. **278**(24): p. 21344-51.

216. Ge, H., et al., *Differential regulation and properties of angiopoietin-like proteins 3 and 4.* J Lipid Res, 2005. **46**(7): p. 1484-90.

217. Fernandez, J.A., et al., *Direct assessment of brown adipose tissue as a site of systemic tri-iodothyronine production in the rat.* Biochem J, 1987. **243**(1): p. 281-4.

218. Silva, J.E. and P.R. Larsen, *Potential of brown adipose tissue type II thyroxine 5'-deiodinase as a local and systemic source of triiodothyronine in rats.* J Clin Invest, 1985. **76**(6): p. 2296-305.

219. Mantha, L. and Y. Deshaies, *beta-Adrenergic modulation of triglyceridemia under increased energy expenditure.* Am J Physiol, 1998. **274**(6 Pt 2): p. R1769-76.

220. Esteva, F.J. and G.N. Hortobagyi, *Comparative assessment of lipid effects of endocrine therapy for breast cancer: implications for cardiovascular disease prevention in postmenopausal women.* Breast, 2006. **15**(3): p. 301-12.

221. Osman, K.A., M.M. Osman, and M.H. Ahmed, *Tamoxifen-induced non-alcoholic steatohepatitis: where are we now and where are we going?* Expert Opin Drug Saf, 2007. **6**(1): p. 1-4.

222. Gunschmann, C., et al., *Transgenic mouse technology in skin biology: inducible gene knockout in mice.* J Invest Dermatol, 2014. **134**(7): p. e22.

223. Shan, T., W. Liu, and S. Kuang, *Fatty acid binding protein 4 expression marks a population of adipocyte progenitors in white and brown adipose tissues.* FASEB J, 2013. **27**(1): p. 277-87.

224. Heffner, C.S., et al., *Supporting conditional mouse mutagenesis with a comprehensive cre characterization resource.* Nat Commun, 2012. **3**: p. 1218.

225. Siersbaek, M.S., et al., *Genome-wide profiling of peroxisome proliferator-activated receptor gamma in primary epididymal, inguinal, and brown adipocytes reveals depot-selective binding correlated with gene expression.* Mol Cell Biol, 2012. **32**(17): p. 3452-63.

226. Wang, Z., et al., *Rapid and highly efficient transduction by double-stranded adeno-associated virus vectors in vitro and in vivo.* Gene Ther, 2003. **10**(26): p. 2105-11.

227. Graham, F.L., et al., *Characteristics of a human cell line transformed by DNA from human adenovirus type 5.* J Gen Virol, 1977. **36**(1): p. 59-74.

228. Klaus, S., et al., *Characterization of the novel brown adipocyte cell line HIB 1B. Adrenergic pathways involved in regulation of uncoupling protein gene expression.* J Cell Sci, 1994. **107 (Pt 1)**: p. 313-9.

229. Green, H. and O. Kehinde, *An established preadipose cell line and its differentiation in culture. II. Factors affecting the adipose conversion.* Cell, 1975. **5**(1): p. 19-27.

230. Vegiopoulos, A., et al., *Cyclooxygenase-2 controls energy homeostasis in mice by de novo recruitment of brown adipocytes.* Science, 2010. **328**(5982): p. 1158-61.

231. Orlicky, D.J. and J. Schaack, *Adenovirus transduction of 3T3-L1 cells.* J Lipid Res, 2001. **42**(3): p. 460-6.

232. Chan, D.A., et al., *Targeting GLUT1 and the Warburg effect in renal cell carcinoma by chemical synthetic lethality.* Sci Transl Med, 2011. **3**(94): p. 94ra70.

233. Horn, C.C., H. Ji, and M.I. Friedman, *Etomoxir, a fatty acid oxidation inhibitor, increases food intake and reduces hepatic energy status in rats.* Physiol Behav, 2004. **81**(1): p. 157-62.

234. Maarbjerg, S.J., et al., *Genetic impairment of AMPKalpha2 signaling does not reduce muscle glucose uptake during treadmill exercise in mice.* Am J Physiol Endocrinol Metab, 2009. **297**(4): p. E924-34.

235. Schmidt, S., et al., *Neuronal functions, feeding behavior, and energy balance in Slc2a3+/- mice.* Am J Physiol Endocrinol Metab, 2008. **295**(5): p. E1084-94.

236. Rose, A.J., et al., *Skeletal muscle eEF2 and 4EBP1 phosphorylation during endurance exercise is dependent on intensity and muscle fiber type.* Am J Physiol Regul Integr Comp Physiol, 2009. **296**(2): p. R326-33.

237. Mattijssen, F., et al., *Hypoxia-inducible lipid droplet-associated (HILPDA) is a novel peroxisome proliferator-activated receptor (PPAR) target involved in hepatic triglyceride secretion.* J Biol Chem, 2014. **289**(28): p. 19279-93.

238. Tschop, M.H., et al., *A guide to analysis of mouse energy metabolism.* Nat Methods, 2012. **9**(1): p. 57-63.

Hartl DL, Jones EW (2005). *Genetics: Analysis of Genes and Genomes* (6 edition). Missisauga: Jones & Bartlett, Canada. page 477. ISBN 0-7637-1511-5.